DESIGN AND DEVELOPMENT OF CATALYSTS & ADSORBENTS FOR CO_X FREE H_2 PRODUCTION

by

Burcu Selen Çağlayan

B. S., Chemical Engineering, Boğaziçi University, 2001

M. S., Chemical Engineering, Boğaziçi University, 2003

Submitted to the Institute for Graduate Studies in
Science and Engineering in partial fulfillment of
the requirements for the degree of
Doctor of Philosophy

Graduate Program in Chemical Engineering
Boğaziçi University

2011

to Emre

ACKNOWLEDGEMENT

First of all, I would like to express my truthful gratitude to my thesis supervisor Prof. Ahmet Erhan Aksoylu for his guidance, encouragement and trust in me. As a mentor, he never once hesitated to spare time for me. It was a privilege for me to work with Prof. Aksoylu during my PhD thesis.

I would like to express my great appreciations for Prof. Ayşe Nilgün Akın, Prof. Prof. Zeynep İlsen Önsan and Prof. Ramazan Yıldırım who devoted their valuable time to guiding me, helping me all the time. I am very grateful to Prof. Hüsnü Atakül who gave his precious time for reading and commenting on my thesis.

I would like to thank Assist. Prof. Ahmet Kerim Avcı for his guidance, support and friendship.

Very special thanks to my friends Feyza Gökaliler and Tuğba Davran Candan for their everlasting help and encouragement on any matter. Their friendship is the biggest asset that I have gained in my life.

I would also like thank Melek Selcen Başar, and Görkem Oğur for their contribution in the experimental systems. Thanks are for Mustafa Karakaya who helped me with my computer problems. I was very lucky to work with the CATREL team; I would like to thank the whole team for their support.

Cordial thanks are for Bilgi Dedeoğlu and Nurettin Bektaş for their technical assistance and friendship during my thesis. Heartfelt thanks are for Melike Gürbüz and Kamuran Taylan Çevre and Belgin Balkan for their friendship and kindness to me. My thanks are also for Yakup Bal for his friendly attitude.

I would like to thank my colleague Ayla Türkekul Bıyık for her support and friendship.

I would like to express my thanks to Bilge Gedik Uluocak and Muhammed Erkan Karabekmez for their friendship and kindness. They spent considerable time and effort in electron microscopy and X-ray diffraction studies conducted at Boğaziçi University Advanced Technologies R&D Center.

Deepest thanks to Semra Türe and Ayşe Çetin for their everlasting support, valuable advice and motivation. I would like to thank Derya Bektaş and Ziya Aydemir for their friendship and support.

Finally; I would like to thank my husband, Ertuğrul Çağlayan, and all my family for their patience, encouragement, understanding and continuous support all these years. They believed in me and loved me all the time. This thesis would not have been possible without their everlasting support.

Financial support provided by Scientific-Technological Research Council of Turkey (TUBITAK) through project 105M282 and State Planning Organization (DPT) through projects DPT03K120250 and DPT07K120630.

ABSTRACT

DESIGN AND DEVELOPMENT OF CATALYSTS & ADSORBENTS FOR CO_X FREE H_2 PRODUCTION

The overall purpose of this research study is to produce, characterize and investigate the performance of catalysts and adsorbents which will play a role in CO_x-free hydrogen production via fuel processing for fuel cell applications. In the first three parts of the study; the purpose was to design and develop Pt-Ni/Al_2O_3 and Au-Re/CeO_2 bimetallic catalysts for water gas shift (WGS) reaction. Results showed that Pt-Ni/Al_2O_3 catalysts were not suitable for fuel processors since methanation was observed under real feed conditions, although Pt-Ni/Al_2O_3 catalysts were found highly active and stable for WGS reaction with ideal feed including only main reactants. Gold addition by deposition precipitation technique on impregnated Re/Ceria catalysts led to higher dispersion and stronger interaction between Au and Re particles. 1%Au-0.5%Re/Ceria (imp+dp) catalyst was found highly active for WGS reaction, especially at high H_2O/CO feed ratios. DRIFT profiles indicated that the reaction took place between the OH groups present on the catalyst and linearly adsorbed CO to produce surface formate along with surface carbonate and bicarbonate species. In the fourth section, DRIFTS and CO/CO_2 adsorption studies were conducted on Pt-Sn and Pt catalysts supported on HNO_3-oxidized activated carbon (AC3) with the aim of understanding the reasons behind the superior PROX performance of Pt-Sn/AC3. Studies revealed that Pt_3Sn alloy formation on AC3 support has led to CO adsorption in higher amounts, and faster surface reaction involving intermediate OH groups which bring along increase in CO conversion and selectivity as the temperature decreases within the range 110-135^oC. The last part consisted of SEM, DRIFTS and CO_2 adsorption studies over activated carbon (AC) adsorbents prepared by subjecting a commercial sample to oxidative, alkali and thermal treatments aiming to develop an efficient AC based CO_2 adsorbent. With Na_2CO_3 impregnation the CO_2 mass uptakes at 20 bars and 25ºC were improved by ca. 8 and 7 folds and at 1 bar were increased ca. 15 and 16 folds, on the average, for air and HNO_3 oxidized samples, respectively.

ÖZET

CO_X'TEN ARINDIRILMIŞ H_2 ÜRETİMİNE YÖNELİK KATALİZÖR VE ADSORBANLARIN TASARIMI VE GELİŞTİRİLMESİ

Bu çalışmanın genel amacı yakıt pili uygulamaları için yakıt işlemcisi yardımıyla CO_x'ten arındırılmış H_2 üretiminde kullanılacak katalizör ve adsorbanları üretmek, karakterize etmek ve performanslarını incelemektir. Çalışmanın ilk üç bölümünün amacı gaz-buhar geçişi reaksiyonunda kullanılan Pt-Ni/Al_2O_3 ve Au-Re/CeO_2 katalizörlerini hazırlamak ve geliştirmektir. Sonuçlar, ideal besleme koşulları için yüksek WGS aktiflik ve kararlılığına sahip olmalarına rağmen Pt-Ni/Al_2O_3 katalizörlerinin gerçekçi besleme koşullarında metanasyon aktifliği göstermeleri nedeniyle yakıt işlemcisinde kullanıma uygun olmadıklarını göstermiştir. Empregnasyonla hazırlanmış Re/CeO_2 katalizörlerine biriktirmeli çöktürme yöntemiyle altın eklenmesi yüksek metal dağılımı ve Au ile Re arasında yoğun etkileşime sebep olmuştur. 1%Au-0.5%Re/CeO_2 katalizörlerinin WGS reaksiyonunda, özellikle yüksek H_2O/CO oranları için, yüksek aktifliğe sahip olduğu bulunmuştur. DRIFT profilleri formik asit tuzu ve yanısıra karbonat ile bikarbonat oluşumunu sağlayan reaksiyonun yüzeyde yer alan OH grupları ile doğrusal tutunmuş CO arasında gerçekleştiğini işaret etmiştir. Pt-Sn/AC3 katalizörünün PROX reaksiyonunda gösterdiği üstün performansın nedenlerinin anlaşılmasının amaçlandığı dördüncü bölümde AC3 destekli hazırlanan Pt-Sn ve Pt katalizörleri üzerinde DRIFT ve CO/CO_2 adsorpsiyon çalışmaları gerçekleştirilmiştir. Çalışmalar Pt_3Sn oluşumunun artan CO adsorpsiyonuna ve OH ara ürünü içeren hızlı yüzey reaksiyonuna imkan tanımasının 110-135^oC aralığında sıcaklık düşüşü ile yükselen CO çevrim ve seçimliliğinin nedeni olduğunu ortaya koymuştur. Son bölümü ise aktif karbon bazlı etkin CO_2 adsorbanlarının geliştirilmesi amacıyla ticari aktif karbonun oksidatif, alkali eklenmesi ve termal işlemlere tabi tutulmasıyla hazırlanmış adsorbanlar üzerinde gerçekleştirilen SEM, DRIFTS ve CO_2 adsorpsiyon çalışmalarını içermektedir. Na_2CO_3 eklenen adsorbanlar üzerindeki testler CO_2 tutma kapasitesinin sırasıyla hava ve HNO_3 ile okside edilmiş örnekler için 20 bar ve 25^oC'de 8 ve 7 kat; 1 bar ve 25^oC'de ise 15 ve 16 kat arttığını göstermiştir.

TABLE OF CONTENTS

LIST OF FIGURES

LIST OF TABLES

LIST OF SYMBOLS

A	Lattice constant
A	Avogadro's number
A_g	Area of an individually adsorbed molecule
A_p	Adsorption potential of the system
b	The equilibrium constant
d	Crystallite size
E	The characteristic energy of the system
E_l	The heat of adsorption for the first layer
E_L	The heat of adsorption for the second and higher layers
m	Saturated amount of gas adsorbed
M	Molar volume of the gas
n	Adsorbent heterogeneity parameter
N	Amount of gas adsorbed
P	Pressure
P_0	Saturation pressure
R	Universal gas constant
S	Surface area
t	Adsorbent heterogeneity parameter
T	Temperature
W	The volume adsorbed
W_0	The limiting micropore volume
ΔH	The isosteric enthalpy of adsorption
λ	The ratio of actual air to fuel ratio to stoichiometry for a given mixture
υ	The adsorbed gas quantitiy
υ_m	The monolayer adsorbed gas quantity

LIST OF ACRONYMS/ABBREVIATIONS

AC	Activated carbon
AC1	HCl treated activated carbon
AC2	Air oxidized activated carbon
AC3	Nitric acid oxidized activated carbon
AC4	Air oxidized and Na_2CO_3 impregnated activated carbon
AC5	Nitric acid oxidized and Na_2CO_3 impregnated activated carbon
ATR	Autothermal reforming
BET	Brunauer-Emmett-Teller
BCI	Backscattering composition imaging
bç	Biriktirmeli çöktürme
BSE	Back-scattering electron
dp	Deposition precipitation
D-R	Dubinin-Radushkevich
DRIFTS	Diffuse reflectance infrared Fourier transform spectroscopy
DSMS	Dynamic sampling mass spectrometer
DTP	Decreasing temperature progression
EDS	Energy dispersive X-ray spectroscopy
emp	Empregnasyon
ESEM	Environmental scanning electron microscopy
FC	Fuel cell
FP	Fuel processor
FTIR	Fourier transform infrared
GHG	Green-house gas
GHSV	Gas hourly space velocity
HRTEM	High resolution transmission electron microscopy
IGA	Intelligent gravimetric analyzer
imp	Impregnation
IR	Infra red
MS	Mass spectrometry

PEMFC	Proton exchange membrane fuel cell
POX	Partial oxidation
PROX	Preferential oxidation
Redox	Reduction-oxidation
SE	Secondary electron
SEM	Scanning electron microscopy
si	Sequential impregnation
SR	Steam reforming
TOX	Total oxidation
TPD	Temperature programmed desorption
vol	Volume
WGS	Water gas shift
WHSV	Weight hourly space velocity
wt	Weight
XPS	X-Ray Photoelectron Spectroscopy
XRD	X-ray diffraction

1. INTRODUCTION

From the beginning of the 20th century, all electric power systems have been built and operated based on a monopolistic system consisting of large electric power grids transmitting energy from the generation systems to the distribution system using one directional of energy flow. With the aim of lowering the price of electric energy supply for the consumers while enhancing the energy production through the use of renewable generation technologies, new energy generation systems have been sought based on dispersed generation of electricity instead of producing it centrally. The new system will consist of both large production facilities and small, dispersed energy generation units of limited power connected to distribution grids which will enable bidirectional energy flow, i.e., a unit such as an apartment or group of houses, will be able to sell its excess production to the distribution grid, and buy from the grid whenever its production is lower than its demand. This new concept will help getting rid of ca. 20% energy loss during transmission, and it will support significant technical changes that favor renewable energy technologies such as solar, geothermal, biomass, wind, hydrogen energy and energy from the sea. However, since energy production from sun, sea and wind are intermittent and flow-limited, new problems will emerge in the management of these new generation energy transmission and distribution systems [1]. In this respect, the combined 'fuel processor – fuel cell' (FP-FC) systems have a major advantage in their use for small-scale stationary applications as they produce energy non-intermittently.

The use of hydrogen as an energy source for these new generation energy grids will be possible with FP-FC systems since the lack of hydrogen distribution network and technical limitations make it difficult to supply, distribute and store hydrogen in necessary quantities [2]. Therefore the hydrogen gas will likely be generated on site by reforming available fuels such as natural gas, gasoline, diesel, propane, LPG, biogas and methanol, all of which have worldwide production, existing infrastructure and distribution networks [3, 4].

Today PEMFC is considered to be the most promising fuel cell system with potential widespread use in small-scale stationary and mobile applications as it offers a

series of advantages such as low operating temperature, sustained operation at high current density, compactness, long stack life and sustainability to discontinuous operation. [3, 5].

The main reactor of a fuel processor system is the reformer which produces a hydrogen-rich gas from the original hydrocarbon feed. Recent studies performed focus on three reforming technologies: (i) Steam reforming (SR), (ii) Partial oxidation (POX) and (iii) Autothermal reforming (ATR) – in which SR and total oxidation (TOX) reactions run simultaneously, increasing the energy efficiency of the process [6]. As the reformate has large quantities of CO regardless of the reforming process and the hydrocarbon feed used, and the PEMFC electrocatalyst has stable activity only if the hydrogen rich feed has lower than 10-40 ppm CO, it is necessary to use a CO clean-up system immediately after the reformer unit. The CO clean-up system generally consists of water-gas shift (WGS) and preferential oxidation (PROX) units run in series; both units usually have multi-stage reactors.

WGS catalyst for the FP-FC system is an essential research concern. Since reversible water-gas shift reaction is moderately exothermic and equilibrium-limited, the desired CO levels can be achieved at low temperatures. In an FP, WGS is normally performed in two serial reactors, namely, high-temperature shift (HTS) reactor operating at 350-500˚C and low temperature shift (LTS) reactor operating at 180-240˚C for obtaining high activity and conversion simultaneously [2]. As the commercial catalysts used for both high-temperature (HTS) and low-temperature (LTS) shift reactions are pyrophoric, the development of active non-pyrophoric catalysts for these systems is crucial. Catalyst formulations which enable the use of a WGS unit with a single reactor operating at a mid-range temperature in a fuel processor are also sought considering the total WGS reactor volume and economical concerns. The critical issue is the design and development of a catalyst which consumes CO while increasing the H_2 content of the WGS product stream compared to that of the product of the reforming unit fed. There are only a few articles addressing WGS catalyst performance under realistic feed conditions and none of them report the change in the hydrogen content.

An efficient PROX unit must reduce carbon monoxide level from 1-2% down to 10-40 ppm while suppressing possible hydrogen oxidation. Considering the energy

efficiency of a combined fuel processor-fuel cell system, the temperature of PROX unit should be ideally in 100˚C-130˚C range. On the other hand, most conventional CO oxidation catalysts require high temperatures, which prevent irreversible CO adsorption and guarantee stable operation. Catalytic low temperature CO oxidation has two important reaction steps, which must occur simultaneously; CO chemisorption and dissociative adsorption of O_2. Therefore, in order to minimize the problems that may result from adsorption competition, new catalysts having distinct active sites for each of the reactants and/or chemisorption processes should be designed for providing high and stable activity [6].

The hydrogen rich stream from the fuel processor, being cleaned-up from poisonous CO is therefore suitable for PEMFCs since a PEMFC can operate on reformed hydrocarbon fuels without the removal of the by-product carbon dioxide [3]. However discharge of carbon dioxide - which is a greenhouse gas - in large quantities to the atmosphere has become one of the most serious global environmental problems. Carbon dioxide capture and storage technologies enable the production of hydrogen with strongly reduced CO_2 emissions [7].

Among a number of techniques that can be used for the separation of carbon dioxide from fuel gas streams in hydrogen production, adsorption of carbon dioxide on adsorbent materials is becoming increasingly important [8]. The first and the most important issue in adsorption process is to find the appropriate adsorbent. The adsorbent must have (i) high selectivity and adsorption capacity for carbon dioxide at high temperature; (2) adequate adsorption/desorption kinetics for carbon dioxide at operating conditions; (3) stable adsorption capacity of carbon dioxide after repeated adsorption/desorption cycles; (4) adequate mechanical strength of adsorbent particles after cyclic exposure to high pressure streams [8]. Therefore, developing efficient adsorbent materials for carbon dioxide adsorption is a key for the development of economically feasible capture technologies.

The overall purpose of this research study is to produce, characterize and investigate the performances of catalysts and adsorbents which will play a role in CO_x-free hydrogen production via fuel processing for fuel cell applications. The thesis consists of

five parts. In the first part of the study; the purpose was to investigate the WGS performances of bimetallic Pt-Ni/Al_2O_3 catalysts. In the second part of the thesis, the aim was to design and develop Au-Re bimetallic catalysts supported on ceria for WGS reaction. An effective catalyst assuring high activity and stability was searched through a parametric study using impregnation and deposition precipitation techniques in catalyst preparation. Based on the superior WGS performance of the 1%Au-0.5%Re/Ceria (imp+dp) catalyst especially at high H_2O/CO feed ratios, real feed experiments in addition to DRIFTS studies were performed on the ceria based catalysts in the third part of the study aiming to obtain a complete set of WGS performance specs of Au-Re/Ceria system. In the fourth section of the thesis, DRIFTS and CO/CO_2 adsorption studies were conducted on both Pt-Sn and Pt catalysts supported on HNO_3-oxidized activated carbon (AC3) with the aim of understanding the reasons behind the superior PROX performance of Pt-Sn/AC3. The last part of the research consisted of SEM, DRIFTS and CO_2 adsorption studies over activated carbon adsorbents prepared by subjecting a commercial sample to different oxidative, alkali and thermal treatments aiming to develop an efficient activated carbon based CO_2 adsorbent.

Chapter 2 contains a detailed literature survey on theoretical background of water gas shift and preferential oxidation reactions as well as CO_2 adsorption and activated carbon adsorbents. Chapter 3 presents the experimental work carried out. The results obtained are presented and discussed in Chapter 4. Chapter 5 consists of the conclusions drawn from the present study and recommendations for future work.

2. LITERATURE SURVEY

2.1. Water Gas Shift Reaction

Water gas shift reaction [Eq. (2.1)] is a well established catalytic industrial process which has been particularly applied in ammonia production [9]. More recently, it has attracted increasing interest since it is a key step in fuel processing for hydrogen production; it enables CO clean up and additional hydrogen generation in fuel cell applications [2, 10, 11]. The WGS units are placed downstream of the reformer to further reduce the CO concentration from ca. 10% to 0.5-1% [2, 11]. Since the feed stream to WGS reactor contains CO, CO_2, H_2O and H_2, additional reactions such as methanation [Eq. (2.2)] can occur depending on the temperature, catalyst used and the H_2O/CO ratio [9].

$$CO + H_2O = CO_2 + H_2 \qquad (\Delta H° = -41.2 \text{ kJ mol}^{-1}) \qquad (2.1)$$

$$CO + 3H_2 = CH_4 + H_2O \qquad (\Delta H° = -206.2 \text{ kJ mol}^{-1}) \qquad (2.2)$$

The WGS reaction is reversible, equilibrium-limited and moderately exothermic; to take advantage of the fast reaction kinetics at higher reaction temperatures and the shift to equilibrium to lower CO concentrations at lower temperatures, existing applications typically combine a high-temperature shift stage (350-500˚C) and low-temperature shift stage (180-260˚C) through serial HTS-LTS units[2, 12].

There has been great interest in the development of active, selective, thermally stable, poison resistant and non-pyrophoric noble metal based WGS catalyst formulations supported on metal oxide carriers since standard HTS (Fe_3O_4/Cr_2O_3 oxide) and LTS ($Cu/ZnO/Al_2O_3$) catalysts cannot be used in fuel processors due to their disadvantages such as thermodynamic limitations at high temperatures, sensitivity to air, the need of long pre-conditioning, and slow kinetics at low temperatures [2, 11, 13, 14]. Both metal and support play an important role in WGS reaction [15]. Catalyst combinations involving noble

metals, mainly Au, and Pt, supported on various oxide supports (Al_2O_3, TiO_2, CeO_2 and ZrO_2) have been reported as promising WGS catalysts.

2.1.1. Pt-Based WGS Catalysts

Platinum, as a noble metal, has attracted interest to be used in mixed oxide supported water-gas shift catalysts; Pt/ZrO_2 [15-17], Pt/TiO_2 [16, 18-22], Pt/CeO_2-ZrO_2 [23, 24], Pt/Al_2O_3 [22, 25-27], Pt/CeO_2 [9, 10, 28-31] and Pt/CeO_2-Al_2O_3 [27, 32] are some examples of the catalysts tested for their WGS activity at low and high temperature regions.

Support modification is widely used to enhance the catalytic activity of the Pt-based WGS catalysts. The enhanced reducibility brought by the monovanadate species formed at lower loadings of vanadia on the zirconia support surface resulted in increased WGS activities for Pt/ZrO_2 catalysts [15]. The effect of vanadium promotion on Pt/CeO_2 catalyst was also studied by the same group and the improvement in WGS kinetics is suggested to be associated with V-O-Ce bonds when vanadium surface density was below the monolayer coverage [9]. Gonzales *et. al.* [20] investigated the WGS activity behavior of Pt deposited over cerium modified TiO_2 catalyst. They suggested that the modifications in the reducibility of the support and the stability of the metallic particles when Pt was supported on cerium-modified TiO_2 were responsible for the better catalytic performance of the catalyst in WGS reaction. The promoting effect of Ce, Ni and Co on the WGS performance of Pt/ZrO_2 catalyst was investigated by Lee and his coworkers under hydrogen rich conditions (10% CO, 10% CO_2, 80% H_2 in dry base gas; $H_2O/CO = 6$) at 250°C [16]. Ce-doped Pt/ZrO_2 catalyst was reported to reach 95.1% CO conversion when low temperature reduction was applied prior to reaction.

Panagiotopoulou et. al. have investigated a series of Pt/Ceria catalysts doped with various cations (Ca, La, Mg, Zn, Zr, Yb, Y, Gd) prepared by urea-nitrate combustion method [31]. They concluded that the WGS activity of the catalyst is enhanced by cation promotion due to the increasing reducibility of the surface cell of ceria and oxygen ion mobility of the ceria support.

The effect of a second noble metal addition, especially rhenium, on the WGS reaction over TiO_2 [17-19, 21], ZrO_2 [17] and ceria-zirconia mixed oxide [11, 23] supported Pt catalysts was studied by several groups. The Fourier transform infrared spectroscopy (FTIR) analyses of the adsorbed species during reaction revealed the enhancement of the adsorbed CO peaks in lower wavenumber region with the increasing Re content [18] and reaction studies hint catalytically active site formations between Pt and Re on titania support surface which are effective for the activation of water and acceleration of WGS reaction [19]. Sintering of Pt/TiO_2 which caused catalyst deactivation during WGS reaction was prevented by the addition of Re as the second metal [21]. Furthermore, the addition of Re increased the catalytic activity through the formation for ReO_x under WGS reaction conditions [21]. It was found that Re enhanced the WGS activity of ceria-zirconia supported Pt catalysts and that $Re_2(CO)_{10}$ was an optimal source for introducing Re to Pt/ceria-zirconia catalysts. The kinetic model suggested a larger positive order dependency of H_2O concentration with lower inhibitory orders for CO_2 and H_2 concentration for the Pt-Re catalyst compared to the Pt catalyst [23].

Radhakrishnan *el. al*. [24] have investigated the WGS activity of Pt/ceria-zirconia oxides under two different realistic feed gas compositions: HTS feed composition (4.9% CO, 10.5% CO_2, 33% H_2O, 30.3%H_2, balance N_2) and LTS feed composition (1.5% CO, 5% CO_2, 45% H_2O, 25% H_2, balance N_2). The catalyst with Pt loadings in 2-4% range reached the equilibrium CO conversion level at 320°C.

2.1.1.1. Al_2O_3 Supported Pt Catalysts for WGS. Al_2O_3 is a very high surface area support that has been reported to result in significant enhancement of activity, selectivity, and stability of dispersed noble metals for a number of catalytic reactions including WGS. The WGS performance and kinetics of Pt/Al_2O_3 catalysts are investigated extensively in the literature. For instance the kinetics of Pt catalysts supported on alumina under fuel reformer conditions (6.8% CO, 8.5% CO_2, 22% H_2O, 37.3% H_2 and 25.4% Ar) in the temperature range 180-345°C has been studied by Phatak et al [25]. In another study, the mechanistic aspects of the WGS reaction on 0.5wt%Pt/Al_2O_3 catalyst was investigated using steady-state isotropic transient kinetic analysis together with *in situ* diffuse reflectance infrared Fourier transform spectroscopy (DRIFTS) [26]. Germani et. al. [27] reported a highly active platinum/ceria/alumina WGS catalyst prepared by sol-gel method

and deposited on stainless steel platelets. They claimed that deposition of catalysts on microstructured platelets led to a better platinum utilization under a feed composition which is typical of the outlet of a gasoline autothermal reformer (9.6% CO, 8.4% CO_2, 23% H_2O, 32.2% H_2 and 26.8% Ar) and equilibrium CO conversion levels could be reached within the temperature range 380-420°C. Pt/ceria/alumina catalysts were also investigated by another group [32], however they reported no H_2 formation nor CO conversion at 300°C with GHSV of 64000 h^{-1} (120 ml/min CO and 0.5 ml/min liquid H_2O). The same catalyst was highly active for ultra high temperature (700°C) WGS reaction; its CO conversion was 76.3% with 94.7% H_2 selectivity. Panagiotopoulou *et al.* [22] have investigated the catalytic performance of Pt-Al_2O_3 and 0.5%Pt-MO_x-Al_2O_3 mixed oxide catalysts in the low and high temperature range of WGS reaction and reported that the Al_2O_3 supported catalysts become active at high temperatures (450°C). They also reported that Pt-MO_x-Al_2O_3 catalysts, where M = Co, Ni, Ti, Fe, and Cr, exceed Pt-Al_2O_3 catalysts in catalytic performance at lower temperatures.

2.1.2. Au/Ceria Catalysts for WGS Reaction

Catalyst formulations involving supported gold on ceria have shown to exhibit high WGS activity comparable to that of conventional catalysts [10, 12, 33-44]. Ceria has been emphasized as a reducible oxide support [34, 45, 46]; hence, a source of oxygen [45] and stabilizing agent for highly dispersed Au in the active nanostructured form [34, 36, 47] and a promoter for WGS reaction [36, 47]. Ce^{4+}/Ce^{3+} redox reaction is believed to be the reason of the high oxygen storage capacity of ceria. The oxygen produced via the redox process [Eq. (2.3)] can be utilized under reduction conditions [36]. On the other hand, the promotion by noble or transition metal enhances the ceria reducibility and facilitates the generation of very active centers at the interface between metal and support [37].

$$2CeO_2 = Ce_2O_3 + ½\ O_2 \qquad (2.3)$$

The reactivity of the gold-ceria catalysts is strongly influenced by the Au particle size and structure, which are sensitive to a number of variables, including preparation method [48], state and structure of the support [36, 45, 46, 48], the interaction between gold and support [36, 37], and catalyst pretreatment [13]. Among the employed methods of

preparation, highly dispersed, low particle size gold is reported to be achieved via deposition precipitation (dp) method [28, 35, 38, 39]. dp technique was also reported to modify ceria via the formation of oxygen vacancies that changes the average size of ceria particles, which play an important role in WGS activity of Au/ceria catalysts [38, 41]. Ceria crystallite size was reported to be as important as the Au particle size in WGS reaction performance [38], considering the fact that two Au/ceria catalysts with different loadings (2.8 and 4%), Au particle sizes and BET surface areas have shown comparable CO conversion levels at temperatures between 50-250°C (1.3% CO, 3.1% H_2O, 0.5% CO_2, 5.7% H_2 and balance He; GHSV = 51500 h^{-1}ml/g catalyst). In another study, it was reported that gold was stabilized more strongly on nanorod ceria enclosed by {110} and {100} planes than on nanocube and nanopolyhedra ceria; 1%Au deposition precipitated on nanorod ceria was observed to reach higher CO conversion levels under 2% CO, 10% H_2O and balance helium feed within 150-350°C temperature range [41].

The influence of the preparation method on the gold particle size and therefore the WGS activity of the Au/ceria catalysts are studied extensively. Fu et. al. [34] have compared two commonly used preparation methods: Coprecipitation and deposition precipitation. They reported that between the Au loading range of 1-9 %, the gold particle size did not increase with loading, indicating a strong interaction between gold and ceria for the catalysts prepared by dp method. On the other hand, they observed the significant effect of calcination temperature on the gold particle size; the gold particle size of catalysts calcined at 650°C were much higher (9.2 nm) than those of which were calcined at 400°C (4.6 nm). They also claimed that the catalyst with lower ceria particle size had higher activity for low temperature water gas shift reaction under ideal feed conditions (2% CO, 10.7% H_2O and balance He) even though it had higher gold particle size. Another group [35] has prepared two Au/ceria catalysts by dp method using ceria with different pretreatment procedures. They reported that the preparation technique strongly influenced the catalytic activity due to the large differences in gold size and to the availability of the gold sites in close contact to ceria defects on the surface. The more active catalyst was reported to reach equilibrium level for CO conversion at 300-350°C with a feed stream containing 4.5% CO in argon, water partial pressure and space velocity being 31.1 kPa and 4000 h^{-1}, respectively.

Andreeva et al. [36] have investigated the effects of gold content, space velocity and H_2O/CO ration the WGS activity of Au/ceria catalysts prepared by dp technique under ideal feed conditions (4.5% CO in Ar; P_{H2O} = 31.1 kPa; GHSV = 4000, 8000, 12000 h^{-1}) in the temperature range 140-350°C. Results indicated that an optimal gold loading, 3% Au, existed amongst 1, 3 and 5% Au loaded samples, and increased H_2O/CO ratios in the feed resulted in higher activities. The authors reported lower activities with increasing space velocities; however they claimed that as the loading and temperature increased, the effect of space velocity became negligible. Low temperature WGS reaction activity studies of 1%Au/ceria prepared by co-precipitation method were conducted by another group [43]. They reported Au and CeO_2 crystallite sizes less than 5 nm and 14.5 nm, respectively. Although their catalyst could only reach 10% CO conversion under the reaction conditions studied at 120-360°C (4% CO, 2.6% H_2O, balance He; 30000 $mlg^{-1}h^{-1}$), they reported the positive effect of the water addition to the system. The stability test results conducted at 360°C with a stream consisting of 2% CO, 20% H_2O and balance helium revealed that the catalyst had low stability; its CO conversion decreased from 60% to 10% within 48 h.

In a study by Sandoval *et. al.* [39], the WGS reaction performance of deposition precipitated gold on ceria as well as other supports (TiO_2, Al_2O_3 and SiO_2) has been investigated. The reducible oxide supported (TiO_2 and CeO_2) Au samples were shown to exhibit higher activities at the temperature range 50-400°C. The gold loadings used in that study were 4 and 8%; the reaction tests were conducted with a stream containing 5% CO and 10% H_2O with space velocity 9000 h^{-1}. Six hours of calcination pretreatment were applied to all catalyst samples at different temperatures (200, 300 and 400°C); for Au/ceria samples, higher WGS activities were obtained at 250-400°C for the ones calcined at 400°C.

In another study by Andreeva et. al. [40], a highly active and stable ceria-alumina supported gold WGS catalyst was prepared by mechanochemical activation. The higher WGS activity compared to Au/ceria catalysts was attributed to the strong modification of ceria in the presence of gold and the formation of oxygen vacancies on the catalyst surface.

The effect of realistic feed conditions on the catalytic LTS activity and deactivation of Au/ceria catalyst prepared by DP technique was investigated by Denkwitz et al [44].

They have studied the reaction under different feed conditions (2-10% CO, 20-31.5% H_2O, 0-11% CO_2, 0-43% H_2, balance He; 80 $Nmlmin^{-1}$, 75-100 mg catalyst diluted with Al_2O_3) with different calcination and reduction procedures applied on the catalysts. Their results revealed that H_2 in the feed significantly reduced the initial reaction rate but had little effect on deactivation. Contrarily, the effect of CO_2 on the initial rate was small; however CO_2 in the feed resulted in significant deactivation.

Ceria is also used as a dopant to modify other reducible oxide based Au catalysts in several studies. Idakiev et al. [37] have studied the effect of ceria modification on mesoporous titania based Au catalysts. Under ideal feed conditions (4.5% CO in Ar; P_{H2O} = 31.1 kPa; GHSV = 4000 h^{-1}) ceria modified samples prepared by dp method reached higher conversion levels at the temperature range 140-250°C. As the temperature increased further to 300°C, Au/ceria catalyst reached CO equilibrium conversion levels.

While ceria supported noble metal catalysts are promising candidates to be used in FP applications, efforts have been made to increase stability and catalytic activity of these catalysts further [49]. In our knowledge however, this is not the case for gold/ceria catalysts; only a few groups have tried to dope rare earth metals into ceria [50, 51] or add another metal besides gold [28, 52] to achieve better yields.

Recently, Andreeva et al. [50] have investigated the influence of preparation method on structure and catalytic performance of gold supported on rare earth metal (La, Sm, Gd, Yb, Y) doped ceria catalysts. They carried out the WGS activity tests under the following conditions: T = 140-350°C, GHSV = 4000 h^{-1}, partial pressure of water vapor = 31.1 kPa and CO composition = 4.42%vol. They concluded that higher WGS activity was achieved for catalysts promoted by Yb and Sm compared to the other gold/ceria based catalysts. The same group has published another study, in which they reported the influence of the dopants Al and Sm on the water gas shift activity and the structure of the catalysts [51]. Hurtado-Juan and his coworkers [28] have claimed to be the first ones who systematically study bimetallic, gold-on-ceria based promoted catalysts. They reported the highest LTS activity (3 ml/min CO, 40.5 ml/min H_2O; WHSV = 52000 h^{-1}) in the temperature range 150-450°C belonged to 1.75%Pt-1.05%Au/ceria in the group of Au-M/ceria (M: Pt, Pd, Ca, W, Ni) catalysts. They also proposed that the role of the Au-M

system is to alter the local band structure of ceria facilitating its redox properties at low temperatures. Very recently bimetallic Au-M/CeO_2 catalysts (M = Ni and Pt) have been reported to exhibit higher LTS activities (0.5 cm^3 catalyst, 10 ml/min CO, 31.1 kPa water vapor) than monometallic Au/CeO_2 [52]. The authors emphasized the positive effect of especially Pt addition to the catalyst on the WGS performance as well as the importance of the preparation sequence.

2.1.3. WGS Reaction Mechanism on Au/Ceria Catalysts

Although Au/CeO_2 catalysts are well accepted as promising WGS catalysts, there is still a lack of knowledge on the kinetics and mechanism of the reaction over these catalysts [53-55]. The main frame including the roles of ceria support and Au nanoparticles, nature of active sites and possible reaction intermediates in the WGS reactions has not yet been established. There are two main mechanisms under question: Reduction-oxidation (redox) and formate mechanisms. The redox process involves the reduction of active sites by CO in the first step and subsequent catalyst oxidation by H_2O in the second step [Eq (2.4)-(2.6)] whereas the formate mechanism involves the reaction of CO with ceria hydroxyl groups to generate surface formates and formate decomposition [53, 54]. Researchers use several techniques (mainly DRIFTS) to provide information on the reaction mechanism, particularly on whether formates act as a reaction intermediates or not. A review of DRIFTS data for Au/CeO_2 catalysts is given in Table 2.1.

$$CO + M \rightarrow CO_a\text{-}M \qquad \text{(M:metal)} \tag{2.4}$$

$$CO_a\text{-}M + 2CeO_2 \rightarrow CO_2 + Ce_2O_3 + M \tag{2.5}$$

$$H_2O + Ce_2O_3 \rightarrow 2CeO_2 + H_2 \tag{2.6}$$

Chen et. al. claimed to analyze all the possible elementary steps in the redox and formate mechanisms of WGS reaction on Au/CeO_2 [56]. They focused on the O-H bond breakage resulting in surface oxygen regeneration which is common to both mechanisms. They calculated the barriers of four possible reactions for regeneration (three of which belonged to redox mechanism) and concluded that it was difficult to reproduce surface oxygen at low temperatures. A study of Rodriguez [55] focused on the mechanistic studies for WGS reaction on Au (111) and inverse CeO_x/Au (111) catalysts. He reported for

CeO_x/Au (111) catalysts, the presence of Ce^{3+} led to the dissociation of H_2O to give OH groups and both formate and carbonate groups could be the intermediates for the WGS reaction between 300-375°C.

Table 2.1. Reported peak positions of species on Au/CeO_2 catalysts.

Assignment	**Region**	**υ (cm^{-1})**
OH mono-coordinated on Ce^{3+}	O-H	3696 [33]
OH two-coordinated on Ce^{3+}	O-H	3663 [33], 3658 [57]
Bridged OH_{ad} groups/Geminal OH groups	O-H	3650 [58], 3647 [43], 3645 [53], 3650 [54]
Hydrogen-bonded hydroxyl groups	O-H	3700-2800 [33, 59], 3700-2500 [57]
Formate species on Ce^{4+}/Bridged-bonded formates	C-H	2950 [54], 2949 [33], 2947 [60], 2945 [44, 53, 57], 2942 [59], 2940[58]
Formate species on Ce^{3+}/Bidentate formates	C-H	2850 [53], 2848 [33], 2843 [59], 2841 [60], 2840 [54], 2833 [44], 2832 [57], 2830 [53]
Linear CO_2 interacting with ceria/Gas phase CO_2	C-O	2363 [44, 53], 2343 [33], 2342 [53], 2332 [44]
CO linearly adsorbed on Ce^{3+}	C-O	2157 [33], 2132 [57], 2093 [53]
CO linearly adsorbed on Ce^{4+}	C-O	2170 [33], 2151 [33], 2148 [33, 53], 2142 [53]
CO co-adsorbed with oxygen species on Au step sites	C-O	2127 [33], 2119 [33], 2118 [53]
$^2F_{5/2} \rightarrow {}^2F_{7/2}$ electronic transition of Ce^{3+}	C-O	2127 [33], 2126 [53]
CO on Au^0 step sites of metallic particles	C-O	2100 [33]
CO on slightly negatively charged Au	C-O	2094 [33], 2090 [33]
CO on $Au^{\delta-}$ sites	C-O	2065 [33], 2060 [33], 2040 [33]
Bending mode of undissociated H_2O	COO	1640 [33]
Bicarbonate species on ceria	COO	1590 [33], 1390 [33], 1212 [33]

Table 2.1. Reported peak positions of species on Au/CeO_2 catalysts. (cont.)

Assignment	Region	υ (cm^{-1})
Formate species on Ce^{3+}	COO	1595 [43], 1588 [44], 1585 [33, 53, 54], 1580 [58], 1575 [59], 1375 [54, 58], 1370 [33, 53]
Formate species on Ce^{4+}/Bridged bonded formates	COO	1550 [33, 53], 1374 [44], 1370 [33], 1333 [53]
Carboxylate species on ceria	COO	1510 [33], 1320 [33]
Carbonate species on ceria	COO	1570 [53], 1480 [33], 1463 [53], 1460 [56], 1430 [33], 1422 [53], 1420 [44], 1390 [53], 1385 [33], 1356 [33], 1340 [33], 1334 [44], 1300 [53], 1291 [44], 1070-1045 [33], 1051 [44], 1049 [53], 1007 [53], 866 [60], 860 [53], 856 [59], 855 [57], 853 [33, 53, 57], 851 [60], 850 [44], 847 [53]

The most comprehensive study on the mechanism of WGS reaction on Au/CeO_2 catalyst was reported by Prof. Behm's group in 2006 [53]. Leppelt *et. al.* have compared the CO adsorption behaviors of reduced ceria support and 2.6%Au/CeO_2 catalyst by *in situ* DRIFTS measurements in a mixture of 200-10000 ppm CO in N_2 at 180°C. On CeO_2, due to CO exposure, they observed the emergence of new peaks in C-H and COO stretching vibration regions assigned to adsorbed formate and bi-carbonate species. They observed the formation of the same bands on Au/CeO_2 under CO flow, but with a much lower intensity than on pure CeO_2. The results of their *in situ* DRIFTS WGS tests (1 kPa CO, 2 kPa H_2O, N_2 as balance) indicated i) formate species resulted from the reaction between adsorbed CO and OH groups on the surface, ii) formate formation was catalyzed by the Au nanoparticles either directly by offering a reaction pathway with a lower activation barrier or indirectly by modifying the oxide surface and/or increasing local reactant coverages by spillover processes, and iii) the buildup of carbonate species in addition to formate species were the reasons of catalyst deactivation.

The group has also conducted transient DRIFTS experiments in order to understand the main role of the formate species in the WGS reaction on Au/CeO_2 catalysts. Based on their results, the mechanism was reported to involve i) adsorption of CO directly on the Au nanoparticles and on the ceria support, and subsequent reverse spillover on the Au nanoparticles, ii) formation of surface formates mainly at active Au sites, iii) decomposition of bidendate formates on the same active sites as they were formed, favored by the presence of water vapor, iv) spillover of formates formed by reaction of CO_{ad} and OH_{ad} at the active Au sites onto the ceria support to form a mobile layer on the support, v) reverse spillover of the adsorbed formate species involving their return to the active sites and decomposing into CO_2 and H_2 (Figure 2.1) [53].

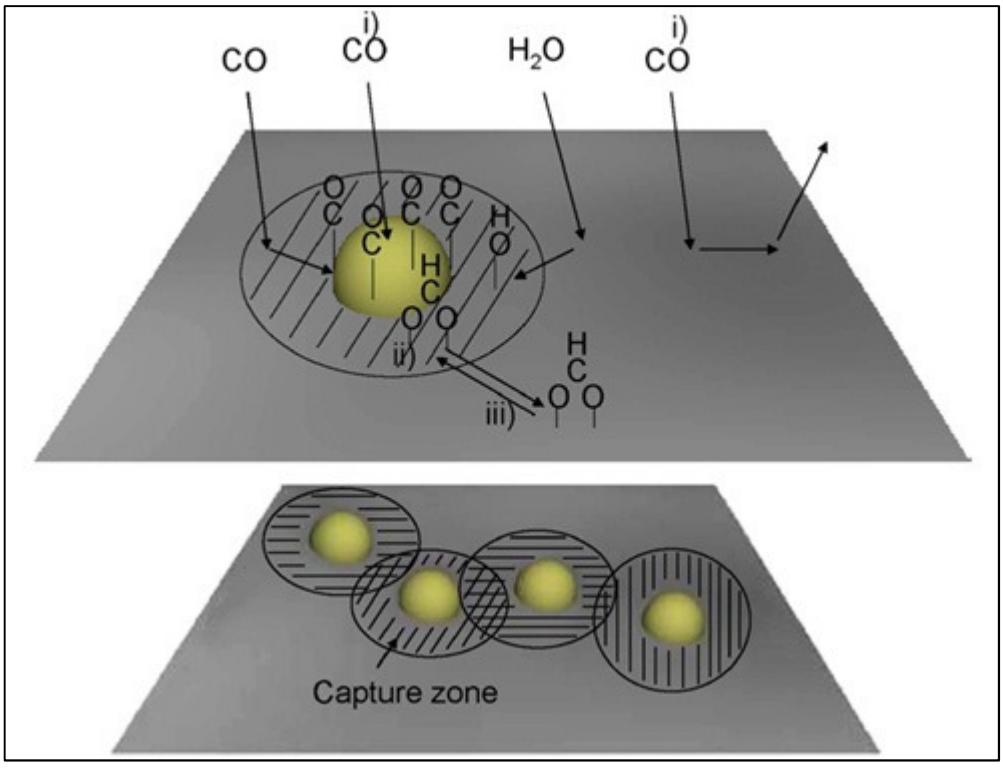

Figure 2.1. Schematic representation of reaction mechanism involving i) CO adsorption on Au nanoparticles and support, followed by reverse spillover, ii) the formation and decomposition of formates, iii) the spillover and reverse spillover of surface formates [53].

Another study on WGS mechanism on Au/Ceria catalysts with very important results is the one conducted by Tabakova *et. al.* in 2003 [33]. As a result of their DRIFTS studies in which they examined the interaction of ceria support and the catalyst with CO

and H_2O, and conducted forward and reverse WGS reaction tests. They concluded that i) forward reaction proceeded at the boundary between small metallic gold particles and ceria, where CO adsorption on gold and H_2O dissociation on ceria defects took place, ii) formates were intermediates in WGS reaction, and iii) the stability of Au/CeO_2 catalysts stemmed from the interactions between small gold metallic particles and ceria.

Sakurai et. al. [38] proposed a formate mechanism involving equations (2.7) and (2.8) based on their findings during CO and water pulse experiments: CO_2 and H_2 were formed at the same time when H_2O was added; which could not be explained by redox mechanism proposed earlier [Eq (2.4)-(2.6)].

$$CO + HO_a\text{-}CeO_{2-x} \rightarrow HCOO_a\text{-}CeO_{2-x} \quad (2.7)$$

$$HCOO_a\text{-}CeO_{2-x} + H_2O \rightarrow HO_a\text{-}CeO_{2-x} + CO_2 + H_2 \quad (2.8)$$

With the aim of seeking a reaction-rate-limiting surface intermediate, Jacobs *et. al.* have examined the surface of Au promoted CeO_2 catalysts after adsorption of CO and H_2O and during steady-state WGS reaction [54]. They concluded that the formates arising on the ceria surface upon adsorption/reaction of CO with surface germinal OH groups were rate limiting for WGS reaction under high H_2O/CO ratios where the rate was first order in CO.

Adversely, Meunier *et.al.* [58] have reported that the formates they detected during WGS reaction with an ideal feed (2% CO, 7% H_2O, balance Ar) over $Au/Ce(La)O_2$ catalyst were not important reaction intermediates in CO_2 formation. They claimed that the specific rate of CO_2 formation was ca. 60 times higher than that of formate decomposition showing that the formates detected by DRIFTS were not important in the WGS reaction.

There are works in literature focusing on the reactivity and state of active gold nanoparticles, also. As an example, Fu et. al. have compared the activity of CN-leached and nonleached Au/CeO_2 catalysts and concluded that positively charged $Au^{\delta+}$ species acted as active sites in the WGS reaction on Au/CeO_2 and that the Au nanoparticles were present as inert spectators [10].

2.2. Preferential Oxidation of Carbon Monoxide

The final catalytic conversion in a fuel processor occurs in the preferential oxidation of CO (PROX) unit. The effluent of reformer, which is fed to WGS unit, has ca. 10% CO. The CO concentration at the exit of WGS unit drops down to 1-2%. The WGS effluent is rich in H_2 and has CO_2, water vapor and CH_4 regardless of the original hydrocarbon/hydrocarbon mixture fed to the reformer inlet. The following preferential CO oxidation [Eq (2.9)] step is necessary since platinum based cathode catalysts of PEM fuel cells require carbon monoxide levels as low as 1-100 ppm for stable operation [6, 61]. Therefore, an efficient PROX unit must reduce carbon monoxide level from 1-2% down to below 100 ppm while suppressing possible hydrogen oxidation [Eq (2.10)] under the presence of CO_2, water vapor and CH_4.

$$CO + ½\ O_2 \rightarrow CO_2 \qquad (\Delta H^\circ = -283.6\ kj/mol) \qquad (2.9)$$

$$H_2 + ½\ O_2 \rightarrow H_2O \qquad (\Delta H^\circ = -243.5\ kj/mol) \qquad 2.10)$$

Considering the energy efficiency of a combined fuel processor-fuel cell system, the temperature of PROX unit should be ideally in 100˚C-130˚C range. On the other hand, most conventional CO oxidation catalysts require high temperatures (ie. above 150˚C), which prevent irreversible CO adsorption, for guaranteeing stable operation. Catalytic low temperature CO oxidation has two important reaction steps, which must occur simultaneously; CO chemisorption and dissociative adsorption of O_2. Therefore, in order to minimize the problems that may result from adsorption competition, the catalyst should have distinct active sites for each of the reactants and/or chemisorption processes for guaranteeing high and stable activity. Controlling the oxygen/CO ratio in the feed is very important; in some cases, two PROX units operating at different temperatures may be necessary [6].

While CO oxidation is a well-studied reaction, preferential oxidation of CO for the feed streams having H_2, CO_2, and H_2O is not fully investigated. Indeed most of the studies in literature deal with dry streams with no CO_2 in the feed. As CO_2, CO, H_2 and H_2O are all present at the exit stream of the water gas shift unit of a practical/commercial fuel

processor, it is important to study selective CO oxidation by using feed mixtures including those in realistic concentrations. [62].

Catalytic formulations involving supported noble metals, such as Au [63-71], Pt [62, 67, 73-82], Ru [83-85], Rh [86], and bimetallic Pt-Sn system [72, 87, 88] were found applicable for PROX reaction.

2.2.1. Pt-Based PROX Catalysts

Pt-based catalysts have been reported to be very robust CO oxidation catalysts [72], therefore there are many studies in literature dealing with the PROX performance of Pt metal supported on Al_2O_3 [62, 67, 73, 74], CeO_2 [61, 75], ceria-zirconia mixed oxides [76-79] and zeolites [80-82]. The use of Pt/alumina catalysts go back to 1963 when Engelhard first proposed that they selectively oxidize CO in hydrogen [62].

Manasilp and Gulari have reported that their 2%Pt/alumina catalyst prepared by single-step sol-gel method could selectively oxidize CO to a few ppm with constant selectivity and high space velocity, which is necessary in fuel processor – fuel cell combinations [62]. They stated the essence of their preparation method as the enhancement in degree of interaction between the support and metal crystallites led by the produced high surface area support having a narrow pore size distribution. They investigated the effect of oxygen/CO ratio and CO concentration in the feed, space velocity, H_2O addition and CO_2 addition to dry feed (1% CO, 1% O_2, 60% H_2 and balance He) on the activity and selectivity of the catalyst. They proposed two reasons for the observed enhancement in CO conversion without any selectivity change upon water addition: Water enhances the water-gas shift reaction, and hydroxyl groups formed upon adsorption of water on the surface of the catalyst is a better oxidant than O_2, therefore enhances the CO oxidation rate. They reported that CO_2 in the feed, however, had a negative effect due to reverse water gas shift reaction, formation of carbonates on the surface or the increase in surface CO concentration due to dissociative adsorption of CO_2.

Kahlich et al. [73] studied the kinetics of the selective CO oxidation in H_2-rich gas on Pt/Al_2O_3 over a wide range of CO concentrations (0.02-1.5%) and observed that it was

not possible to have more than 80% conversion over 0.5% Pt/alumina in the presence of hydrogen for a feed stream having 1% CO and 1% O_2 even at temperatures as high as 250°C. They also observed that hydrogen presence increased the rate of CO oxidation by a factor of five. Based on their kinetic model they estimated that the best temperature for preferential oxidation of CO over a Pt/alumina catalyst was 200°C and that 2.5 times the stoichiometric amount of oxygen would be needed to completely oxidize 1% CO. Another kinetic study was conducted by Bissett et. al. [74]. They have combined experimental work and simulations in order to obtain rate expressions for the PROX reaction on Pt/alumina catalyst under conditions similar to those used in fuel processor – fuel cell combinations (30-10000 ppm CO, 30-10000 ppm O_2, 30% H_2, 17% CO_2, 15% H_2O and balance N_2; 83 cm^3/s) within 80-200°C temperature range.

The mechanism of PROX over Pt/CeO_2 catalyst were investigated extensively using catalytic reaction tests, and in situ DRIFTS, XPS, HRTEM and TDS techniques by Pozdnyakova et. al. [61]. They observed significant amount of adsorbed water in a hydrogen-bonded structure suppressing hydrogen oxidation, which allowed them to propose a mechanism including the contribution of surface water in a low temperature water-gas shift- type reaction, for the PROX feed (1% CO, 0.4-1% O_2, balance H_2; 100 Nml/min) used.

Ayastuy et. al. [75] have reported about an active ceria-supported Pt catalysts which showed 45% selectivity at very low temperature (~ 80ºC). They observed that for complete conversion in the presence of 60% hydrogen between 81-93°C occurred with oxygen/CO ratio of 3. They have also observed the inhibition effect of CO_2 below 90°C although at higher temperatures it had a positive effect on the catalyst performance. The same group have also compared a series of ceria-zirconia mixed oxides as supports for Pt, obtaining complete CO depletion at temperatures as low as 75ºC and observed a selectivity of 50% with supports containing 80%, 68% and 50% of ceria (in mol%) [76]. They claimed that unlike alumina, ceria and ceria-zirconia mixed oxides have an active role in CO oxidation supplying their lattice oxygen to oxidize CO. In the presence of CO_2 and H_2O, however, there was a general decrease of CO conversion.

Wootsch and his coworkers have studied the preferential CO oxidation in the presence of hydrogen over $Pt/Ce_xZr_{x-1}O_2$ (x = 0, 0.15, 0.5, 0.68) catalysts [77]. They examined the effect of the temperature and excess O_2 (λ = 0.8-2). A noncompetitive Langmuir-Hinshelwood type mechanism on the metal/oxide interface was proposed by the authors in the temperature range 90-130ºC.

Oxide promoters are widely used in PROX studies to enhance the activity and selectivity of the monometallic Pt catalysts. A ceramic monolith washcoated with 5% Pt promoted by Fe oxide impregnated onto γ-Al_2O_3 was tested for PROX performance in 90-150°C temperature range [78]. The test gas contained 1000 ppm CO, 20% H_2, 10% H_2O and varying O_2/CO ratios with the balance N_2. The effect of CO_2 in the activity and selectivity of the catalyst was also tested with the addition of 20% CO_2 gas to the stream. Its enhanced activity was attributed by the authors to the presence of a metal oxide promoter, which provides the site for O_2 adsorption and dissociation, eliminating the inhibition observed in the oxidation of CO on Pt catalysts. As a continuation of this work, Liu et. al. [79] have studied the structural properties of active and selective Fe-oxide promoted Pt/γ-alumina catalyst. Their results showed that Fe oxide must be in intimate contact with the Pt particles in order to enhance PROX activity. They have shown that Fe oxide partially covered the Pt particles, interacted with them and changed the electronic properties of the particles by providing oxygen to the adsorbed CO on the Pt nearby and creating a dual site for CO oxidation.

Igarashi et. al. [80] proposed Pt-supported zeolite catalysts which they claimed oxidizing carbon monoxide much more selectively in a large excess of hydrogen with the addition of lower concentration of oxygen than that used for conventional Pt-supported alumina catalysts. In a feed stream of 1% CO and 1% O_2 in hydrogen, their catalysts showed conversions of 60-80% above 200°C and selectivities of 30-60% with a catalyst weight to flow rate ratio of 0.006 g/(scm^3). Additionally, they reported that with decreasing oxygen content to 0.7%, they have obtained an enhanced selectivity, approaching 100%. Among the catalysts prepared with different zeolite types, Pt/mordenite showed the highest conversion from CO to CO_2 and high selectivity. The group continued their studies by adding second metal to the catalyst and observed fairly high conversion with a high selectivity of ca. 90% over a wide fuel-flow rate conditions at 150°C [81]. The same group

also reported that Pt-Fe/mordenite catalyst showed complete removal of CO with the stoichiometric O_2 addition in a simulated reformate (1% CO, 0.5% O_2, 0-20% H_2O, 0-25% CO_2, balance H_2; 50 cm^3/min, 0.025 g catalyst) at 80-150°C with 100% selectivity [82].

2.2.2. Pt-SnO_x System for PROX reaction

Among the oxide promoters investigated for Pt-based catalysts for the PROX reaction, SnO_x is perhaps the most promising one. The Pt-SnO_x system has been studied for many years as it has shown to catalyze the CO oxidation at moderate temperatures (ca. 120ºC), where neither platinum nor tin dioxide alone has stable activity. The high activity of Pt-SnO_x system has been ascribed to a synergistic bifunctional mechanism in which Pt provides the adsorption sites for CO, while oxygen adsorbs dissociatively on SnO_x [89]. On the other hand, the reactive sites situated at the border between SnO_x and Pt particles could not be distinguished; thus the possibility of oxygen spillover from tin dioxide onto Pt has been considered for Pt-SnO_x/Al_2O_3 catalysts [90].

Very recently Ayastuy et. al. [72] published their work on CO-PROX over sequentially impregnated Pt-Sn/Al_2O_3 catalysts. They tried to optimize the catalyst composition by keeping the Pt loading constant (1wt%) and varying the Pt/Sn atomic ratio (Pt/Sn = 1.92, 0.53, 0.28). As a result of their characterization and performance test studies conducted using idealistic and realistic feed streams (1% CO, 0.4-1.5% O_2, 0-5% CO_2, 0-5% H_2O and balance He; GHSV = 12000 h^{-1}) the optimum Pt/Sn ratio was found to be 0.53. Interestingly they concluded that in PROX, the addition of Sn to Pt did not substantially increase the activity at low temperatures; however, the temperature range where the CO conversion was maximum was increased significantly suggesting that the addition of Sn weakened the adsorption of hydrogen.

With the aim of selectively creating Pt-promoter oxide interfacial sites, Jain et. al. [87] have prepared Pt-Sn/Al_2O_3 catalysts among other oxide promoted catalysts by depositing 0.15-0.25% Sn onto the surface of 5% monometallic Pt/Al_2O_3 catalyst. They conducted dry (0.5% CO, 1.25% O_2, 25% H_2 and balance He) and wet (0.1% CO, 0.15% O_2, 60% H_2, 20% CO_2, 10% H_2O and balance He) tests within 40-250°C temperature range in order to investigate the PROX activity and selectivity of the catalysts. In the dry tests Pt-

Sn bimetallic catalyst showed a slight improvement in the activity compared to the monometallic catalyst; the CO conversion profiles were similar, but shifted to lower temperatures for the bimetallic catalyst. In the wet tests, the bimetallic catalyst was reported to show high activity with a trend indicating less dependence on the GHSV.

Schubert et al. [88] have investigated PROX on vulcan supported Pt-Sn catalysts and obtained higher activity and selectivity than commercial Pt/Al_2O_3 catalyst at low temperatures. Their temperature-programmed desorption (TPD), *in situ* diffuse reflectance IR Fourier transform spectroscopy, and x-ray photon spectroscopy measurements revealed that i) CO surface coverage on the metallic particles was high and decreased with temperature, ii) only part of the Sn was reduced and included in PtSn alloy particles, while another part formed SnO_x islands beside the active particles. They suggested that the reaction took place either in a bifunctional way at the perimeter of the SnO_x islands on/adjacent to PtSn particles or by a spill-over process. They also reported the exact position of the C-O stretch vibration which depends on the catalyst, temperature and CO coverage at different temperatures under a mixture of 1 kPa CO, 75 kPa H_2 and balance N_2. The CO adsorption peak positions for Pt- and PtSn-based catalysts reported in the literature are given in Table 2.2.

2.2.2.1. Activated Carbon Supported Pt-SnO_x Catalysts for PROX. Activated Carbon (AC) is known for its high surface area and a surface chemistry that allows tailoring of surface chemical properties [99-101]. The textural and chemical properties of the AC surface can be modified in order to enhance the catalytic properties of the AC supported catalysts [100, 101]. The surface chemical properties of the activated carbons will be discussed in section 2.3. Because of its advantageous properties as a catalyst and catalyst support, activated carbons are used in various catalytic applications such as oxidation of sulfur dioxide, hydrogenation, chlorination and ozone decomposition. AC supported catalysts were tested for CO oxidation in the last few decades and shown to exhibit higher catalytic performance than Al_2O_3 supported ones [102].

Table 2.2. Reported peak positions of CO adsorption bands for Pt- and PtSn-based catalysts.

Assignment	Region	υ (cm^{-1})
CO linearly adsorbed on Pt	C-O	2095 [61], 2070 [91], 2063 [92], 2065-2060 [93], 2051-2042 [93]
CO linearly adsorbed at the Pt step sites	C-O	2068-2041 [61], 2050 [88], 2048 [94], 2039 [95]
CO linearly adsorbed on the extended terraces of Pt	C-O	2083-2075 [61], 2073 [88, 94]
CO linearly adsorbed on the Pt sites on the PtSn alloyed surface	C-O	2075-2066 [88], 2072-2043 [96], 2071 [93], 2068-2043 [97], 2067 [91], 2060 [98], 2060-2050 [93]
Bridged bonded CO on Pt sites	C-O	1882-1877 [61], 1826 [92], 1815 [95], 1791 [94], 1780 [91]
Bridged bonded CO on Pt sites on the PtSn alloyed surface	C-O	1840 [91]

In a series of papers, firstly several Pt-Sn/AC catalysts were prepared, characterized in a detailed fashion [101, 102] and tested for their CO oxidation activities [102]. The results clearly showed that the CO oxidation performance of the catalysts strongly depended on Pt:Sn loading ratio, preparation procedure and AC pretreatment. The results hinted that the active phase on Pt-Sn catalyst prepared on nitric acid oxidized activated carbon (AC3) is the Pt_3Sn alloy. Pt_3Sn is formed with the help of the carboxylic acid rich surface chemistry of the support and/or through the interaction between the metallic Pt phase and the SnO_x interface, and have resulted in enhanced CO oxidation ability [102]. The activated carbon supported Pt-Sn and Pt-Ce catalysts were then used in PROX reaction under hydrogen rich feed conditions by Özkara et al. [103]. In that paper, the activity tests for the 1%Pt-0.25%Sn/AC catalysts prepared by sequential impregnation were performed for a feed stream having 1% CO, 1% O_2, 60% H_2 and inert He (100 ml/min, 0.25 g. catalyst) at 150°C. 80% CO conversion was obtained with the catalyst prepared by air oxidized activated carbon support. Baltacioglu et. al. reported their PROX test (5% CO, 2% O_2, 5-45% H_2, balance He; 150 cm^3/min, 100 mg catalyst) results at 110°C and compared them to the results of their CO oxidation studies; significant

enhancement in CO oxidation rates were observed with 46% selectivity, especially for H_2 concentrations higher than 30% [104]. Afterwards, Pt-Sn/AC catalysts were tested further by Şimşek et al. at 150^{o}C for the feed additionally containing CO_2 and water vapor [105]. The results showed that 1%Pt-0.25%Sn/AC3 prepared by using HNO_3 oxidized AC support, reached 100% CO conversion level in the presence of only CO_2 or both CO_2 and H_2O in the feed (1% CO, 1% O_2, 60% H_2, 15% CO_2, 0-10% H_2O and balance He; 100 ml/min, 0.25g catalyst). Recently, Ilgaz Soykal has tested the same catalyst for its PROX activity and selectivity with a feed stream containing 1% CO, 1.25% O_2, 60% H_2, 10% CO_2, 15% H_2O, 3% CH_4 and balance helium at 110-135°C temperature range as a part of his MS thesis [106]. His results showed that bimetallic Pt-Sn/AC3 catalyst reached the same CO conversion levels of ca. 88% under realistic feed conditions as in the case of idealistic feed stream (1% CO, 1% O_2, 60% H_2 and balance He.). Based on the results of those initial studies, the Pt-Sn catalyst prepared on AC3 was found promising for practical applications, considering that the effluent of the water gas shift reactors in an on-board fuel processor has both CO_2 and water vapor. As the active phase on Pt-Sn/AC3 is probably Pt_3Sn alloy, a series of density functional studies have been carried out on CO-Pt_3Sn and (CO+O)-Pt_3Sn systems; the results of those works, which also include simulations on CO-Pt system as the comparison basis, well revealed that (i) the alloy leads to a decrease in CO adsorption strength, (ii) it limits the number of possible sites for CO adsorption compared to those on Pt surface, and (iii) it provides specific and distinct sites for oxygen adsorption in the close neighborhood of the CO-adsorbing sites. [107-109].

2.3. Carbon Dioxide Adsorption on Activated Carbon

2.3.1. Activated Carbon

Activated carbons are non-hazardous, processed carbonaceous products with a complicated porous structure and internal surface area that is predominantly contained within the micropores [110]. Micropores which have widths less than 2 nm provide high adsorptive capacities for molecules of small dimensions such as gases and most solvents [111]. A schematic representation of the structure of activated carbon is illustrated in Figure 2.2. They are produced from various raw materials such as woods, coconut shell, coal, lignite, peat, etc in two ways: Chemical and physical activation [112, 113].

Chemically activated carbons are manufactured by the simultaneous carbonization and activation of the raw material with an activating agent (H_3PO_4 or $ZnCl_2$) at 600-800°C. Whereas physically activated carbons are manufactured from thermally decomposed (at 600-800°C) carbonaceous precursors in the absence or presence of controlled air flow. The activation step is performed in the presence of steam and/or CO_2 at 800-1100°C. As a result of these activation treatments non-graphitic raw material is gasified and a highly porous and disordered graphitic material with surface oxide groups is formed. Following the activation treatments, the activated carbons may be washed with pure water or mineral acids to diminish the ash content which otherwise would result in pore blockage, since substituent groups or impurities on the carbon surface may limit the adsorption capacity, by repelling or failing to attract the adsorbate molecules [113, 114].

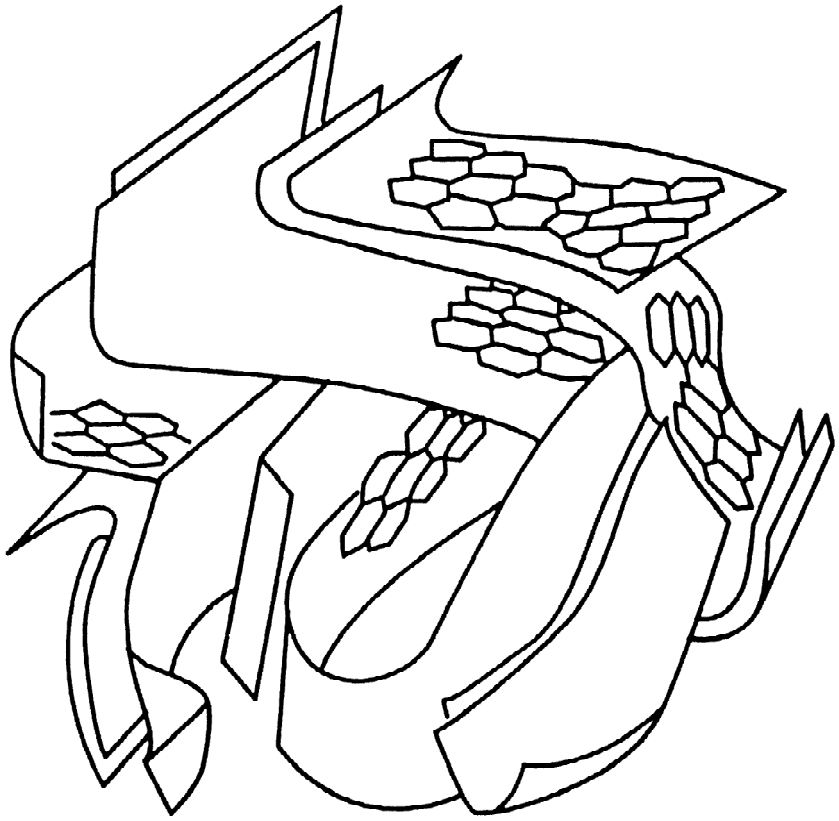

Figure 2.2. Schematic representation of the activated carbon structure [111].

The base material and the activation conditions affect the pore structure and the surface chemistry of the activated carbon samples tremendously [115]. The size of the pores is very important for the adsorption properties of activated carbon. Adsorption

strength increases with the decreasing pore size due to the increase in the number of contact points between the adsorbate, and the adsorbent and if the micropore width is less than twice the diameter of the adsorbate, adsorption potentials between the opposing pore walls start to overlap [115].

Surface chemistry is another important factor affecting the adsorption properties of activated carbons. There are atoms other than carbon – heteroatoms – at the edges of the condensed, polyaromatic building blocks of activated carbons that define their chemical characteristics as the carbon atoms located at the edges of carbon crystallites act as active sites showing strong tendency to chemisorb elements like oxygen, hydrogen, chlorine, bromine, iodine and sulfur forming non-stoichiometric stable surface compounds called surface groups/complexes [115, 116]. Amongst these surface groups, surface oxygen complexes are counted as the most important and common ones [115, 116]. Carbon-oxygen surface groups are the most important factors influencing the surface reactions, surface behavior, hydrophilicity and electrical/catalytic properties of carbons [117]. And since the oxygen atoms are bonded to the carbon atoms at the edges of the molecules which constitute the main adsorbing surface, they influence the adsorption of characteristics of activated carbons [117]. The identification of the surface oxygen groups is very important since it provides information on the detailed gasification mechanism and surface characterization of carbonaceous materials [117, 118]. Temperature programmed desorption is the most common method in the identification and quantification of the surface oxygen groups formed on the surface due to oxidative treatments or CO_2 chemisorption [118]. The groups proposed consist of lactones, ethers, pyrones, carbonyls, semiquinones, quiones, acid anhydrides, keto-enols, ketenes and epoxy oxygens [95, 113, 115, 116, 118-120]. Figure 2.3 presents the surface oxygen groups and their decomposition temperature ranges reviewed by Figueiredo et. al [120].

The surface oxygen groups are formed on activated carbons when they are treated with oxidizing agents such as concentrated nitric or sulfuric acid, sodium hypochlorite, permanganate, bichromate, hydrogen peroxide [116, 121]. As a result of these treatments acidic, basic and neutral surface oxygen groups are introduced to the activated carbon surface and the surface becomes more hydrophilic; the associated changes in the surface area and pore texture affect the adsorption and catalytic behaviors of the samples [116].

Table 2.3. Surface oxygen groups and their decomposition temperatures [120].

Group	Decomposing Species	Decomposition Temperature (K)
Carboxylic	CO_2	523 - 673
Lactone	CO_2	623 - 923
Phenol	CO	873 - 973
Carbonyl	CO	1073 – 1173
Anhydride	CO + CO_2	623 – 873
Ether	CO	973
Quinone	CO	973 - 1253

Although TPD is the most common method used for the identification and quantification of the surface oxygen groups formed on the activated carbon surface upon oxidative treatments, additional methods such as FTIR/DRIFTS are widely used. Identification of surface groups is possible with transmission/absorbance curves; Table 2.4 presents a brief review of the peak assignments for the functional surface groups formed on activated carbon samples.

2.3.2. Carbon Dioxide Adsorption on Activated Carbon

Discharge of carbon dioxide to the atmosphere in large quantities as a result of consumption of fossil fuels has become one of the most important environmental issues [135, 136]. In order to break the direct link between energy production and GHG emissions, new technological solutions, either in energy production and/or GHG capture and sequesteration need to be developed. Among the available CO_2 capture technologies, adsorption is considered as one of the most promising ones in the commercial and industrial applications because of the low energy requirement, cost advantage, and ease of applicability over a relatively wide range of temperatures and pressures [127, 137]. CO_2 adsorption at different temperatures (e.g. 25 or 0°C) has been used since 1964 [138]. However, the success of this approach is dependent on the development of adsorbents which should have the following properties: (1) high selectivity and adsorption capacity for carbon dioxide at different temperatures; (2) adequate adsorption/desorption kinetics for carbon dioxide at operating conditions; (3) stable adsorption capacity of carbon dioxide

after repeated adsorption/desorption cycles; (4) adequate mechanical strength of adsorbent particles after cyclic exposure to high pressure streams [137, 139].

Table 2.4. Reported infrared assignments for surface oxygen groups of activated carbons.

Assignment	**Reference**
O-H str. vib. in free O–H	3594 [122]
O-H str. vib. in hydroxyl, carboxylic acids and phenolic groups	3620-2500 [120], 3600-3200 [123], 3500-3100 [124], 3495 [125], 3429 [126], 3417 [126], 3400 [116, 127], 3400-2400 [128], 3300 [129], 3212 [122]
C-H str. vib. in formates, methyls and methylenes	3000-2700 [127], 2960 [123], 2950 [125], 2920 [123], 2900 [128], 2880 [125], 2850 [123]
C=O str. vib. in ketone groups	2300 [126, 130], 1732 [122], 1695 [122], 1670-1660 [131], 1657 [122], 1631 [122], 1612 [122], 1719 [116]
C=O str. vib. in carboxylic anhydride, carboxylic carbonate and lactone groups	1790-1675 [120], 1787 [132], 1780 [129], 1750-1630 [127], 1750 [133], 1745 [125], 1740 [131], 1730 [124], 1729 [126], 1724 [131], 1720 [130, 134], 1710-1680 [131], 1710 [128], 1700 [123], 1680 [134], 1660 [116]
C=C str. vib. in aromatic rings of quinones and ceto-enols	1680-1550 [120], 1620 [126], 1600 [133], 1590 [128], 1580 [130]
C=C str. vib. in aromatic rings	1640-1430 [125], 1603 [129], 1600-1585 [120], 1600-1450 [127], 1600-1400 [131], 1585 [122], 1583 [134], 1580 [107, 124], 1570 [122], 1559 [122]
C-O str. vib. in carboxylic anhydrides, phenols, ethers and lactones	1500-1100 [120], 1450-1100 [124], 1300-1120 [124], 1300-1000 [116, 120], 1275 [129], 1264 [131], 1260 [125], 1250 [116, 133], 1250-1235 [131], 1220-1000 [120], 1200 [130], 1200-1180 [123], 1175 [116], 1162-1114 [131], 1125 [116],
C-H out-of plane bending vibration in aromatic rings	890 [123], 875 [132], 874 [134], 820 [123], 817 [125, 134], 802 [132], 760 [123], 757 [134]

It is well known that CO_2 is strongly adsorbed at room temperatures on microporous solids having pores with diameters close to or exceeding the diameter of adsorbate by a factor of 2 to 5, such as activated carbons (ACs) and zeolites [139, 140]. The activated carbons are often preferred over zeolites because of their relatively moderate strengths of adsorption for gases, which facilitate the desorption process, resulting in robustness in cyclic operations [141]. Moreover, they do not require any moisture removal; they present a high CO_2 adsorption capacity at ambient pressure [142].

In the chemisorption reaction, a gas phase CO_2 molecule chemisorbs on an active site of activated carbon, C_s, to produce a surface carbon-oxygen complex, $C(CO_2)$ [Eq (2.11.)]. The CO_2 chemisorption reaction becomes complicated by the heterogeneity and the structural complexity of the carbonaceous surface [143, 144].

$$CO_2\ (g) + C_s \leftrightarrow C(CO_2) \qquad (2.11)$$

The large adsorption capacity of AC is stemmed from the well-developed internal pore structure, large surface area and the surface functional groups [143]. As discussed above, physical and surface chemical properties of ACs can be modified via several different oxidation procedures, heat treatments and/or impregnation procedures; during those treatments, the types and amounts of oxygen and nitrogen-bearing surface groups, which play an important role in the adsorption behaviors of the ACs, are changed [142, 145, 146].

Pellerano et. al. [147] have compared the CO_2 adsorption properties of four different activated carbon and two zeolite samples. Activated carbon samples have reported to exhibit higher CO_2 adsorption performance than the zeolite samples on mass basis at 25°C between 2-8 bars. In that study, ACs were reported to be easier to regenerate; the adsorption capacity of the samples remained the same even after the 15^{th} cycle, whereas the zeolites have lost 40% of their adsorption capacity after the 3^{rd} cycle [147].

Similarly, Himeno et. al. [148] have compared the CO_2 adsorption capacities of five commercial activated carbon samples which predominantly have micropores. They obtained CO_2 adsorption isotherms for the samples at 0, 25 and 50°C under pressures up to

6 MPa. They concluded that the order of the adsorption capacity of activated carbons was almost the same as the order of the BET surface area and pore volume. The authors used Toth equation [Eq (2.13)] and Dubinin-Astakhov model [Eq (2.14)-(2.15)] to correlate their experimental adsorption data. They also reported the Henry's law constant determined from the Toth equation as a measure of adsorption affinity and isosteric enthalpy of adsorption calculated by the Clasius-Clapeyron equation [Eq (2.12)]:

$$\frac{\Delta H}{RT^2} = -\left[\frac{\partial lnP}{\partial T}\right]_N \tag{2.12}$$

where ΔH is the isosteric enthalpy of adsorption, P is the pressure and T is the temperature. The value of the isosteric enthalpy of adsorption at low surface coverage is inversely related to the pore size of the adsorbent [148].

Toth equation can be represented by

$$N = \frac{mP}{(b+P^t)^{1/t}} \tag{2.13}$$

where N is the amount adsorbed, m is the saturated amount adsorbed, P is the equilibrium pressure, b is the equilibrium constant, and t is the parameter that indicates the heterogeneity of the adsorbent. The Toth model is commonly used for activated carbons due to both its simplicity and the fact that it reflects the correct adsorption behavior at both low and high pressures. The Dubinin-Astakhov equation can be written as

$$W = W_0 exp\left[-\left(\frac{A_p}{E}\right)^n\right] \tag{2.14}$$

where W is the volume adsorbed, W_0 is the limiting micropore volume, E is the characteristic energy of the system, n is the heterogeneity parameter, and A is the adsorption potential. The adsorption potential A is given by

$$A_p = RTln\left(\frac{P_s}{P}\right) \tag{2.15}$$

where R is the universal gas constant, T is the equilibrium temperature, and P_s is the saturation pressure. Dubinin-Astakhov model applies to the adsorption equilibria of several vapors and gasses including CO_2 on microporous activated carbons. For a large variety of microporous carbons such as activated carbons, the adsorption data can be fitted to Equation (2.12) with exponent n=2, which corresponds to Dubinin-Radushkevich equation (D-R) [Eq (2.16)] over a wide range of relative pressures [149]:

$$W = W_0 exp\left[-\left(\frac{A}{E}\right)^2\right] \tag{2.16}$$

In another study, An and his coworkers [150] have reported to reach 4.5 mmol/g CO_2 adsorption capacity at 0 °C and atmospheric pressure for an activated carbon they derived from carbon fibre-phenolic resin composites.

Due to acidic character of CO_2, introduction of Lewis bases onto the AC surfaces may favor the CO_2 sorption performance. General ways used for the preparation of AC with increased surface basicity are to remove/neutralize the acidic surface groups and to replace acidic groups with proper basic ones [142]. It has been shown that the surface basicity of the ACs can be increased by heat treatment with gaseous or aqueous ammonia, leading to a higher amount of nitrogen-bearing surface groups which result in higher CO_2 adsorption capacity [115, 132, 137, 142, 146, 149, 151, 152]. As an example, Pevida et. al. [146] claimed that the basic character of two commercial activated carbons was increased through the use of heat-treatments with ammonia at different temperatures, in the 200-800°C range. At room temperature under atmospheric pressure, the CO_2 adsorption capacity of an activated carbon was increased from 7 wt% to 8.4 wt% with ammonia treatment. CO_2 adsorption capacities of 9.6 and 3.2 wt% were reported for a sample, which was ammonia heat-treated at 800°C, for 25 and 75°C, respectively, under atmospheric pressure [146].

The introduction of alkali metal or alkaline earth metals on the surface of an adsorbent also creates basic sites [135]. It is well known that as the ratio of electric charges to the radius of the metal ion increases, the basicity of a metal oxide decreases [135]. Slurry and solution impregnation techniques are widely used to modify surface chemistry

of ACs though pore blockage and decreased surface area are common problems reported [146]. Somy et al. [153] reported a 20% increase in CO_2 adsorption capacity upon impregnation of Cr_2O and zinc carbonate on ACs under 30-110 kPa CO_2 pressure at room temperature. They also observed that washing the impregnated samples with metal oxide resulted in 15% increase in CO_2 adsorption capacity and that the increase in the adsorption capacity was significant when the impregnation temperature was decreased from 95 to 25°C. Yong and his coworkers have developed 0.28 and 0.22 mmol/g carbon dioxide adsorption capacity for magnesium oxide and calcium oxide impregnated carbon-based adsorbents at 300ºC [139]. The activation procedures of carbons with NaOH, KOH and Na_2CO_3 have been investigated by Lillo-Rodenas et. al [154]. They followed the chemical reactions occurring during heat treatments up to 730°C with Fourier transform infrared spectroscopy and temperature programmed desorption. They concluded that the use of Na_2CO_3 should be avoided since no porosity development occurred in the presence of carbonate. However, CO_2 capture capacity increase was reported to be markedly higher for the Na_2CO_3-treated zeolite samples, in spite of the lower surface area, lower crystallinity and higher Si/Al ratio of the NaOH-treated material [155].

Guo et. al. [156] have investigated the CO_2 adsorption properties of modified activated carbon samples at four different temperatures (30, 40, 50 and 60°C) under a pressure of 0-40000 Pa and compared them to those of a commercial activated carbon. In order to modify the samples, they used i) 4% KOH solution, ii) a mixture of ethylenediamide and ethanol and iii) a mixture of 4% KOH, ethylenediamide and ethanol. The adsorption data were fit to Dubinin-Radushkevich and Freundlich isotherms. The isosteric heat of adsorption of the adsorbents was derived from isotherm equations. The authors concluded that the physical properties, surface area, pore volume and micropore volume of activated carbon samples had no influence on the amount of CO_2 adsorbed. However, the active ingredients impregnated on the samples were found to have significant influence; the CO_2 amount adsorbed on the modified samples were nearly 1.7-1.9 times the amount adsorbed on the nonmodified one. The sample which was impregnated with a mixture of 4% KOH, ethylenediamide and ethanol had the highest adsorption capacity especially at lower temperatures.

There are a few studies in literature covering the adsorption of carbon dioxide on chemically modified carbon-based adsorbents at high temperature. As an example to those studies, Yong et. al. [135] have investigated the adsorption capacity of CO_2 on a high surface area commercial activated carbon before and after chemical modification with MgO and S-CaO-MgO. The CO_2 adsorption capacities of MgO and S-CaO-MgO impregnated samples were reported to be 0.28 and 0.22 mmol/g at 300°C and 1 bar, respectively. Song and Lee [157] have reported that 1.2 and 0.7 μmol/m^2 CO_2 was adsorbed on calcium oxide modified activated carbons at 100 and 250°C, respectively. The adsorbed amounts of CO_2 for the nonmodified activated carbon were 0.8 and 0.16 μmol/m^2. The authors claimed that calcium oxide modified activated carbons could be used for separation of CO_2 directly from effluent gas due to their adsorption capacity at high temperatures.

3. EXPERIMENTAL WORK

3.1. Materials

3.1.1. Chemicals

The chemicals used for catalyst and adsorbent preparation are listed in Table 3.1. All chemicals used are research grade.

Table 3.1. Chemicals used in catalyst and adsorbent preparation.

Chemicals	**Formula**	**Source**	**Molecular Weight (g/mole)**
Activated Carbon (ROX 0.8)	C	NORIT	12
Ammonium carbonate	$CH_6N_2O_2.CH_5NO_3$	Merck	157.13
Ammonium perrhenate	NH_4ReO_4	Merck	268.24
Cerium(III) nitrate hexahydrate	$Ce(NO_3)_3.6H_2O$	Merck	434.23
Gamma alumina	γ-Al_2O_3	Alcoa	101.96
Hydrochloric acid	HCl	Merck	36.40
Nickel (II) nitrate hexahydrate	$Ni(NO_3)_2.6H_2O$	Merck	290.81
Nitric acid	HNO_3	Merck	63
Sodium carbonate	Na_2CO_3	Merck	105.99
Tetraammineplatinum (II) nitrate	$Pt(NH_3)_4(NO_3)_2$	Aldrich	387.22
Tetrachloroauric (IV) acid trihydrate	$AuCl_4H.3H_2O$	Aldrich	393.83
Tin (IV) chloride	$SnCl_4.5H_2O$	Riedel - de Haën	350.5

3.1.2. Gases

All of the gases used in this research were supplied by the Linde Group. Table 3.2. and Table 3.3 list the specifications and applications of the liquids and gases employed in this research.

Table 3.2. Specifications and applications of the liquids used.

Liquid	**Specification**	**Application**
Nitrogen	HABAŞ	BET cold trap FT-IR detector
Water	De-ionized	Aqueous solution Reactant

Table 3.3. Specifications and applications of the gases used.

Gas/Standard	**Specification**	**Application**
Argon	99.998%	Inert, GC Carrier Gas
Carbon dioxide	99.995 %	GC calibration, Reactant, Adsorbate
Carbon monoxide	99.999 %	GC calibration, Reactant, Adsorbate
Dry air	99.998 %	Calcination, GC 6-way pneumatic valve
Helium	99.999 %	Inert, GC Carrier Gas, BET
Nitrogen	99.998 %	Inert, BET, Air treatment
Oxygen	99.998 %	Reactant
Methane	99.5 %	GC calibration

3.2. Experimental Systems

The experimental systems used can be divided into five groups:

- Catalyst/Adsorbent Preparation Systems: The set-ups used for incipient-to-wetness impregnation and deposition precipitation techniques; the set-ups used for adsorbent preparation and modification are also involved in this group of experimental systems.

- Catalyst Characterization Systems: This group involves eight different analytical and spectroscopic techniques and the systems used to characterize the physical, microstructural and electronic properties of the catalyst samples prepared and to examine the changes during and/or after reaction.

- Catalytic Reaction System: This continuous flow microreactor system includes gas and liquid flow control, temperature controlled transfer lines, gas/liquid mixing, temperature controlled reaction chamber, and feed and product sampling sections. This system is used for determining the catalytic activity, selectivity and stability.

- Product Analysis System: The quantitative determination of the composition of the species, both in the reactor effluent and feed stream, is conducted by two gas chromatographs that are connected on-line to the microreactor flow system.

3.2.1. Catalyst and Adsorbent Preparation Systems

The system used for preparing catalysts by incipient-to-wetness impregnation technique (Figure 3.1) includes a Retsch UR1 ultrasonic mixer, a vacuum pump, a Büchner flask and a MasterFlex computerized-drive peristaltic pump. This system was also used for adsorbent modification. The system used for deposition precipitation method (Figure 3.2) includes a Julabo water bath, a 400 ml beaker, a Heidolph impeller and a Mettler Toledo pH-meter.

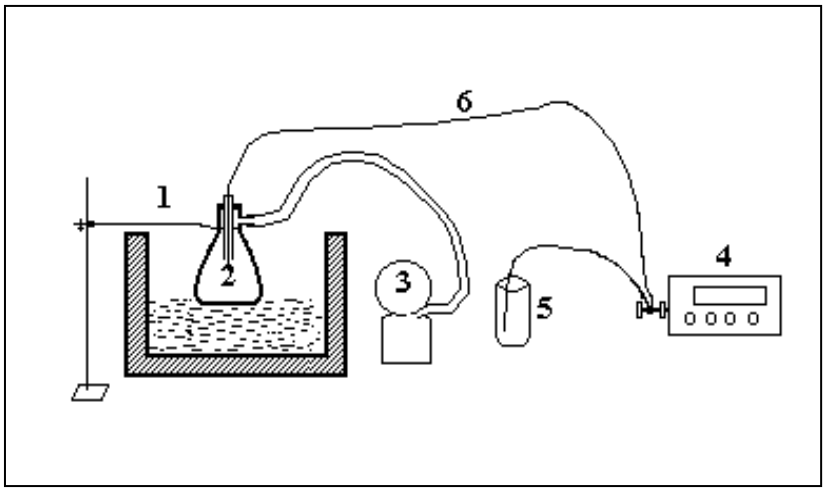

Figure 3.1. Schematic diagram of the impregnation system [158]. (1. Ultrasonic mixer, 2. Büchner flask, 3. Vacuum pump, 4. Peristaltic pump, 5. Reactant storage tank, 6. Silicone tubing).

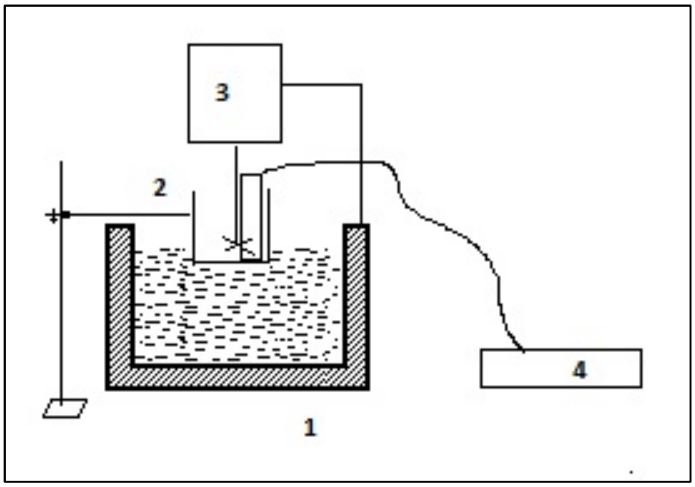

Figure 3.2. Schematic diagram of the deposition precipitation system. (1. Water bath, 2. Beaker, 3. Impeller, 4. pH-meter).

The adsorbent preparation system which was used for HCl and HNO_3 treatments of activated carbons consists of an Electro-mag heating mantle, a Nüve MK 318 mixer, a soxhlet appatus and a round bottom flask and a 2 Lt beaker. The air treatment of the activated carbon samples were employed in a Lenton furnace equipped with a Eurotherm

controller; the nitrogen and dry air gasses were supplied by gas regulators and Aalborg mass flow controllers.

3.2.2. Catalyst Characterization Systems

3.2.2.1. Total Surface Area. The total surface area of the adsorbents and supports were measured on a Micromeritics Flowsorb II 2300 constant pressure dynamic apparatus (Figure 3.3) by N_2 adsorption from N_2-He mixtures at liquid nitrogen temperature using a multi-point technique and the Brunauer-Emmett-Teller (BET) equation [Eq.(3.1)-(3.2)].

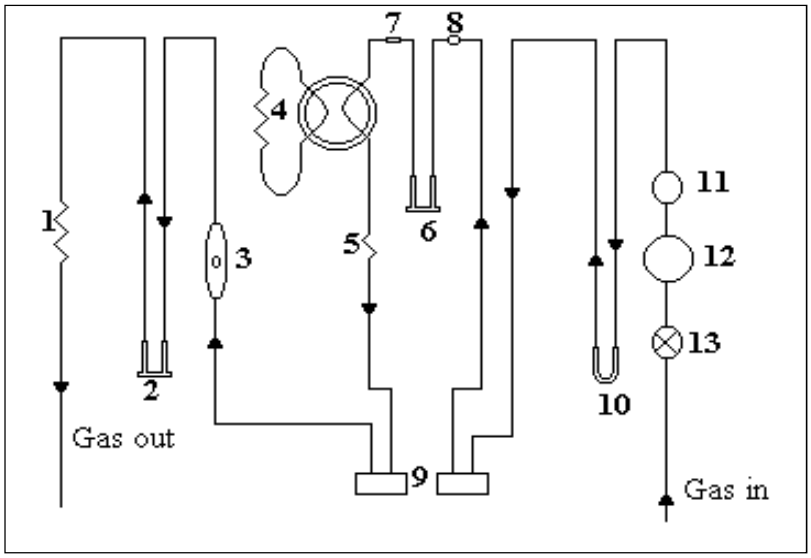

Figure 3.3. Schematic diagram of the BET equipment [158]. (1.Back diffusion restrictor 2.Degas 3.Flowmeter 4.Long Path 5.Short Path 6.Test Sample 7.Filter 8.Septum 9.Thermal conductivity cells 10.Cold trap 11.Adjustment valve 12.Flow controller 13.On-off valve).

The BET equation can be written as

$$\frac{1}{v[(P_0/P)-1]} = \frac{c-1}{v_m C}\left(\frac{P}{P_0}\right) + \frac{1}{v_m c} \qquad (3.1)$$

where P and P_0 are the equilibrium and saturation pressure of adsorbates/supports at the temperature of adsorption, υ is the adsorbed gas quantity, and υ_m is the monolayer adsorbed gas quantity. The BET constant, c, can be expressed as

$$c = exp\left(\frac{E_1 - E_L}{RT}\right) \quad (3.2)$$

where E_1 is the heat of adsorption for the first layer and E_L is that for the second and higher layers, R is the universal gas constant and T is the adsorption temperature.

3.2.2.2. Scanning Electron Microscopy (SEM). Micrographs of the fresh and reduced catalyst samples as well as the adsorbents were taken using an environmental scanning electronic microscope (ESEM), to observe the morphology differences. X-ray analytical mapping and Energy Dispersive X-Ray Spectroscopy (EDS) tests were also conducted on catalyst/adsorbent samples in order to clarify their elemental analysis and to obtain information on the dispersion of the metals on the catalyst surface. The tests were conducted in a Philips XL 30 ESEM-FEG system, having a maximum resolution of 2 nm. Apart from the secondary electron (SE) images obtained at high resolution for all samples studied, back-scattered electron (BSE) images were also obtained for modified activated carbon adsorbents in order to provide better information about the distribution of Na species. The experiments were performed at the Advanced Technologies Research and Development Center of Boğaziçi University.

3.2.2.3. High Resolution Transmission Electron Microscopy (HR-TEM). To obtain information on the surface morphology variation of the reduced catalyst samples, HR-TEM analyses were carried out using JEOL 2100 LaB_6 HRTEM operating at 200 kV. The analyses were performed at the Institute of Materials at TUBITAK-MAM.

3.2.2.4. X-Ray Diffraction (XRD). The crystalline phases of the catalyst samples and their particle sizes were identified by using a Rigaku D/MAX-Ultima+/PC X-Ray diffraction equipment having an X-ray generator with Cu target and scan speed of 2º/min. The experiments were performed at the Advanced Technologies Research and Development Center of Boğaziçi University.

3.2.2.5. X-Ray Photoelectron Spectroscopy (XPS). The extent of electronic interaction between metal components of the freshly reduced samples as well as the oxidation states of the metallic species present on the fresh and used samples was investigated through determination the amounts of metallic phases by X-ray photoelectron spectroscopy (XPS).

The tests were performed at the Middle East Technical University Central Laboratory using SPECS spectrometer equipped with a hemispherical electron analyzer and Al-K_α 282 W dual X-ray source.

3.2.2.6. Fourier Transform Infrared Spectroscopy. The FTIR transmittance/ absorbance spectra have been collected on a Bruker Vertex 70V equipped with a MCT detector. PIKE Technologies DRIFTS cell with ZnSe window with PIKE Technologies temperature controller and Brooks mass flow controllers allowed thermal treatments under controlled atmospheres and spectrum scanning at controlled temperatures (25-400°C) (Figures 3.4 and 3.5).

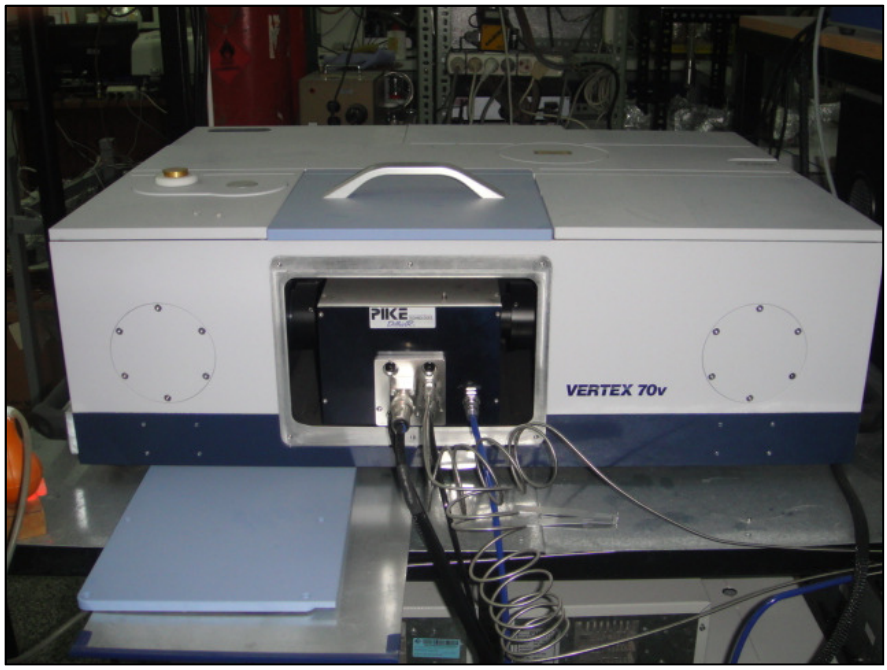

Figure 3.4. Photograph of the DRIFTS cell.

The feed section was composed of mass flow control systems, 1/4", 1/8" and 1/16" stainless steel tubing and fittings for feeding gaseous species, i.e. carbon monoxide, carbon dioxide, oxygen, helium, argon and hydrogen (see Table 3.3 for specifications). The high purity gases were supplied by pressurized cylinders and were passed through the gas flow regulators. The flow rates of the gasses were controlled by Brooks Instrument mass flow controllers and the set values of were adjusted by two Brooks Instrument 0154 series control boxes. On-off valves were placed in front of the mass flow controllers to protect

them from possible back-pressure fluctuations. In order to meter the flow of individual species and adjust desired feed ratios, each gas was fed from an independent line.

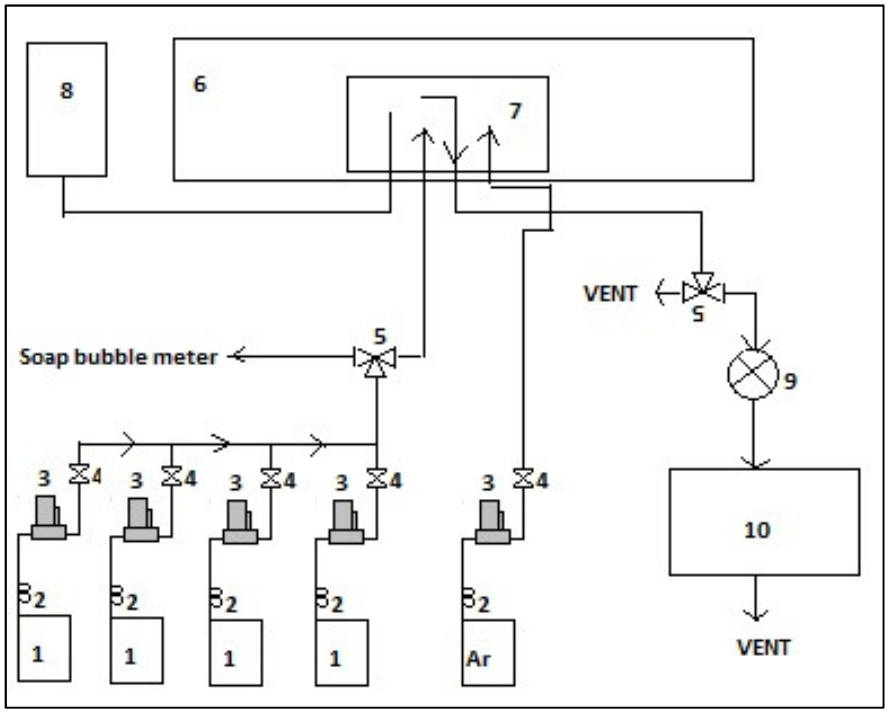

Figure 3.5. Schematic representation of FTIR-DRIFTS-MS System. 1.Gas cylinder, 2. Gas Regulator, 3. Mass flow controller, 4. On-off valve, 5. Three-way valve, 6. FTIR, 7. DRIFTS cell, 8. Heating chamber, 9. Cold trap, 10. MS.

Hiden Analytical HPR 20 QMS Sampling System was used to analyze the concentration of the gasses leaving the DRIFTS cell. The product stream from the DRIFTS cell was allowed to pass through two cold traps since steam in the product stream should be removed prior to the product analysis to avoid any condensation in the mass spectrometer.

3.2.2.7. Intelligent Gravimetric Analyzer (IGA). CO_2 and CO adsorption tests of the adsorbents and PROX catalysts were conducted using IGA system (Hiden Isochema) (Figure 3.6). The adsorption/desorption isotherms were obtained within 0-20000 mbar pressure and 25-200°C temperature ranges. While the static mode of the system was used at atmospheric pressure, the concentration of the gasses leaving the adsorption unit was analyzed by Hiden Analytical Dynamic Sampling Mass Spectrometer (DSMS).

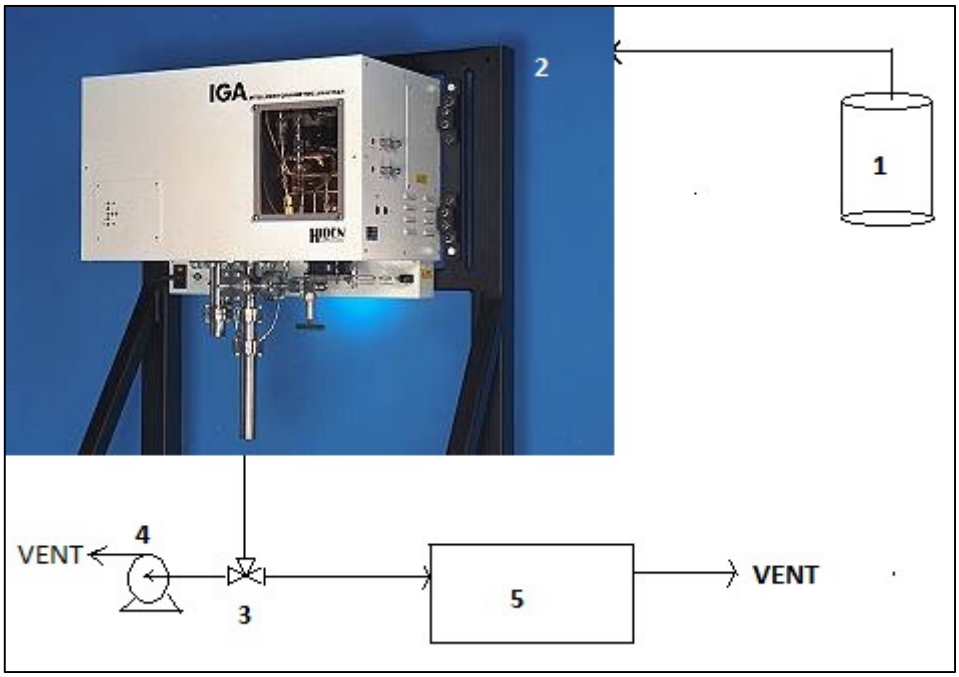

Figure 3.6. Experimental setup for adsorption experiments using IGA: 1. High pressure gas cylinder with high pressure regulator, 2. IGA, 3. Three-way valve, 4. Vacuum pump, 5. DSMS.

3.2.2.8. HSC-Chemistry Software The equilibrium calculations for the water gas shift reaction were conducted using HSC-Chemistry 4.1.; the effect of different reactants and temperature on the product composition was determined.

3.2.3. Catalytic Reaction System for WGS Reaction

The catalytic reaction system (Figure 3.7) was designed and constructed in the Catalysis and Reaction Engineering Laboratory of Chemical Engineering Department, Boğaziçi University and involves three characteristic sections: Feed, reaction and product analysis.

The feed section was composed of mass flow control systems, 1/4", 1/8" and 1/16" stainless steel tubing, valves and fittings for feeding liquid water and gaseous species, i.e. carbon monoxide, carbon dioxide, nitrogen and hydrogen (see Table 3.3 for specifications). The high purity gases were supplied by pressurized cylinders and were passed through the gas flow regulators. The flow rates of the gasses were controlled by

Brooks Instrument mass flow controllers and the set values of were adjusted by the Brooks Instrument 0154 series control box. On-off valves were placed in front of the mass flow controllers to protect them from possible back-pressure fluctuations. In order to meter the flow of individual species and adjust desired feed ratios, each gas was fed from an independent line. It was possible to divert the flow direction of feed gases before entering the reactor through the direction of bypass line by using a three way valve, so that the dry feed composition could be measured using gas chromatographs.

Water was introduced to the system at constant flow rates using an Agilent 1100 series HPLC pump. In order to feed water in the form of steam the 1/16" stainless steel tubing, through which water was allowed to flow, and the line going to reactor after the on-off valve, including the reactant mixing zone, were kept at 130 ± 5 °C using a 1 m Cole-Parmer heating tape, a 16-gauge wire K type sheathed thermocouple and Omron E5AN temperature controller. The heating tape was covered with ceramic wool insulation to prevent heat losses.

The reactants, metered and mixed in the feed section, were allowed to flow through the reaction section. This section was composed of a 45 cm × 20 cm × 20 cm furnace with 2.4 cm ID controlled by a Eurotherm 3216P programmable temperature controller, a K-type sheathed thermocouple and a down-flow, 55 cm long ¼”. OD, stainless steel tubular microreactor. During the reaction tests, the catalyst bed (ca. 0.4 cm) which was stabilized by silane treated glass wool was placed in the center of the reactor. Ceramic glass wool insulations were placed in top and bottom ends of the reactor furnace in order to prevent heat loss and provide a stable temperature profile.

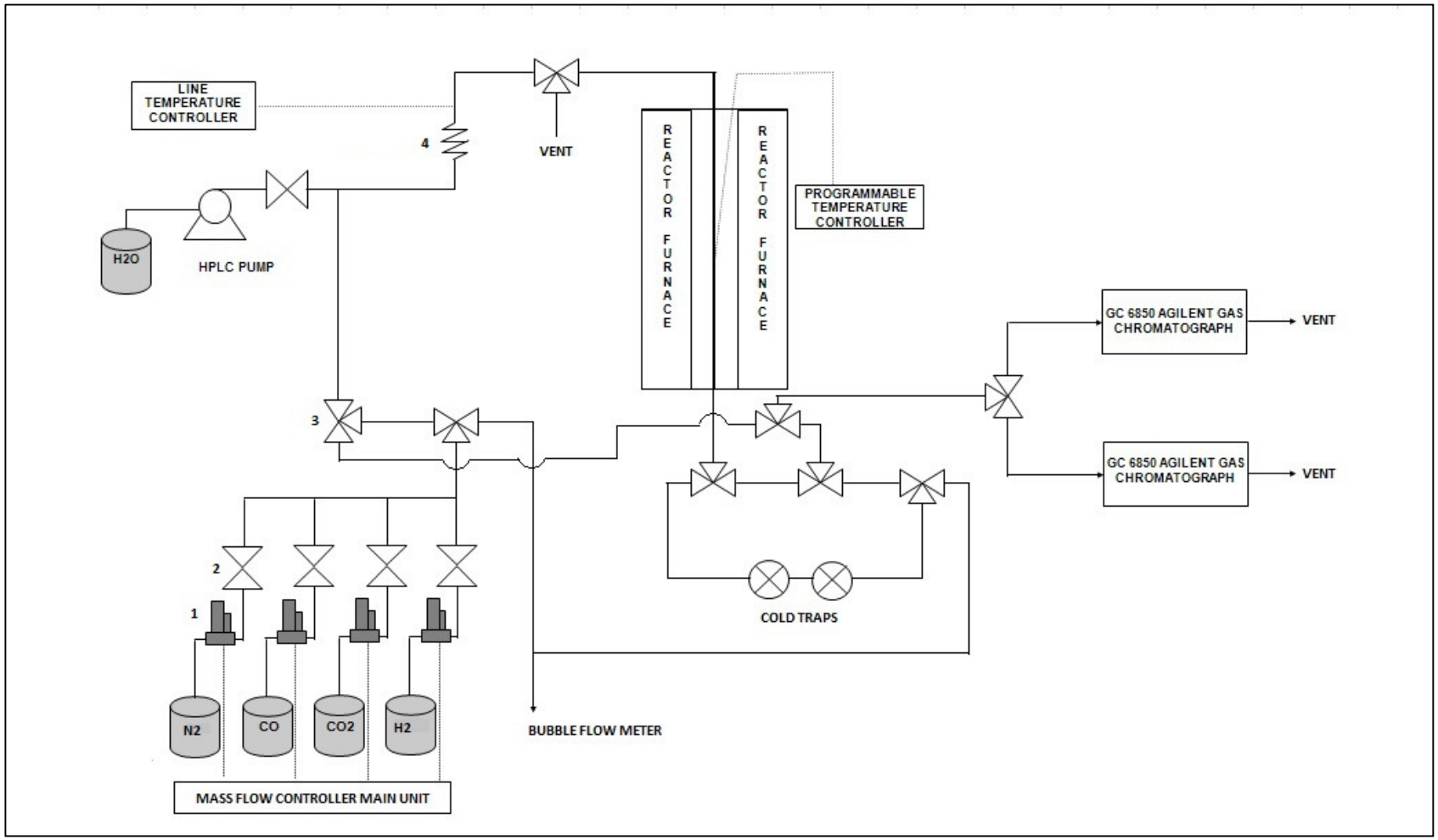

Figure 3.7. Schematic diagram of the microreactor flow system (1. Mass flow controller, 2. On-off valve, 3. Three-way valve, 4. Mixing zone).

Since steam in the product stream should be removed prior to the product analysis to avoid any condensation in the gas chromatograph columns, two cold traps were placed after the reactor. The line between the cold traps and the reactor was kept at 130 ± 5 °C using a 1 m Cole-Parmer heating tape, a 16-gauge wire K type sheathed thermocouple and Omron E5AN temperature controller to avoid the condensation of steam along the stainless steel tubing.

3.2.4. Product Analysis System for WGS Reaction

Two Agilent Technologies 6850 gas chromatographs equipped with Porapak Q and Molecular Sieve 5A columns were used for analyzing feed and dry product streams. 1 h time-on-stream data were used while reporting the catalyst performance. Analysis conditions of the gas chromatographs are given in Table 3.4 below.

Table 3.4. Reactant and product gas analysis conditions.

GC	**Agilent Technologies 6850 – GC1**	**Agilent Technologies 6850 GC2**
Detector type	TCD	TCD
Column temperature, °C	80	80
Inlet Temperature	65	65
Detector Temperature	200	200
Carrier Gas	Helium	Argon
Carrier Gas flow rate, mL/min	20	20
Column packing material	Porapac Q	Molecular Sieve 5A
Column tubing material	Stainless steel	Stainless steel
Column length & ID	2m × 3 mm	2 m × 3 mm
Sample loop	1 ml	1 ml

Before proceeding with the experiments, the gas chromatographs were calibrated by known values of the species to be analyzed under the conditions given in Table 3.4 and by reading the area under the peak calculated by the integrator. Using this procedure,

volume versus peak area curves were constructed for each gas and the corresponding calibration factors were determined by linear regression.

3.3. Catalyst/Adsorbent Preparation and Pretreatment

In this thesis, four sets of catalysts/adsorbents were used:

- Bimetallic Pt-Ni/Al_2O_3 catalysts
- Bimetallic Au-Re/CeO_2 catalysts
- Bimetallic Pt-Sn/AC3 catalysts
- Modified AC adsorbents

The preparation procedure of each catalyst/adsorbent sample is explained in detail below. In order to obtain high catalytic activities, a pretreatment involving the reduction of the active metals from their oxide state –which was formed while calcinations- to their metallic state was required prior to the reaction, since catalysts in their oxide forms are usually inactive for the reactions.

3.3.1. Preparation and Pretreatment of Pt-Ni/Al_2O_3

γ-Al_2O_3 is a high surface area support material. However it is reported to have low stability at temperatures higher than 600°C and tends to facilitate carbon formation in the presence of steam due to its high acidity. The most thermally stable version of alumina is obtained when γ-phase is transformed into α-phase at temperatures greater than 1100 °C. However, its low surface area, which is less than 5 m^2 g^{-1}, is likely to end up with poor catalytic activities due to the low dispersion of active metals. Hence using a support such as δ-alumina – an intermediate phase between γ and α - having relatively high thermal stability and an acceptable surface area can be optimum in terms of obtaining an efficient catalytic performance [159, 160].

The support preparation procedure used in this study involved crushing and sieving γ-Al_2O_3 into 250-354 μm (45-60 mesh) particle size and drying of γ-Al_2O_3 at 200

°C for 2 h. followed by calcinations at 900 °C for 4 h in a muffle furnace. BET surface area of the δ-Al_2O_3 support obtained was found as 81.6 m^2g^{-1} [161].

The bimetallic Pt-Ni/δ-Al_2O_3 catalyst was prepared through a sequential route, in which Pt precursor solution was impregnated over initially prepared and calcined Ni/δ-Al_2O_3 catalyst. Ni/δ-Al_2O_3 catalyst was prepared by the incipient-to-wetness impregnation technique using aqueous solution of $Ni(NO_3)_2.6H_2O$. The aqueous solution were prepared by dissolving the calculated amount of the precursor salt in definite amount of distilled water (ca. 1 ml solution/g support). The support, δ-Al_2O_3, was placed in a Büchner erlen and mixed ultrasonically for 25 min. under vacuum. The aqueous solution was then impregnated through dropwise addition on the support via a peristaltic pump. The resulting slurry, which was formed after ultrasonic mixing of the aqueous solutions and the support under vacuum for 1.5 h, was then dried overnight at 115 °C and calcined at 600 °C for 4 h to obtain (NiO/δ-Al_2O_3). The aqueous Pt solution was then added to NiO/δ-Al_2O_3 and mixed ultrasonically under vacuum for 1.5 h. The resulting slurry involving two metals was dried overnight at 115°C and finally calcined at 500°C for 4 h. Table 3.5 represents the Pt-Ni/δ-Al_2O_3 catalysts studied.

Table 3.5. List of Pt-Ni/Al_2O_3 bimetallic catalysts.

Denoted as	**Pt wt.%**	**Ni wt.%**	**Preparation method**
0.2Pt-5Ni	0.2	5	Sequential Impregnation
0.2Pt-10Ni	0.2	10	Sequential Impregnation
0.2Pt-15Ni	0.2	15	Sequential Impregnation

TPR studies have shown that reduction using pure hydrogen flow at 500°C for 4 h is a suitable procedure for pretreating the bimetallic catalyst [159]. Preliminary tests have shown that reduction under 50 ml/min pure hydrogen flow for 2 h was the optimum reduction procedure for Pt-Ni/δ-Al_2O_3 bimetallic catalysts to be tested for WGS performances. The reduction of catalysts involves placing the calcined catalyst into the constant temperature zone of the microreactor, through which N_2 was allowed to flow at 50 ml/min and the heating of the catalyst bed from room temperature to 500°C at a rate of 7.5°C/min. At 500°C, the gas flow was switched from N_2 to H_2 and the latter was set to

flow at 50 ml/min. The temperature was kept constant at 500°C for 2 h. After reduction, the system was allowed to cool down to the reaction temperature under 50 ml/min N_2 flow.

3.3.2. Preparation and Pretreatment of Au-Re/CeO_2

Ceria support was prepared by homogeneous precipitation of cerium nitrate using Na_2CO_3. Ca. 20 g of cerium (III) nitrate hexahydrate was mixed with 100 ml of deionized (DI) water. The pH of the solution was adjusted to 8 with the controlled addition of aqueous Na_2CO_3 solution. The resulting suspension was allowed to mix for 1 h in a water bath at 60°C under controlled temperature and pH. It was then filtered by using Watman filter paper and washed with deionized water a couple of times. It was then dried overnight at 105˚C and calcined in a muffle furnace at 400˚C for 4 h.

Au/Ceria catalysts were prepared by the dp technique, which was carried out under fully controlled pH, stirring speed and temperature. Ceria support was suspended in DI water at a pH of 8.0-8.5. The pH was adjusted by adding aqueous ammonium carbonate solution. Subsequently, the desired amount of tetrachloro auric (IV) acid was added dropwise under vigorous stirring and then the precipitate was aged for 1 h, filtered and washed with DI water at 65˚C. The filtrate was then dried overnight at 75˚C under vacuum and calcined at air in a muffle furnace at 400˚C for 4 h.

Re addition to all catalysts were conducted via incipient-to-wetness impregnation technique using aqueous solution of ammonium perrhenate (using ca. 2 ml DI water/g ceria support). The ceria support was placed in a Büchner erlen and mixed ultrasonically for 25 min. under vacuum. The aqueous solution was then impregnated on the support via a peristaltic pump. The resulting slurry, which was formed after ultrasonic mixing of the aqueous solutions and the support under vacuum for 1.5 h, was then dried overnight at 115˚C and calcined at 400˚C for 4 h. Sequential impregnation was also employed for a catalyst sample by first adding gold, using appropriate solutions of tetrachloroauric (IV) acid trihydrate and ammonium perrhenate solutions for gold and rhenium additions, respectively. The preparation methods of all catalysts tested for WGS activity are given in the text in brackets next to the catalyst as impregnation (imp), sequential impregnation

(si) and deposition precipitation (dp). For example, 1%Au-0.5%Re/Ceria (imp+dp) implies first the impregnation of Re on to ceria support and then the deposition precipitation of gold. Table 3.6 represents the Pt-Ni/δ-Al_2O_3 catalysts studied. Among the Au-Re bimetallic catalysts prepared, only for the (dp+imp) catalyst, consecutive calcinations were applied upon gold precipitation and rhenium impregnation steps. On the other hand, only one calcination step upon dp was applied to (imp+dp) and (si) catalysts.

Table 3.6. List of Au-Re/Ceria bimetallic catalysts.

Denoted as	**Au wt.%**	**Re wt.%**	**Preparation method**
1Au-0.5Re/Ceria (imp+dp)	1	0.5	Impregnation + dp
0.5Au-0.25Re/Ceria (imp+dp)	0.5	0.25	Impregnation + dp
0.5Re-1Au/Ceria (dp+imp)	1	0.5	dp + Impregnation
0.5Re-1Au/Ceria (si)	1	0.5	Sequential Impregnation
1Au/Ceria (dp)	1	-	dp
0.5Re/Ceria (imp)	-	0.5	Impregnation

Preliminary tests have shown that reduction under flow of 5% hydrogen/balance nitrogen mixture for 1 h at 200°C was the optimum reduction procedure for Au monometallic and Au-Re bimetallic catalysts to be tested for WGS performances. After placing the catalyst into the constant temperature zone of the microreactor, N_2 was allowed to flow at 95 $mlmin^{-1}$ and the catalyst bed was heated from room temperature to 200°C at a rate of 7.5°Cmin^{-1}. At 200°C, 5 $mlmin^{-1}$ hydrogen was introduced in addition to nitrogen flow. The temperature was kept constant at 200°C for 1 h. After reduction, the system was allowed to cool down or heat up to the reaction temperature under 95 $mlmin^{-1}$ N_2 flow.

3.3.3. Preparation and Pretreatment of Pt-Sn/AC3

Commercial activated carbon supplied by NORIT was crushed and sieved into 355-250 μm (45-60 mesh) particle size and exposed to different thermal and chemical pretreatments indicated below prior to being used as support:

As the initial step, activated carbon material was treated with 200 ml of 2 N HCl acid solution to remove some ash content and sulfur accompanied with it. This treatment was carried out in a Soxhlet apparatus. Approximately 15 g of commercial activated carbon was placed in an extraction unit held by an extraction thimble. Extraction process was continued under reflux for 12 hours. The slurry was then rinsed with 250 ml DI water and washed again for 6 hours inside the Soxhlet apparatus to remove HCl remaining on the support surface. Finally, the slurry was dried at 115°C overnight. This support is referred to as AC1.

15 g of AC1 was put into a round bottom flask containing 350 ml of 5 N HNO_3 solution. This flask was heated up under total reflux for 3 hours. The suspension was allowed to precipitate through the night. The resulting precipitate was put in a 2 Lt beaker, 1.5 Lt DI water was added and the mixture was boiled for ca. 4 h on a Nüve mixer. The suspension was again allowed to precipitate through the night. The rinsing procedure was repeated 3 times, and then the slurry was dried at 115°C overnight. The obtained support is called AC3.

1wt%Pt-0.25wt%Sn/AC3 catalyst was prepared by sequential impregnation in which Pt solution was impregnated over initially prepared and calcined Sn/AC3 catalyst. Sn/AC3 catalysts were prepared by the incipient-to-wetness impregnation technique using aqueous solution of tin chloride. The aqueous solutions were prepared by dissolving the calculated amount of the precursor salt in definite amounts of distilled water and HCl mixture (ca. 2.1 ml solution/g support). Five grams of AC3 was placed in a Büchner erlen and mixed ultrasonically for 25 min. under vacuum. The aqueous solution was then impregnated on the support via a peristaltic pump. The resulting slurries, which were formed after ultrasonic mixing of the aqueous solutions and the support under vacuum for 1.5 h, were then dried overnight at 115 °C. The aqueous Pt solution prepared using aqueous hexachloroplatinic acid precursor was then added to the monometallic catalyst and mixed ultrasonically under vacuum for 1.5 h. The resulting slurry involving two metals was dried overnight at 115 °C.

The catalysts were calcined *in situ* under He with flow rate of 50 ml/min at 400°C for 2 hours and then reduced by H_2 with flow rate of 50 ml/min at 400°C for 10 hours

prior to the reactions. The reduction was conducted for 10 hours in order to enable the surface stabilization.

3.3.4. Preparation and Pretreatment of Activated Carbon Adsorbents

The activated carbon adsorbents used in this study were prepared by subjecting the commercial sample to different oxidative, alkali and thermal treatments described below.

Commercial activated carbon supplied by NORIT was crushed and sieved into 355-250 μm (45-60 mesh) particle size. As the initial step, activated carbon material was treated with 200 ml of 2 N HCl acid solution to obtain AC1 as described in section 3.3.3.

AC1 was oxidized in a down flow reactor, heating it from room temperature up to 450°C under the flow of 150 ml/min N_2 with 10°C/min heating rate. It was kept at 450°C under the flow of 150 ml/min N_2-50 ml/min dry air mixture for 10 hours and was cooled down to room temperature under the flow of 150 ml/min N_2. This procedure resulted in the second type of AC adsorbent called AC2.

AC1 was subjected to HNO_3 solution as described in section 3.3.3. to obtain AC3.

AC2 was impregnated with 10% Na_2CO_3 solution (ca. 2.1 ml DI/g support) and was subjected to calcination at different temperatures under the flow of 5% O_2–95% N_2 mixture for 2 h. The resulting adsorbents were named as AC4. The calcination temperatures for AC4 samples were 200, 250 and 300 °C.

Similarly, AC3 was impregnated with 10% Na_2CO_3 solution (ca. 2.1 ml DI water/g support) and was subjected to calcination at different temperatures under the flow of 5% O_2–95% N_2 mixture for 2 h. These samples were called as AC5 and the calcination temperatures for these samples were 175, 200 and 250 °C.

All adsorbents (AC1, AC2, AC3, AC4 and AC5) were used as such or were subjected to thermal treatment under 50 ml/min helium flow for 2 h at 400 ºC or 600ºC and

denoted as AC1-400He and AC4-250-600He, etc. The adsorbents used in this study are given in Table 3.7.

Table 3.7. List of activated carbon adsorbents.

Name	Treatment
AC0	NORIT ROX
AC1	HCl washed NORIT ROX
AC2	HCl washed and air oxidized NORIT ROX
AC3	HCl washed and HNO_3 oxidized NORIT ROX
AC4-200	Na_2CO_3 impregnated and calcined (200°C) AC2
AC4-250	Na_2CO_3 impregnated and calcined (250°C) AC2
AC4-300	Na_2CO_3 impregnated and calcined (300°C) AC2
AC5-175	Na_2CO_3 impregnated and calcined (175°C) AC3
AC5-200	Na_2CO_3 impregnated and calcined (200°C) AC3
AC5-250	Na_2CO_3 impregnated and calcined (250°C) AC3

3.4. Catalyst Characterization

3.4.1. Total Surface Area Experiments

Total surface area measurements were performed using the multi-point BET method. The equations used in the total surface area calculations are Equations (3.1) and (3.2) in addition to Equation (3.3) which is given as follows:

$$S = \frac{A v_m A_g}{M} \tag{3.3}$$

where S is the surface area A is the Avogadro's number (6.02×10^{23}), A_g is the area of an individually adsorbed molecule, which is 16.2×10^{-20} m^2 for nitrogen, M is the molar volume of the gas, and υ_m is the monolayer volume. A straight line results for P/P_o values

from about to 0.05 to 0.25 when experimental data are plotted as $1/\upsilon[(P_o/P)-1]$ on the ordinate against P/P_o on the abscissa. Relative pressures within the prescribed range are typically obtained with gas compositions between about 5% and 25% nitrogen and inert helium.

Each sample was first dried and degassed under nitrogen flow for two and a half hours at 523 K and then cooled to room temperature. The Flowsorb 2300 unit was calibrated by injecting one milliliter of nitrogen at ambient conditions, calculating the corresponding volume of gas at standard conditions and setting the instrument to indicate thereafter adsorbed and desorbed gas volumes at standard conditions. Then a flow of the measuring gas (5% to 25% nitrogen/helium mixture) was allowed to pass over the sample at liquid nitrogen temperature of 77.4 K and equilibrate. After the adsorption equilibrium was established as indicated by the threshold indicator, the temperature of the sample was raised to ambient temperature and the amount of nitrogen desorbed was measured by the thermal conductivity detector. This nitrogen adsorption-desorption procedure was repeated at least four times with different nitrogen-helium gas concentrations. The total surface area was calculated by using software supplied by Micromeritics Inc. together with the Flowsorb 2300 unit.

3.4.2. X-Ray Photoelectron Spectroscopy

X-ray photoelectron spectroscopy (XPS) analyses were conducted on reduced monometallic and bimetallic ceria supported catalysts before and after reaction. The tests were performed using SPECS spectrometer equipped with a hemispherical electron analyzer and Al-K_α (h= 1486.56 eV; 1 eV = 1.6302×10^{-19} J) 282 W dual X-ray source. The vacuum in analysis chamber was always $< 1 \times 10^{-9}$ mbar. The spectra were collected at pass energy of 48 eV. The XPS data analysis was performed with the XPSPeak 4.1 program. The intensities were estimated by calculating the integral of each peak, after subtraction of the S-shaped background, and by fitting the curve to a combination of Lorentzian (30%) and Gaussian (70%) lines. All binding energies were referenced to the C 1s line at 284.6 eV, which provided binding energy values with an accuracy of $\pm$ 0.2 eV.

3.4.3. FTIR Spectroscopy Experiments

The FTIR-DRIFTS-MS system described in Section 3.2.2.6 was used for conducting four types of experiments: (i) Experiments for obtaining the transmittance/absorbance spectra of ceria based catalysts, Pt/AC3 and Pt-Sn/AC3 samples, and activated carbon adsorbents under inert atmosphere, (ii) CO adsorption tests for ceria based catalysts, Pt/AC3 and Pt-Sn/AC3 samples, (iii) O_2 adsorption tests for Pt/AC3 and Pt-Sn/AC3 catalysts and (iv) PROX experiments for Pt-Sn/AC3 catalysts.

For the experiments on the ceria supported catalyst samples and ceria support, *in situ* reduction procedure was employed. The sample was put in the DRIFTS cell without any dilution and the chamber is subjected to 5 ml argon flow. The IR spectrum obtained under these conditions was used as background. The mass flow controller system was adjusted to 47.5 ml/min He flow and the temperature of the cell is increased gradually until 200°C, which was the reduction temperature. 5 ml/min hydrogen flow was added to the inlet flow and after 1 h of reduction the cell was allowed to cool down to the room temperature under 47.5 ml/min He flow. CO adsorption experiments were conducted under 3, 10 and 20% CO/He mixture with 50 ml/min total flow. A total of 256 scans were recorded per spectrum over the range 4000-600 cm^{-1} at a resolution of 2 cm^{-1}.

A total of 256 scans were recorded per spectrum over the range 4000-600 cm^{-1} at a resolution of 2 cm^{-1} for Pt/AC3 and Pt-Sn/AC3 catalyst samples. To improve the reflectivity of the samples, the previously calcined and reduced catalysts were diluted with KBr at ratio of KBr:catalyst, 20:1. A spectrum of KBr recorded in 50 ml/min He taken at room temperature served as background. Operando FTIR spectra of Pt-Sn/AC3 and Pt/AC3 catalysts were obtained under PROX reaction conditions which resulted in the highest CO conversion levels (50 ml/min; 1% CO, 1.25% O_2, 60% H_2, balance He) at 135 °C and 110 °C. The DRIFTS cell outlet was connected to a Hiden Analytical Mass Spectrometer to monitor the conversion levels. Transmission experiments such as CO adsorption and O_2 adsorption in which no reactions were involved, were carried out with different compositions of CO (1, 6, 10, 20%) or O_2 (1.25, 6, 10 and 20%) under helium flow. For both experiments, KBr spectrum recorded under inert flow was used as background.

The IR spectra of modified activated carbon adsorbent samples were obtained under 50 ml/min helium flow at room temperature. A total of 64 or 256 scans were recorded per spectrum over the range 4000-600 cm^{-1} at a resolution of 4 cm^{-1}. To improve the reflectivity of the samples, the samples were diluted with KBr at ratio of KBr:sample, 20:1. A spectrum of KBr recorded in He served as background.

3.4.4. Adsorption Experiments

The CO_2 adsorption/desorption isotherms of activated carbon adsorbents as well as the CO and CO_2 adsorption/desorption isotherms of Pt/AC3 and Pt-Sn/AC3 PROX catalyst samples were obtained using the gravimetric system described in Section 3.2.2.7.

The CO_2 adsorption capacities and CO_2 adsorption isotherms of the activated carbon adsorbents were obtained in the range of 0-20 bar. High purity CO_2 gas was connected directly to the analyzer. The adsorption and desorption isotherms of all samples were obtained at room temperature, 120 or 180 and 200ºC. In order to eliminate humidity and trapped gasses, 60-90 mg samples were outgassed at room temperature for 24 h prior to the adsorption runs. In the adsorption tests, CO_2 pressure was increased by 1000 mbar in each step starting from 5×10^{-3} mbar and the equilibrium pressure was assumed to be reached after 20 min. Cyclic adsorption/desorption tests were also performed for some of the adsorbent samples. Some of these tests were conducted to show the effect of temperature on the adsorption/desorption cycles.

Adsorption/desorption isotherms of fresh Pt/AC3 and Pt-Sn/AC3 PROX catalyst samples were obtained in the range of 0-1200 mbar. High purity CO and CO_2 gasses were connected directly to the analyzer. The adsorption and desorption isotherms of all samples were obtained at room temperature, 110ºC, 115ºC, 125ºC and 135ºC. Before adsorption runs 50-100 mg samples were outgassed at room temperature for 24 hours to remove water vapor. CO/CO_2 pressure was increased by 100 mbar in each step starting from 5×10^{-3} mbar and the equilibrium pressure was assumed to be reached after 20 min. For the CO adsorption experiments at lower pressure region (0-200 mbar), 10 mbar increments were used. Evaluating the CO adsorption capacity of the catalyst samples at 110ºC, 115ºC,

125ºC and 135ºC at pressures as low as ca. 25 mbar was possible by using the gravimetric analyzer.

3.5. WGS Reaction Tests

3.5.1. Blank Tests

Blank tests were conducted to ensure that the material of construction, glass wool and the reactor did not interfere with the reaction test outputs. The results indicated that the glass wool and the reactor were inert under the conditions used in the reaction experiments. Catalyst supports (δ-Al_2O_3 and ceria) were also found inert under the conditions studied.

3.5.2. Preliminary Tests

Decreasing (Decreasing Temperature Progression, DTP) and increasing (Increasing Temperature Progression, ITP) reaction temperature programs were followed for selected feed compositions. The reaction was studied at 50°C intervals within the temperature range. For WGS over Pt-Ni/Al_2O_3 catalysts ITP and DTP reaction curves coincided under the conditions studied indicating the usability of the temperature programs. Whereas for WGS over Au-Re/Ceria catalysts, ITP and DTP were found not usable since the two reaction curves belonging to the temperature programs did not coincide. There, each reaction test was performed for a single temperature (and reaction mixture) on freshly reduced samples.

The effect of reduction procedure was investigated for Au/Ceria (dp) catalyst; experiments were designed in order to find the conditions which would lead to increased activity of the metallic particles. A series of tests were performed without any reduction treatment, with reduction at 200 and 400°C under the reduction conditions given in Section 3.3.2. Some preliminary tests were also performed for obtaining the favorable reduction procedure for Re/Ceria and Au-Re/Ceria (imp+dp).

3.5.3. WGS over Pt-Ni/Al_2O_3 Catalysts – Ideal Feed

The water gas shift reaction has been studied over Pt-Ni/Al_2O_3 catalysts at different temperatures and feed compositions. The platinum metal loading was kept fixed as 0.2 wt.% for all samples. The experiments were carried out by using ITP in the temperature range 200-500°C. The reaction was studied at 50°C intervals starting from 200°C within the temperature range. Prior to reaction tests, the catalyst was reduced in 50 ml/min of pure hydrogen flow at 500°C for 2 h. The experiments were designed to investigate the effects of reaction parameters such as temperature, Ni content, steam/carbon monoxide ratio (H_2O/CO), and space velocity on the activity and selectivity of the catalyst in WGS. The reaction conditions are given in the Table 3.8. Experiments were duplicated and, in some cases, triplicated.

Table 3.8. The WGS conditions studied over Pt-Ni/Al_2O_3 catalysts.

#	Ni %	GHSV ($mlg^{-1}h^{-1}$)	H_2O/CO	CO (ml/min)	Total (ml/min)
1	5	120000	10/3	4.5	150
2	10	120000	10/3	4.5	150
3	15	120000	10/3	4.5	150
4	5	120000	2	4.5	150
5	10	120000	2	4.5	150
6	15	120000	2	4.5	150
7	5	60000	10/3	4.5	150
8	15	60000	10/3	4.5	150
9	5	180000	10/3	4.5	150
10	15	180000	10/3	4.5	150

3.5.4. WGS over Pt-Ni/Al_2O_3 Catalysts – Real Feed

The WGS performance of Pt-Ni/Al_2O_3 catalysts with carbon dioxide and hydrogen present in the feed was investigated within the temperature range of 200-450°C for two different feed compositions. The experiments were performed under different real feed conditions presented in Table 3.9 at atmospheric pressure using 75 mg of freshly reduced catalyst with 120000 $mlg^{-1}h^{-1}$ GHSV and balance N_2.

Table 3.9. Real feed compositions of WGS reactions studied over Pt-Ni/Al_2O_3 catalysts.

Feed #	H_2O/CO	CO (%)	H_2O (%)	H_2 (%)	CO_2 (%)
1	2	3.0	6	35.0	7.0
2	3.33	3.0	10.0	35.0	7.0

3.5.5. WGS over Au-Re/Ceria Catalysts - Ideal Feed

The purpose of this part of the study was to design and develop Au-Re bimetallic catalysts supported on ceria for WGS reaction. An effective catalyst assuring high activity and stability was searched through a parametric study using impregnation and deposition precipitation techniques in catalyst preparation. The effects of temperature, Re incorporation, metal addition sequence, GHSV and H_2O/CO ratio on the WGS activity were investigated and compared to those of monometallic Au/Ceria catalysts.

Prior to reaction tests, the catalyst samples were reduced *in situ* under 5% hydrogen/nitrogen flow for 1 h at 200°C. The reaction tests were performed in the temperature range of 200-500°C over freshly reduced catalysts for 3 h time-on-stream (TOS). The various gas feed compositions used are listed in Table 3.10.

Table 3.10. The WGS conditions studied over ceria based catalysts.

Catalyst	**CO (ml/min)**	**H_2O (ml/min)**	**N_2 (ml/min)**	**H_2O/CO**	**GHSV ($mlg^{-1}h^{-1}$)**
1Au/Ceria (dp)	4.5	4.5	141	1	120000
1Au/Ceria (dp)	4.5	9	136.5	2	120000
1Au/Ceria (dp)	4.5	15	130.5	10/3	120000
1Au/Ceria (dp)	4.5	22.5	123	5	120000
1Au/Ceria (dp)	4.5	9	136.5	2	86800
1Au/Ceria (dp)	4.5	9	136.5	2	180000
1Au-0.5Re/Ceria (imp+dp)	4.5	4.5	141	1	120000
1Au-0.5Re/Ceria (imp+dp)	4.5	9	136.5	2	120000
1Au-0.5Re/Ceria (imp+dp)	4.5	22.5	123	5	120000
1Au-0.5Re/Ceria (imp+dp)	4.5	9	136.5	2	180000
0.5Au-0.25Re/Ceria (imp+dp)	4.5	9	136.5	2	120000
0.5Re-1Au/Ceria (dp+imp)	4.5	4.5	141	1	120000
0.5Re-1Au/Ceria (dp+imp)	4.5	9	136.5	2	120000
0.5Re-1Au/Ceria (dp+imp)	4.5	22.5	123	5	120000
1Au-0.5Re/Ceria (si)	4.5	4.5	141	1	120000
1Au-0.5Re/Ceria (si)	4.5	9	136.5	2	120000
1Au-0.5Re/Ceria (si)	4.5	22.5	123	5	120000
1Au-0.5Re/Ceria (si)	4.5	4.5	141	1	180000
0.5Re/Ceria (imp)	4.5	9	136.5	2	120000

3.5.6. WGS over Au-Re/Ceria Catalysts – Real Feed

The WGS performance of the monometallic and bimetallic ceria based catalysts (given in Table 3.10) with carbon dioxide and hydrogen present in the feed was investigated within the temperature range of 250-350°C. Each test was conducted over freshly reduced samples. The experiments were performed under different real feed conditions presented in Table 3.11 at atmospheric pressure using 75 mg of catalyst with

120000 $mlg^{-1}h^{-1}$ GHSV and balance N_2.

Table 3.11. Real feed compositions of WGS reactions studied over ceria based catalysts.

Feed #	**H_2O/CO**	**CO (%)**	**H_2O (%)**	**H_2 (%)**	**CO_2 (%)**
1	16.30	2.1	34.1	23.7	12.3
2	6.73	2.1	14.4	23.7	12.3
3	6.73	4.9	32.7	30.0	10.4
4	5.00	6.7	33.3	50.0	10.0
5	3.33	3.0	10.0	35.0	7.0

4. RESULTS AND DISCUSSION

The results of this study will be presented and discussed in five sections:

- Characterization and water-gas shift reaction studies over bimetallic Pt-Ni/Al_2O_3 catalysts using ideal and real feeds,
- Characterization and water-gas shift reaction studies over ceria supported catalysts using ideal feeds,
- Characterization of ceria based catalysts using FTIR-DRIFTS-MS system and water-gas shift reaction studies using real feed compositions,
- DRIFTS and adsorption studies over highly active preferential oxidation catalyst Pt-Sn/AC3,
- Carbon dioxide adsorption studies over modified activated carbon adsorbents.

4.1. WGS Reaction over Pt-Ni/Al_2O_3 Catalysts

4.1.1. Characterization

The detailed catalyst characterization of Pt-Ni/Al_2O_3 samples has been reported previously [160, 162, 163] point out the changes on the catalyst surface and active metallic sites due to reduction. Those characterization studies have shown that (i) Pt-rich Pt and Ni islands were formed on the catalyst surface where Pt centers are in the very close neighborhood of the Ni sites, as confirmed by SEM/SEM-BCI analyses (Figure 4.1), and (ii) there was no Pt–Ni alloy formation either locally or in the bulk as confirmed by EDS and XRD (Figure 4.2), respectively.

In this study, the crystalline phases were identified and no alloy formation was observed by both XRD and EDS analyses. SEM and EDS studies show that Ni particles almost cover the whole Al_2O_3 surface; the detailed mapping at high magnification (× 100000) showed that Pt-rich Pt and Ni islands are formed on the catalyst surface where Pt centers are located very close to Ni sites.

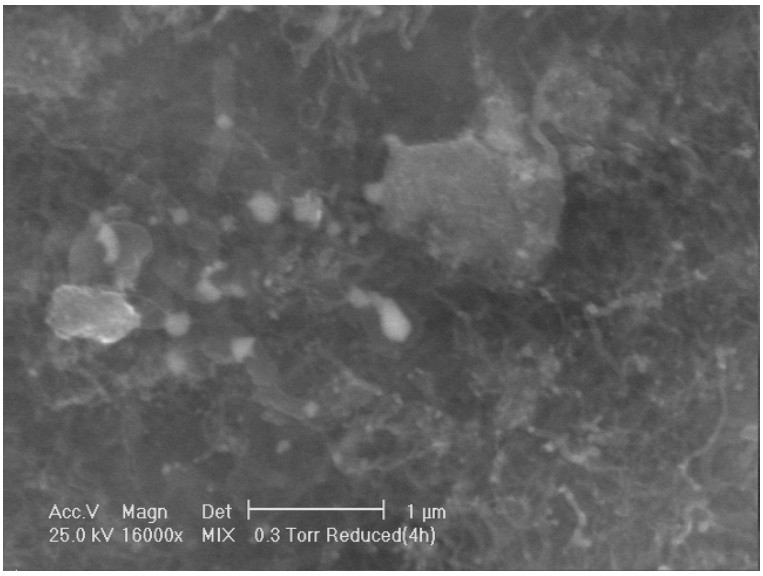

Figure 4.1. SEM micrograph of the reduced 0.2wt%Pt-15wt%Ni/δ-Al_2O_3 catalyst [154].

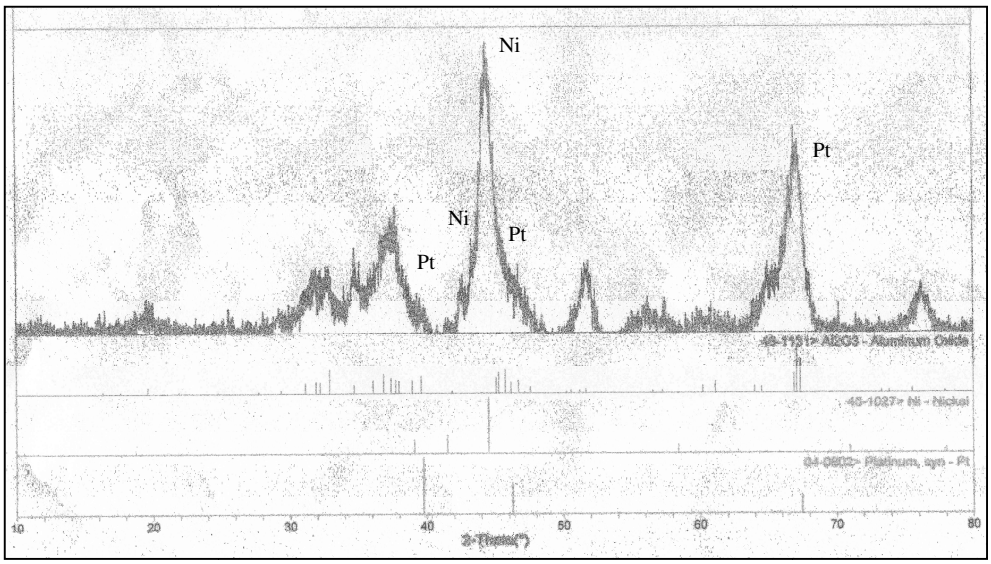

Figure 4.2. XRD pattern of the reduced 0.2wt%Pt-15wt%Ni/δ-Al_2O_3 catalyst [154].

In the X-ray analytical mapping images (Figure 4.3) these Pt and Ni sites are clearly distinguished. As the nickel content is increased from 5% to 10% and to 15% by weight, distinct and bigger Ni islands are formed which makes it possible for more platinum atoms to get into direct contact with Ni atoms. Therefore, it can be easily

assumed that the Pt-Ni interaction is more effective for the samples that have higher Ni contents.

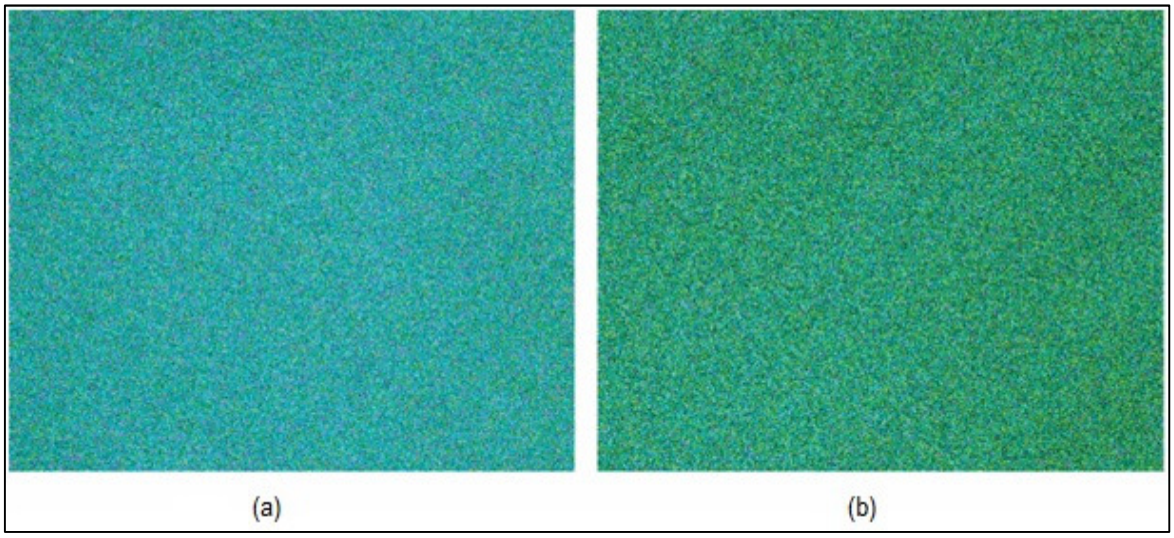

Figure 4.3. X-ray analytical mapping image of 0.2%Pt-5%Ni/Al_2O_3 (a) and 0.2%Pt-15%Ni/Al_2O_3 (b). Al_2O_3: Blue; Ni: Green; Pt: Purple. (Magn: 100000×).

4.1.2. WGS Performance Tests – Ideal Feed

In the present study, the performance test conditions were designed to investigate the effects of the Ni content, GHSV and H_2O/CO ratio on the WGS activity of the bimetallic Pt-Ni/Al_2O_3 catalysts, which were reported to have secondary water gas shift activity in addition to their high activity for autothermal reforming of propane [162] and LPG [163, 164].

Results presented were obtained using an idealized feed composition consisting of 3% CO, 6-10% H_2O and 87-91% inert, resembling a medium temperature range feed composition between the values of low and high temperature shift reactions; since the typical reformate in a fuel processor will contain 8-10% and 3-5% CO for high and low temperatures shifts [44], and H_2O/CO ratio will be 1-3.5 and >3.5 for low and high temperature shifts. Results of catalytic performance tests obtained over bimetallic catalysts with different nickel amounts are shown in Figure 4.4. For each test, the H_2O/CO ratio and GHSV were 10/3 and 120000 ml/g.h, respectively. It is observed that with the increase in

the Ni loading, equilibrium conversions can be reached at lower temperatures. In the literature, there are several factors proposed to be responsible for the enhanced catalytic activity with the addition of metal oxides to high surface area oxide supported noble metal catalysts. These factors are: increased reducibility of the support [22, 165], stabilization of the noble metal crystallites against sintering [22, 166] and formation of new active sites [22, 165, 166]. Therefore, increase in the amount of nickel added may have strengthened one or more of these effects in the current study. Furthermore, Pt crystallites, which are in direct contact with the reducible NiO_x species confirmed by our catalyst characterization studies, are also responsible for the enhancement of activity; as the Ni loading was increased, the Pt-Ni interaction was enhanced.

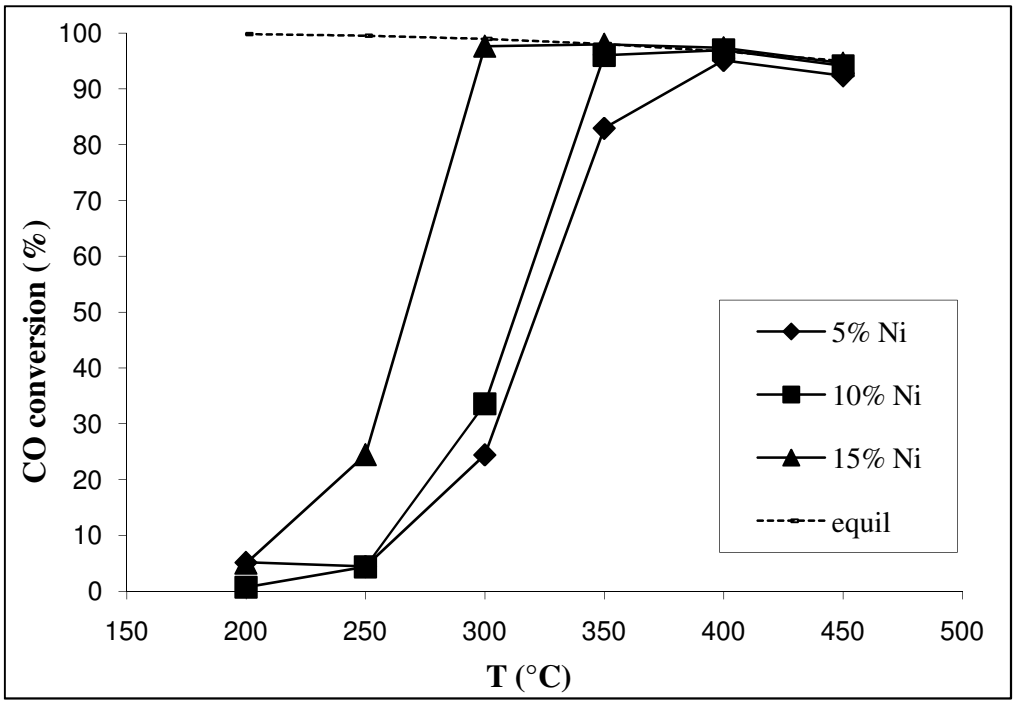

Figure 4.4. Effect of Ni loading of Pt-Ni catalysts on WGS activity profile given as a function of temperature. Equilibrium conversion is also indicated. (3% CO; 10% H_2O; 87% N_2; GHSV=120000 $mlg^{-1}h^{-1}$).

The effect of H_2O/CO ratio on WGS activity was investigated using two different feed ratios: 10/3 and 2 (Figure 4.5). The results showed that H_2O/CO has a similar effect on carbon monoxide conversion as Ni loading: With the increase in H_2O/CO ratio, CO conversion increases and equilibrium conversions can be reached at lower temperatures.

The results are very reasonable since the equilibrium conversion of carbon monoxide for H_2O/CO ratio of 10/3 is higher than that of H_2O/CO ratio of 2 for the temperature range studied as shown in Figure 4.5. It should be noted that the equilibrium conversion levels are given in Figures 4.4 and 4.5 for the reaction conditions investigated.

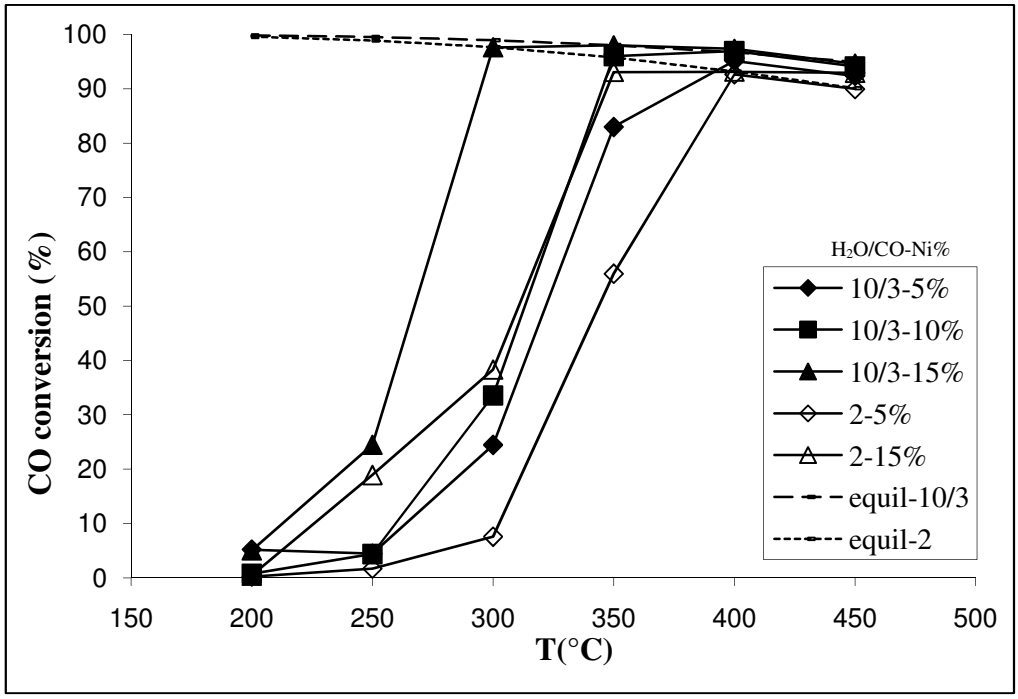

Figure 4.5. Effect of H_2O/CO ratio on WGS activity profile given as a function of temperature (GHSV=120000 $mlg^{-1}h^{-1}$). Equilibrium conversions are also indicated.

Aiming to investigate the effect of GHSV on the catalytic activity, the flowrate of the reaction mixture was kept constant, whereas the amount of catalyst was varied. No significant trend in the CO conversion was observed with increasing GHSV for the whole temperature range (Figure 4.6); though an enhancement in WGS activity would be expected with a decrease in space velocity. According to our results so far, it is very obvious that there should be an optimum space velocity value for the water-gas shift reaction conditions that were studied. Further work is needed to find this optimum point and figure out the trend (Figure 4.7). There, it is seen that medium level of GHSV, ca. 12×10^4 $mlg^{-1}h^{-1}$, for the tested interval is the optimum in terms of the CO conversion level reached.

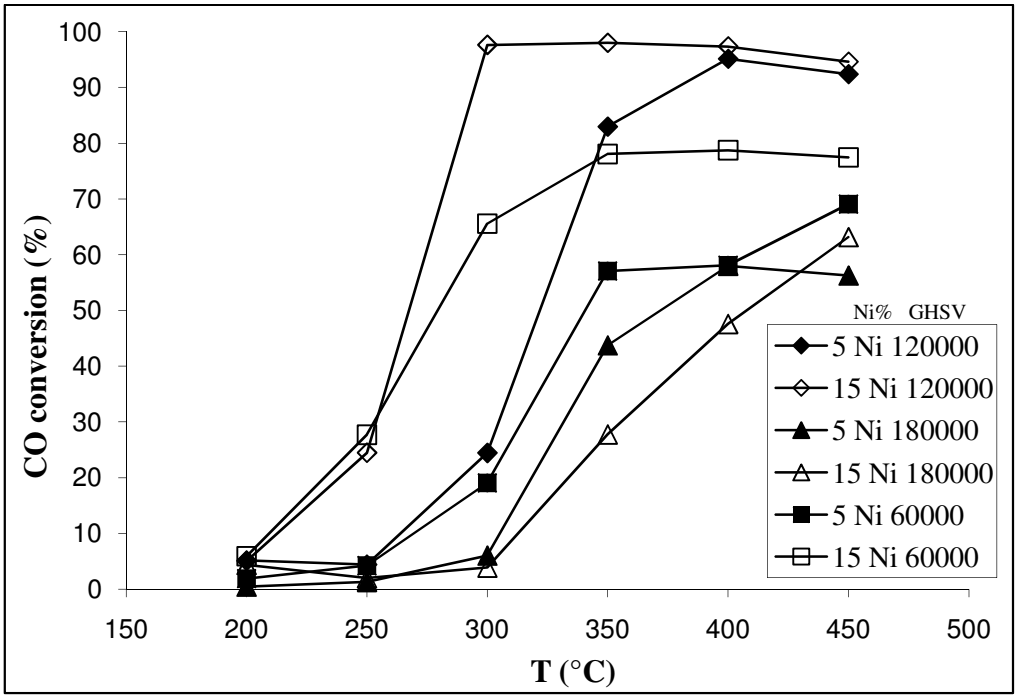

Figure 4.6. Effect of space velocity on WGS activity profile given as a function of temperature. (3% CO; 10% H_2O; 87% N_2).

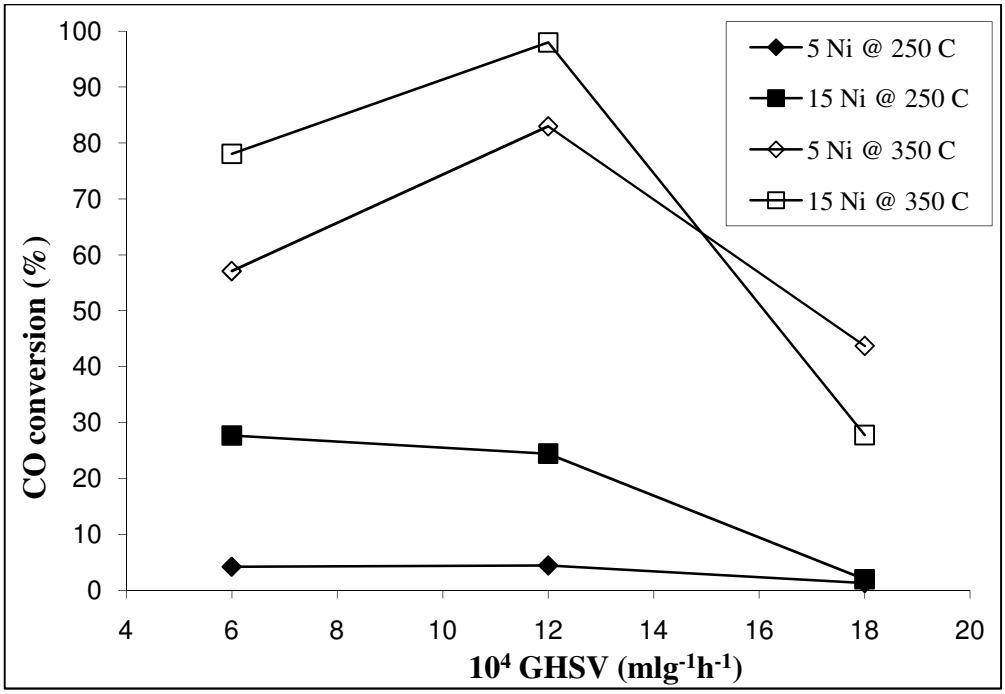

Figure 4.7. CO conversion as a function of GHSV (3% CO; 10% H_2O; 87% N_2).

Selectivity is one of the most important qualities of a water-gas shift reaction catalyst: side reactions, especially methanation that would consume hydrogen should be avoided for a range of H_2O/CO ratios and space velocities [44]. No detectable methane formation was observed in the catalytic reaction tests conducted using different idealized feed compositions.

4.1.3. WGS Performance Tests – Real Feed

The effect of CO_2 and H_2 addition to the feed stream was investigated in order to observe the WGS activity of the Pt-Ni/Al_2O_3 catalysts under conditions very close to those in a fuel processor. Results presented were obtained using feed compositions consisting of 3% CO, 6-10% H_2O, 7% CO_2, 35% H_2 and 49-45% inert, resembling a medium temperature range feed composition between the values of low and high temperature shifts. Results of catalytic performance tests obtained over bimetallic catalysts with different nickel amounts are shown in Figures 4.8 and 4.9.

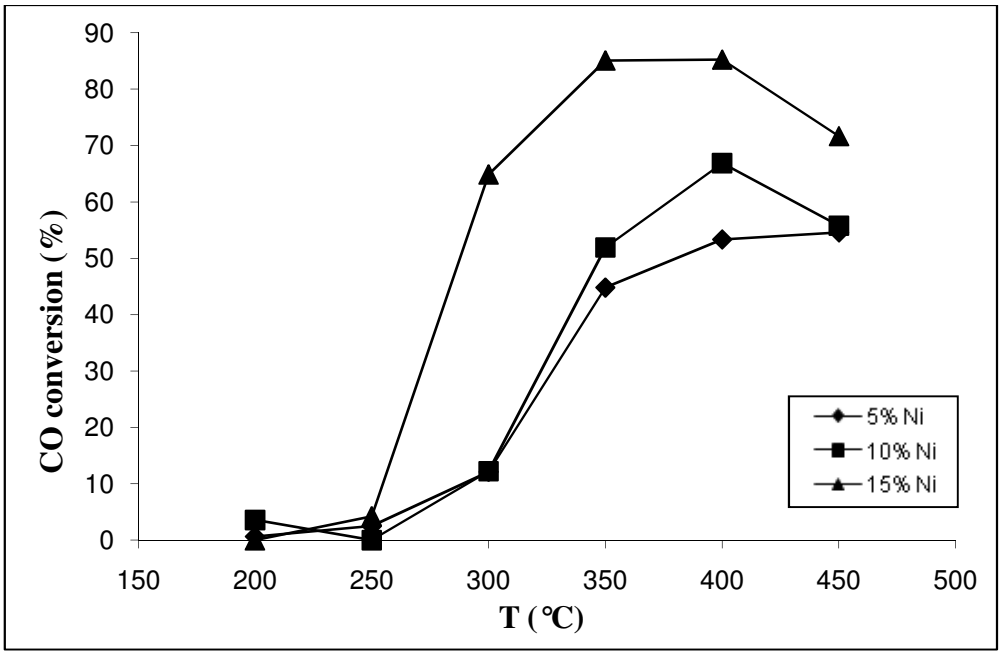

Figure 4.8. Effect of Ni loading of Pt-Ni catalysts on WGS activity profile given as a function of temperature. (3% CO; 6% H_2O; 7% CO_2, 35% H_2O, 49% N_2; $H_2O/CO=2$).

It is observed that with the increase in the Ni loading, carbon monoxide conversion increases for feed compositions having H_2O/CO ratio of 2 (Figure 4.8) and 10/3 (Figure 4.9). These results highly resemble the results of the WGS study under idealistic feed conditions with the CO conversion levels of the latter being higher.

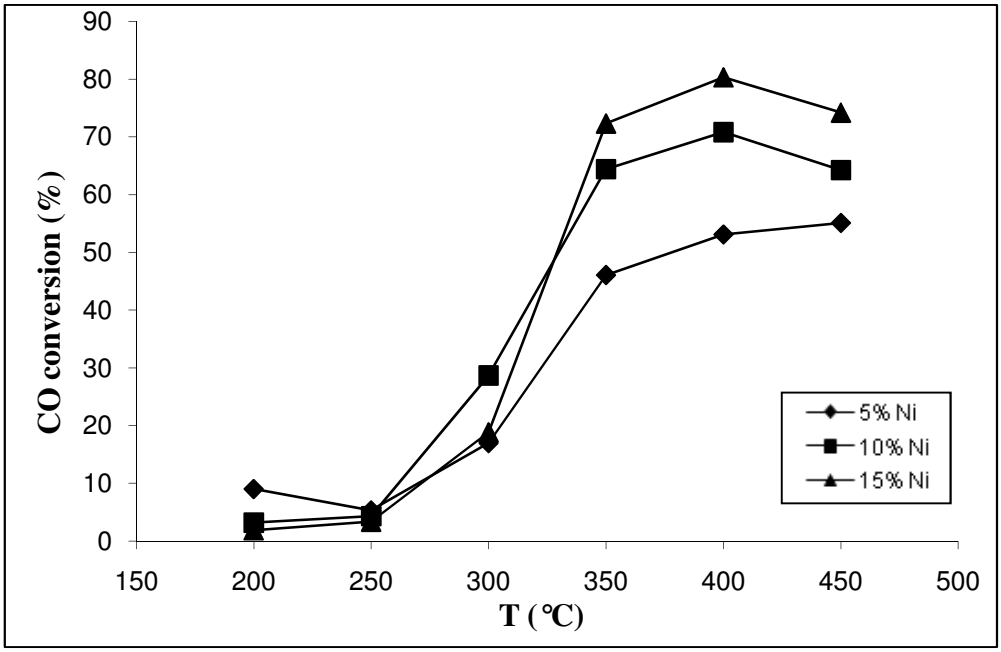

Figure 4.9. Effect of Ni loading of Pt-Ni catalysts on WGS activity profile given as a function of temperature. (3% CO; 10% H_2O; 7% CO_2, 35% H_2O, 45% N_2; H_2O/CO=10/3).

Reporting only the CO conversion levels is not the best way to represent the WGS performance results when the feed used is the real feed. It is evident from the results of the WGS reaction tests under real feed conditions, there is a pronounced decrease in H_2 concentration in the product streams compared to its level in the feed stream, ca. 35%, for all the conditions and catalysts studied (Figure 4.10). The CO conversion levels reached, may point to an active and co-selective WGS catalyst, however when the hydrogen levels in the product stream are considered, it is very clear that the main product is actually being consumed. This consumption arose from the fact that methanation occurs as a side reaction, and it becomes dominant as the temperature increases (Figure 4.11).

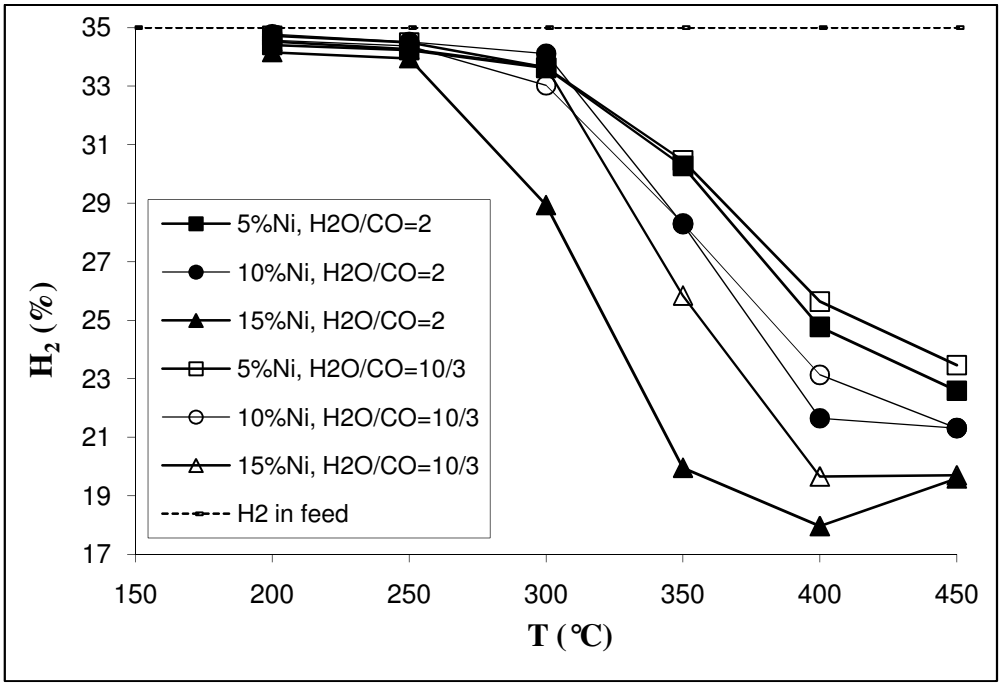

Figure 4.10. Hydrogen concentrations of the product streams under real feed conditions.

In Figure 4.11, the methane concentrations in the product streams are given as a function of temperature. Methane production increases as the Ni amount in the catalyst increases for the H_2O/CO feed ratios studied. This result is reasonable since Ni based catalysts have been reported as active catalysts for the selective methanation of CO above 250°C [167-169]. For 0.2%Pt-15%Ni/Al_2O_3 catalyst, as the H_2O/CO ratio in the feed increases from 2 to 10/3, methanation slows down. However for the catalysts with less Ni amounts this is not the case; H_2O/CO ratio has no effect on methane production. Once higher amount of nickel particles are present on the catalyst surface, water can dissociate into hydroxyl groups, which are the intermediates of the WGS reaction, on the NiO_x sites more easily [170]. The decreased CH_4 production at higher H_2O/CO ratio in the feed over 0.2%Pt-15%Ni/Al_2O_3 catalyst may be attributed to this surface process leaving fewer sites for methanation in comparison to the feed with lower amount of water.

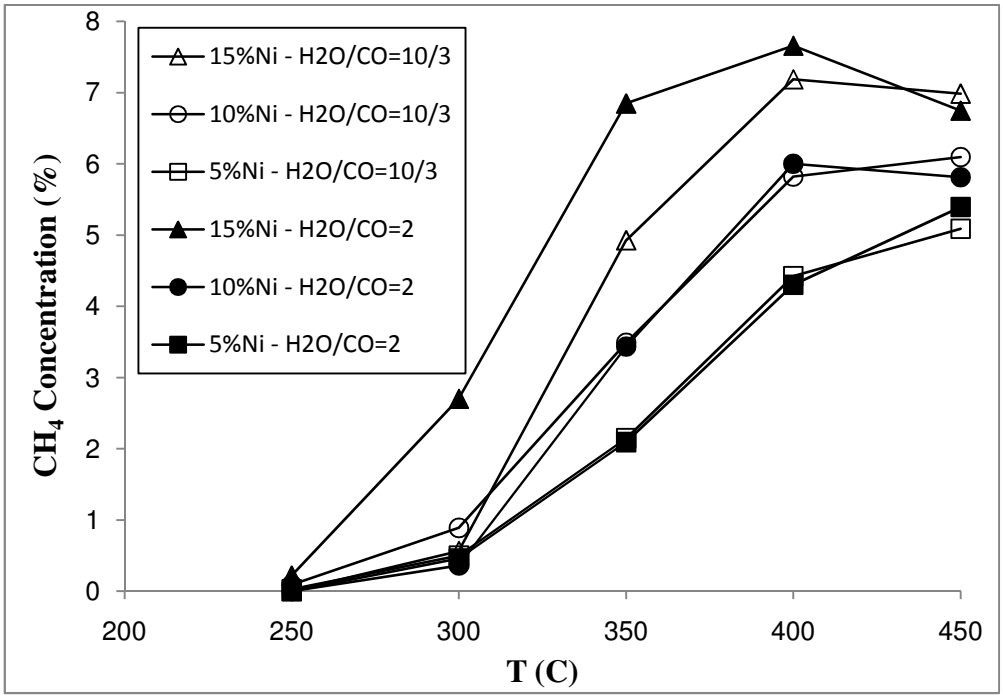

Figure 4.11. Methane formation under real feed conditions as a function of temperature.

4.2. WGS Reaction over Ceria-Based Catalysts – Ideal Feed

4.2.1. Characterization

The XRD patterns of all calcined and reduced samples showed the presence of CeO_2 in the cubic crystal structure of fluorite-type. Rhenium impregnation and gold deposition did not influence the size of ceria crystallites to a great extent (Table 4.1); therefore, neither the extent of crystallization nor the structure of the support are the reasons of the differences observed in the catalytic activity of bimetallic catalysts. No detectable diffraction peaks of gold or rhenium crystallites were obtained, suggesting both metals are highly dispersed with very small particle sizes. The decrease in the calculated ceria lattice constants in the bimetallic catalysts (Table 4.1) can be attributed to the incorporation of Re^{+7}, which has smaller ionic radius (0.53 Å), into ceria lattice of ionic radius 0.97 Å [31]. This incorporation is evident in the case of 0.5%Re-1%Au/Ceria (dp+imp) considering the shift in the XRD peaks towards higher diffraction angles.

Table 4.1. Ceria lattice constants and crystallite sizes of reduced catalysts.

Sample	Lattice constant, a[a] (nm)	Crystallite size[b] (nm)
1%Au-0.5%Re/ceria (imp+dp)	0.542	12.0
0.5%Re-1%Au/ceria (dp+imp)	0.540	13.8
1%Au/ceria (dp)	0.542	12.3
Ceria	0.542	11.6

[a] Calculated using $d^2= a^2/(H^2+K^2+L^2)$
[b] Calculated using the Scherrer Equation

Considering the redox properties of CeO_x, detailed analysis of Ce oxidation states is an important parameter. Figure 4.12 represents the XPS spectra of Ce 3d core level electrons of the freshly reduced catalysts and the catalysts used in WGS reaction as well. Ce 3d region of the XPS spectra were evaluated and relative amount of Ce^{3+} compound was estimated using the following equation [12, 171]:

$$[Ce^{3+}]= I\text{-}Ce^{3+}/(I\text{-}Ce^{3+} + I\text{-}Ce^{4+}) \quad (4.1)$$

where $I\text{-}Ce^{3+}$ and $I\text{-}Ce^{4+}$ represent the sum of intensities of two doublets resulting from Ce_2O_3 and three doublets resulting from CeO_2, respectively.

The higher Ce^{3+} content (Table 4.2) on 1%Au/Ceria (dp) and 1%Au-0.5%Re/Ceria (imp+dp) samples compared to that of 0.5%Re-1%Au/Ceria (dp+imp) implies higher electron transfer ability from the support to metallic sites resulting in higher catalytic activity [33, 42]. As a result of this electron transfer during reaction, the amount of Ce^{3+}decreased for 1%Au/Ceria (dp) and 1%Au-0.5%Re/Ceria (imp+dp), whereas for 0.5%Re-1%Au/Ceria (dp+imp), low WGS activity level led to increased Ce^{4+} content on the surface due to limited oxygen utilization by the active sites.

The O 1s spectra of the catalysts are shown in Figure 4.13. In all cases, the 1s peak is complex; the components observed after deconvolution of the O 1s peak are given in Table 4.2. For the freshly reduced samples, the low energy side of the O 1s binding energy scale (~529 eV) corresponds to the oxygen in the ceria lattice [172, 173]. The other two

peaks at ca. 531 and 533 eV are attributed to the chemisorbed water and hydroxyls, and to the weakly adsorbed water only on the ceria in oxidized state [42, 174], respectively. Comparably higher amount of adsorbed water and hydroxyls are evident for freshly reduced 1%Au-0.5%Re/Ceria (imp+dp) catalyst sample.

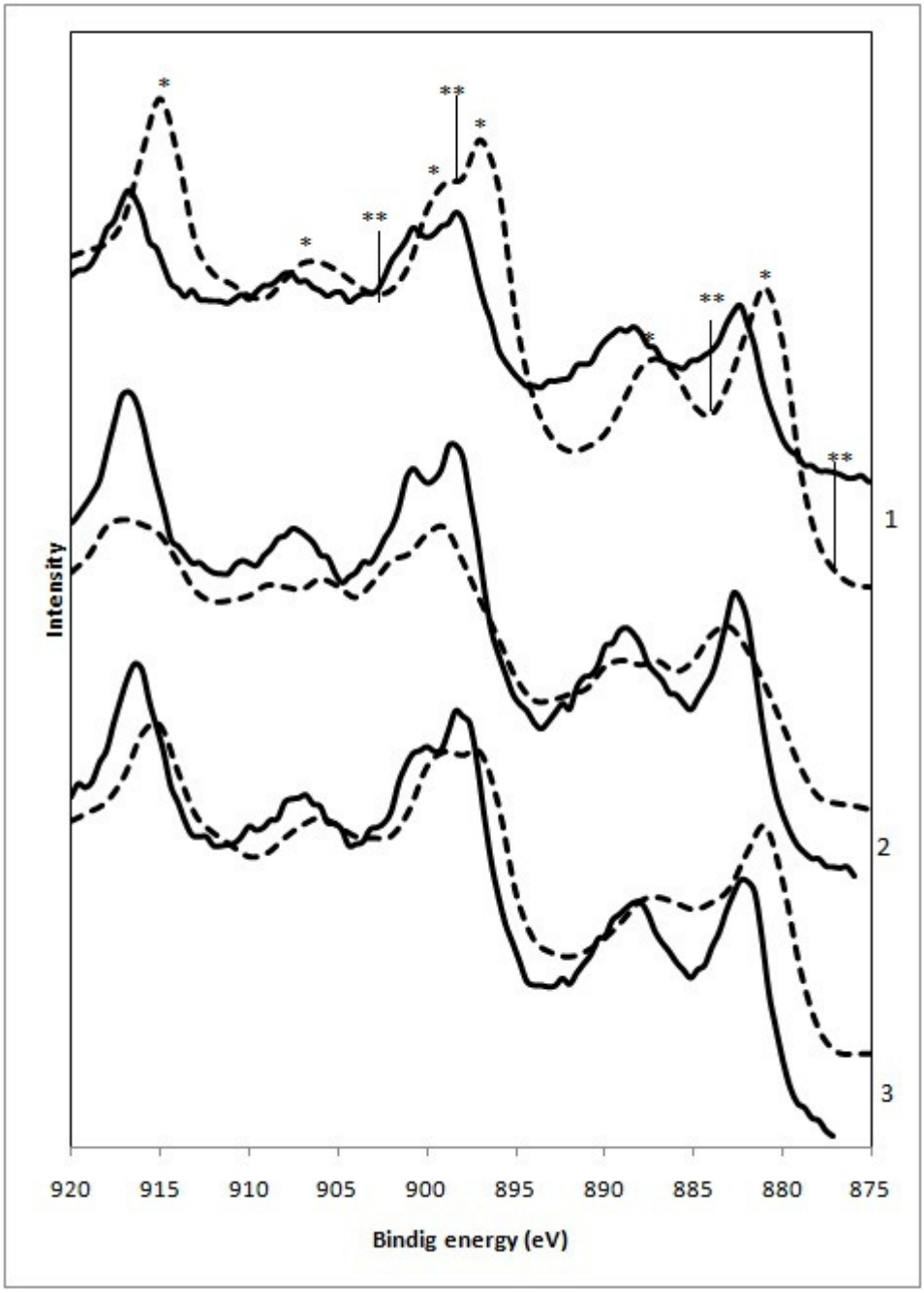

Figure 4.12. XP spectrum of Ce 3d region of catalyst samples. (1) 1%Au/Ceria (dp); (2) 1%Au-0.5%Re/Ceria (imp+dp); (3) 0.5%Re-1%Au/Ceria (dp+imp). (Continuous lines: freshly reduced samples; dashed lines: samples used in WGS reaction; * Ce^{+4}; ** Ce^{+3}).

Table 4.2. XPS results of freshly reduced and used catalyst samples.

Sample	**Ce 3d**	**O 1s**	
	Ce^{3+} (%)	Peak position (eV)	Area (%)
1%Au-0.5%Re/ceria (imp+dp)	4.7	533.30	1.2
		530.97	25.0
		528.84	73.8
0.5%Re-1%Au/ceria (dp+imp)	2.3	533.00	1.4
		530.86	17.5
		528.96	81.2
1%Au/ceria (dp)	7.5	532.39	3.0
		531.00	13.1
		529.39	83.9
1%Au-0.5%Re/ceria (imp+dp)-used	4	533.00	3.8
		529.95	76.4
		527.60	19.7
0.5%Re-1%Au/ceria (dp+imp)-used	6.5	530.50	17.9
		528.17	74.5
		526.90	7.6
1%Au/ceria (dp)-used	4.5	531.10	7.0
		528.02	79.4
		526.90	13.7

Due to the water gas shift reaction, the intensity of the 531 eV peak decreased significantly for 1%Au/Ceria (dp) and 1%Au-0.5%Re/Ceria (imp+dp) implying the spent hydroxyls during reaction. This result is in agreement with the catalytic performance tests which run with the feed having $H_2O/CO=5$; the most active catalyst is 1%Au-0.5%Re/Ceria (imp+dp) which has the lowest amount of hydroxyls after the reaction. As a result of the WGS reaction, the peak related to the adsorbed water molecules on the ceria in the oxide state disappears and peaks corresponding to the lattice oxygen and oxygen ions associated with a (-2) formal charge (527 eV) evolved at the low energy side of the O 1s spectra for all samples studied [42]. It should be noted that for the 0.5%Re-1%Au/Ceria

(dp+imp) sample, which has lower Ce^{4+} content after WGS reaction, the lowest 527 eV peak is observed.

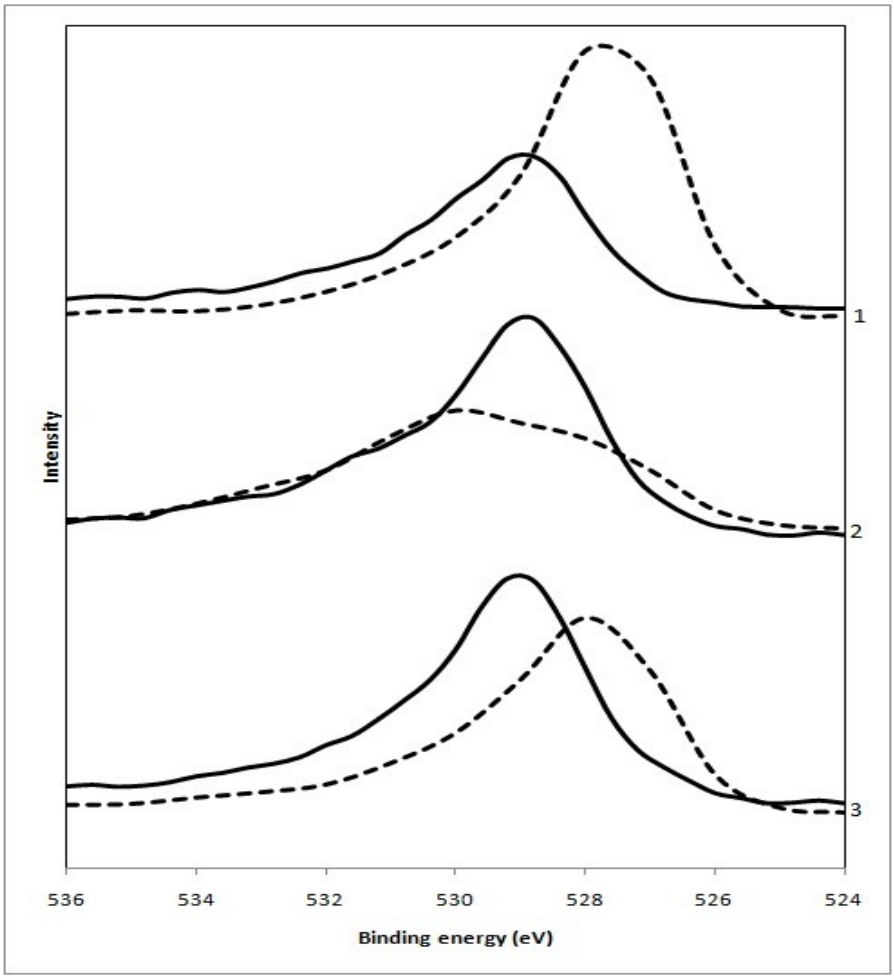

Figure 4.13. XP spectrum of O 1s region of catalyst samples. (1) 1%Au/Ceria (dp); (2) 1%Au-0.5%Re/Ceria (imp+dp); (3) 0.5%Re-1%Au/Ceria (dp+imp). (Continuous lines: freshly reduced samples; dashed lines: samples used in WGS reaction).

A very porous blossom-like texture is observed in the SEM micrographs of all catalysts; as an example, the SEM micrographs of 0.5%Re-1%Au/Ceria (dp+imp) sample are given in Figures 4.14 and 4.15. Some aggregates formed by very small particles, which are confirmed by the X-ray analytical mapping analysis, are also present especially on 0.5%Re-1%Au/Ceria (dp+imp).

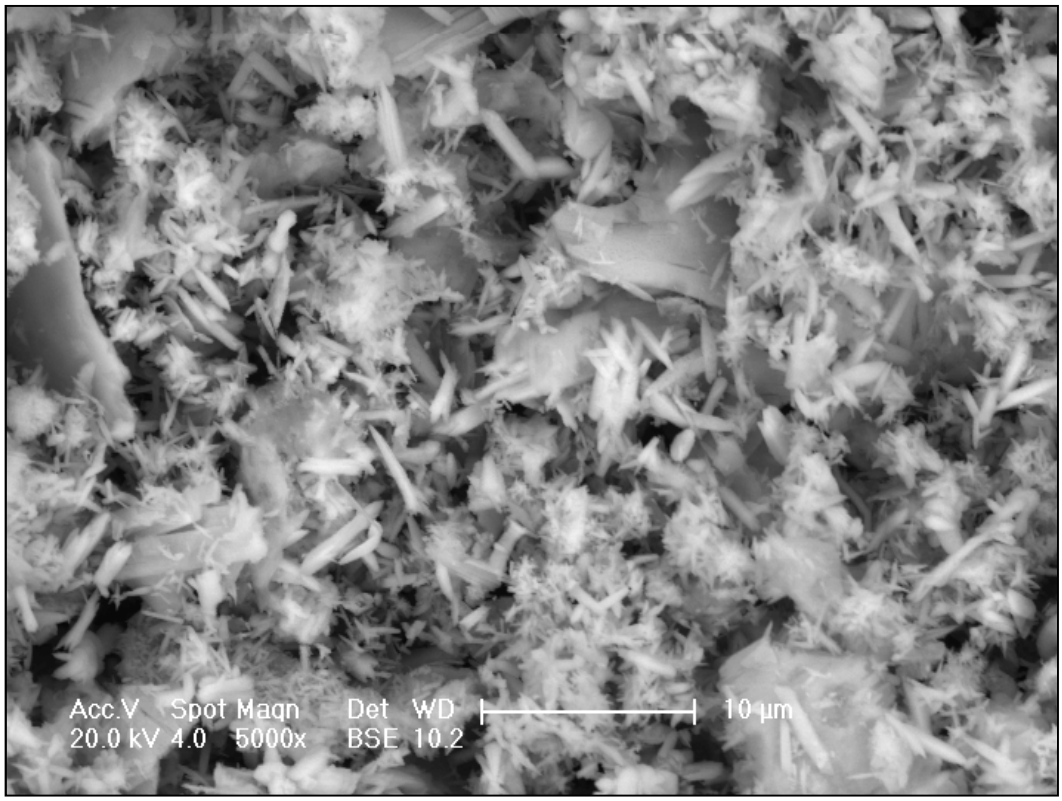

Figure 4.14. SEM micrograph of reduced 0.5%Re-1%Au/Ceria (dp+imp) (x5000).

EDS studies prove that the bright areas in Figure 4.15 are mainly composed of gold particles. SEM images confirm there is no significant change in surface morphology due to the changes in metal addition sequence or Re addition. For all catalysts examined, both x-ray mapping images and EDS studies clearly indicate the uniform dispersion of metals on ceria surface.

The samples were also characterized by HRTEM-EDS in detail. The HRTEM image of Au nanocluster observed in the monometallic sample is given in Figure 4.16. The Au, Re and ceria nanoclusters, each of which was confirmed by the EDS analysis, are seen on the HRTEM image of bimetallic 1%Au-0.5%Re/Ceria (imp+dp) sample 4.17. The detail of the interfacial region(s) formed on the bimetallic sample is also given in Figure 4.18.

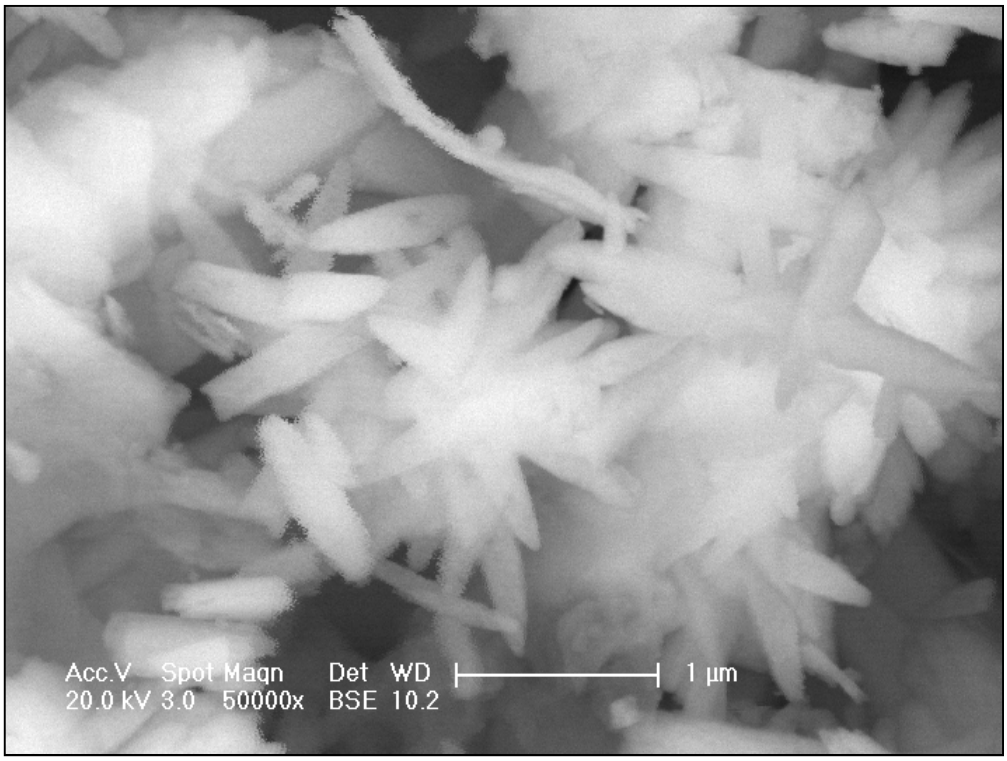

Figure 4.15. SEM micrograph of reduced 0.5%Re-1%Au/Ceria (dp+imp) (x50000).

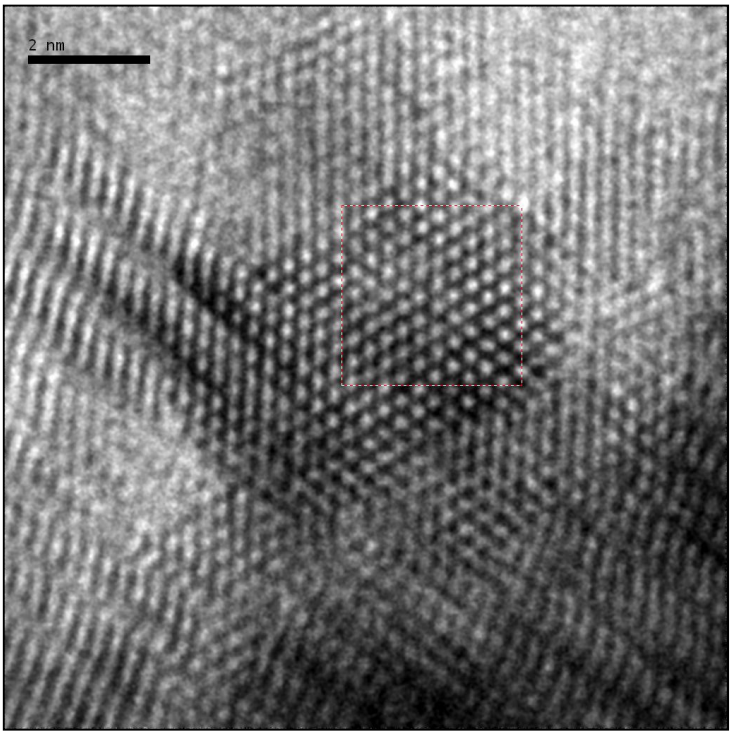

Figure 4.16. HRTEM image of Au nanocluster from 1%Au/Ceria.

The results of the HRTEM studies hint the possible Au-Re surface alloy (skin-type bimetallic alloy) formations in the interfacial boundaries of the nanoclusters in the 1%Au-0.5%Re/Ceria (imp+dp) sample. HRTEM studies reveal that ceria in all catalysts consists of particles with an average size of 10-12 nm, verifying the results of the crystallite size calculations based on Scherrer's equation from the XRD data. Average size of Au nanoclusters/particles are measured as 4-5 nm according to HRTEM studies.

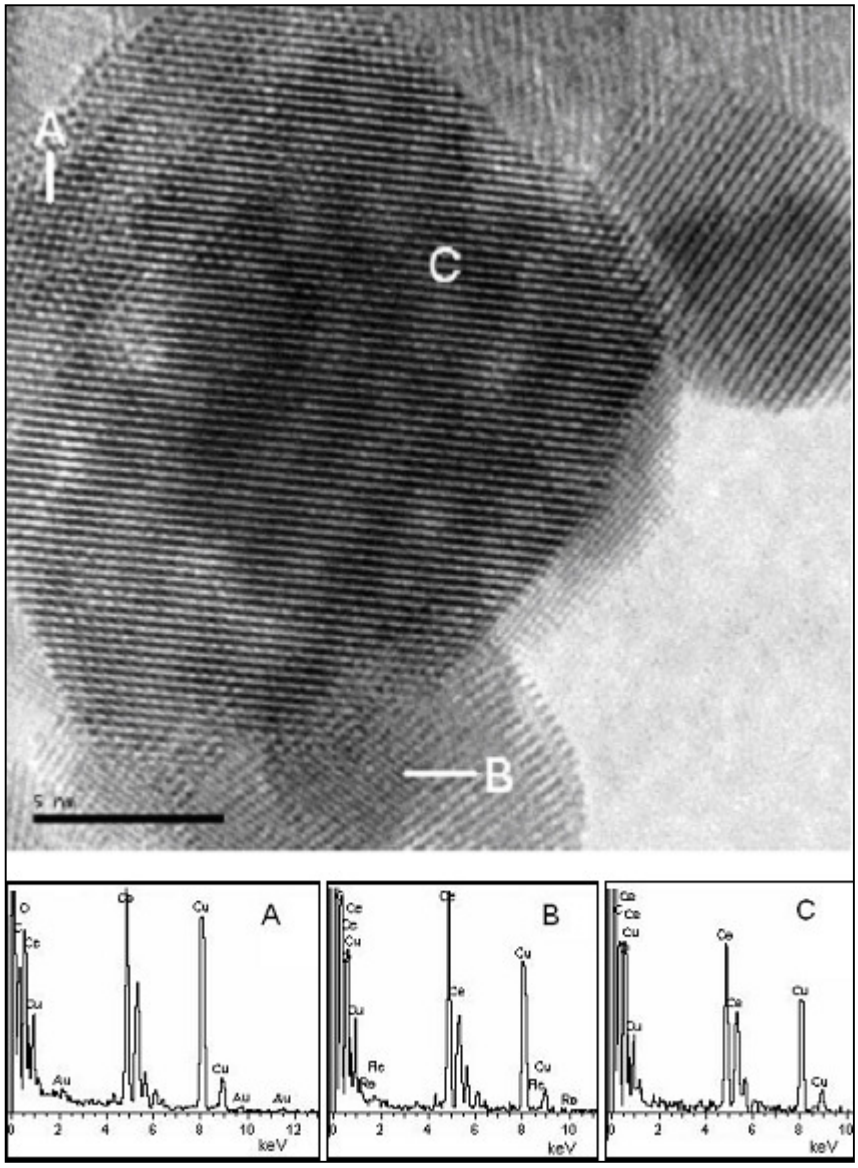

Figure 4.17 HRTEM image of 1%Au-0.5%Re/Ceria (imp+dp) and its regional EDS analysis: (A) gold and ceria nanocluster; (B) rhenium and ceria nanocluster; (C) ceria alone. The presence of the Cu signal in the EDS spectra is due to the employed grids.

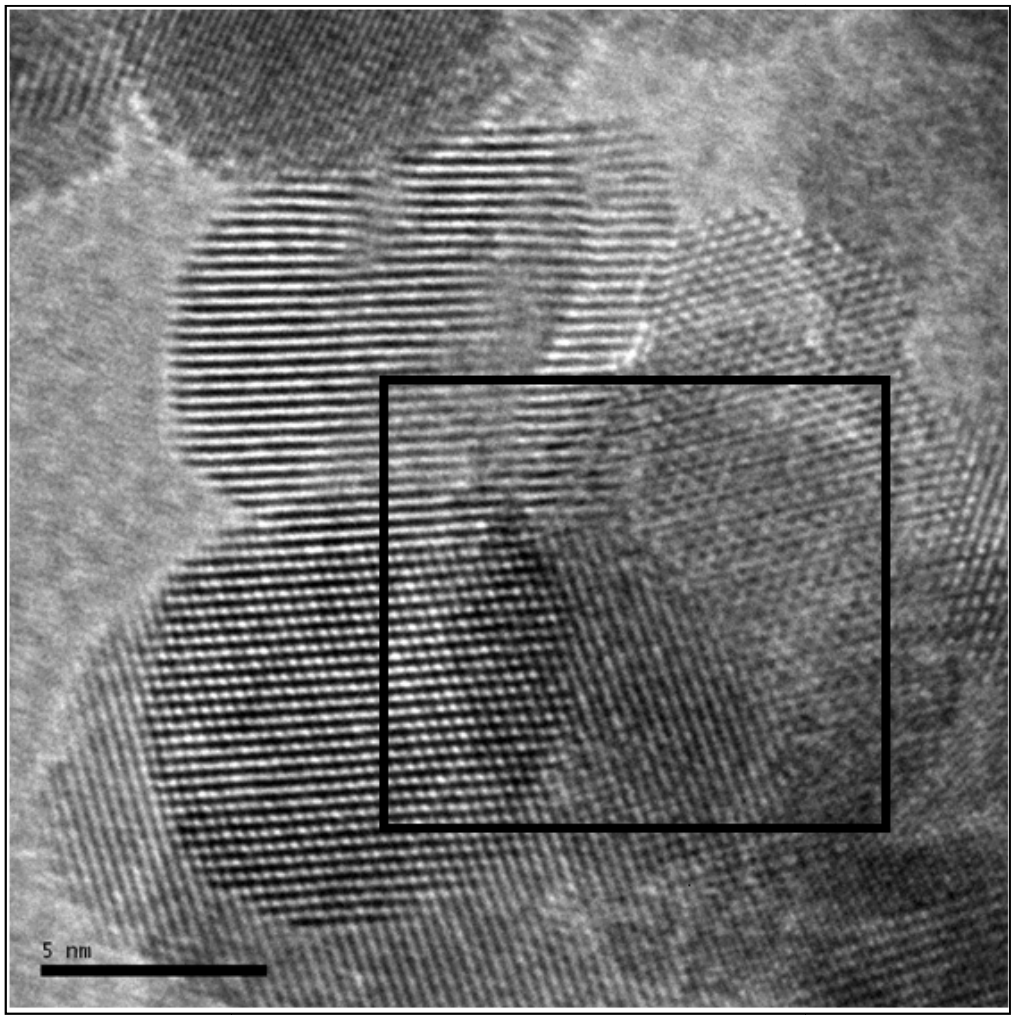

Figure 4.18. HRTEM image of 1%Au-0.5%Re/Ceria (imp+dp) showing the layered structures/formations in the interfacial region.

4.2.2. WGS Performance Tests

No detectable methane formation was observed in the catalytic reaction tests. Increasing the GHSV from 120000 to 180000 $mlg^{-1}h^{-1}$ by varying the catalyst amount led to a decrease in CO conversion for all monometallic and bimetallic catalysts. As an example, the CO conversion values for 1%Au/Ceria (dp) at different gas hourly space velocities are given in Figure 4.19.

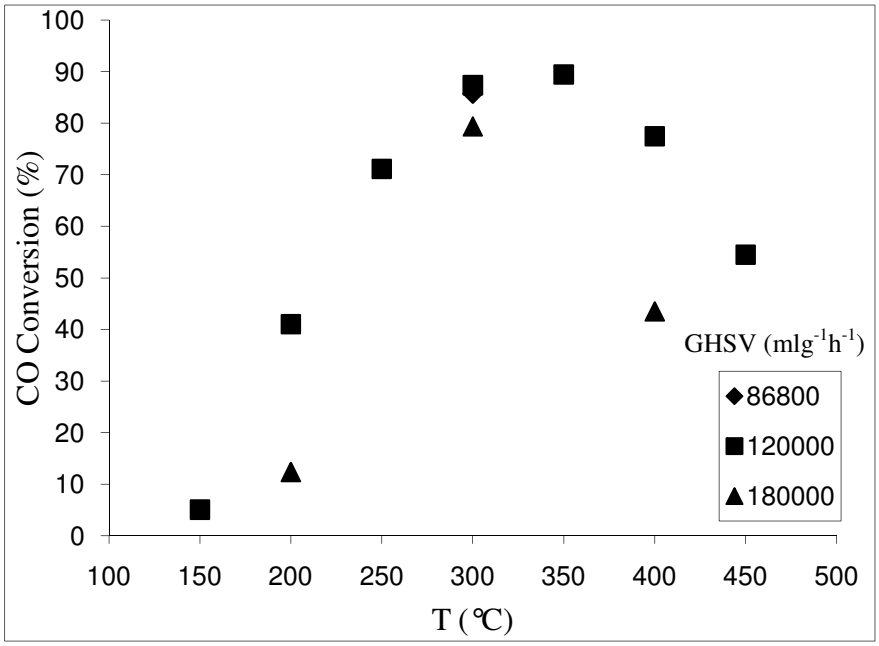

Figure 4.19. Effect of GHSV on the catalytic activity of 1%Au/Ceria (dp).

The conversion – temperature data showed that conversion makes a maximum for lower H_2O/CO ratios, ie. $H_2O/CO=1$ and 2, and the temperature for the maximum conversion level shifted from 350 C to 300 C as H_2O/CO increases from 1 to 2 (Figure 4.20). On the other hand, no distinct maximum for conversion – temperature curve was observed for $H_2O/CO=5$. It seems that at H_2O/CO ratio of 5, as a consequence of high steam content leading suppressed reverse WGS, no significant loss of WGS activity was observed.

The influence of the preparation method of Au-Re catalysts on the catalytic activity was investigated by comparing the catalytic performances of 1%Au-0.5%Re/Ceria (imp+dp), 0.5%Re-1%Au/Ceria (dp+imp) and 0.5%Re-1%Au/Ceria (si). Amongst them, the most active catalyst was found as 1%Au-0.5%Re/Ceria (imp+dp) (Figure 4.21). As previously reported in literature [21, 26, 31], dp method clearly enhances the catalytic activity of the gold based catalysts through the achievement of better dispersion due to lower particle size. Figure 4.21 shows that the sequentially impregnated catalyst exhibited 0-25 % CO conversion within 250-400˚C temperature range, whereas 1%Au-0.5%Re/Ceria (imp+dp) and 0.5%Re-1%Au/Ceria (dp+imp) reached 85% and 65% CO conversion levels, respectively. The application sequence of the impregnation and dp

methods which were used in Re and Au addition, respectively, was found crucial; gold addition by dp technique on impregnated Re/Ceria catalysts led to a higher dispersion and, consequently, higher CO conversion values. On the other hand, impregnation of Re on Au/Ceria catalysts resulted in slight blockage of active sites, agglomeration of gold particles and decrease in Ce^{3+} content which was confirmed by the EDS, x-ray analytical mapping and XPS studies.

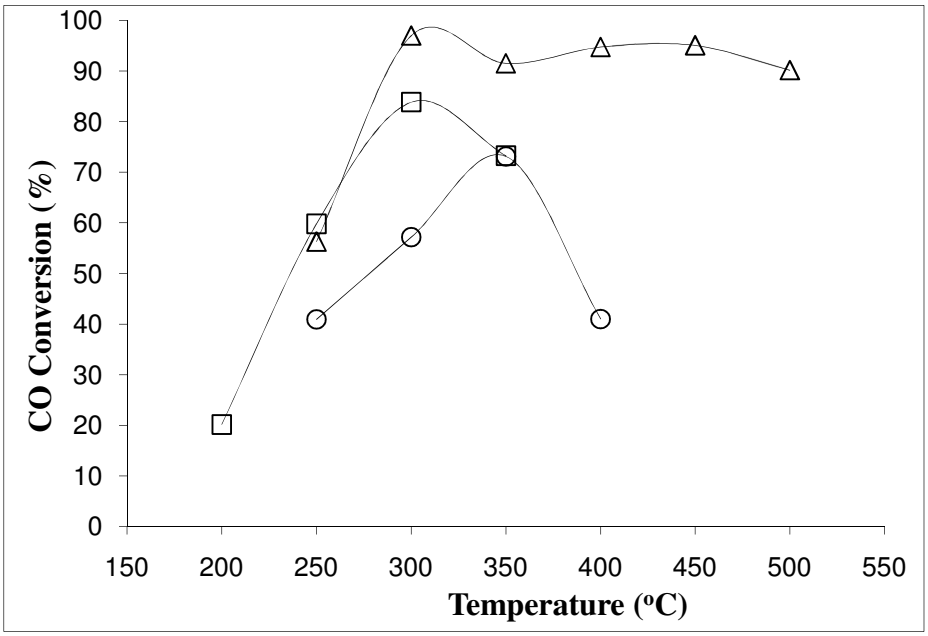

Figure 4.20. Effect of H_2O/CO on the catalytic activity of 1%Au-0.5%Re/Ceria (imp+dp) (3% CO, GHSV=120000 ml/g.h); (Δ) H_2O/CO=5; (□)H_2O/CO=2; (○) H_2O/CO=1. Note that the equilibrium profiles are given in Figure 4.21 and 4.22.

Since Au-Re bulk alloy formation requires very high temperatures [175], this significant activity difference between the two catalysts prepared by (imp+dp) and (dp+imp) may also be explained by surface alloy formation or interaction between Au and Re atoms. For the (dp+imp) catalysts, consecutive calcinations were applied upon gold precipitation and rhenium impregnation steps, making sure that Re particles are added and stabilized on previously stabilized surface; as a consequence, the procedure lessens the possibility for Au-Re surface alloy formation. On the other hand, only one calcination step upon dp was applied to (imp+dp) catalysts; thus, stabilization of both Re and Au particles

was simultaneous on the ceria surface, leading higher potential for bimetallic interactions starting from precursor states, which can easily result in Au-Re surface alloy formation.

Figures 4.21 and 4.22 show the influence of Re addition on the WGS activity of the catalysts. Au-Re/Ceria catalysts showed better performances at higher H_2O/CO ratio while the monometallic catalysts suffered from steam inhibition. Figure 4.22 clearly illustrates the superior performance of 1%Au-0.5%Re/Ceria (imp+dp) especially at elevated (above 300 ^oC) temperatures for H_2O/CO ratio of 5. Since Re/Ceria catalysts were found inactive in WGS (Figure 4.21), the performance of Au-Re/Ceria catalysts can be attributed to steam tolerance of catalytically active sites formed on the bimetallic system.

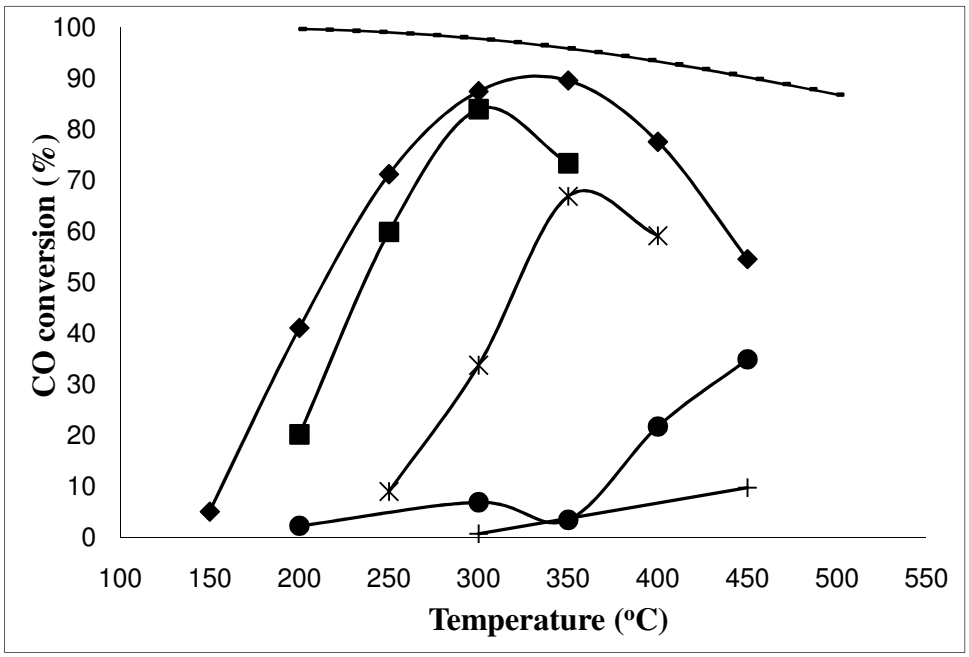

Figure 4.21. Temperature dependence of the catalytic activity: 3% CO; 6% H_2O; 91% N_2; (120000 ml/gh) (♦)1%Au/Ceria(dp); (■)1%Au-0.5%Re/Ceria(imp+dp); (∗)0.5% Re-1%Au /Ceria(dp+imp); (•)0.5%Re-1%Au/Ceria(si); (+)0.5%Re/Ceria (imp); (-)equil.curve.

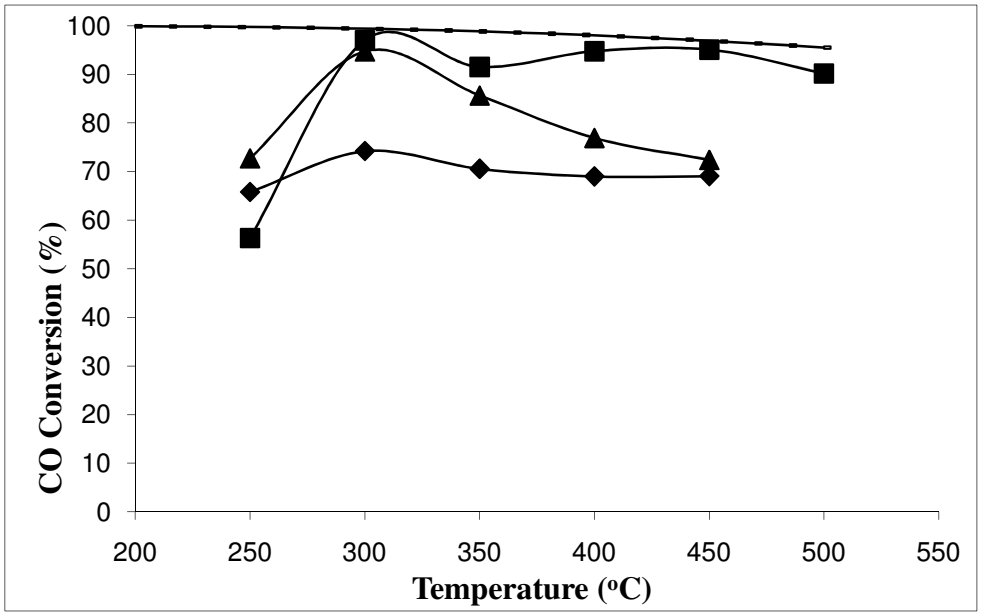

Figure 4.22. Temperature dependence of the catalytic activity 3% CO; 15% H_2O; 82% N_2; GHSV=120000 ml/g.h; (■) 1%Au-0.5%Re/Ceria (imp+dp); (▲) 0.5%Au-0.25%Re/Ceria (imp+dp);(♦) 1%Au/Ceria (dp); (-) equilibrium curve.

Sato et al. [19] have reported in their FT-IR studies that additional adsorbed CO peaks toward lower wavenumbers were strongly related to higher water amount used in WGS reaction performed over Pt-Re/TiO_2 and Ir-Re/TiO_2 catalysts. They also stated that the role of Re would be the stabilization of formate species and to accelerate the rate of hydrogen formation, and possible catalytically active sites formed between Re and the second metal could be effective for water activation.

The catalytic stability of 1%Au-0.5%Re/Ceria (imp+dp) catalyst, which showed the maximum conversion during performance studies, was tested for 48 h at 350°C. The test was carried out with a feed stream consisting of 3% CO, 15% H_2O and nitrogen. At first the catalyst deactivated rapidly, losing about 37% of its initial activity within 8 h, but then lost only another 3% over the next 40 h (Figure 4.23).

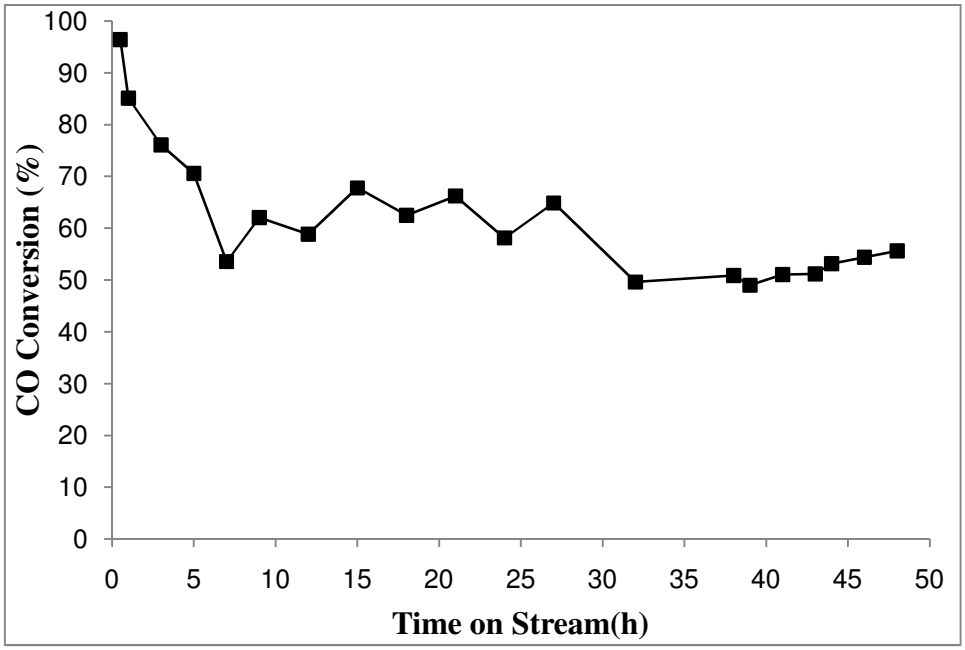

Figure 4.23. Stability test for WGS reaction. (3% CO, 15% H_2O, 82% N_2; 350°C).

4.3. WGS Reaction over Au-Re/Ceria Catalysts – Real Feed and DRIFTS Studies

The results of the WGS reaction tests performed on the ceria based catalysts revealed that the bimetallic 1%Au-0.5%Re/Ceria (imp+dp) catalyst was highly active and selective especially at high H_2O/CO ratios. Considering no methane formation was observed over ceria based catalysts during preliminary tests under real feed conditions, WGS reaction activities of the catalysts were decided to be investigated under several realistic feed conditions aiming to have complete WGS performance specs of Au-Re/Ceria system.

Moreover, in order to get more information on the WGS reaction over the synthesized catalysts and particularly on the surface reaction mechanism, DRIFTS studies were performed on the catalysts as well as the ceria support.

4.3.1. DRIFTS Studies

In order to analyze the processes taking place over the catalysts during reduction and CO exposure in detail, the catalysts have been analyzed by operando-FTIR-DRIFTS-

MS. Figures 4.24-4.29 show the DRIFT spectra of the catalysts used in this part of the study and that of the ceria support. Figures 4.30 and 4.31 are also given in order to distinguish the different species formed on the surface of each catalyst under inert and 3% CO – 97% He flow.

As explained in Section 3.4.2, *in situ* reduction procedure was employed prior to DRIFTS tests on the ceria supported catalyst samples. The sample was placed in the DRIFTS cell without any dilution and the chamber was subjected to 5 ml argon flow first; the IR spectrum obtained under these conditions was used as background. Then the mass flow controller system was adjusted to 47.5 ml/min He flow and the temperature of the cell was increased gradually until 200°C, which is the reduction temperature. During the reduction, 5 ml/min hydrogen flow was added to the inlet flow and after 1 h of reduction; the cell was allowed to cool down to the room temperature under 47.5 ml/min He flow. CO adsorption experiments were conducted under 3, 10 and 20% CO/He mixture with 50 ml/min total flow.

For the ceria support, *in situ* reduction procedure was employed. However, interaction with CO was not investigated since preliminary tests had shown that ceria support was not active for the WGS reaction. The DRIFT spectra of the ceria support are presented in Figure 4.24. At room temperature under inert flow, one peak at 3700 cm^{-1} is evident in the high frequency range which can be attributed to mono-bridging OH groups [33]. In the lower frequency region, carbonates represented by 1050 cm^{-1} band are observed. The bands at 1498 and 1325 cm^{-1} can be attributed to either carbonates [33, 44] or carboxylate [33] species on the ceria surface.

The peak at 3658 cm^{-1} on the 200°C spectrum of ceria is characteristic of doubly bridged OH groups [57]. Formate formation (2850 cm^{-1} [64]) was observed as a result of temperature increase under inert atmosphere. The increasing intensity and the red shift of 1498 and 1050 cm^{-1} bands to 1470 and 1030 $cm^{-1}$with increasing temperature in addition to formate formation indicates the reoxidation of the ceria surface. The emerging bands at 1270, 1255 and 1116 cm^{-1} can be attributed to carbonates on the ceria surface [53]. Similarly the new band at 1315 cm^{-1} can be ascribed to carboxylates [33, 176]. Upon reduction almost no change in the DRIFT spectrum of the ceria support was observed, as

the reduction treatment is usually used to remove oxygen from the metal sites on a catalyst. The broad band between 3350 and 3150 cm^{-1} gained intensity due to the increase in the amount of hydrogen bonded hydroxyl groups as a result of hydrogen introduction to the DRIFTS cell [33, 57, 59].

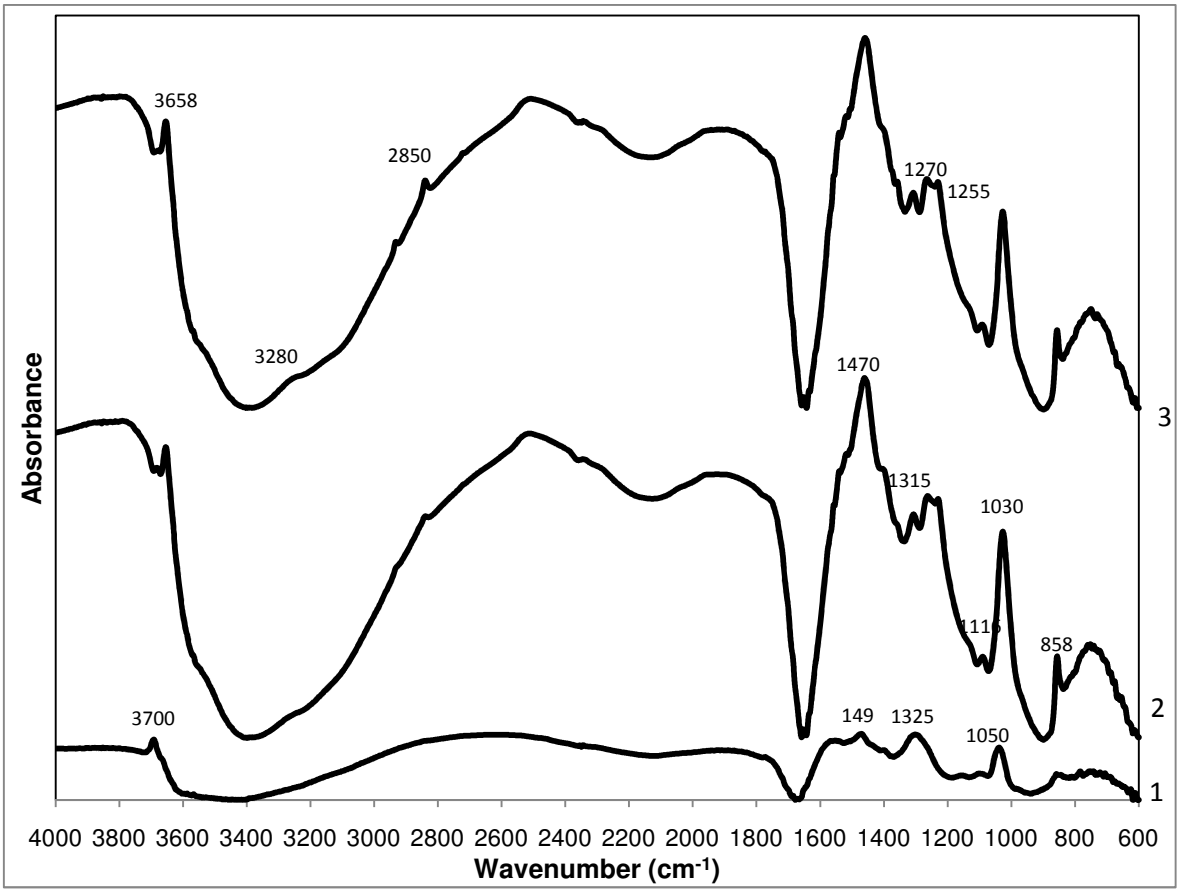

Figure 4.24. DRIFT spectra of ceria support (1) under He flow at room temperature, (2) under He flow at 200°C, (3) during reduction.

Although WGS performance test conducted using ideal feeds have shown that 0.5Re/Ceria (imp) catalyst is not active for the reaction, the DRIFT spectra under various conditions involving the spectra obtained under inert flow at room temperature, at 200°C, during reduction, after reduction at room temperature and under 3% and 10% CO flows are given in Figure 4.25, as a reference for surface species formed on the rhenium sites of the bimetallic catalysts.

The DRIFT spectrum of 0.5%Re/Ceria (imp) sample reveals the formation of carbonate (1475, 1405, 1272, 1182, 1045 and 973 cm^{-1} bands [33]) species on the catalyst surface. Bicarbonate species were also observed as indicated by the 1602 cm^{-1} [33] band. In the OH region of the spectrum, weak bands associated with the presence of mono-bridging (3693 and 3685 cm^{-1} [33]) and hydrogen bonded (3380-3120 cm^{-1} [33, 57, 59]) hydroxyl species are evident.

Changes in the DRIFT spectra of the of 0.5%Re/Ceria (imp) catalyst occur as a result of heating it up to 200°C and reduction treatment. Apart from the increase in the amount of hydroxyl species under reduction conditions which is evident from the intensity increase of the broad band in the OH region (3380-3120 cm^{-1}), a number of new bands with high intensities evolve in the O-C-O region as well. All the new bands in addition to the ones with increased intensities point out to carbonate species formation (1525, 1471, 1427, 1338, 1272, 1259, 1095, 1033, 993, 895, 862 [33, 53]). The disappearance of the bicarbonate band at ca. 1600 cm^{-1} is worth mentioning, and 2858 cm^{-1} band confirms the formation of formate species on Ce^{+3} [44, 53]. The spectrum taken at room temperature after reduction under inert atmosphere is very close to the one taken during reduction which confirms the stable surface species after reduction.

In order to characterize the CO adsorption behavior of the 0.5%Re/Ceria (imp) catalyst, DRIFTS measurements under 3% CO-balance He and 10% CO-balance He atmospheres were made. On this catalyst, new peaks emerge in the C-O region as a result of CO exposure. CO adsorption resulted in a peak at 2021 cm^{-1} which can be attributed to CO linearly adsorbed on isolated Re metal (Re^0) particles [177-180]. Similarly, the bands appearing at 2196 and 2158 cm^{-1} indicate the linear adsorption of CO on Ce^{4+} and Ce^{3+} sites, respectively [33]. However these two bands coincide with the gas phase CO doublet [181], and it is hard to distinguish. The band attributed to bridge type CO adsorption on Re metal is also present (1785 cm^{-1}) [182]. The 2389 cm^{-1} band can be assigned to the gas phase CO_2 or linear interaction of CO_2 with ceria.

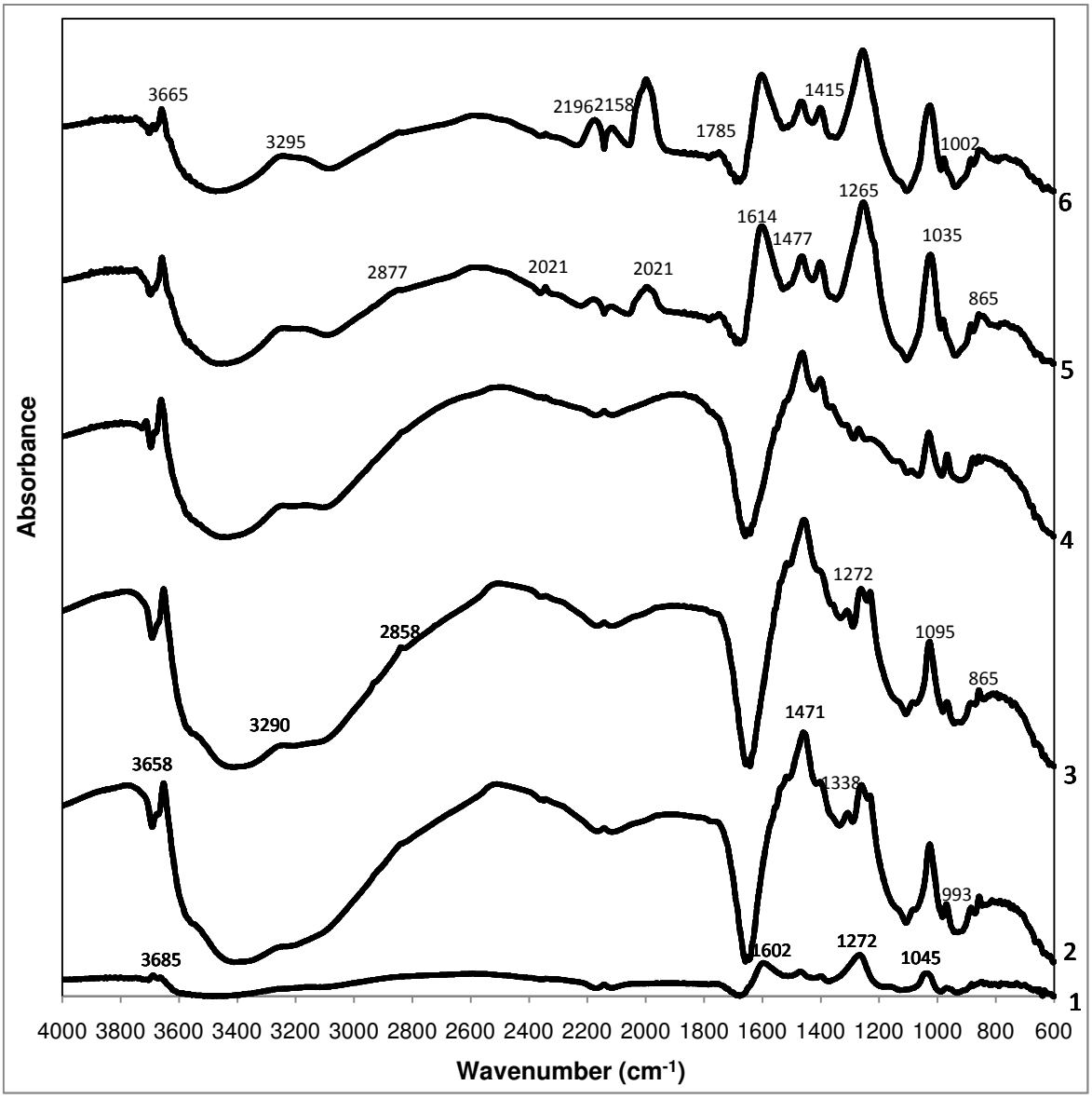

Figure 4.25. DRIFT spectra of 0.5%Re/Ceria (imp): (1) under He flow at room temperature, (2) under He flow at 200°C, (3) during reduction, (4) after reduction at room T, (5) under 3% CO-97% He flow, (6) under 10%CO-90% He flow.

The peaks in the O-C-O (1700-1200 cm^{-1}) and C-H (1200-600 cm^{-1}) regions (1477, 1415, 1265, 1035, 1002, 892 and 865 cm^{-1} bands) are all attributed to carbonate species, although the 1614 cm^{-1} band should not be excluded since formates are considered as reaction intermediates in the formate mechanism proposed for the water gas shift reaction (See Section 2.1.3). The reoccurrence of 1614 cm^{-1} band with the 2877 cm^{-1} band in the C-H region indicates the presence of formates on the catalyst surface [53]. Moreover, with

the increasing CO partial pressure in the DRIFTS cell, the intensity of the broad OH band increases.

The DRIFT spectra of the other monometallic catalyst, 1%Au/Ceria (dp), is given in Figure 4.26. Similar to the DRIFT spectrum of 0.5%Re/Ceria (imp) at room temperature, the OH region of the first spectrum of monometallic gold catalyst is dominated by a weak broad band between 3400-3100 cm^{-1} which is characteristic of hydrogen bonded hydroxyl groups [33, 57, 59], and 3699 cm^{-1} band with a shoulder at 3685 cm^{-1} which can be attributed to the mono-coordinated OH on Ce^{3+} [33]. In the carbonate and formate region (1800-800 cm^{-1}) of the same spectrum (Spectrum 1 in Figure 4.26), strong peaks attributed to carbonates can be observed at 1604, 1487, 1427, 1288, 1116, 1049 and 877 cm^{-1}. The 1604 cm^{-1} band is also assigned to carbonates since no formate band in the C-H region between 2900-2800 cm^{-1} is observed.

Through spectra 2 to 4 in Figure 4.26, i.e. throughout heating up to 200°C, reduction and cooling down to room temperature procedures, rearrangement of the carbonate region is observed in addition to hydroxyl peak intensity increase. The carbonate peaks are settled at the end of the reduction treatment and formate species on Ce^{3+} which are evident from the 2860 and 1588 cm^{-1} bands [33, 44, 53, 54], are also formed. The formation of the band near 2140 cm^{-1} after reductive conditioning is observed, as well. This peak is assigned to the forbidden electronic transition $^2F_{5/2} \rightarrow {}^2F_{7/2}$ of Ce^{3+} on surface defect sites [33, 53].

In contradiction to the spectrum obtained from 0.5%Re/Ceria (imp) catalyst under CO exposure, when CO was introduced to the DRIFTS cell on 1%Au/Ceria (dp) sample, a little change in the O-C-O and C-H regions was observed. This may be related with the fact that formate species which have been already formed on the catalyst sample during/after the reduction treatment. The changes in the carbonate bands consist of the decrease in the 1487 cm^{-1} band intensity and the reformation of the 1245 cm^{-1} band. The increase in the amount of hydroxyl species is also evident in the OH regions of the spectra belonging to the catalyst under different amounts of CO exposure.

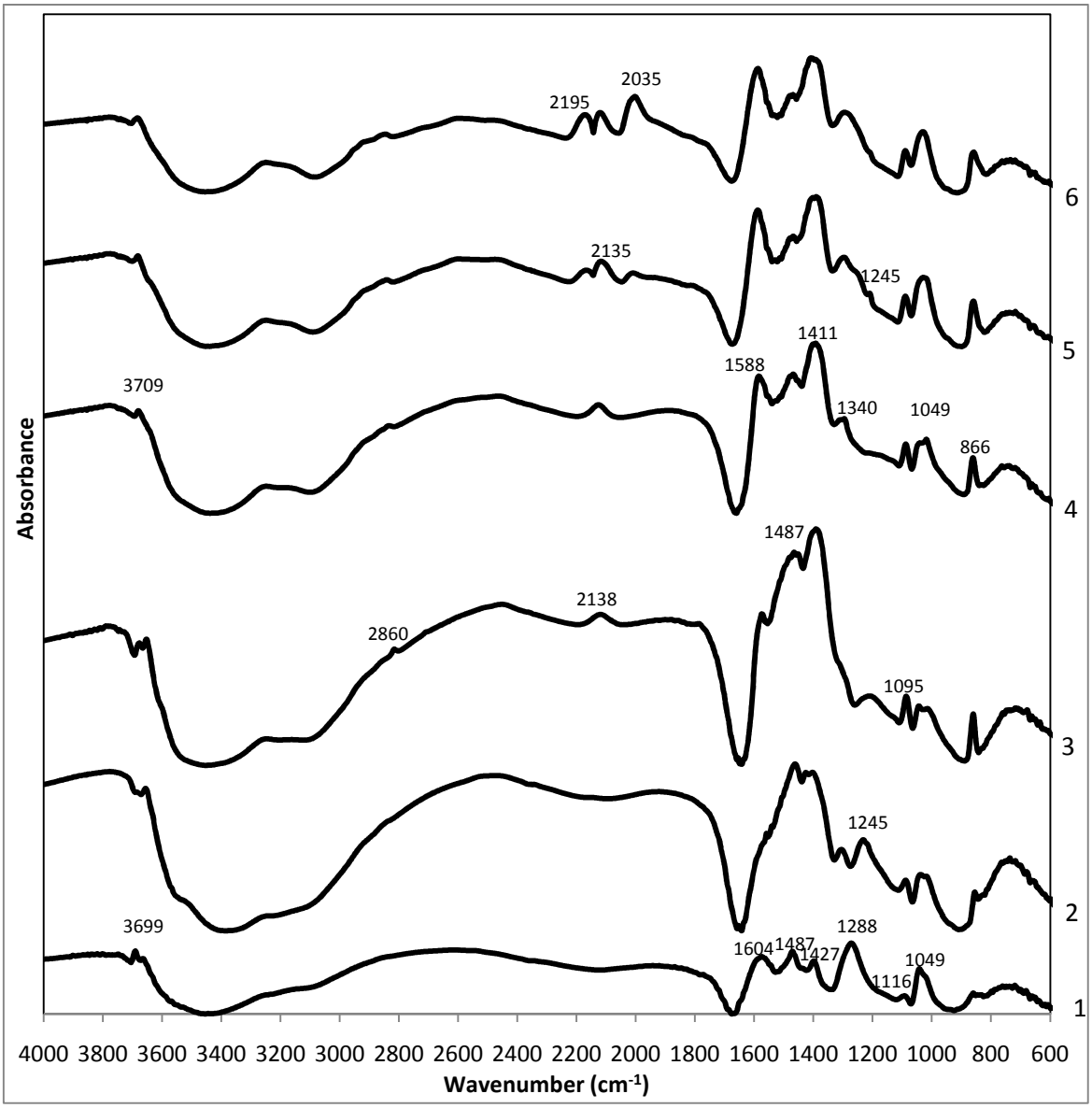

Figure 4.26. DRIFT spectra of 1%Au/Ceria (dp): (1) under He flow at room temperature, (2) under He flow at 200°C, (3) during reduction, (4) after reduction at room T, (5) under 3% CO-97 % He flow, (6) under 10%CO-90% He flow.

CO adsorption can be clearly observed on the monometallic Au catalyst with the band at 2035 cm^{-1} which can be attributed to CO linearly adsorbed on negative Au sites [33]; and those at 2195 and 2135 cm^{-1} which can be assigned to the linear CO adsorption bands on the Ce^{4+} and Ce^{3+} sites, respectively [33]. As in the case of the monometallic Re catalyst those two peaks coincide with the band resulting from the contribution the the gas phase CO. The 2195 cm^{-1} band can be perceived as a combination of gas phase CO and

linear CO adsorption on Ce^{4+} and $Au^{\delta+}$ sites [182]. It can be easily concluded from the integrals of the linear adsorption peaks that CO adsorption first starts on the Ce^{3+} sites. This result is evident from the fact that the integrals of the 2135 cm^{-1} band is nearly the same for the two spectra under CO exposure; whereas both the intensity and integral of the other adsorption sites, Ce^{4+}/ $Au^{\delta+}$ and $Au^{\delta-}$, increase as the CO concentration in the cell increases.

The changes in the DRIFT spectra of 0.5%Au-0.25%Re/Ceria (imp+dp) and 1%Au-%0.5Re/Ceria (imp+dp) can be observed through curves 1 to 6 in Figure 4.27 and 4.28, respectively. The spectra of those catalysts will be considered together in spite of the loading difference, as their method of preparation is the same. At room temperature under inert atmosphere apart from the mono- (3695 cm^{-1}) and two-coordinated (3668 cm^{-1}) OH bands and broad hydrogen bonded hydroxyl band (ca. 3250 cm^{-1}), there are virtually no distinct peaks in the spectra of the bimetallic catalysts. The indistinct bands in the O-C-O and C-H regions (1423, 1305, 1296, 1058 and 1045 cm^{-1} bands) can be attributed to carbonate species on the ceria support according to Table 2.1. When compared to the 1st spectrum of the monometallic gold catalyst, the carbonate region of the bimetallic catalysts prepared by the (imp+dp) sequence seems unsettled. As the temperature was increased from the room temperature to 200°C, formate formation was observed for both catalysts. Although vibrations of formate species formed on Ce^{3+} [53, 54] in the C-H region can be seen on the spectra (2827 and 2840 cm^{-1} bands for 0.5%Au-0.25%Re/Ceria (imp+dp) and 1%Au-0.5%Re/Ceria (imp+dp), respectively); the formate vibrations in the O-C-O region (ca. 1600 cm^{-1}) are missing or indistinct. During reduction, the formation of 2146 cm^{-1} band was observed which is assigned to the forbidden electronic transition $^2F_{5/2} \rightarrow {}^2F_{7/2}$ of Ce^{3+} on surface defect sites as discussed above. The 4th spectrum of the 1%Au-0.5%Re/Ceria (imp+dp) catalyst taken under inert atmosphere after reduction at room temperature indicates a significant decrease in the hydrogen bonded hydroxyl species (broad 3250 cm^{-1} band). Since no species other than helium was detected in the mass spectrum of the exit stream form the DRIFTS cell, one can suspect that water may have been formed during/after reduction and swept away by the inert helium to the water traps located before the mass spectrometer.

CO adsorption was clearly observed on the 0.5%Au-0.25%Re/Ceria (imp+dp) catalyst by the bands at ca. 2030 cm^{-1} which can be attributed to CO linearly adsorbed on negative Au sites [33] and/or on metallic Re sites [180]; and those at 2185 and 2130 cm^{-1} which can be assigned to the linear CO adsorption bands on the Ce^{4+} and Ce^{3+} sites, respectively [33]. The latter two bands coincide with the band resulting from the contribution of the gas phase CO as discussed previously. The 2185 cm^{-1} band can be perceived as a combination of gas phase CO, linear CO adsorption on Ce^{4+} and $Au^{\delta+}$ sites [182]. Similarly, band corresponding to the linear CO adsorption on the metallic gold sites which would appear at ca. 2100 cm^{-1} [33] could have been covered by the gaseous CO doublet. In addition, as in the case of the monometallic gold catalyst, supposedly CO adsorption first starts on the Ce^{3+} sites comparing the integrals of the adsorption bands in the 5^{th} and 6^{th} spectra: The integrals of the 2130 cm^{-1} band is nearly the same for the two spectra under CO exposure; whereas both the intensity and integral of the other adsorption sites, $Ce^{4+}/Au^{\delta+}$ and $Re/Au^{\delta-}$, increase as the CO concentration in the cell increases.

The insignificant peaks near 1840 and 1780 cm^{-1} can be attributed to the bridged CO on Au or Re metal surfaces since the vibrations attributed to the bridge type molecular CO adsorption appear between 1950-1750 cm^{-1} [180, 183]. The DRIFT spectra of 0.5%Au-0.25%Re/Ceria (imp+dp) catalyst represent an increase in the hydroxyl species proven by the slight intensity increase in the broad 3260 cm^{-1} band, and the formation of formate and bicarbonate species besides the carbonates is observed. The characteristic bicarbonate band is observed at 1210 cm^{-1} [33]. The 1319 cm^{-1} band can be attributed to carbonate or carboxylate species [33]. Simultaneously, the formation of formate species is observed with vibrations in the C-H (2868 cm^{-1} band) and O-C-O (1614 cm^{-1} band) regions.

Surface groups formed on the 1%Au-0.5%Re/Ceria (imp+dp) catalyst under CO exposure show similar changes. The formation of formate (2880 and 1600 cm^{-1} bands), carbonyl (1430, 1310, 1100, 1040 and 870 cm-1 bands), carboxylate (1310 cm^{-1} band) and bicarbonyl (1212 cm^{-1} band) species was observed as in the case of 0.5%Au-0.25%Re/Ceria (imp+dp) catalyst sample. The slight increase in the hydroxyl groups is evident from the intensity increase of the broad band between 3400-3100 cm^{-1}.

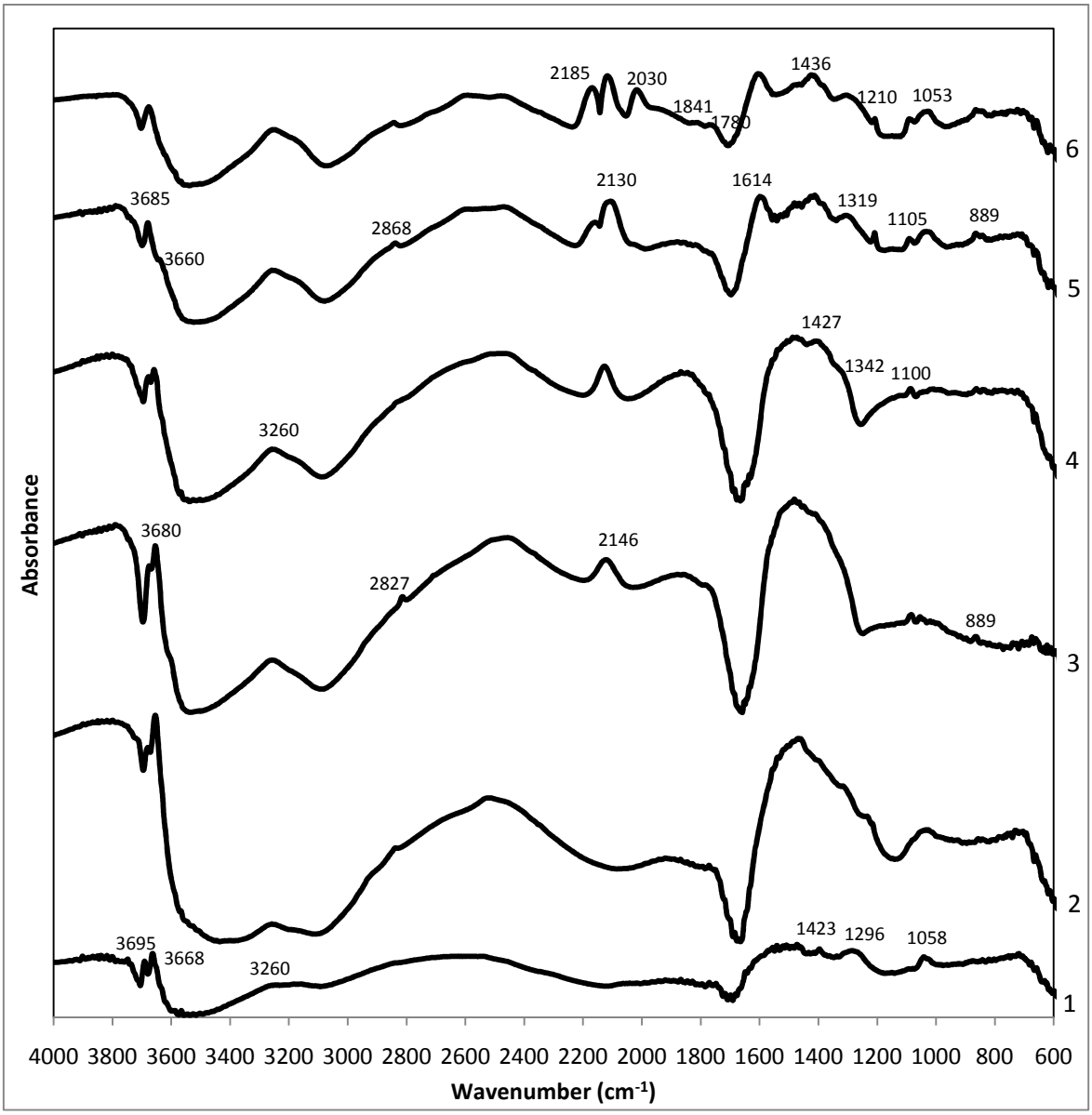

Figure 4.27. DRIFT spectra of 0.5%Au-0.25%Re/Ceria (imp+dp): (1) under He flow at room temperature, (2) under He flow at 200°C, (3) during reduction, (4) after reduction at room T, (5) under 3% CO-97% He flow, (6) under 10% CO-90% He flow.

The bridged bonded CO bands are also present on the 5th and 6th spectra of the bimetallic catalyst. As in the case of 0.5%Au-0.25%Re/Ceria (imp+dp) catalyst sample, 1837 and 1776 cm^{-1} bands are attributed to bridge type-adsorbed CO molecules on the metal surfaces. The red shift from 1841 and 1780 cm^{-1} to 1837 and 1776 cm^{-1}, respectively, can be explained by less CO species which are bridged bonded on the 1%Au-0.5%Re/Ceria (imp+dp) catalyst.

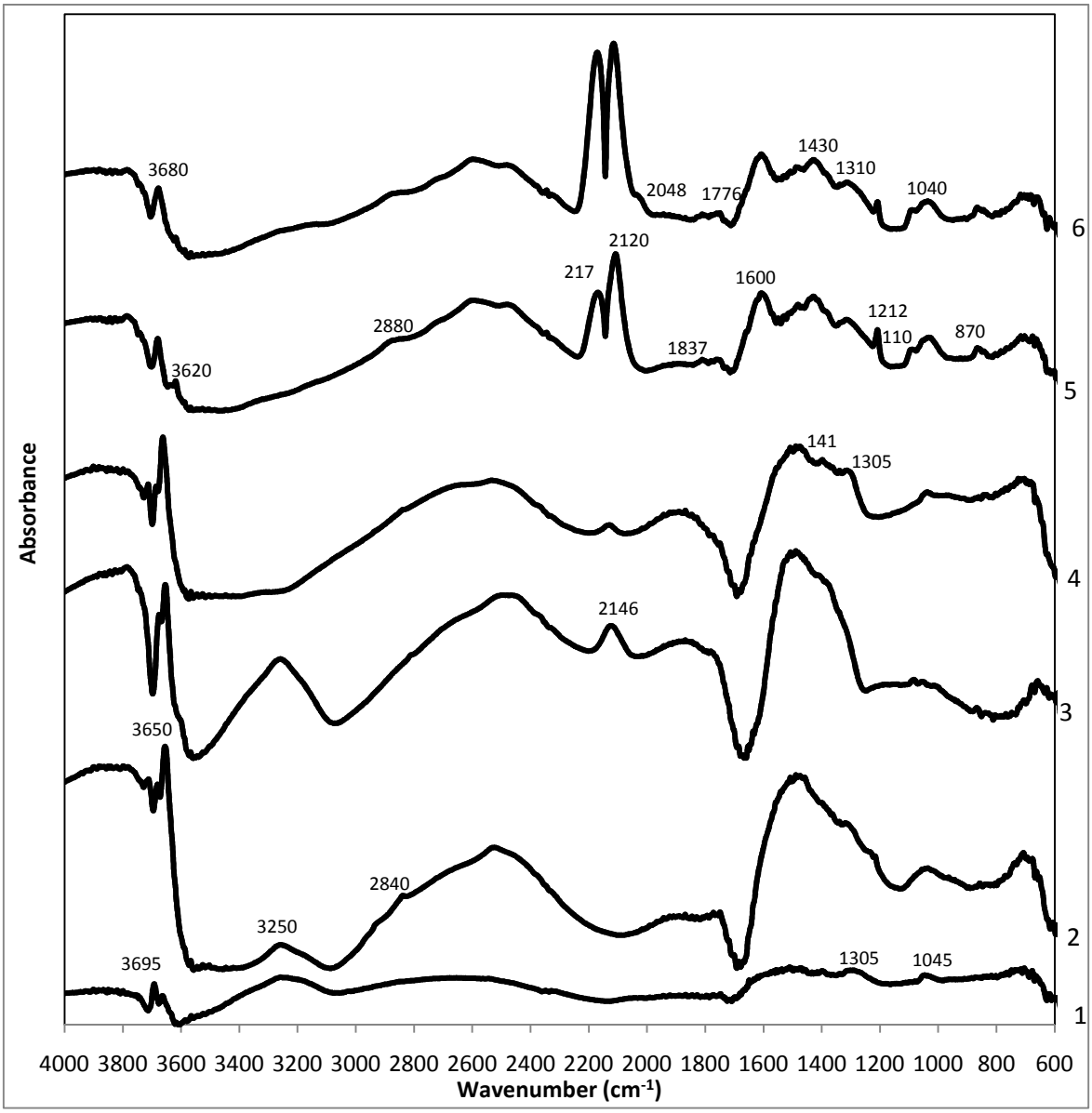

Figure 4.28. DRIFT spectra of 1Au-0.5Re/Ceria (imp+dp): (1) under He flow at room temperature, (2) under He flow at 200°C, (3) during reduction, (4) after reduction at room T, (5) under 3% CO-97% He flow, (6) under 10% CO-90% He flow.

Supporting this fact, the linear CO adsorption bands (2170 and 2120 cm^{-1} bands) intensities are much higher for 1%Au-0.5%Re/Ceria (imp+dp) catalyst compared to those of 0.5%Au-0.25%Re/Ceria (imp+dp). Since the CO gas amount sent to the DRIFTS cell is the same in both cases, the contribution of the linear adsorbed CO on $Au^{\delta+}$ and Au^{0} bands are much higher for the active 1%Au-0.5%Re/Ceria (imp+dp) catalyst sample. A weak band at 2048 cm^{-1} is also observed attributed to CO linearly adsorbed on negatively

charged Au particles when the CO concentration in the cell is increased (6^{th} spectrum of Figure 4.28).

The DRIFT spectra of 0.5%Re-1%Au/Ceria (dp+imp) catalyst under inert, reduction and CO-He atmospheres are given in Figure 4.29. As the previous characterization tests have proven the distinction between 0.5%Re-1%Au/Ceria (dp+imp) and the rest of the bimetallic catalysts led by the impregnation sequence, a consequent difference in its DRIFT spectra was also expected. At room temperature under inert atmosphere, the broad band between 3400-3100 cm^{-1}, which appeared on most of the catalyst samples under consideration, does not exist or cannot be distinguished. The only distinct band in the O-H region is the 3698 cm^{-1} band which is attributed to mono-coordinated hydroxyl species on Ce^{3+} [33]. In the O-C-O and C-H regions, distinct carbonate bands at 1490, 1420, 1309, 1053 and 980 cm^{-1} are observed. The 1587 cm^{-1} band can be assigned to bicarbonates [33] rather than formates [44] since the formate species contribution in the C-H region around ca. 2900 cm^{-1} is missing.

As in the case of other catalyst samples, rearrangement of the carbonate region was observed for 0.5%Re-1%Au/Ceria (dp+imp) catalyst in addition to hydroxyl peak intensity increase, through spectra 2 to 4 in Figure 4.29, i.e. throughout heating up to 200°C, reduction and cooling down to room temperature procedures. However, as a distinction, no formate band was observed in the C-H (3000-2600 cm^{-1}) or in O-C-O (1800-1200 cm^{-1}) regions. The formation of the band near 2146 cm^{-1} after reductive conditioning was observed which is assigned to the forbidden electronic transition $^2F_{5/2} \rightarrow {}^2F_{7/2}$ of Ce^{3+} on surface defect sites [33, 53].

As the feed was changed from pure helium gas to 3% CO – 97% He gas mixture, CO adsorption bands are observed along with formate formation and an increase in the amount of hydroxyl species. As can be seen from the 5^{th} and 6^{th} spectra of Figure 4.29, formate formation is evident from the 2890 cm^{-1} and 1612 cm^{-1} bands in the C-H and O-C-O regions, respectively. The other bands in the O-C-O (1800-1200 cm^{-1}) and C-H (1200-600 cm^{-1}) regions (i.e. 1427, 1336, 1112, 1050 and 867 cm^{-1}) are characteristic of carbonates on the support surface. The intensity increase in the broad band between 3400-3100 cm^{-1} points out to formed hydroxyl species.

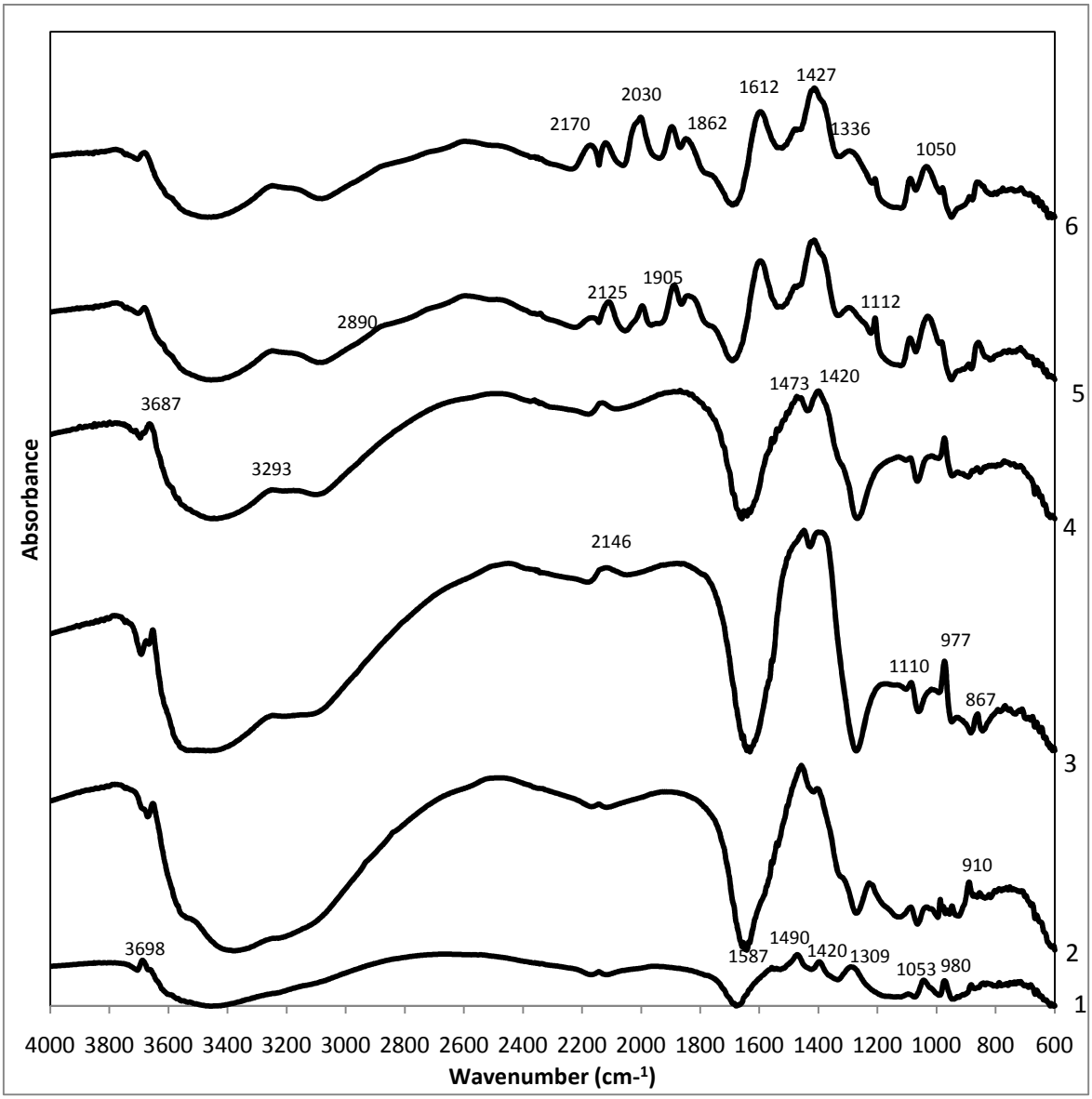

Figure 4.29. DRIFT spectra of 0.5%Re-1%Au/Ceria (dp+imp): (1) under He flow at room temperature, (2) under He flow at 200°C, (3) during reduction, (4) after reduction at room T, (5) under 3% CO-97 % He flow, (6) under 10% CO-90% He flow.

In the CO adsorption region of the spectra 5 and 6 (2300-1700 cm^{-1}), bridge-type adsorbed CO bands were observed at 1905 and 1862 cm^{-1} with high intensities. These two bands are attributed to bridge-type CO adsorption on metallic surfaces; in this case, it indicates adsorption on Au and Re, and more likely on rhenium metallic particles, since the preparation procedure applied includes the Re impregnation as the last step. Linear CO adsorption on the rhenium metal combined with the contribution from linear adsorption on

the negatively charged gold particles is represented by the 2030 cm^{-1} band. The doublet at 2070 and 2025 cm^{-1} is attributed to the CO linearly adsorbed on Ce^{4+} and Ce^{3+} along with the contribution from the gas phase CO and linear adsorption on metallic gold particles. Taking into account the gas phase contribution, it can be concluded that for 0.5%Re-1%Au/Ceria (dp+imp) catalyst, carbon monoxide was adsorbed as bridge type on metallic gold, and bridged/linear adsorption takes place on metallic Re sites.

Figure 4.30 is given in order to compare the species present on the fresh ceria support and the catalyst surfaces. A quick glance at the O-H region (3800-3000 cm^{-1}) of the spectra is sufficient to conclude that the catalysts prepared by (imp+dp) method are rich in hydroxyl groups. This conclusion is based on the higher intensity of the 3695 (mono-coordinated OH on Ce^{3+}), 3660 (two-coordinated OH on Ce^{3+}) and 3250 cm^{-1} (hydrogen-bonded hydroxyl groups) bands.

The section between 3000 and 1700 cm^{-1} in Figure 4.30 has been removed since there are no peaks in the C-H or C-O vibration regions. Considering the C-H vibrations of the formate species were not observed, the peaks ca. 1600 cm^{-1} can be attributed to bicarbonates rather than formates as in the cases of 0.5%Re/Ceria (imp), 0.5%Re-1%Au/Ceria (dp+imp) and 1%Au/Ceria (dp) catalysts. The carbonates on the support and catalyst samples can be seen clearly in the O-C-O (1700-1200 cm^{-1}) and C-H (1200-600 cm^{-1}) regions. The distinction between the catalysts prepared by (imp+dp) method and the other bimetallic or monometallic samples is very clear: The carbonate species are also observed in the spectra of 0.5%Au-0.25%Re/Ceria (imp+dp) and 1%Au-0.5%Re/Ceria (imp+dp) catalysts but with lower intensity than the carbonates on the other catalyst samples.

Figure 4.31 compares the CO adsorption characteristics of the samples as well as the species formed under CO atmosphere on the catalysts; it shows the DRIFT profiles obtained from the five monometallic and bimetallic catalysts under 3% CO–97% He atmosphere at room temperature.

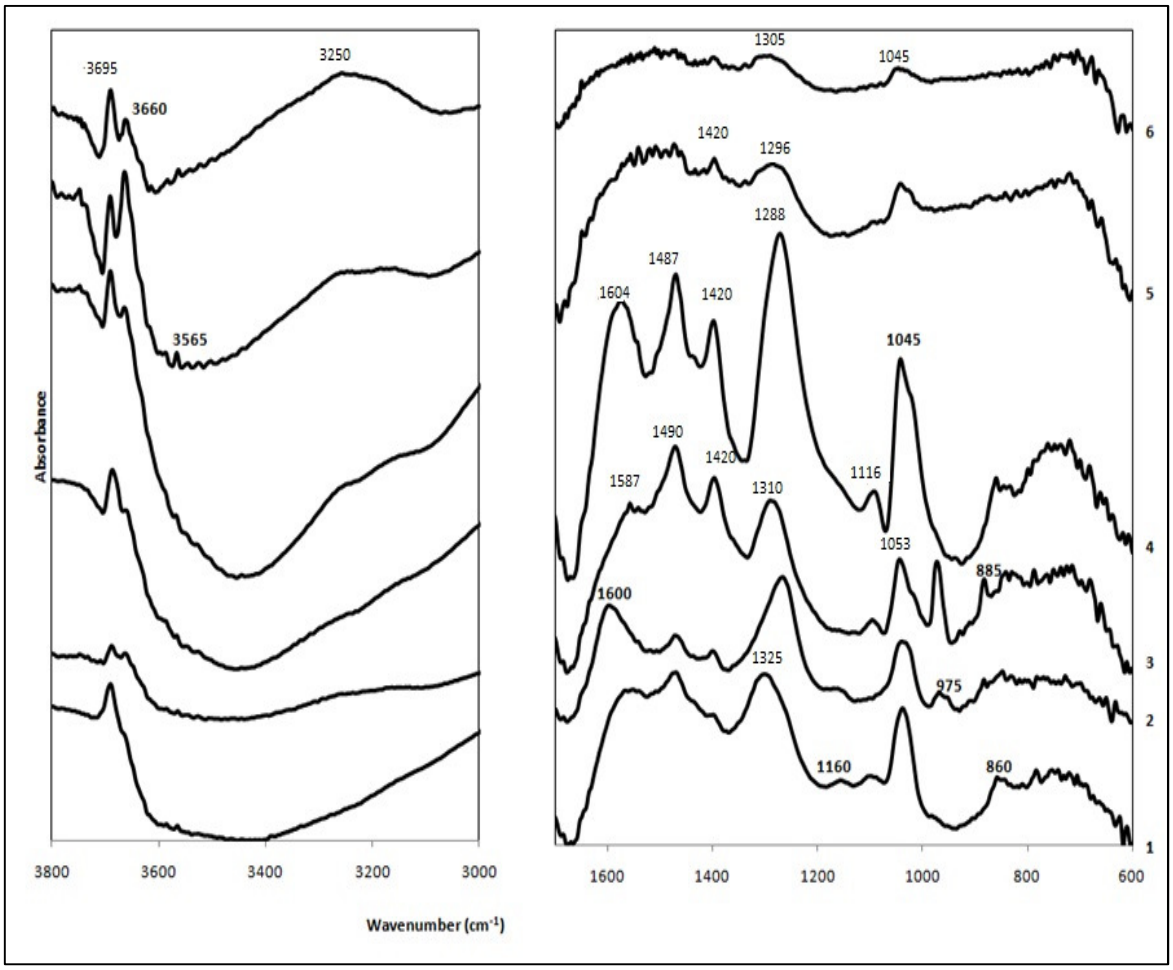

Figure 4.30. DRIFT spectra of fresh support and catalyst samples under inert atmosphere at room T: (1) Ceria, (2) 0.5%Re/Ceria (imp), (3) 0.5%Re-1%Au/Ceria (dp+imp), (4) 1%Au/ Ceria (dp), (5) 0.5%Au-0.25%Re/Ceria (imp+dp), (6) 1%Au-0.5%Re/Ceria (imp+dp).

The DRIFT profiles indicate that the reaction on the 1%Au-0.5%Re/Ceria (imp+dp) catalyst takes place between the OH groups present on the catalyst and CO. The IR intensity of the broad 3250 cm^{-1} band has decayed due to CO exposure. Simultaneously, the formation of the surface formate ($CHOO^-$) species in C-H (ca. 2900 cm^{-1}) and O-C-O (ca. 1600 cm^{-1}) regions, along with surface carbonates (CO_3^{-2}) and bicarbonate (HCO_3^-) species (1212 cm^{-1}) was observed. No intensity decrease in the OH bands was observed for the other catalyst samples although it was expected since formate formation is common to all samples. It can be concluded that carbonate formation is dominant for the other catalyst samples as a result of the reaction between CO gas and ceria lattice oxygen.

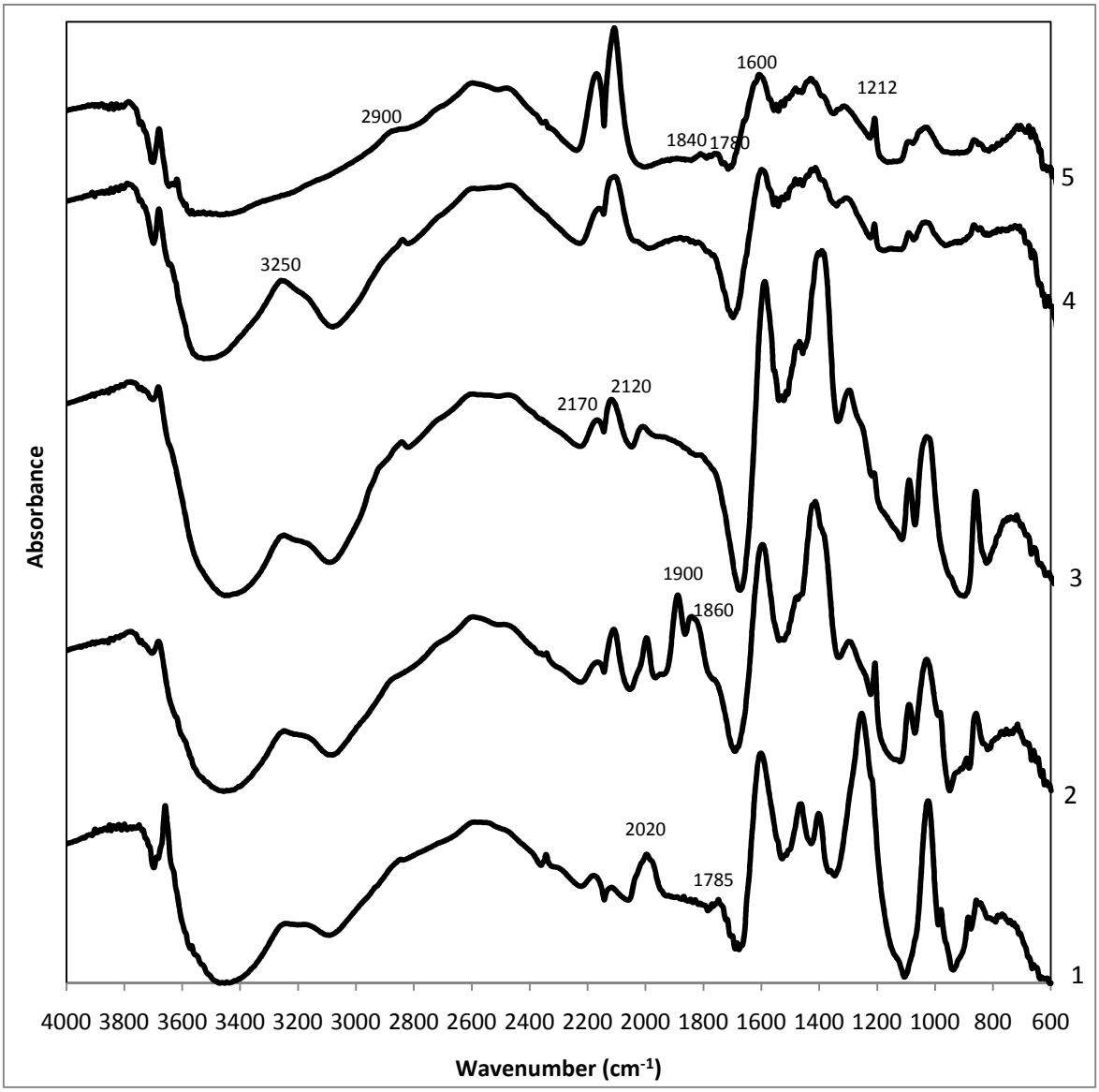

Figure 4.31. DRIFT spectra of reduced catalyst samples under 3%CO-97%He flow at room temperature: (1) 0.5%Re/Ceria (imp), (2) 0.5%Re-1%Au/Ceria (dp+imp), (3) 1%Au/ Ceria (dp), (4) 0.5%Au-0.25%Re/Ceria (imp+dp), (5) 1%Au-0.5%Re/Ceria (imp+dp).

A comparison in the C-O region reveals the difference in the adsorption characteristics of the catalyst samples. Under the same conditions (3% CO balance He flow), linear (2010 cm^{-1}) and bridged (1785 cm^{-1}) adsorption of CO on the Re metal sites of the monometallic Re catalyst were observed. As discussed above, the doublet at ca. 2170 and 2120 cm^{-1} is attributed to the linear adsorption of CO on Ce^{4+} and Ce^{3+} sites, respectively, with the contribution from the gas phase CO. This doublet is common to all catalyst samples, though its intensity and area vary. The intensity difference stems from the

contribution of the linear CO adsorption on Au^0 particles which should appear at 2100 cm^{-1}, to the 2120 cm^{-1} band. The results show that, CO is linearly adsorbed on gold metal particles on the catalysts following the order 1%Au-0.5%Re/Ceria (imp+dp) > 0.5%Au-0.25%Re/Ceria (imp+dp) > 1%Au/Ceria (dp) = 0.5%Re-1%Au/Ceria (dp+imp). It can be clearly seen from Figure 4.31 that bridge-type CO adsorption is evident on 0.5%Re-1%Au/Ceria (dp+imp) catalyst on Au^0 and Re^0. When 0.5%Re-1%Au/Ceria (dp+imp) and 1%Au-0.5%Re/Ceria (imp+dp) samples are compared on the basis of bridged adsorbed CO molecules, the red shift from ca. 1900 and 1860 cm^{-1} to 1840 and 1780 cm^{-1}, respectively, accompanied by the intensity decrease, can be explained by less bridge-type adsorbed CO species on the 1%Au-0.5%Re/Ceria (imp+dp) catalyst.

It should be noted that the DRIFTS experiments conducted may give an insight to what would go on during the WGS experiments, it would be wrong to state a WGS mechanism merely based on those results. The surface/intermediate species which would form on the catalysts' surfaces under a feed containing both CO and H_2O is of crucial importance.

4.3.2. WGS Performance Tests – Real Feed

In order to accomplish a complete WGS study on the Au-Re/Ceria catalysts, performance tests under real feed conditions have been conducted. The effect of CO_2 and H_2 addition to the feed stream was investigated aiming to observe the WGS activity of the monometallic and bimetallic ceria based catalysts under reaction conditions very close to those in a fuel processor. The performance test results presented were obtained using feed compositions presented in Table 3.11. The tests were conducted at atmospheric pressure, within the temperature range 250-350°C using 75 mg of catalyst with 120000 $mlg^{-1}h^{-1}$ GHSV and balance N_2.

Results of catalytic performance tests obtained over bimetallic and monometallic catalysts under two different feed conditions are shown in Figures 4.32 and 4.33 as CO conversion and hydrogen production percentages. The feed compositions used in Figure 4.32 and 4.33 are the 3rd and the 1st feeds in Table 3.11, respectively. For the other three feed conditions studied no hydrogen production was observed; the hydrogen in the feed

was consumed to produce water. No methane production was observed as in the preliminary tests. A comparison of the catalysts' performance under feeds having H_2O/CO feed ratios of 6.73 and 16.13 reveals that with the increase in the H_2O/CO ratio, carbon monoxide conversion increases for the 1%Au-0.5%Re/Ceria (imp+dp) catalyst. The carbon monoxide conversion over the 1%Au/Ceria (dp) catalyst is nearly the same for the two H_2O/CO feed ratios. These results highly resemble the results of the WGS study under idealistic feed conditions; at high H_2O/CO ratios bimetallic 1%Au-0.5%Re/Ceria (imp+dp) catalyst is more active than the monometallic gold catalyst despite CO_2 and H_2 addition to the feed.

CO conversion level is not the best way to represent the WGS performance results if the feed dealt with is the real feed having large hydrogen content. It is evident from the results of the WGS reaction tests conducted under real feed conditions that there is a pronounced decrease in H_2 concentration in the product streams compared to that in the feed for the samples studied except for 1%Au-0.5%Re/Ceria (imp+dp) catalyst (Figures 4.32-b and 4.33-b). The CO conversion levels reached for 1%Au/Ceria (dp) sample especially at lower H_2O/CO ratios, may point to an active and selective WGS catalyst, however when the hydrogen levels in the product stream are considered, it is very clear that the main product is being consumed.

The best WGS performances for the bimetallic 1%Au-0.5%Re/Ceria (imp+dp) catalyst are obtained at 300°C under realistic feed conditions with high H_2O/CO ratios in the feed. The results obtained reveal 1%Au-0.5%Re/Ceria (imp+dp) catalyst is a potential candidate which enables the use of a single WGS unit operating at a mid-range, i.e. HTS-LTS transition, temperatures in a fuel processor instead of a two-stage WGS operation in separate HTS and LTS units.

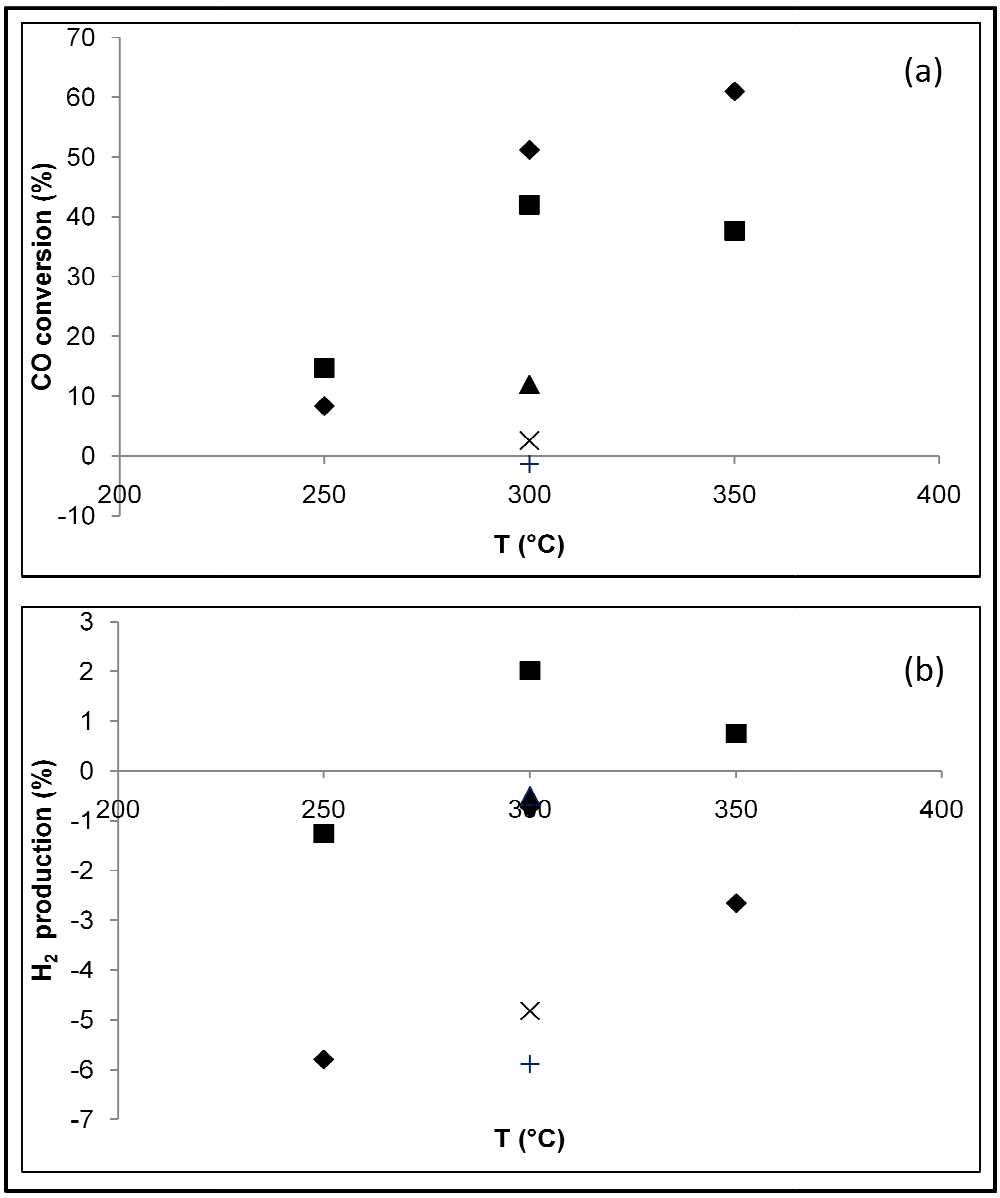

Figure 4.32. (a) CO conversion, (b) H_2 production as a function of T (4.9%CO, 32.7%H_2O, 30.0%H_2, 10.4%CO_2, balance N_2); (♦)1%Au/Ceria(dp); (■)1%Au-0.5%Re/Ceria(imp+dp); (▲)0.5%Re-1%Au/Ceria(dp+imp); (+)0.5%Re-1%Au/Ceria(si); (×) 0.5%Re/Ceria(imp).

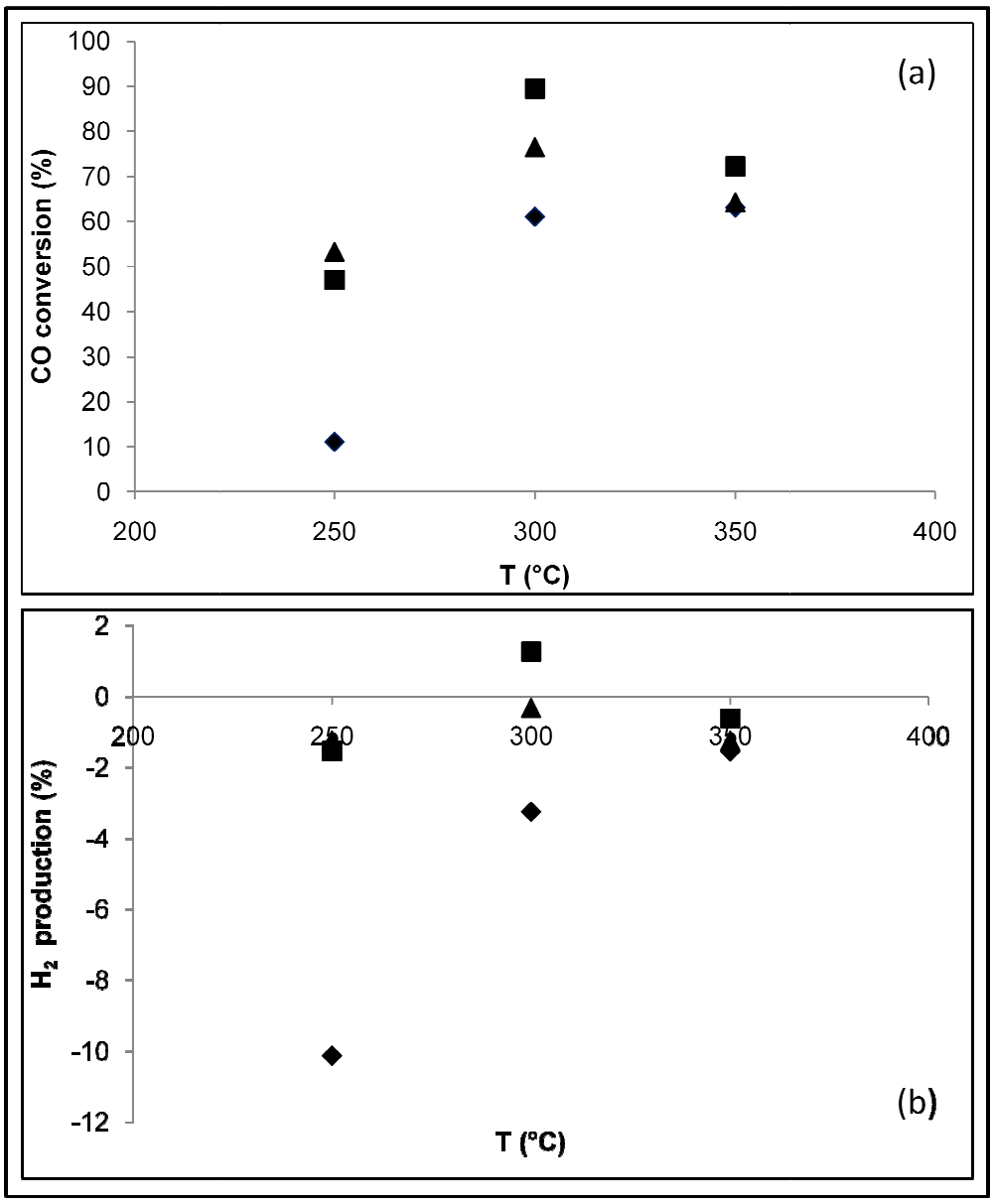

Figure 4.33. (a) CO conversion, (b) H_2 production as a function of temperature (2.1% CO, 34.1% H_2O, 23.7% H_2, 12.3% CO_2, balance N_2); (♦) 1%Au/Ceria (dp); (■) 1%Au-0.5%Re/Ceria (imp+dp); (▲) 0.5%Au-1%Re/Ceria (imp+dp).

4.4. DRIFTS and Adsorption Studies over Pt-Sn/AC3

Pt-Sn/AC3 catalyst has been reported to have high activity and selectivity for the preferential oxidation of CO as discussed in Section 2.2.2.1. With the aim of understanding the reason of superior performance of this catalyst, DRIFTS and CO adsorption studies were conducted on both Pt-Sn/AC3 and Pt/AC3; the latter, which is not active for PROX, will be used as the reference basis. CO_2 adsorption studies were performed as well in order to comprehend the PROX mechanism under real feed conditions.

4.4.1. DRIFTS Studies

In order to analyze the processes taking place over the catalysts during PROX reaction in detail, the catalysts have been analyzed by operando-FTIR-DRIFTS-MS. Figures 4.34 and 4.45 show the DRIFTS results obtained over Pt/AC3 and Pt-Sn/AC3 catalysts, respectively, before reaction and after exposure to reaction mixture (50 ml/min; 1% CO, 1.25% O_2, 60% H_2, balance He).

Figure 4.36 is also given in order to compare the behavior of the catalysts under reaction conditions. Figures 4.34, 4.35 and 4.36 show typical DRIFT spectra obtained under PROX conditions over Pt/AC3 and Pt-Sn/AC3 catalysts. More specifically, the spectra refer to conditions as established 5 min after switching from He to reaction mixture (CO, O_2, H_2, He) at 135ºC and atmospheric pressure. The data collected after 5 min time-on-stream (TOS) correspond to a stable gas phase composition of the reactor effluent as confirmed by MS.

The spectral zone in the 3800–2800 cm^{-1} range displays bands mostly attributable to hydroxyl species. In both cases, the spectra are dominated by a broad band extending along this range and displaying a maximum at ca. 3250 cm^{-1}, which is attributed to O-H stretches from hydroxyl, phenolic and carboxylic groups [116, 122, 124, 126]. This band diminishes for AC1 sample after the HCl treatment and gains intensity due to HNO_3 treatment for AC3 (not shown). The weak and broad band at 3600 cm^{-1} is assigned to the O-H stretching vibration in free –OH [122]. The observed increase in peak intensity of 3250 cm^{-1} band is significant for Pt/AC3 and Pt-Sn/AC3 catalysts during DRIFTS-MS

reaction tests. This increase was ~ 2 folds (190%) for Pt/AC3 and 113% for Pt-Sn/AC3 catalyst which is in agreement with the evolution of PROX; reaction intermediate hydroxyl species diminish to a lower value due to production of water for Pt-Sn/AC3 catalyst having greater activity. The band at ~2875 cm^{-1} appearing in all spectra can be attributed to formate species present on the catalysts which are unaffected from the reaction at any temperature [61, 184].

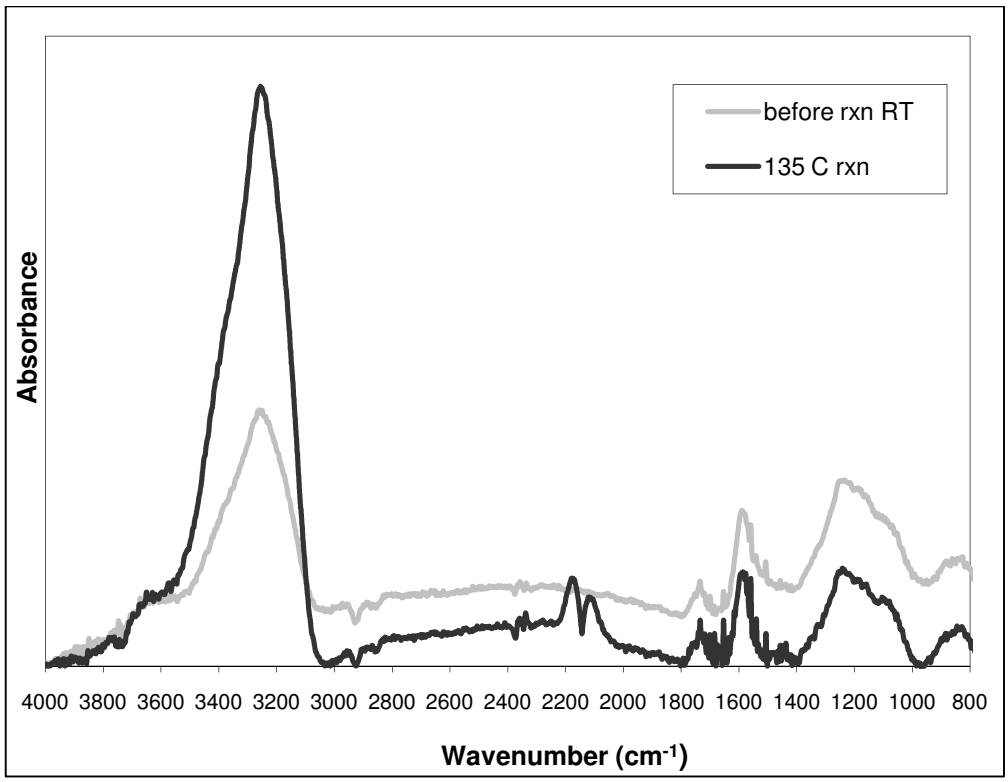

Figure 4.34. DRIFT spectra of Pt/AC3 under He flow at room temperature and in the presence of PROX reaction mixture (1% CO, 1.25% O_2, 60% H_2, balance He).

The feature extending from 2380 to 2270 cm^{-1} is associated with the asymmetric stretching vibration of gas-phase CO_2 [61, 79]. The carbon dioxide signal mainly originates from ambient air absorption in the optical path outside the DRIFTS cell. This spectral region is therefore not evaluated, as CO_2 variations in the ambience are usually larger than those in the DRIFTS cell. The spectra taken under reaction conditions contain vibro-rotational transitions associated with gaseous CO, the maximum of the R-branch appearing at 2166 cm^{-1} and that of the Q-branch appearing at 2105 cm^{-1} [185]. No bands corresponding to linearly adsorbed (~2060 cm^{-1}) or bridge-type adsorbed CO (~1825 cm^{-1}) were observed for neither catalyst [88].

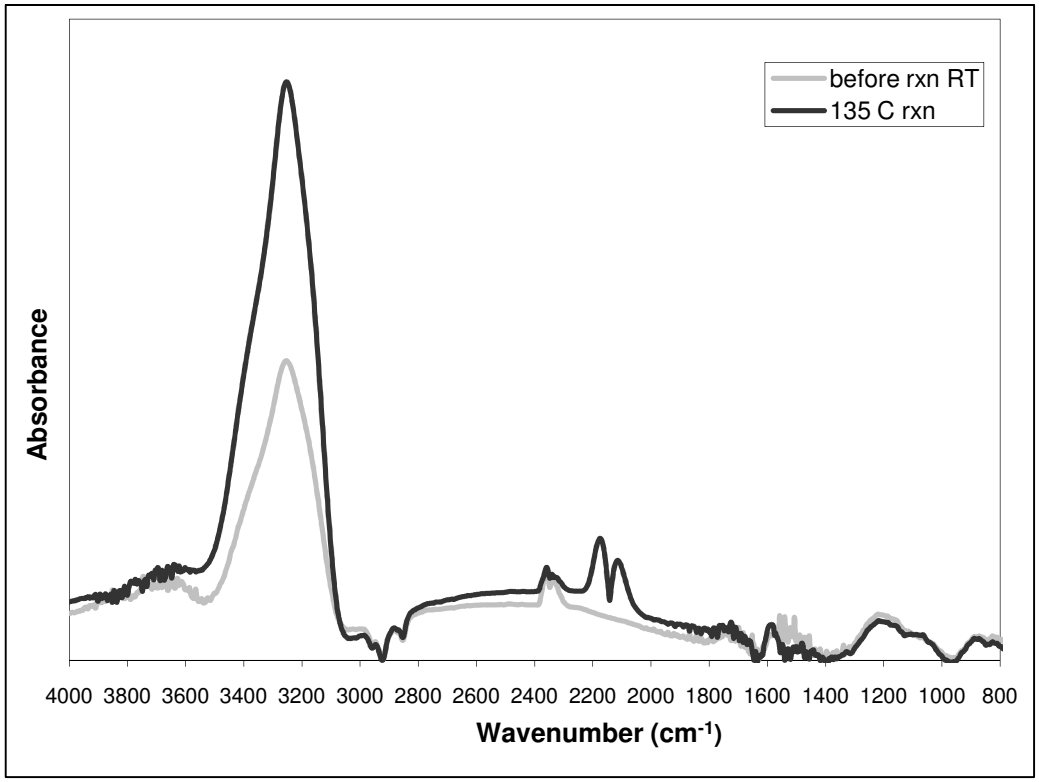

Figure 4.35. DRIFT spectra of Pt-Sn/AC3 under He flow at room temperature and in the presence of PROX reaction mixture (1% CO, 1.25% O_2, 60% H_2, balance He).

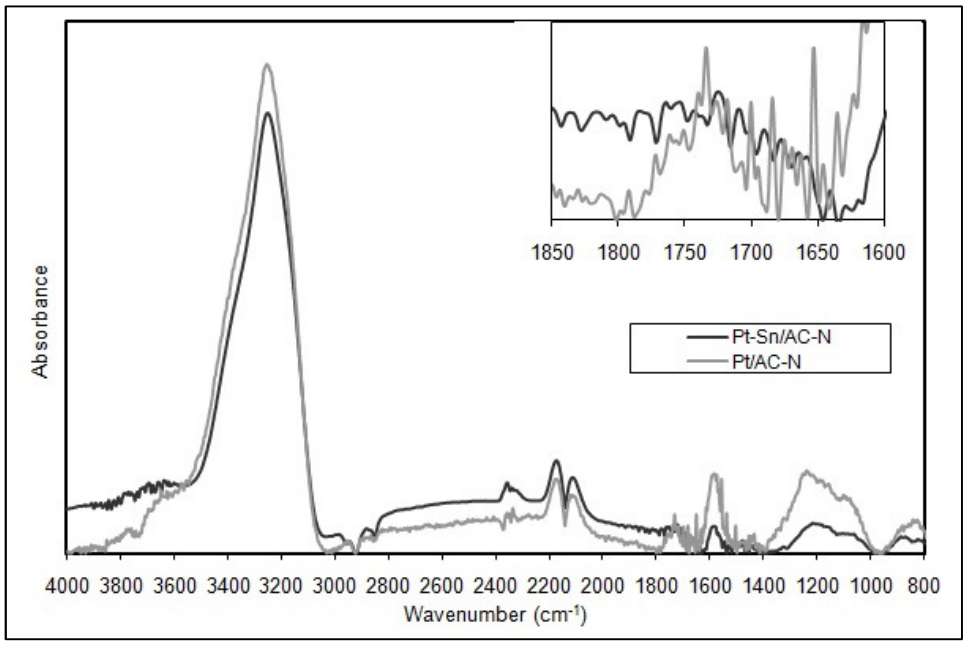

Figure 4.36. DRIFT spectra of Pt/AC3 and Pt-Sn/AC3 in the presence of PROX reaction mixture at 135ºC.

All spectra contain broad bands associated with the chemistry of the AC3 support in the 1800-700 cm^{-1} region. The peak near 1750 cm^{-1} is attributed to C=O band in carboxylic groups, lactones and anhydrides [126, 127, 131, 133]. The peak near 1600 cm^{-1} is associated with the quinone functional groups [126, 133] which are present in AC3 support. The broad peak at 1250 cm^{-1} is the C-O stretching in carboxylic anhydrides, phenols, ethers and lactones [133], and the 800 cm^{-1} band can be attributed to aromatic C-H out-of plane bending vibrations [125, 134].

The 3250 cm^{-1}, 1750 cm^{-1} and 1250 cm^{-1} bands indicates the presence of carboxylic acid groups on the surface of the catalyst. Since Pt-Sn/AC3 does not have the 1750 cm^{-1} band (Figure 4.35) which is present in the DRIFT spectra of the AC3 support (not shown), it can be concluded that upon calcination and reduction treatments of the catalyst, the carboxylic acid groups were decomposed. Decomposition of the carboxylic acid groups during pretreatment steps leads to mobility of the metallic precursors originally anchored to them and enhance the Pt-Sn interaction which results in the formation of Pt_3Sn alloy [101, 102].

Since the gaseous CO signal completely cover the CO adsorption band on the AC-based catalysts [88] under the reaction conditions, it is possible that the linearly adsorbed CO band overlaps the gaseous CO signal. For further investigation of adsorption over catalyst samples, individual CO adsorption and O_2 adsorption DRIFTS tests were conducted on both catalysts at 110ºC. The CO adsorption experiments were conducted under 1%, 6%, 10% and 20% CO levels with balance inert flow. Figures 4.37 and 4.38 show the DRIFT spectra of Pt/AC3 and Pt-Sn/AC3, respectively. The bands attributed to the adsorption of CO on Pt are absent in the spectrum of Pt/AC3. Since Pt/AC3 catalysts is inactive for CO oxidation [102] and our preliminary studies show that it is inactive for PROX as well, no change upon CO exposure was observed over that sample as expected. The intensity of the 3250 cm^{-1} band has slightly increased due to increase in the CO amount in the mixture. This increase was 5.7% under 1%CO-He mixture flow. The percentage increase in the intensity of 3250 cm^{-1} band in the case of Pt-Sn /AC3 is only 2.3%.

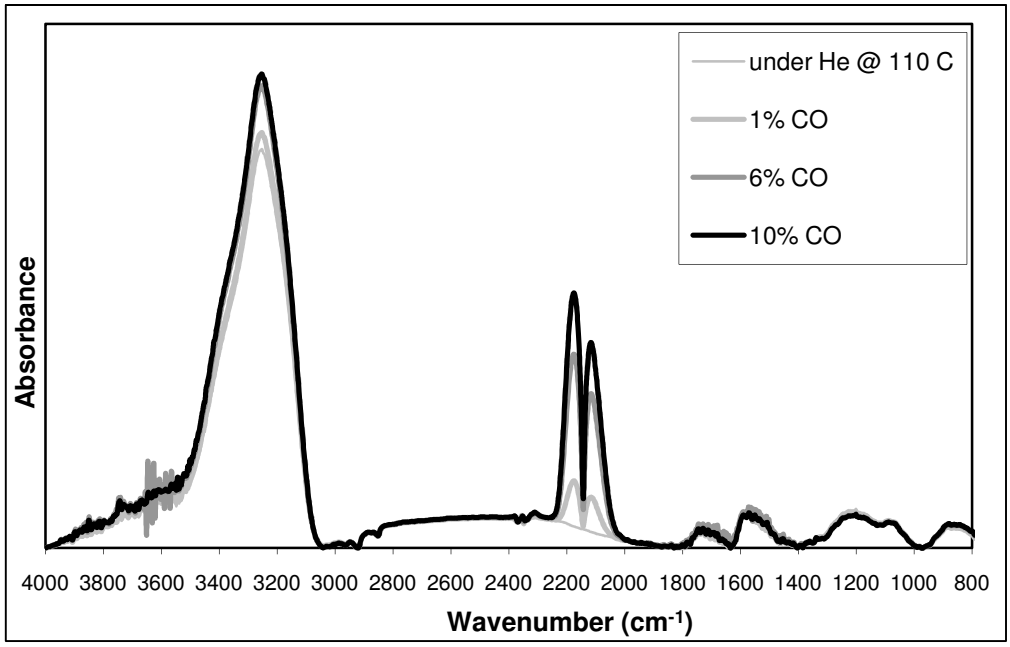

Figure 4.37. CO adsorption DRIFT spectra of Pt/AC3 sample in the presence of different % CO in He.

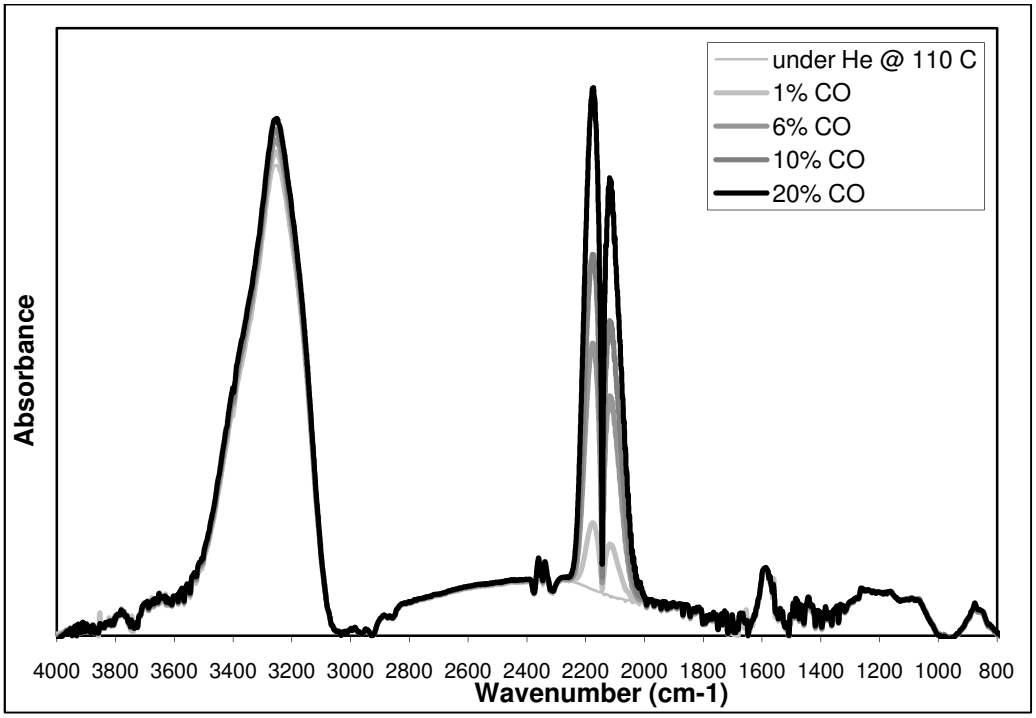

Figure 4.38. CO adsorption DRIFT spectra of Pt-Sn/AC3 sample in the presence of different % CO in He.

Figure 4.39 presents the DRIFT spectra of the two catalyst samples under 1%CO-He mixture flow. The linearly adsorbed CO band (~2054 cm^{-1}) was clearly observed only for Pt-Sn/AC3, however bridge-type adsorbed CO band which would appear near 1820 cm^{-1}, was not present [88]. It is known from surface science studies that CO is linerly adsorbed on Pt (111) surface, but above 0.33 ml coverage limit, direct repulsive forces between adsorbed CO molecules start to dominate due to the decreased distance between CO molecules, and bridge-type adsorption becomes more stable than atop adsorption. On the other hand, the flat potential energy surface accompanied with the lack of a lateral adsorbate interaction enables the existence of linear adsorption on the Pt_3Sn (111) surface [186, 187], which is in accordance with our current results.

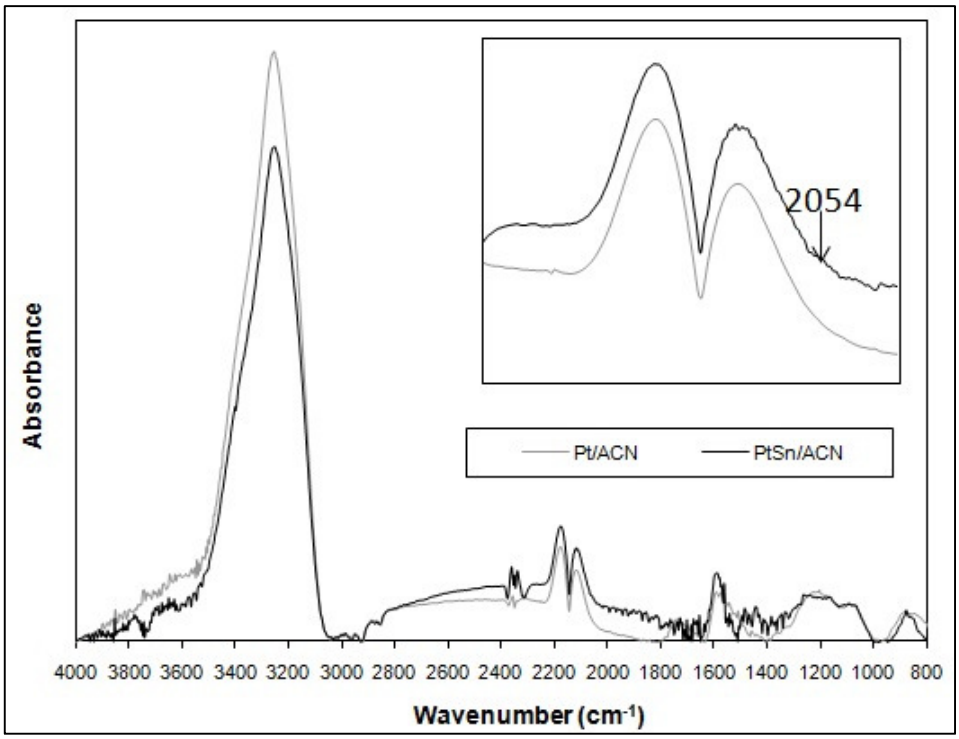

Figure 4.39. CO adsorption DRIFT spectra of Pt/AC3 and Pt-Sn/AC3 samples in the presence of 1 % CO in He.

The O_2 adsorption experiments were conducted under 1.25%, 6% and 20% O_2 and balance inert flow (Figures 4.40 and 4.41). The intensity increase of the 3250 cm^{-1} band as a result of higher oxygen content in the feed was observed for both catalysts; the rise in response to increase in O_2 concentration being more significant for Pt-Sn/AC3 (Figure

4.41). The percentage increase of the band is 18.8 and 21.0 for Pt/AC3 and Pt-Sn/AC3, respectively.

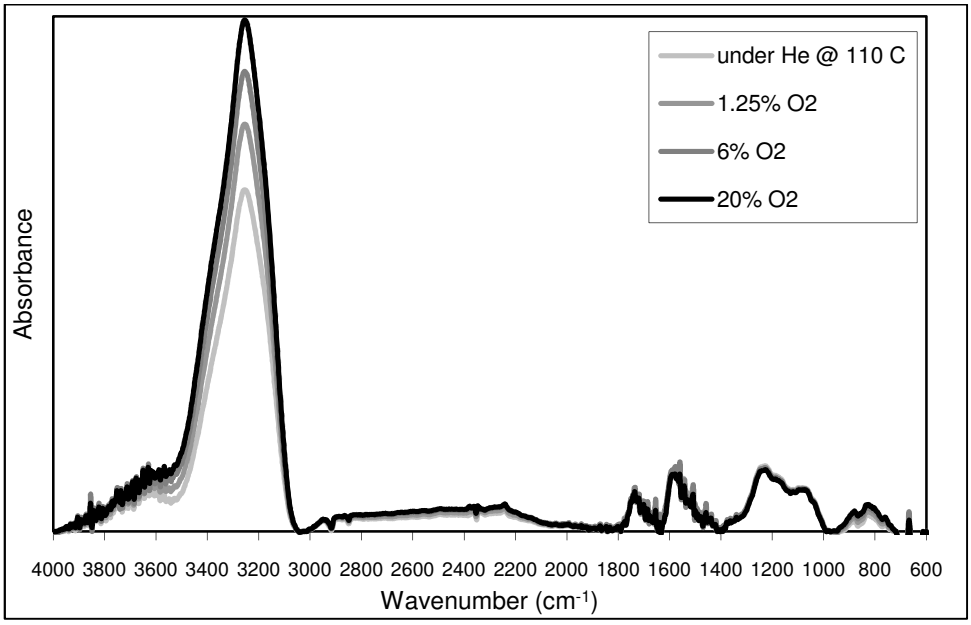

Figure 4.40. O_2 adsorption DRIFT spectra of Pt/AC3 sample in the presence of different % O_2 in He.

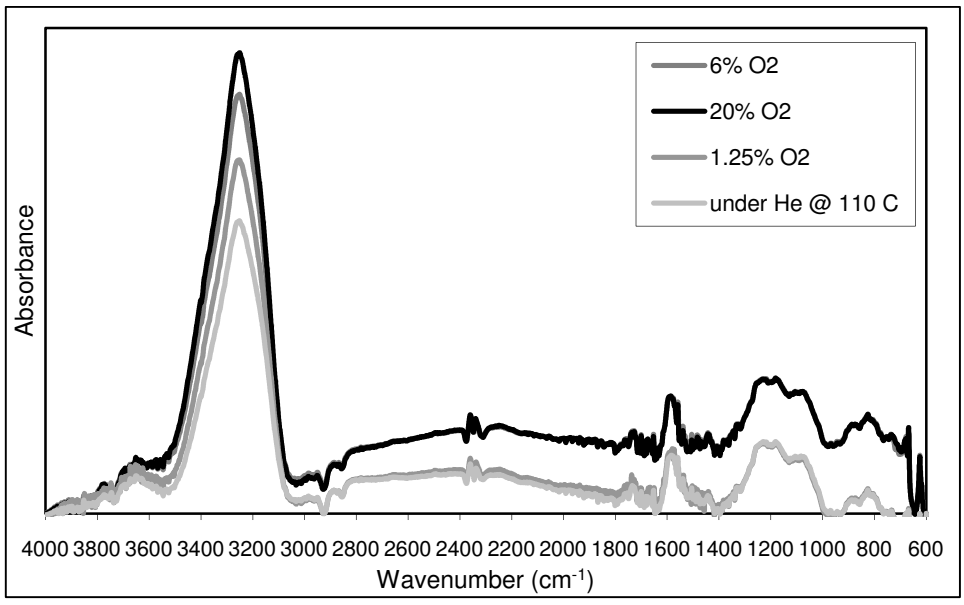

Figure 4.41. O_2 adsorption DRIFT spectra of Pt-Sn/AC3 sample in the presence of different % O_2 in He.

4.4.2. Adsorption Studies

Carbon monoxide and carbon dioxide adsorption isotherms were obtained for fresh AC3, Pt/AC3 and Pt-Sn/AC3 at 25, 110, 115, 125 and 135ºC. A representative plot of CO_2 and CO adsorption isotherms of Pt-Sn/AC3 sample is given in Figure 4.42. The adsorption data were fitted to standard isotherm models; Langmuir and Dubinin-Radushkevich. The best fitting isotherm model was Dubinin-Radushkevich [Eq (2.16)]. The regression coefficients and the constants for the adsorption of CO_2 on the adsorbents are presented in Table 4.3.

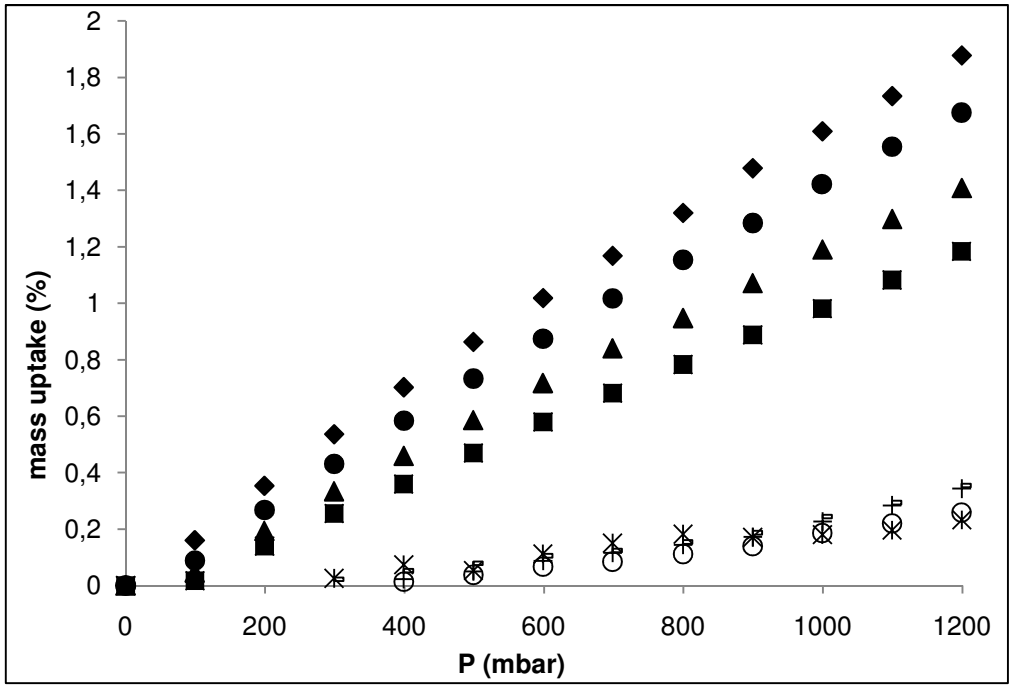

Figure 4.42. CO_2 (♦ 110 ºC, ●115ºC, ▲125ºC, ■ 135ºC) and CO (* 110 ºC, ○115ºC, + 125ºC, - 135ºC) adsorption isotherms of Pt-Sn/AC3 sample.

It should be noted that as a_0 values obtained for AC3 and Pt/AC3 confirm each other for the whole temperature range, those values can be considered as a measure of micropore volume. On the other hand, the a_0 values obtained for Pt-Sn/AC3 sample slightly deviates from those obtained for AC3 and Pt/AC3 most probably due to the double calcination procedures applied on that sample and the consequent changes in its structure.

Table 4.3. Constants of Dubinin-Radushkevich isotherm model for the adsorption of CO_2 on the adsorbent samples.

Adsorbent	T (°C)	Regression Coefficient	E (kJ/mol)	a_0 (g/g adsorbent)
Pt-Sn/AC3	110	0.9997	13.60	0.482
	115	0.9970	13.36	0.583
	125	0.9990	13.36	0.722
	135	0.9981	13.37	0.904
Pt /AC3	110	0.9999	14.20	0.302
	115	0.9997	13.71	0.408
	125	0.9992	13.69	0.503
	135	0.9986	13.92	0.534
AC3	110	0.9960	14.29	0.371
	115	0.9994	14.24	0.426
	125	0.9988	14.26	0.477
	135	0.9985	14.21	0.566

The isosteric heat of adsorption of carbon dioxide, Q, at a given surface loading was calculated from the adsorption isotherms at different temperatures using Clausius Clapeyron equation [Eq (2.12)]. The isosteric heat of adsorption values for the Pt-Sn/AC3, Pt/AC3 and AC3 samples are plotted in Figure 4.43. The value of heat of adsorption on Pt-Sn/AC3 and Pt/AC3 decreased slightly from 33.1 kJ/mol to 28.9 kJ/mol and from 33.7 kJ/mol to 29.0 kJ/mol, respectively, while CO_2 loading (ie. the adsorbed amount of CO_2) increased from 0.4% to 0.8%. As a result of increased CO_2 loading there was a smaller decrease in the isosteric heat of adsorption of AC3 sample led by weak repulsive interactions between adsorbed CO_2 molecules [156] and the value of Q was about 35 kJ/mol. Results indicate that the difference in the strength of CO_2 adsorption on AC3, Pt/AC3 and Pt-Sn/AC3 is within ca. 0.8 kJ/mol (Table 4.3). Thus, the heat of adsorption values of CO_2 on Pt/AC3 and Pt-Sn/AC3 samples are very close. It is known that CO_2 addition to the feed diminishes CO oxidation activity and stability of metal oxide supported Pt-SnO_x systems [62, 105] due to the presence of mobile CO_2 on the support impeding O_2 transfer (Figure 4.44). This negative effect is eliminated for Pt-Sn/AC3 due to the properties of both its support and alloy type active sites. Its support has significantly

greater CO_2 adsorption capacity compared to those of Pt/AC3 and AC3 led by the decomposition of its carboxylic acid groups during its double calcination and reduction steps leaving available sites ready for CO_2 adsorption on its support. Although CO_2 adsorption strength of Pt-Sn/AC3 is slightly lower, its surface has capacity to adsorb and stabilize CO_2. Its alloy type active centers have ensembles of Pt atoms for CO adsorption and Sn- and Sn-Pt ensembles for O- adsorption at the atomic distances. By this way, the necessity of O-spillover (or transfer) through the support is completely eliminated.

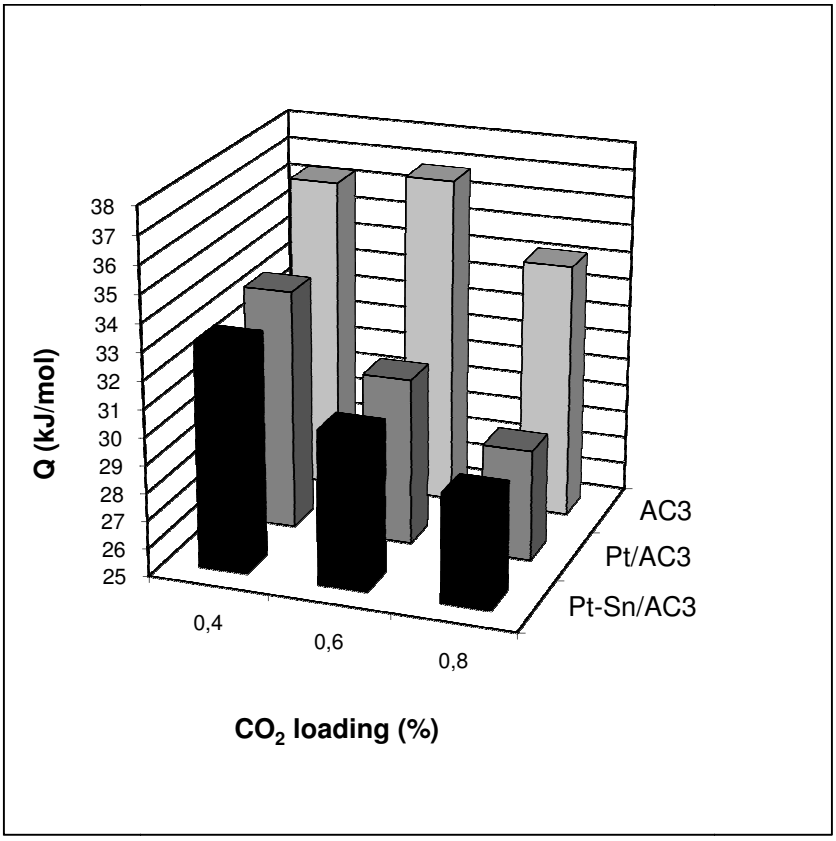

Figure 4.43. Isosteric heat of adsorption values for the Pt-Sn/AC3, Pt/AC3 and AC3 samples.

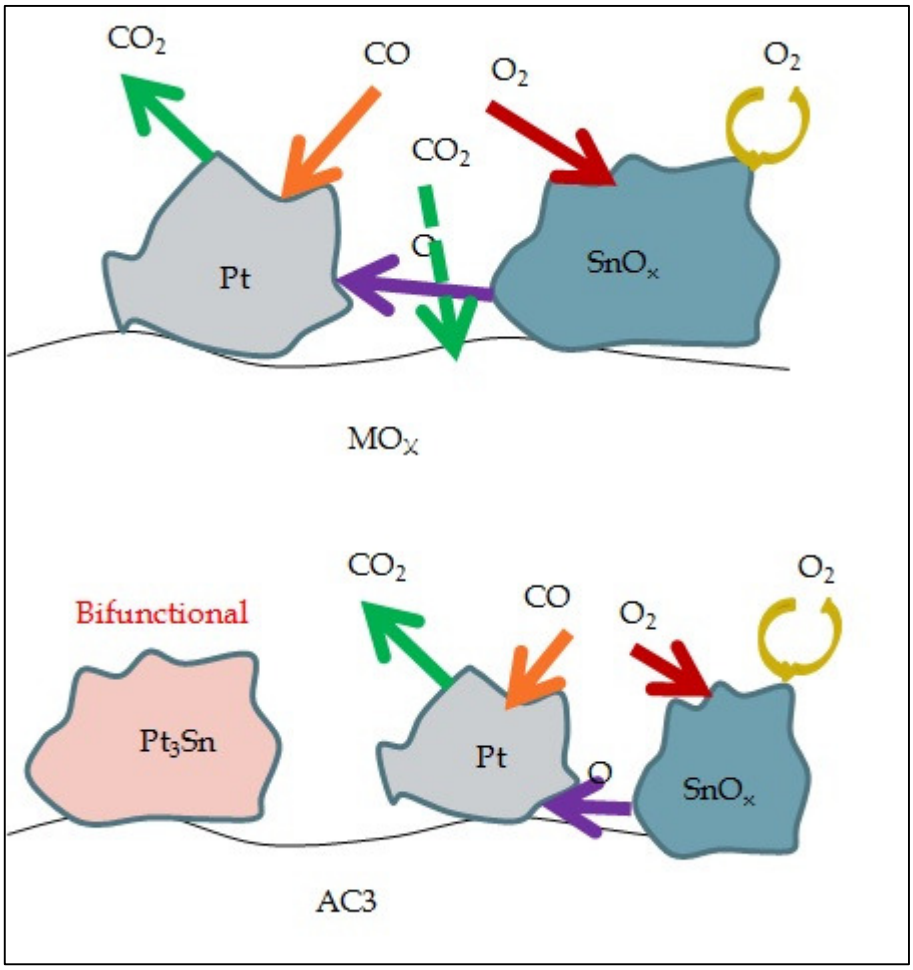

Figure 4.44. Schematic representation of CO oxidation over MO_x (top) and AC3 (bottom) supported Pt-SnO_x system.

The results of the CO adsorption studies indicate that CO adsorption on the samples should have chemical nature. On the other hand, the CO adsorption behavior could not be explained by any of the standard models. Thus, it should be somehow an activated type adsorption besides its –should be- chemical nature. Figures 4.45-4.47 show the adsorption isotherms of Pt/AC3 and Pt-Sn/AC3 catalysts at different pressure ranges. In the pressure range 300-1200 mbar CO adsorption capacity of Pt-Sn/AC3 is much higher than Pt/AC3 and CO mass uptake increases as the temperature increases. Contrarily, the CO mass uptake of Pt-Sn/AC3 sample at 50 mbar at the PROX test temperatures are ca. 0.032% (110ºC), 0.022% (115ºC), 0.01% (125ºC) and 0.005% (135ºC).

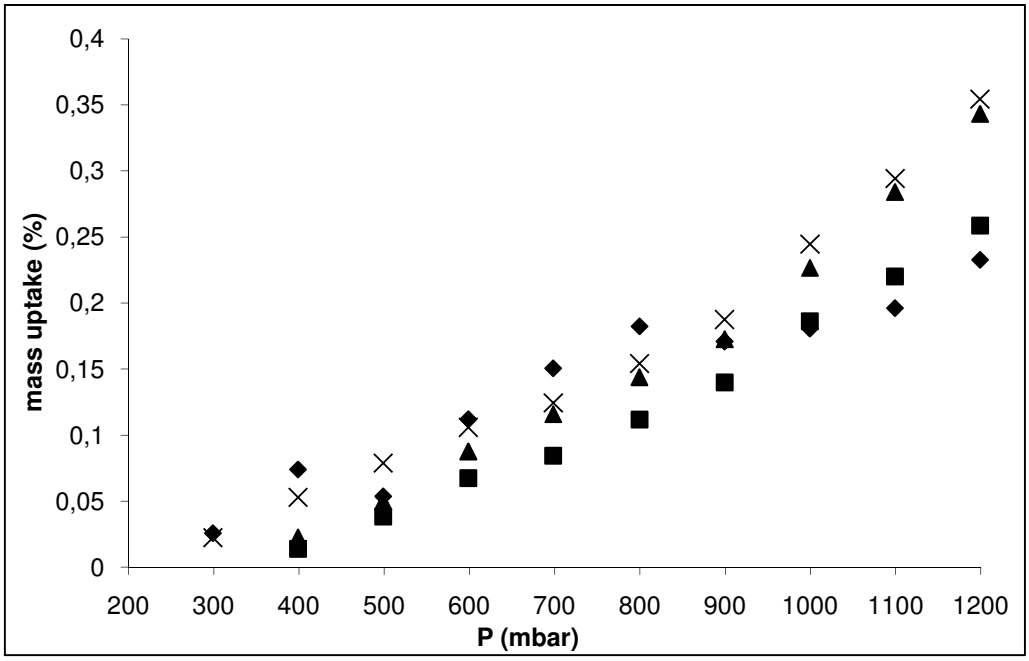

Figure 4.45. CO adsorption isotherms of Pt-Sn/AC3 at 110°C (♦), 115°C (■), 125°C (▲) and 135°C (x).

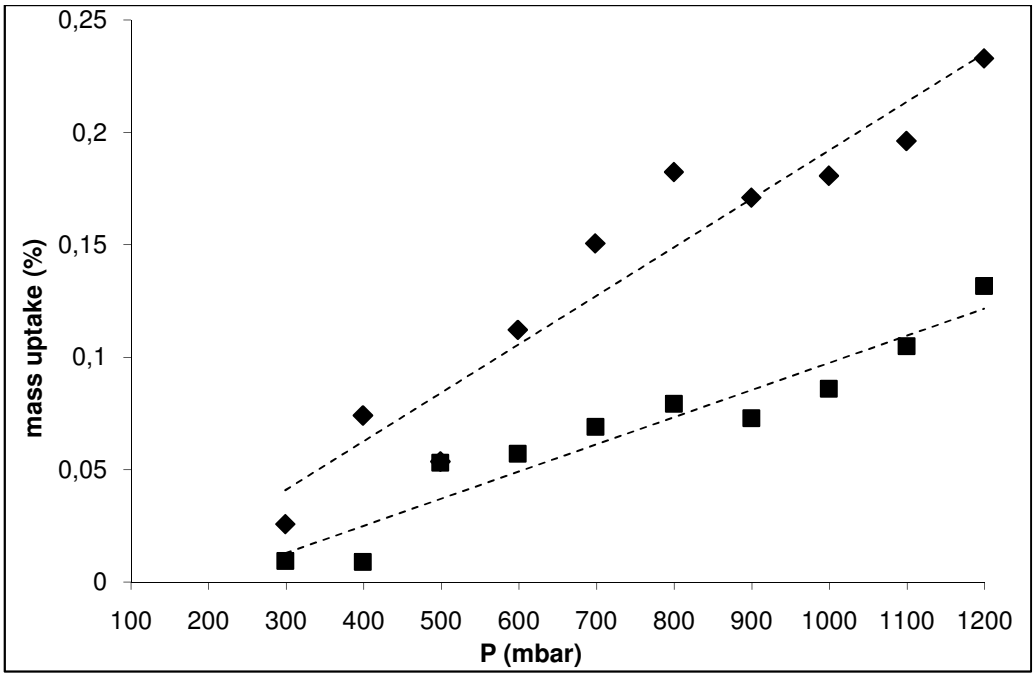

Figure 4.46 CO adsorption isotherms of Pt-Sn/AC3 (♦) and Pt/AC3 (■) samples at 110°C.

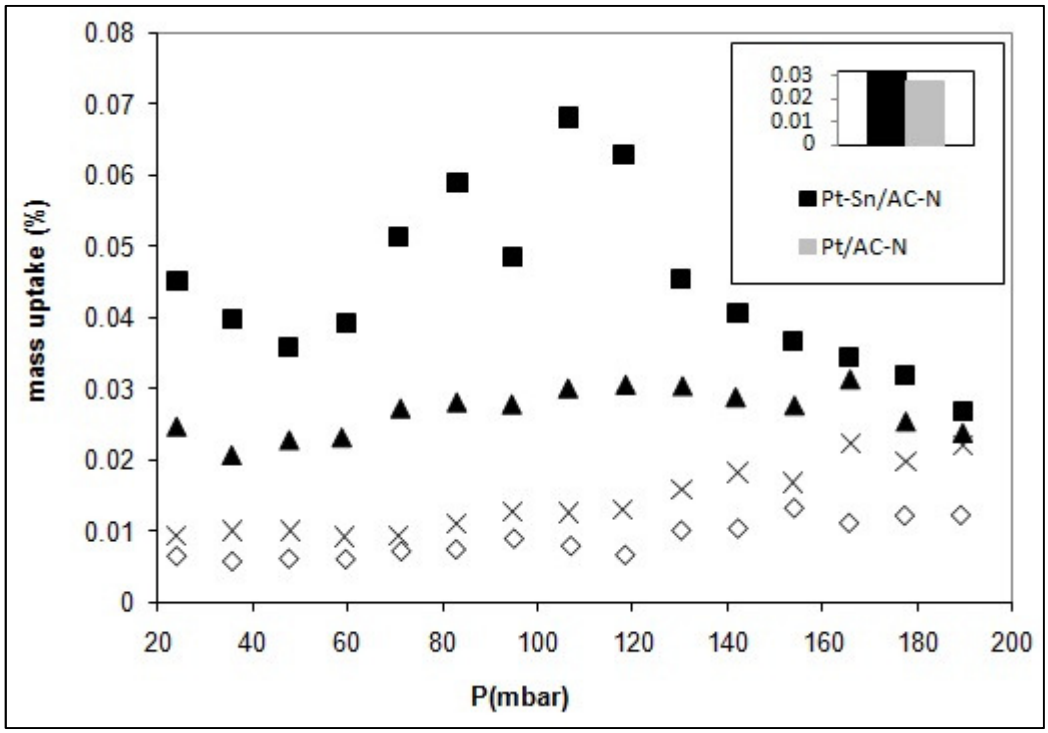

Figure 4.47 CO adsorption isotherms of Pt-Sn/AC3 at low pressure region at (■)110°C, (▲) 115°C, (x) 125°C and (◊) 135°C. Little figure: CO mass uptake % values of Pt-Sn/AC3 and Pt/AC3 at 50 mbar at 110°C.

Repeated tests have shown that the mass uptake of the Pt-Sn/AC3 at 110ºC is significantly higher than that measured at the other temperatures studied for this pressure level, which is very close to the CO partial pressure used in the performance tests. High CO mass uptake of Pt-Sn/AC3 at 110 ºC under PROX conditions is one of the primary reasons of its high activity.

4.5. Carbon Dioxide Adsorption Studies over Modified Activated Carbon Adsorbents

4.5.1. Characterization

Figure 4.48 shows the SEM micrographs of AC2 and AC4-250 adsorbents as examples to the oxidized and Na_2CO_3-impregnated samples. The impregnated particles can be clearly distinguished. In order to compare the morphology of the AC4 and AC5 adsorbents, Figures 4.49 and 4.50 are given. The secondary electron and corresponding

back-scattering electron images of the air oxidized Na_2CO_3-impregnated adsorbents reveal that although a uniform distribution of Na_2CO_3 is thought to be observed (Figures 4.49-a and 4.49-b) on the samples with 2-3% Na^+ on average (EDS results), this is not the case. An agglomeration of Na crystals is evident from the Figures 4.49-c and 4.49-d which is also confirmed by the EDS results (ca. 20% Na^+). On the other hand, the micrograms and EDS studies of the nitric acid oxidized and Na_2CO_3-impregnated (AC5) adsorbents (Figure 4.50) show a uniform distribution of Na_2CO_3 with 5-6% Na^+; the Na^+%, increasing with calcination temperature applied to the adsorbent. Independent of the calcination temperature cracks are observed on the surface of all the nitric acid oxidized and Na_2CO_3-impregnated samples.

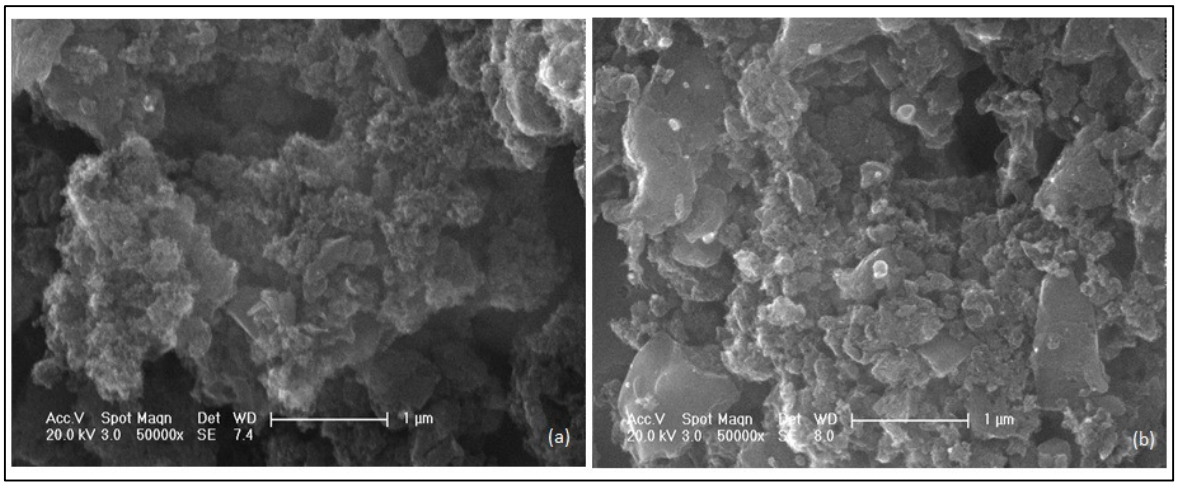

Figure 4.48. SEM micrographs of (a) Air oxidized sample (AC2) (x50000), (b) Air oxidized and Na_2CO_3 impregnated sample (AC4-250) (x50000).

The BET surface areas of all adsorbents studied are given in Table 4.4. The results indicate that total surface area increases with air oxidation, but decreases with HNO_3 oxidation treatment. There is a 50% decrease in BET area of the air oxidized adsorbent as a result of Na_2CO_3 impregnation; no correlation exists between the total surface area and the calcination temperature. For AC5, however, the total surface area increases as the temperature of the calcination step, which was applied upon Na_2CO_3 addition, increases.

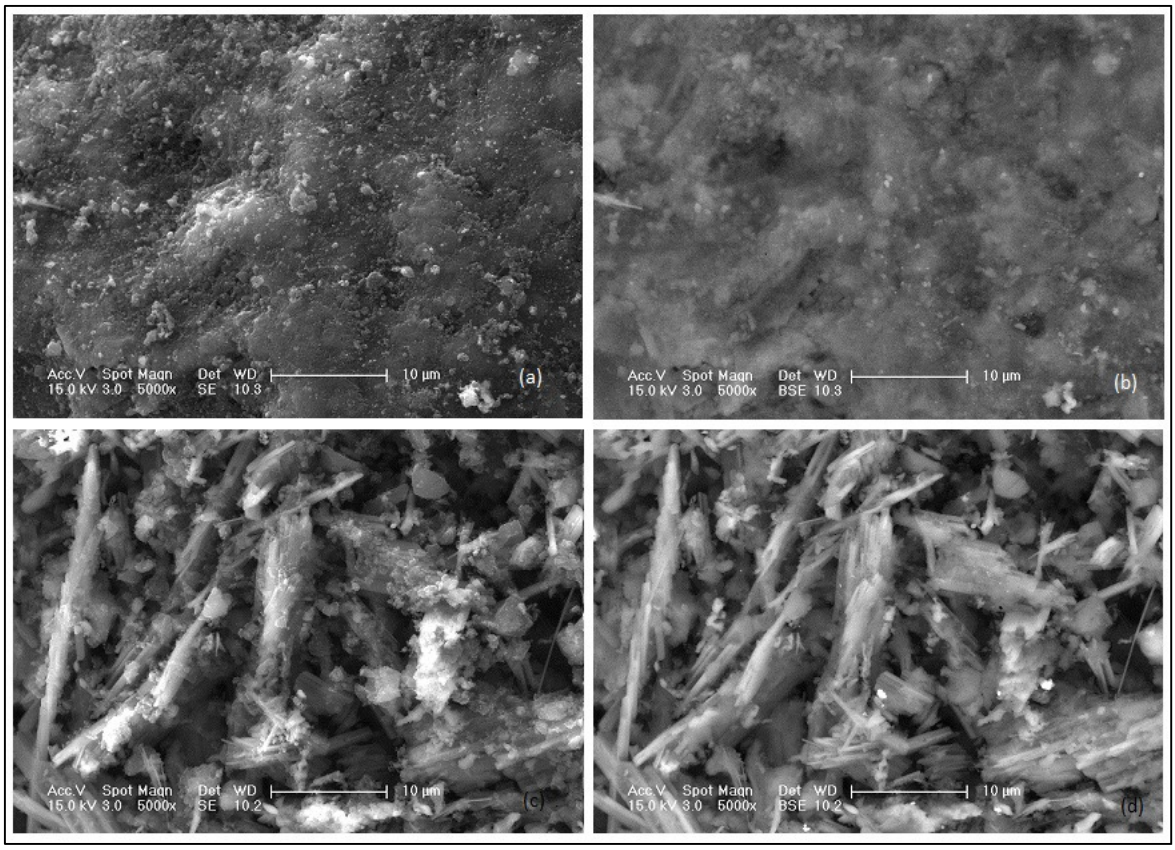

Figure 4.49. Secondary electron images ((a) and (c)) and corresponding back-scattering electron images ((b) and (d)) of air oxidized and Na_2CO_3 impregnated sample (AC4) (x5000).

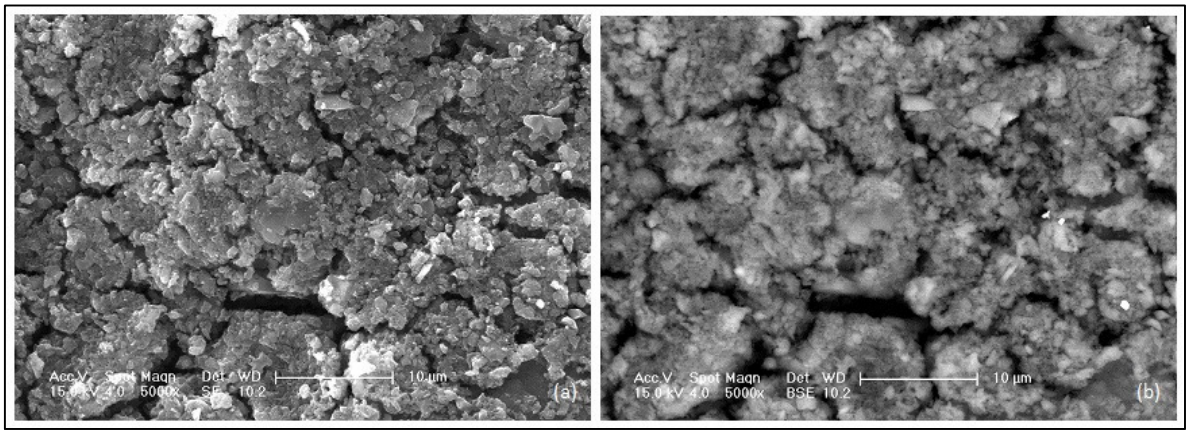

Figure 4.50. Secondary electron (a) and corresponding back-scattering electron images (b) of HNO_3 oxidized and Na_2CO_3 impregnated sample (AC5) (x5000).

Table 4.4. BET surface areas of adsorbents.

Adsorbent	BET (m_2/g)
AC1	856
AC2	1228
AC3	667
AC4-200	687
AC4-250	579
AC4-300	771
AC5-175	564
AC5-200	888
AC5-250	1190

The DRIFT spectra of all adsorbents studied are given in Figure 4.51-4.54, which were obtained from the adsorbents kept under 50 ml/min He flow. Table 4.5 represents the peak integration values of the main bands in the DRIFT spectra. It is convenient to investigate the DRIFT spectra in two regions: 4000- 2800 cm^{-1} and 1800-800 cm^{-1} since there are no peaks in between other than the feature extending from 2380 to 2270 cm^{-1}, which is associated with the asymmetric stretching vibration of gas-phase CO_2 [61, 79]. The carbon dioxide signal mainly originates from ambient air absorption in the optical path outside the DRIFTS cell. This spectral region is therefore not evaluated, as CO_2 variations in the ambience are usually larger than those in the DRIFTS cell, which consist of the decomposition of surface oxygen groups and carbonate.

The spectral zone in the 3800–2800 cm^{-1} range displays bands mostly attributable to hydroxyl species. The weak and broad band at 3600 cm^{-1} is assigned to the O-H stretching vibration in free –OH [122]. All spectra show a strong and wide absorption band at 3500–3050 cm^{-1} with a maximum at about 3250 cm^{-1}. The position of the band is characteristic of the stretching vibration of hydroxyl compounds from carboxyls, phenols or alcohols [116, 120, 122, 124, 126]. This band diminishes after the HCl treatment (Figure 4.51) and gains intensity due to oxidative air and HNO_3 treatments (Figure 4.52); the $NaCO_3$ modification and following heat treatments resulted in high intensities (Figures 4.53 and 4.54).

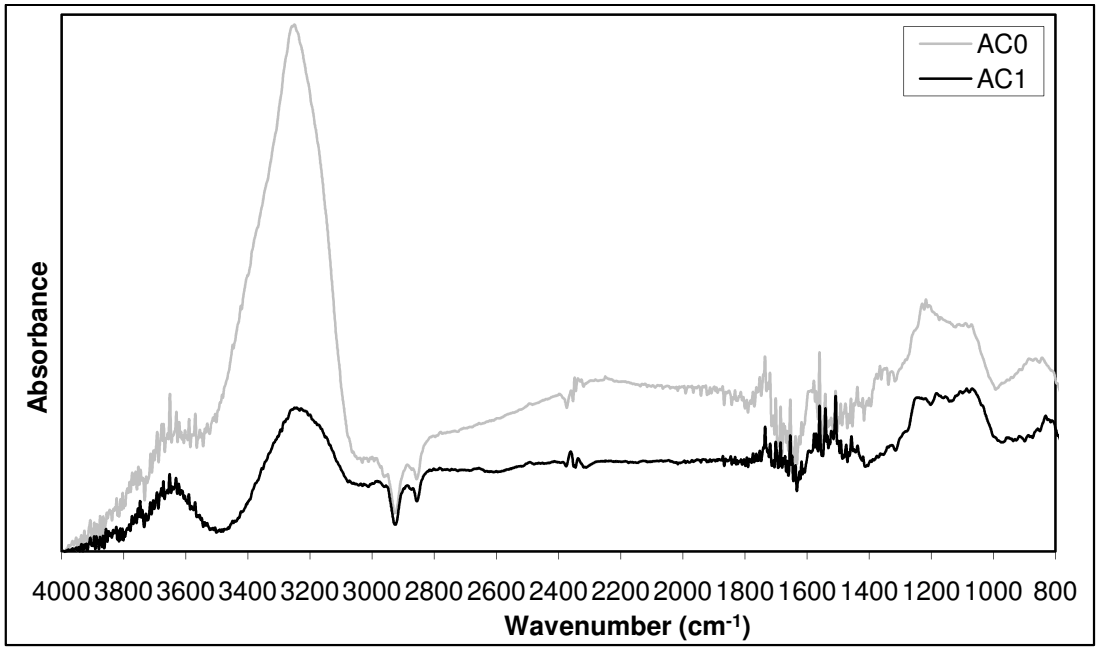

Figure 4.51. DRIFT spectra of the commercial sample and the HCl treated adsorbent under 50 ml/min He flow.

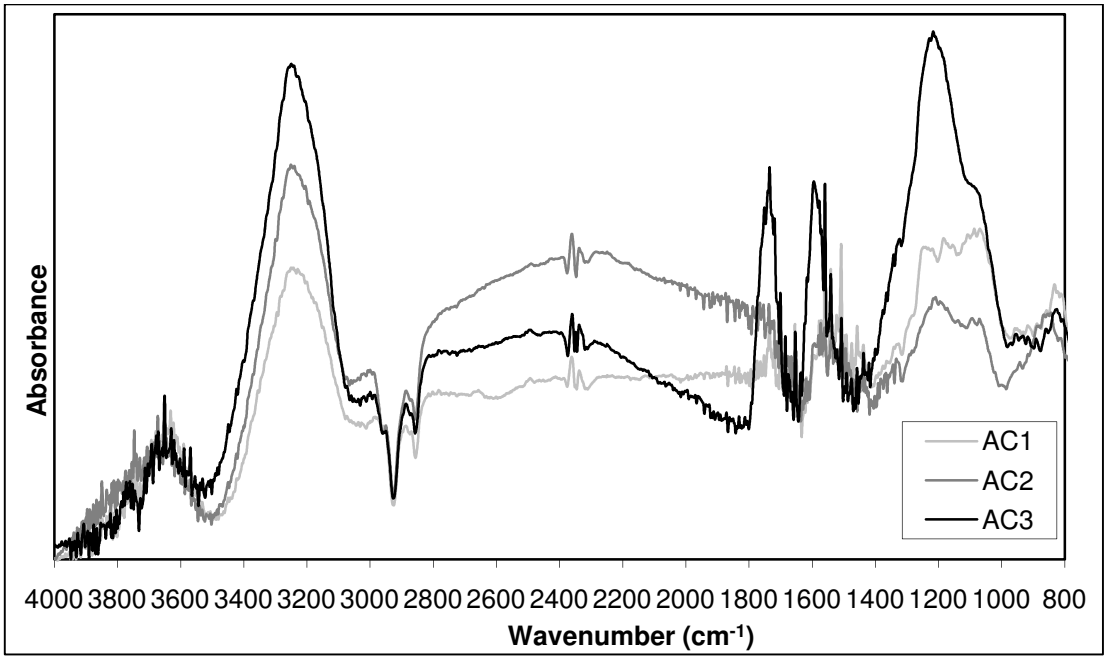

Figure 4.52. DRIFT spectra comparison of HCl treated, air oxidized and HNO_3 oxidized samples under 50 ml/min He flow.

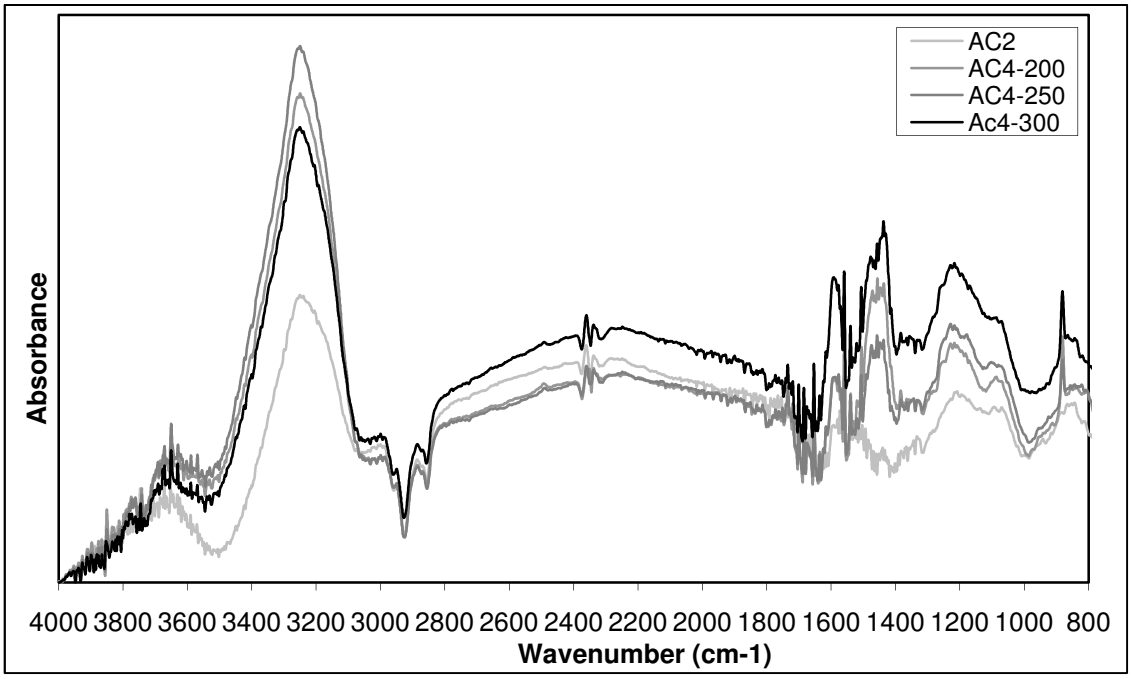

Figure 4.53. DRIFT spectra of air oxidized and Na_2CO_3 modified adsorbents under 50 ml/min He flow.

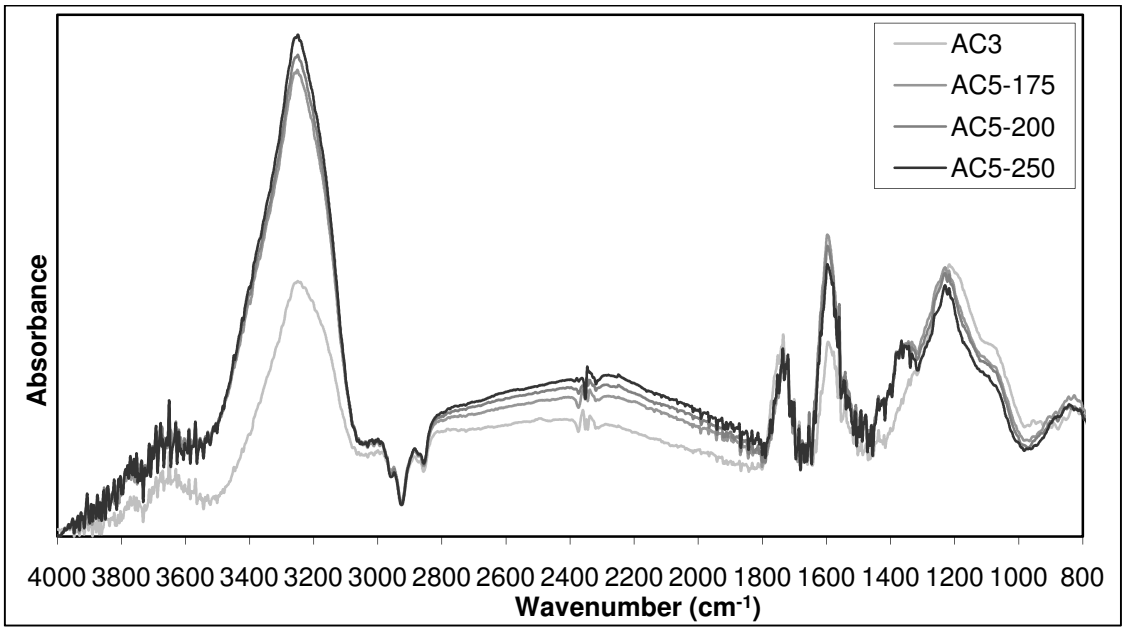

Figure 4.54. DRIFT spectra of HNO_3 oxidized and Na_2CO_3 modified adsorbents under 50 ml/min He flow.

The very high intensity, and therefore high amount of –OH groups, in the commercial sample may be attributed to carboxylic groups, which decompose at ca. 250ºC [120] as a result of heat treatment during AC1 production. Some acidic and basic groups may be formed in the case of HNO_3 and air oxidation treatment, respectively. The two folds increase in the band intensity through production of basic groups due to Na_2CO_3 addition to AC2 and AC3 samples is evident from Table 4.5. The band at ~2875 cm^{-1} appearing in all spectra can be attributed to formate species present on the catalysts which are unaffected by any of the treatment procedures [61, 184].

There are three main bands in the spectral regional 1800-800 cm^{-1} confirming the presence of surface oxygen groups: (i) a band centered near to 1750 cm^{-1} is the characteristic of C=O stretching vibration in carboxylic groups, lactones and anhydrides [120, 126, 127, 131, 133], (ii) a band near 1600 cm^{-1} attributed to C=C stretching vibration in aromatic rings of quinone and keto-enol groups [120, 122, 126, 127-129, 133] and (iii) the broad band centered around 1250 cm^{-1} is the indication of C-O stretching in carboxylic groups, anhydrides, phenols, ethers and lactones [120, 133] or (C-O-C) stretching vibration in lactones and ethers [125, 131]. A decrease in the 1750 cm^{-1} band is observed (Figure 4.51) as a result of the HCl treatment; on the other hand, this band regains intensity due to the formation of acidic carboxylic acid groups (Figure 4.52) upon HNO_3 oxidation [101, 120]. Na_2CO_3 modification results in intensity loss of this band for AC3 sample (Figure 4.54). As expected, 1750 cm^{-1} band is not present in AC2 samples, which do not have any carboxylic groups due to high temperature air treatment [101, 120]. From the integral values of the band around 1600 cm^{-1} and through comparing Figure 4.54 and Figures 4.51-4.53, it can be concluded that the aromatization in AC5 samples are higher than that of any other sample due to the alkali and oxidation treatments. The extent of aromatization decreases as the calcination temperature increases for AC5 adsorbents (Figure 4.54). Among the oxidative HNO_3 and air treatments, HNO_3 oxidation results in higher aromatization (Figure 4.52). The 1250 cm^{-1} band diminishes after the HCl treatment (Figure 4.51). The intensity gain is obvious for AC3 sample due to mostly carboxylic acid formation (Figure 4.52). The intensity of 1250 cm^{-1} band decreases as the calcination temperature increases for AC5 adsorbents (Figure 4.54). There is no correlation between the calcination temperature and band intensity for air oxidized and Na_2CO_3 modified samples (Table 4.5). The simultaneous formation of 3250 cm^{-1} (O-H), 1750 cm^{-1} (C=O)

and 1250 cm^{-1} (C-O) bands points to the production of carboxylic acid groups on the adsorbent surface for AC3 and AC5 samples [188].

Table 4.5. The peak integration values of the main bands in DRIFT spectra under 50 ml/min He common to all adsorbent samples.

Sample	**Peak Integration**				
	O-H 3250 cm^{-1}	**C=O 1750 cm^{-1}**	**C=C 1600 cm^{-1}**	**C-O 1250 cm^{-1}**	**C-H 850 cm^{-1}**
AC0	12.371	0.212	0.291	1.926	1.035
AC1	2.772	0.087	0.452	1.65	0.359
AC2	3.557	0	0.517	1.02	0.445
AC3	5.037	0.912	1.032	4.261	0.278
AC4-200	7.105	0	0.376	1.329	0.759
AC4-250	7.922	0	0.402	1.629	0.915
AC4-300	6.288	0	0.397	1.447	0.388
AC5-175	10.543	0.581	1.870	4.995	0.701
AC5-200	10.676	0.605	1.620	4.764	0.97
AC5-250	10.978	0.577	1.227	4.336	0.891

The spectral region 1000-700 cm^{-1} is attributed to C-H out-of plane bending vibration in aromatic rings [123, 125, 132, 134]. The formation of sharp 880 cm^{-1} band can be assigned to C-H groups in AC4 (Figure 4.53) [132]. The broad band around 1450 cm^{-1} which occurred only in AC4 samples may be attributed to C-H deformation vibration in CH_2 or $C(CH_3)_3$ groups [122]. The evolving of the shoulder at 1350 cm^{-1}, which is only present in AC5 samples, is the evidence of the presence of C-H groups of the aromatic ring (Figure 4.54) [132]. This band and the one at 1600 cm^{-1} show that the extent of aromatization of AC5 samples is very high.

4.5.2. Adsorption Studies

Carbon dioxide adsorption and desorption isotherms were obtained for fresh and helium treated AC1,AC2, AC3, AC4 and AC5 samples at room temperature, 120ºC/180ºC

and 200ºC, in order to investigate the changes in CO_2 adsorption behavior upon the modifications, heat treatments and/or impregnations applied. Table 4.6 summarizes the results obtained in the adsorption studies. The helium treated samples are named as "sample name-400/600He" indicating the helium treatment temperature. All the isotherms and adsorption capacities are presented as mass uptake percentage. The tests were performed in 0-20000 mbar pressure range. A representative plot of CO_2 adsorption-desorption isotherms of AC4-250 sample at three temperature levels is given in Figure 4.55. The fact that adsorption and desorption isotherms coincide for the Na_2CO_3 modified samples proves fully reversible adsorption and easy recovery of the adsorbent. Figure 4.56 shows the results of the cyclic adsorption- desorption tests performed on AC3; the cycle was repeated three times at room temperature. The observed adsorption capacity loss is, ca. 7.4 % between the first and the third cycle, indicating slight capacity decrease. Whereas there is no decrease in the CO_2 mass uptake even after the 10^{th} and 5^{th} adsorption-desorption cycles for AC4-250-400He and AC5-250-400He samples, respectively (Figures 4.57 and 4.58). The role of high temperature helium treatment therefore, is to further stabilize the adsorbent surface. The effect of temperature during cyclic adsorption-desorption tests was also tested for selected samples. As an example, cyclic test results performed on AC5-250-400He is given in Figure 4.59. Since AC5-250-400He sample lost adsorption capacity (~7%) as a result of 6 consecutive adsorption-desorption isotherms at 25ºC, 120ºC, 200ºC, 120ºC, 25ºC and 25ºC (Figure 4.58), it can be concluded that adsorption-desorption experiments at high temperatures may have caused changes in the surface.

There is not much difference between the CO_2 mass uptake % values of the nonimpregnated (AC1, AC2 and AC3) samples (Figure 4.60), and there is no correlation between the CO_2 mass uptake values and the BET surface areas; it is more convenient to correlate the adsorption capacities with the oxygen groups formed on the adsorbent surfaces. As a result of helium treatment at 400ºC, the adsorption capacities of AC2 and AC3 samples increased.

Table 4.6. Results of the adsorption experiments at 1 bar and 20 bars.

	RT (% mass uptake)		**120/180ºC (% mass uptake)**		**200ºC (% mass uptake)**	
Adsorbent	**20 bar**	**1 bar**	**20 bar**	**1 bar**	**20 bar**	**1 bar**
AC1	3.30	0.75	4.29	0.15	4.70	0.55
AC2	2.66	0.53	4.29	0.17	4.58	0.35
AC3	2.30	0.39	1.42	0.10	3.39	0.11
AC4-200	20.19	7.70	8.54	1.43	4.16	0.43
AC4-250	22.74	8.87	13.19	2.51	4.59	0.35
AC4-300	19.49	7.24	10.55	1.84	2.57	0.15
AC5-175	17.08	7.07	6.79	1.14	2.61	0.38
AC5-200	17.80	7.26	7.97	1.82	3.40	0.36
AC5-250	13.57	5.38	9.07	2.12	4.92	0.58
AC1-400He	3.15	0.64				
AC2-400He	5.7	1.27				
AC3-400He	4.36	0.55				
AC4-200-400He	22.38	8.19				
AC4-250-400He	18.17	6.66				
AC4-300-400He	21.18	7.74				
AC5-175-400He	17.47	6.33				
AC5-200-400He	16.6	5.82				
AC5-250-400He	18.38	6.92	8.72	1.91	4.70	0.60
AC1-600He	15.03	4.4				
AC2-600He	11.98	4.4				
AC3-600He	9.34	1.6				
AC4-200-600He	19.62	7.11				
AC4-250-600He	17.85	6.51				
AC4-300-600He	20.82	7.06	9.82	1.59	4.44	0.89
AC5-175-600He	14.88	4.76				
AC5-200-600He	14.5	4.83				
AC5-250-600He	18.32	5.9				

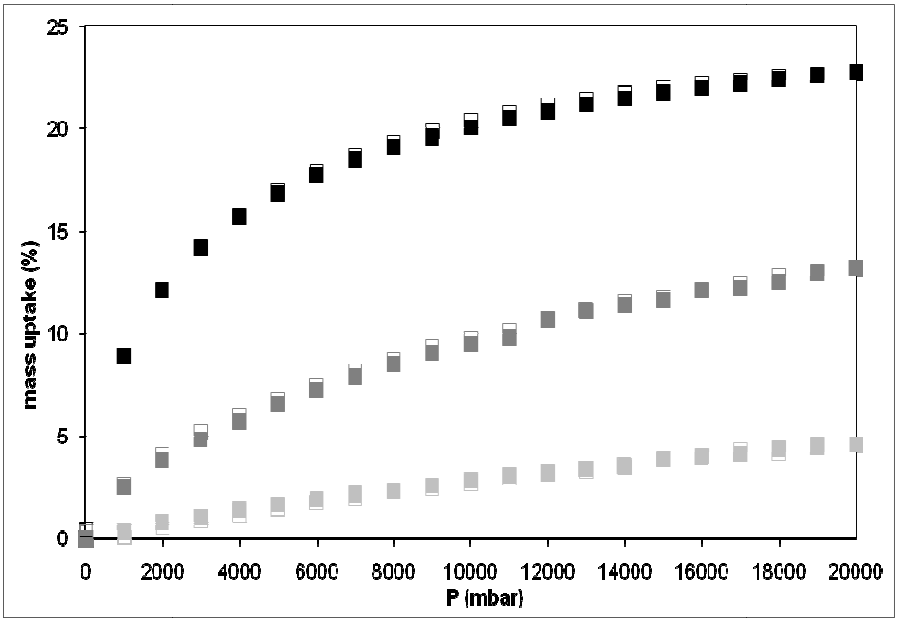

Figure 4.55. Adsorption and desorption isotherms of air oxidized and Na_2CO_3 modified sample AC4-250 at 25ºC (■), 120ºC (■) and 200ºC (■)

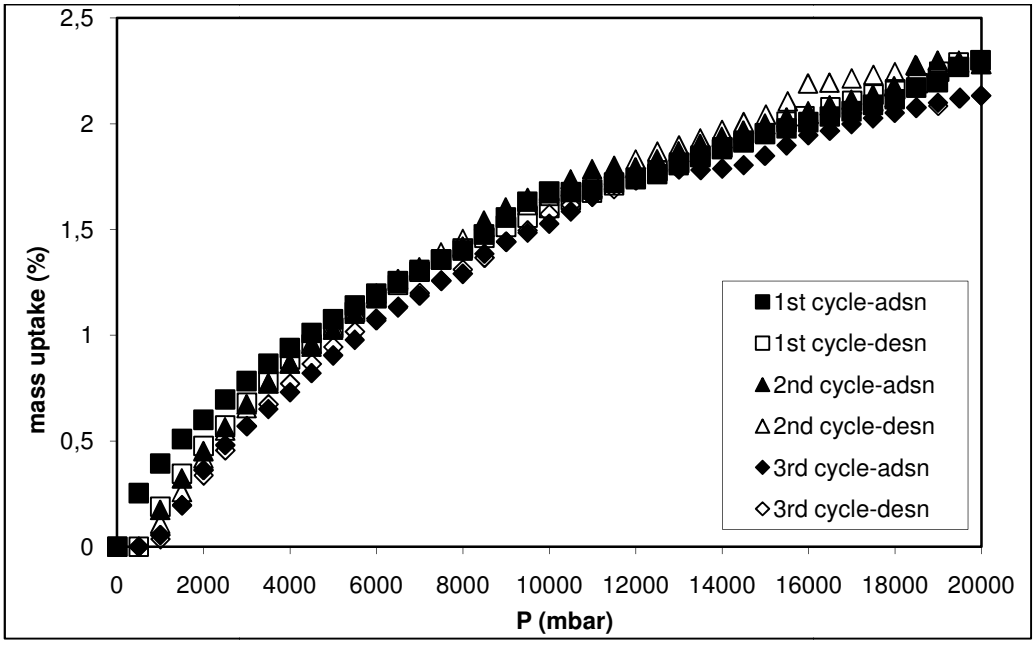

Figure 4.56. Cyclic adsorption and desorption isotherms of HNO_3 oxidized adsorbent (AC3) at 25ºC.

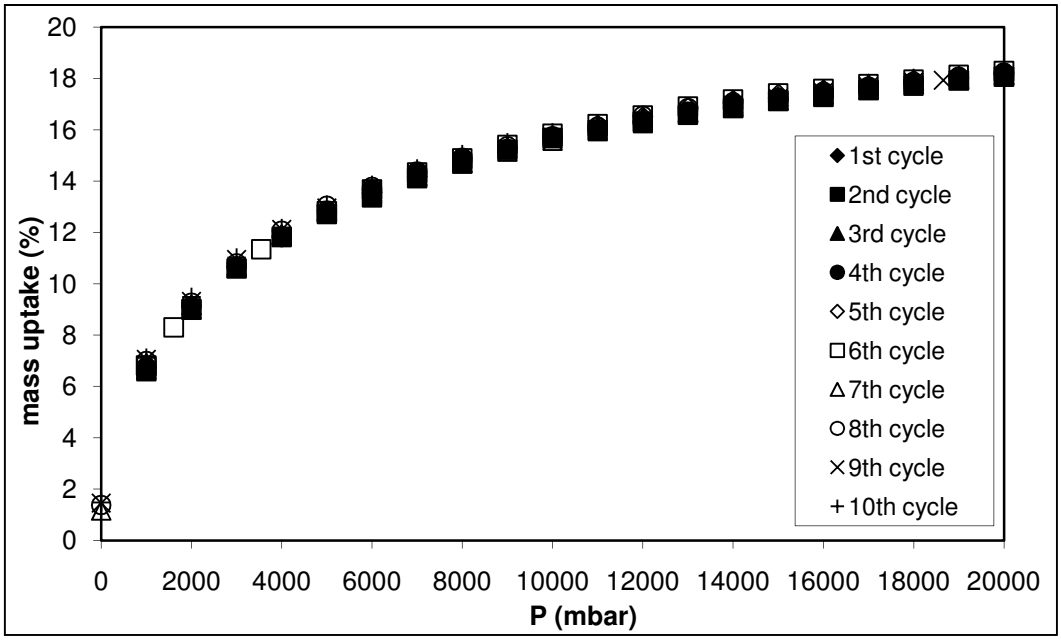

Figure 4.57. Cyclic adsorption/desorption test results of air oxidized, Na_2CO_3 modified and He treated sample (AC4-250-400He) at 25ºC.

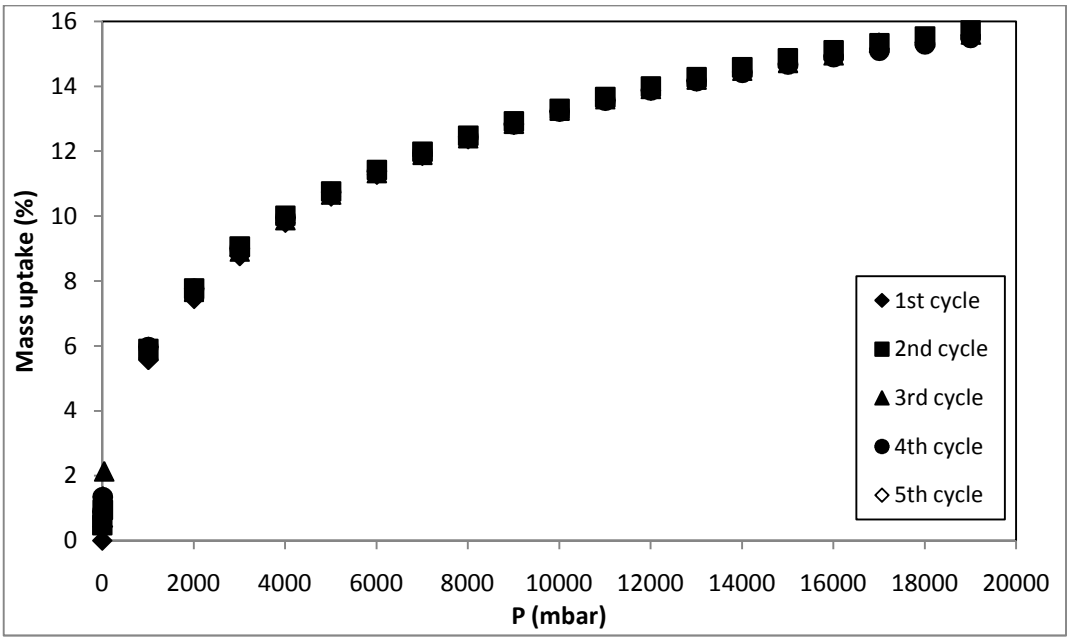

Figure 4.58. Cyclic adsorption/desorption test results of HNO_3 oxidized, Na_2CO_3 modified and He treated sample (AC5-250-400He) at 25ºC.

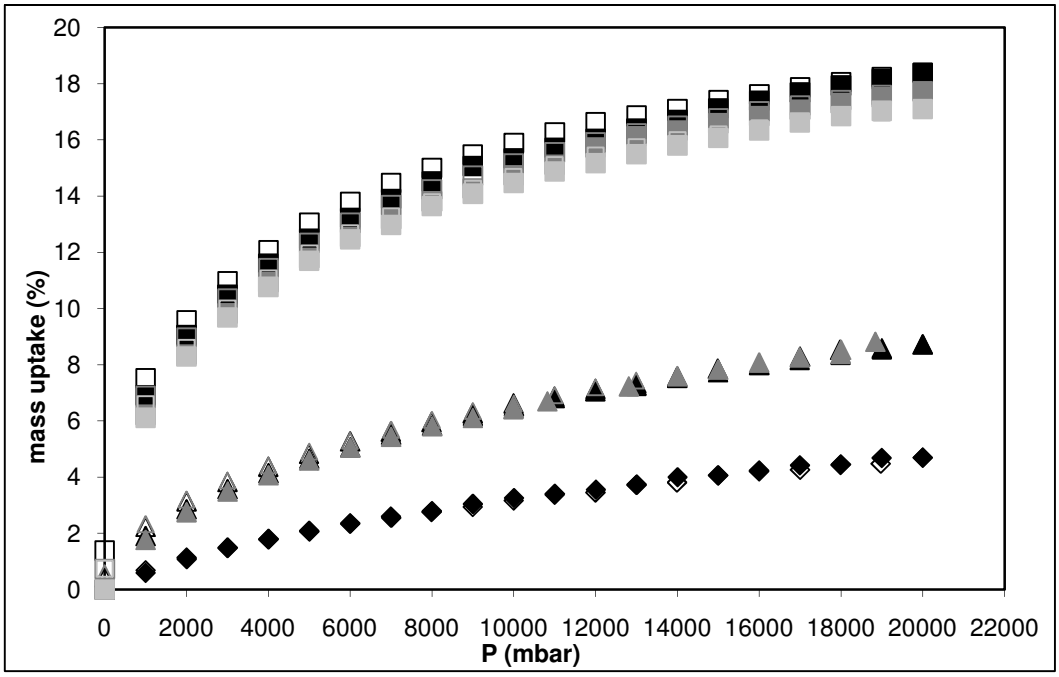

Figure 4.59. Cyclic adsorption/desorption test results of AC5-250-400He at three temperature levels (25ºC (■), 120ºC (▲) and 200ºC (♦)).

On the other hand, the values of % mass uptake capacity of AC1 adsorbent stayed the same upon He treatment at 400ºC. The adsorption capacity increase of the AC3 adsorbent may be explained by the decomposition of the carboxylic acid groups (at ~240ºC), verified by the presence of 1250 cm^{-1}, 1750 cm^{-1} and 3250 cm^{-1} bands in the DRIFTS studies, as a result of helium treatment at 400ºC. Similarly, the increased adsorption capacities of AC2 samples may be attributed to the decomposition of the phenol or alcohol surface groups (3250 cm^{-1} band) as they do not have any carboxylic acid groups. Since HCl treatment is used for removing ash and sulphur from the AC0 sample and, as verified by the DRIFTS studies, only a very limited amount of surface oxygen groups (no carboxylic acid groups) were introduced to the surface; the CO_2 adsorption capacity of AC1 samples stayed unchanged. Likewise, ~3 folds increase in the adsorption capacities of AC1, AC2 and AC3 samples as a result of higher temperature (600ºC) helium treatment may be attributed to the decomposition of surface oxygen groups, like anhydrides (at 550ºC), in addition to the carboxylic acid groups.

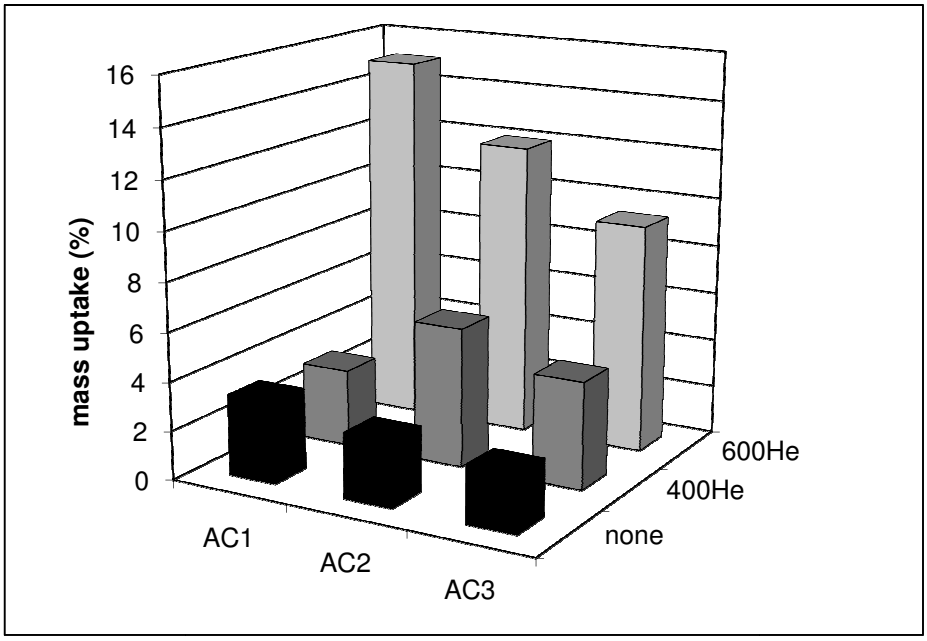

Figure 4.60. The effect of He treatment on the CO_2 mass uptake % values of HCl treated (AC1), air oxidized (AC2) and HNO_3 oxidized (AC3) samples.

Results clearly indicate the enhancement in carbon dioxide adsorption capacities of air oxidized and nitric acid oxidized AC samples upon Na_2CO_3 imregnation (Figures 4.61 and 4.62). For the Na_2CO_3 impregnated samples the increase in mass uptakes at 20 bars and 25ºC are nearly 8 and 7 folds for air oxidized and nitric acid oxidized samples, respectively; and at 1 bar, the difference is even higher (~15 and 17 folds for AC2 and AC3, respectively). Thus, the basic sites generated have an increased affinity for carbon dioxide molecules. Without He-treatment, the CO_2 adsorption capacities of AC4 samples are higher than those of AC5 adsorbents; the highest adsorption capacity belongs to the sample calcined at 250ºC, which has the lowest BET surface area among AC4-group adsorbent samples. For the AC4 samples without helium treatment, as the BET surface area increases the adsorption capacity of the adsorbents decreases. The same relationship does not hold for AC5 samples; there is no correlation between the BET surface areas or the calcination temperatures of the samples and the CO_2 adsorption capacities. As a result of high temperature helium treatments, almost no change is observed for the CO_2 mass uptake values of AC4 and AC5 samples; this result was expected since the surfaces are covered with more basic and stable surface groups as a result of Na_2CO_3 impregnation and calcination procedures applied prior to the He treatments. Therefore the advantage of the

high temperature helium treatment for Na_2CO_3 impregnated samples is limited to a further stabilization of the surface as discussed above.

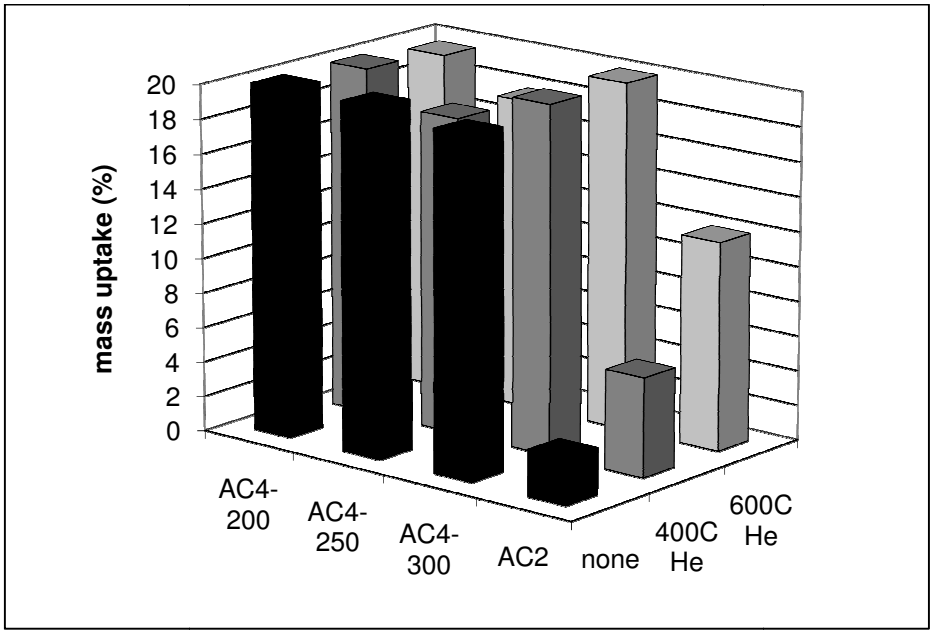

Figure 4.61. The effect of He treatment on the CO_2 mass uptake % values of air oxidized and Na_2CO_3 modified samples (AC4).

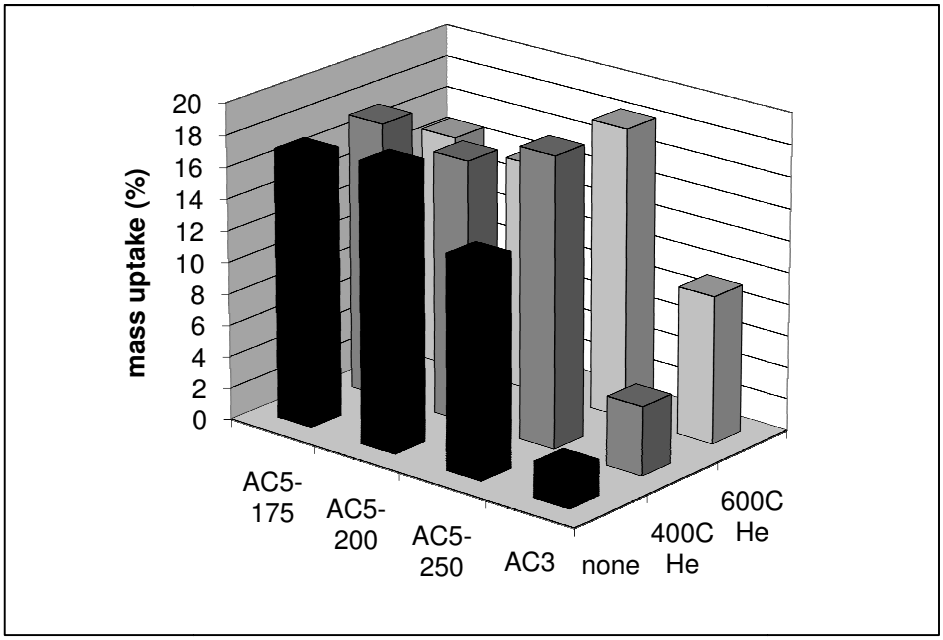

Figure 4.62. The effect of He treatment on the CO_2 mass uptake % values of HNO_3 oxidized and Na_2CO_3 modified samples (AC5).

The amount of adsorbed carbon dioxide on Na_2CO_3 impregnated adsorbents decreases with increasing adsorption temperature (Figures 4.63 and 4.64). However for only HCl treated, air oxidized and HNO_3 oxidized samples, in addition to the non overlapping adsorption and desorption isotherms during cyclic tests, adsorption capacity increases; this can be attributed to the decomposition of the oxygen bearing surface groups, leaving free sites for CO_2 adsorption (Figure 4.65).

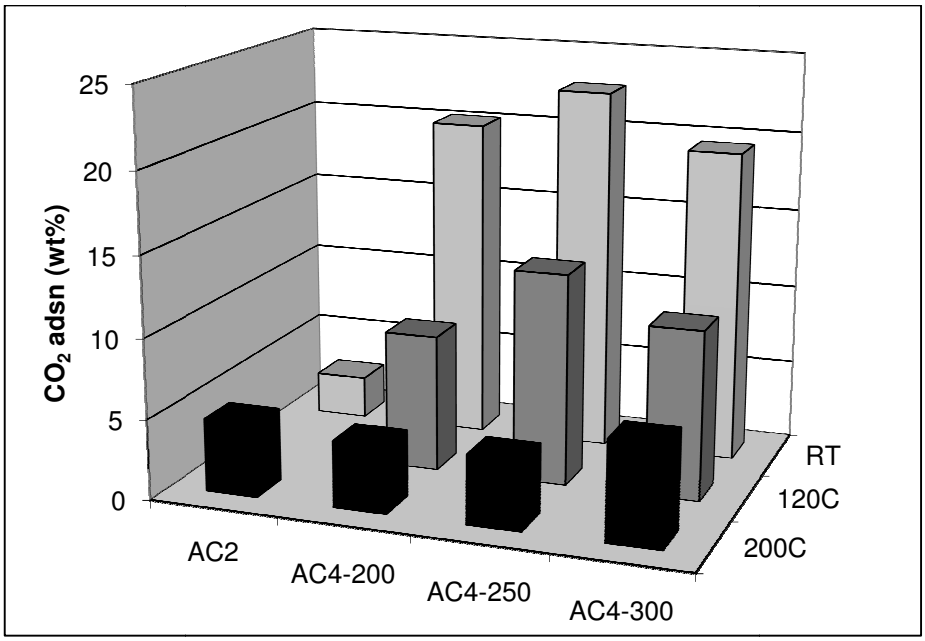

4.63. The effect of temperature on the CO_2 mass uptake % values of air oxidized and Na_2CO_3 modified samples (AC4).

The adsorption data of high surface area activated carbon adsorbents are often fit to Dubinin-Radushkevich (D-R) isotherm and Freundlich isotherm models for low pressures. However, the adsorption data of none of the samples could fit to D-R model. Instead, the isosteric heat of adsorption for the adsorbents is calculated. It should be noted that no estimation could be possible for AC1, AC2 and AC3 since the adsorption data of nonimpregnated samples do not fit Langmuir model – ie. CO_2 adsorption capacities increase with increasing temperature-. The isosteric heat of adsorption of carbon dioxide, Q, at a given surface loading was calculated from the adsorption isotherms at different temperatures using Clausius Clapeyron equation [Eq (2.12)].

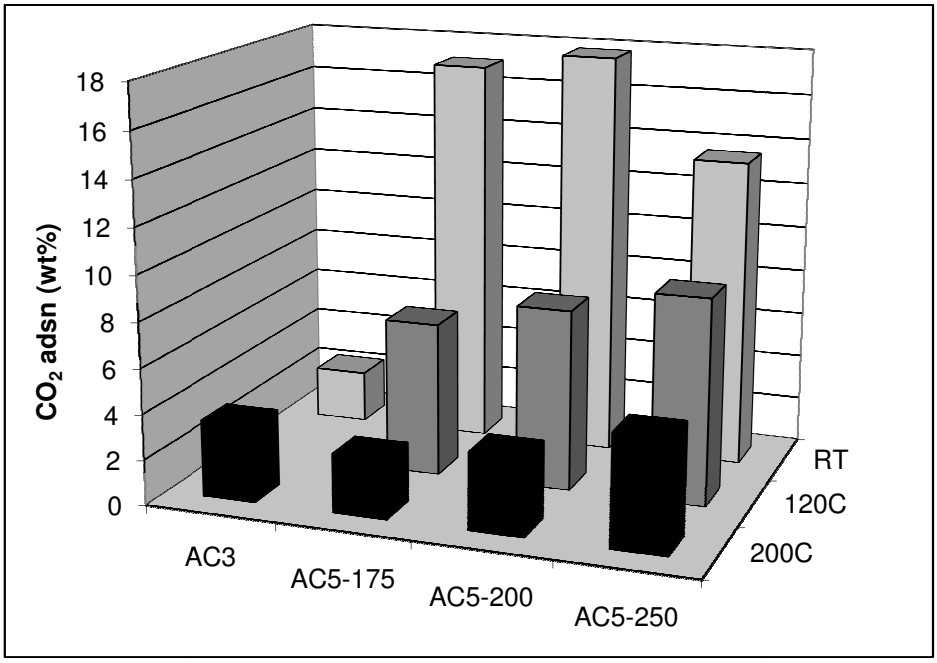

4.64. The effect of temperature on the CO_2 mass uptake % values of HNO_3 oxidized and Na_2CO_3 modified samples (AC5).

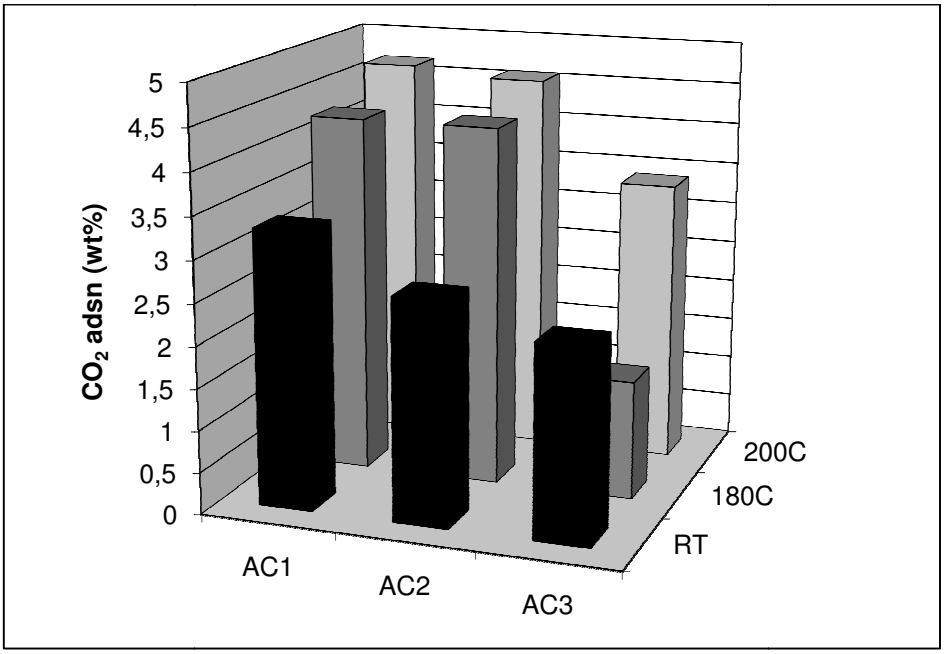

Figure 4.65. The effect of temperature on the CO_2 mass uptake % values of HCl treated (AC1), air oxidized (AC2) and HNO_3 oxidized (AC3) samples.

The isosteric heat of adsorption values for the AC4 and AC5 samples are plotted in Figure 4.66. The general trend is that the value of heat of adsorption of samples increases with the adsorbed amount of CO_2 indicating lateral interactions between the adsorbed CO_2 molecules [189]. The lateral interaction increases as the adsorbate loading increases. The heat of adsorption values of AC4-300 and AC5-250 remain constant over the adsorbed CO_2 range of 1.5-3% indicating an energetically homogeneous surface [189]; then at higher values, the heat of adsorption of AC5-250 increases due to increasing lateral interactions with the increased CO_2 on the surface. The order of isosteric heat of adsorption at any adsorbate amount within the range 2-4 % is AC4-300 > AC5-175 > AC5-200 > AC4-200 > AC4-250 > AC5-250. Results indicate that CO_2 was adsorbed more strongly on AC4-300 than on AC4-250 and AC4-200 adsorbents. Similarly, CO_2 was adsorbed more weakly on AC5-250 than on AC5-175 and AC5-200 samples. For AC4 samples as the BET surface area increases, isosteric heat of adsorption decreases and reversely, for AC5 samples CO_2 is adsorbed more strongly on the adsorbent surface as the BET surface area decreases.

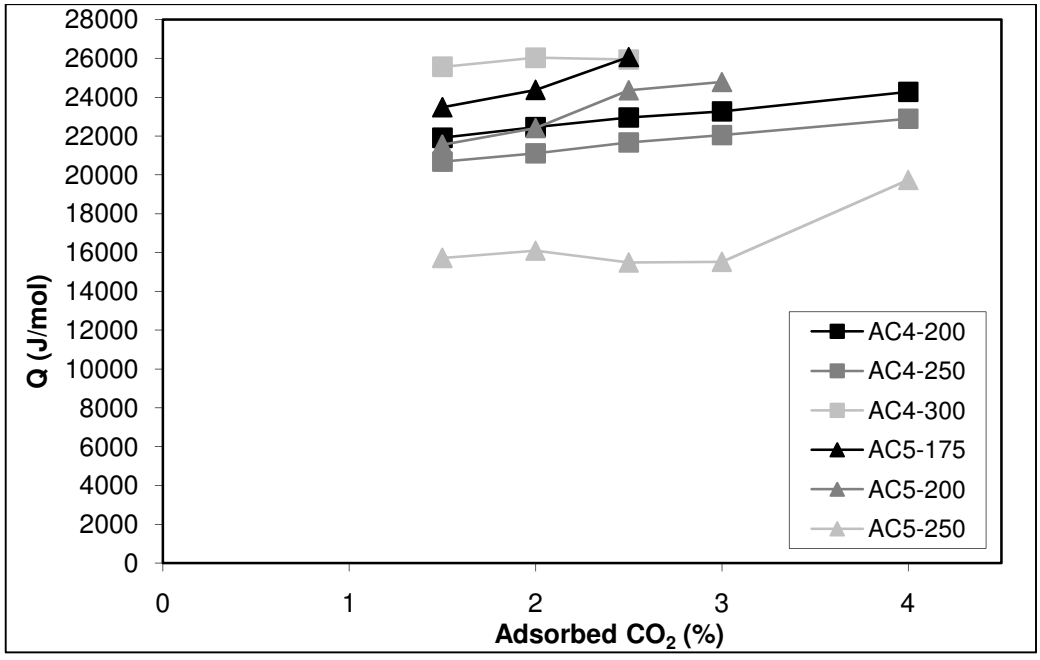

Figure 4.66. The isosteric heat of adsorption values for the air oxidized and Na_2CO_3 modified (AC4) and HNO_3 oxidized and Na_2CO_3 modified (AC5) samples.

5. CONCLUSIONS AND RECOMMENDATIONS

5.1. Conclusions

The overall purpose of this research study was to produce, characterize and investigate the performances of catalysts and adsorbents which will play a role in CO_x-free hydrogen production via fuel processing for FP-FC applications. The conclusions drawn will be presented in five sections. In the first part of the study; the purpose was to investigate the WGS performances of bimetallic Pt-Ni/Al_2O_3 catalysts. The major conclusions that can be drawn from the first part of this study can be given as follows:

- With the increase in the Ni loading, equilibrium conversions was found to be reached at lower temperatures. This enhanced catalytic activity can be attributed to the increased number of Pt crystallites, which are in direct contact with the reducible NiO_x species. As the Ni loading was increased, the Pt-Ni interaction was enhanced.
- Increase in H_2O/CO ratio in the feed led to an increase in CO conversion, and the equilibrium conversions were observed to be reached at lower temperatures.
- Bimetallic Pt-Ni/Al_2O_3 catalysts were found highly active and stable for WGS reaction in the 200-500°C temperature range under ideal conditions.
- Methanation was observed under real feed conditions; thus Pt-Ni/Al_2O_3 catalysts are not suitable for the WGS unit of fuel processors.

In the second part of the thesis, the purpose was to design and develop Au-Re bimetallic catalysts supported on ceria for WGS reaction. An effective catalyst assuring high activity and stability was searched through a parametric study using impregnation and deposition precipitation techniques in catalyst preparation. The following conclusions can be drawn on the basis of the characterization and catalytic activity results:

- Catalytic performance tests clearly showed that Re addition affected the WGS activity of Au/Ceria catalysts strongly.

- Gold addition by dp technique on impregnated Re/Ceria catalysts led to higher dispersion and stronger interaction between Au and Re particles; therefore, high CO conversion levels were obtained. On the other hand, impregnation of Re on Au/Ceria catalyst resulted in blockage of active sites and poor WGS activity.
- Novel Au-Re/ceria catalysts are highly active for WGS reaction under ideal feed conditions, especially at high H_2O/CO ratios, led by the presence of catalytically active and steam tolerant sites formed on the bimetallic catalyst.

Based on the superior WGS performance of the 1%Au-0.5%Re/Ceria (imp+dp) catalyst especially at high H_2O/CO ratios, real feed experiments in addition to DRIFTS studies were performed on the catalysts aiming to have complete WGS performance specs of Au-Re/Ceria system. The conclusions of this section are as follows:

- The DRIFT profiles indicated that the reaction on the 1%Au-0.5%Re/Ceria (imp+dp) catalyst takes place between the OH groups present on the catalyst and CO to produce surface formate along with surface carbonates and bicarbonate species.
- Carbonate formation was dominant for the catalysts other than 1%Au-0.5%Re/Ceria (imp+dp) as a result of the reaction between CO gas and ceria lattice oxygen.
- The results show that, CO was linearly adsorbed on gold metal particles on the catalysts following the order 1%Au-0.5%Re/Ceria (imp+dp) > 0.5%Au-0.25%Re/Ceria (imp+dp) > 1%Au/Ceria (dp) = 0.5%Re-1%Au/Ceria (dp+imp).
- Bridge-type CO adsorption was dominant on 0.5%Re-1%Au/Ceria (dp+imp) catalyst on Au^0 and Re^0.
- There was a pronounced decrease in H_2 concentration in the product streams compared to that in the feed for the samples studied except for 1%Au-0.5%Re/Ceria (imp+dp) catalyst.
- The best WGS performances for the bimetallic 1%Au-0.5%Re/Ceria (imp+dp) catalyst were obtained at 300°C under realistic feed conditions with high H_2O/CO ratios in the feed.

- The results obtained reveal 1%Au-0.5%Re/Ceria (imp+dp) catalyst is a potential candidate which enables the use of a single WGS unit operating at a mid-range temperatures in a fuel processor.

In the fourth section of the thesis, DRIFTS and CO/CO_2 adsorption studies were conducted on both Pt-Sn/AC3 and Pt/AC3 catalysts with the aim of understanding the reasons of superior PROX performance of Pt-Sn/AC3. The following conclusions were drawn:

- The results of the DRIFTS studies indicate that the decomposition of the carboxylic acid groups during pretreatment steps leads to mobility of the metallic precursors originally anchored to them and enhance the Pt-Sn interaction leading Pt_3Sn alloy formation.
- DRIFTS and adsorption studies revealed that Pt_3Sn alloy formation on AC-N support has led to CO adsorption and faster surface reaction involving intermediate hydroxyl groups which bring along increase in CO conversion and selectivity as the temperature decreases within the range 110-135 ^oC.
- High CO mass uptake of Pt-Sn/AC3 at 110ºC under PROX conditions is one of the primary reasons of its high activity.
- Besides the high CO oxidation activity and the fact that CO adsorption does not lead to CO poisoning, weak CO_2 adsorption strength of the catalyst limits CO_2 inhibition during PROX reaction.

The last part of the research consisted of SEM, DRIFTS and CO_2 adsorption studies over activated carbon adsorbents prepared by subjecting a commercial sample to different oxidative, alkali and thermal treatments. The major conclusions of this section are as follows:

- The results clearly indicate the enhanced CO_2 adsorption capacities of the air and HNO_3 oxidized samples as a result of Na_2CO_3 modification.
- With Na_2CO_3 impregnation the CO_2 mass uptakes at 20 bars and 25ºC were improved by ca. 8 and 7 folds and at 1 bar were increased ca. 15 and 16 folds, on the average, for air oxidized and nitric acid oxidized samples, respectively.

- The adsorption capacities of the nonimpregnated samples could be increased by high temperature helium treatments or increasing the adsorption temperature through decomposition of surface oxygen groups, leaving free sites for CO_2 adsorption.
- The loss in the adsorption capacity due to cyclic adsorption-desorption procedures was overcome with further stabilization of the surface of Na_2CO_3 modified samples with high temperature helium treatments.
- DRIFTS studies revealed the formation of carboxylic acid groups on the HNO_3 oxidized adsorbents; increased aromatization was observed for HNO_3 oxidized and Na_2CO_3 impregnated samples. The formation of basic groups due to Na_2CO_3 addition to air and HNO_3 oxidized samples was also proved by the DRIFTS studies.

5.2. Recommendations

According to the results of the present study, the following points are thought to be beneficial for the future studies:

- Kinetic studies can be performed over Au-Re/ceria (imp+dp) catalysts in order to obtain a power-law type WGS rate expression.
- Deposition precipitation technique can be used for Re addition while preparing Au-Re/ceria catalysts to cover the effect of all the possible preparation method strategies on WGS activity.
- Different Au and Re loadings can be studied to find an optimum Au/Re ratio, which will lead to improvement of WGS activity and the stability of Au-Re/ceria catalysts.
- Water can be connected to the FTIR-DRIFTS-MS system in order to observe the changes in the surface concentration during WGS reaction. The surface/intermediate species which would form on the catalysts' surfaces under the flow of a feed containing both CO and H_2O is of crucial importance in determination of surface mechanism.
- The water vapor formed during DRIFTS experiments can be vacuumed so that it is possible to conduct experiments at temperatures above 200°C.

- Selective CO_2 adsorption tests can be conducted on the AC adsorbents and Pt-Sn/AC3 catalyst on the Intelligent Gravimetric Analyzer system in order to investigate their adsorption behaviors under the realistic conditions similar to that of a fuel processor.
- The chemical modification of the activated carbon adsorbents can be done by NaOH impregnation so that the CO_2 adsorption capacities of the Na_2CO_3 modified and NaOH modified samples can be compared.

REFERENCES

1. Sabonnadiere, J. C., *Renewable Energies*, John Wiley & Sons, Inc., New York, NY, USA, 2009.

2. Ghenciu, A. F., "Review of Fuel Processing Catalysts for Hydrogen Production in PEM Fuel Cell Systems", *Current Opinion in Solid State and Materials Science*, Vol. 6, pp. 389-399, 2002.

3. Song C., "Fuel Processing for Low-Temperature and High-Temperature Fuel Cells. Challenges and Opportunities for Sustainable Development in the 21st Century", *Catalysis Today*, Vol. 77, No. 1-2, pp. 17-49, 2002.

4. Cheekatamarla P. and A. M. Lane, "Efficient Bimetallic Catalysts for Hydrogen Generation from Diesel Fuel", *International Journal of Hydrogen Energy*, Vol. 30, No. 11, pp. 1277-1285, 2005.

5. Ghenciu A. F., "Fuel Processing Catalysts for Hydrogen Reformate Generation for PEM Fuel Cell", *Fuel Cell Magazine*, April/May 2003

6. Trimm, D. L., Z. I. Onsan, "Onboard Fuel Conversion for Hydrogen-Fuel-Cell-Driven Vehicles", *Catalysis Reviews Science and Engineering*, Vol. 43, pp. 31-84, 2001.

7. Damen K., M. Troost., A. Faaij, W. Turkenburg, "A Comparison of Electricity and Hydrogen Production Systems with CO_2 Capture and Storage. Part A: Review and Selection of Promising Conversion and Capture Technologies", *Progress in Energy and Combustion Science*, Vol. 33, No. 6, pp. 580-609, 2007.

8. Yong Z., V. G. Mata, A. E. Rodrigues, "Adsorption of Carbon Dioxide at High Temperature – A Review", *Separation and Purification Technology*, Vol. 26, No. 2-3, pp. 195-205, 2002

9. Duarte de Farias, A. M., P. Bargiela, M. G. C. Rocha, M. A. Fraga, "Vanadium-Promoted Pt/CeO_2 Catalyst for Water-Gas Shift Reaction", *Journal of Catalysis*, Vol. 260, pp. 93-102, 2008.

10. Fu, Q., H. Saltsburg, M. Flytzani-Stephanopoulos, "Active Nonmetallic Au and Pt Species on Ceria-Based Water-Gas Shift Catalysts", *Science*, Vol. 301, pp. 935-938, 2003.

11. Choung, S. Y., M. Ferrandon, T. Krause, "Pt-Re Bimetallic Supported on CeO_2-ZrO_2 Mixed Oxides as Water-Gas Shift Catalysts", *Catalysis Today*, Vol. 99, pp. 257-262, 2005.

12. Leppelt, P., B. Schumacher, V. Plzak, M. Kinne, R. J. Behm, "Kinetics and Mechanism of the Low-Temperature Water-Gas Shift Reaction on Au/CeO_2 Catalysts in an Idealized Reaction Atmosphere", *Journal of Catalysis*, Vol. 244, pp. 137-152, 2006.

13. Sun, J., J. DesJardins, J. Buglass, K. Liu, "Noble Metal Water Gas Shift Catalysis: Kinetics Study and Reactor Design", *International Journal of Hydrogen Energy*, Vol. 30, pp. 1259-1264, 2005.

14. Vignatti, C., M. S. Avila, C. R. Apesteguia, T. F. Garetto, "Catalytic and DRIFTS Study of the WGS Reaction on Pt-Based Catalysts", *International Journal of Hydrogen Energy*, Vol 35, pp. 7302-7312, 2010.

15. Nguyen-Thanh, D., A. M. Duarte de Farias, M. A. Fraga, "Characterization and Activity of Vanadia-Promoted Pt/ZrO_2 Catalysts for the Water-Gas Shift Reaction", *Catalysis Today*, Vol. 138, pp. 235-238, 2008.

16. Lee, H. C., D. Lee, O. Y. Lim, S. Kim, Y. T. Kim, E. Y. Ko, E. D. Park, "ZrO_2-Supported Pt Catalysts for Water Gas Shift Reaction and Their Non-pyrophoric Property", *Studies in Surface Science and Catalysis*, Vol. 167, pp. 201-206, 2007.

17. Iida, H., A. Igarashi, "Structure Characterization of Pt-Re/TiO_2 (Rutile) ad Pt-Re/ZrO_2 Catalysts for Water-Gas Shift Reaction at Low-Temperature", *Applied Catalysis A: General*, Vol. 308, pp. 192-198, 2006.

18. Sato, Y. U., K. Terada, S. Hasegawa, T. Miyao, S. Naito, "Mechanistic Stuty of Water-Gas-Shift Reaction over TiO_2 Supported Pt-Re ad Pd-Re Catalysts", *Applied Catalysis A: General*, Vol. 296, pp. 80-89, 2005.

19. Sato, Y. U., K. Terada, Y. Soma, T. Miyao, S. Naito, "Marked Addition Effect of Re upon the Water Gas Shift Reaction over TiO_2 Supported Pt, Pd and Ir Catalysts", *Catalysis Communications*, Vol. 7, pp. 91-95, 2006.

20. Gonzalez, I. D., R. M. Navarro, M. C. Alvarez-Galvan, F. Roza, J. L. G. Fierro, "Performance Enhancement in the Water-Gas Shift Reaction of Platinum Deposited over a Cerium-Modified TiO_2 Support", *Catalysis Communications*, Vol. 9, pp. 1759-1765, 2008.

21. Azzam, K. G., I. V. Babich, K. Seshan, L. Lefferts, "A Bifunctional Catalyst for the Single-Stage Water-Gas Shift Reaction in Fuel Cell Applications. Part 2. Roles of the Support and Promoter on Catalyst Activity and Stability", *Journal of Catalysis*, Vol. 251, pp. 163-171, 2007.

22. Panagiotopoulou, P., D. I. Kondarides, "A Comparitive Study of the Water-Gas Shift Activity of Pt Catalysts Supported on Single (MO_x) and Composite (MO_x/Al_2O_3, MO_x/TiO_2) Metal Oxide Carriers", *Catalysis Today*, Vol. 127, pp. 319-329, 2007.

23. Radhakrishnan, R., R. R. Willigan, Z. Dardas, T. H. Vanderspurt, "Water Gas Shift Activity and Kinetics of Pt/Re Catalysts Supported on Ceria-Zirconia Oxides", *Applied Catalysis B: Environmental*, Vol. 66, pp. 23-28, 2006.

24. Radhakrishnan, R., R. R. Willigan, Z. Dardas, T. H. Vanderspurt, "Water Gas Shift Activity of Noble Metals Supported on Ceria-Zirconia Oxides", *AIChE Journal*, Vol. 52, No. 5, pp. 1888-1894, 2006.

25. Phatak, A. A., Koryabkina N., Rai S., Ratts J. L., Ruettinger W., Farrauto R. J., Blau G. E., Delgass W. N., Ribeiro F. H., "Kinetics of the Water-Gas Shift Reaction on Pt Catalysts Supported on Alumina and Ceria", *Catalysis Today*, Vol. 123, pp. 224-234, 2007.

26. Kalamaras, C. M., G. G. Olympiou, A. M. Efstathiou, "The Water-Gas Shift Reaction on Pt/γ-Al_2O_3 Catalyst: Operando SSITKA-DRIFTS-Mass Spectroscopy Studies", *Catalysis Today*, Vol. 138, pp. 228-234, 2008.

27. Germani, G, P. Alphonse, M. Courty, Y. Schurman, C. Mirodatos, "Platinum/Ceria/ Alumina Catalysts on Microstructures for Carbon Monoxide Conversion", *Catalysis Today*, Vol. 110, pp. 114-120, 2005.

28. Hurtado-Juan, M. A., C. M. Y. Yeung, S. C. Tsang, "A Study of Co-Precipitated Bimetallic Gold Catalysts for Water-Gas Shift Reaciton" *Catalysis Communications*, Vol. 9, pp. 1551-1557, 2008.

29. Meunier, F. C., A. Goguet, C. Hardacre, R. Burch, D. Thompsett, "Quantitative DRIFTS Investigation of Possible Reaction Mechanisms for the Water-Gas Shift Reaction on High-Activity Pt- and Au-Based Catalysts", *Journal of Catalysis*, Vol. 252, pp. 18-22, 2007.

30. Jacobs, G., S. Ricote, P. M. Patterson, U. M. Graham, A. Dozier, S. Khalid, E. Rhodus, B. H. Davis, "Low Temperature Water-Gas Shift: Examining the Efficiency of Au as a Promoter for Ceria-Based Catalysts Prepared by CVC of Au Precursor", *Applied Catalysis A: General*, Vol. 292, pp. 229-243, 2005.

31. Panagiotopoulou, P., J. Papavasiliou, G. Avgouropoulos, T. Ioannides, D. I. Kondarides, "Water-Gas Shift Activity of Doped Pt/CeO_2 Catalysts", *Chemical Engineering Journal*, Vol. 134, pp. 16-22, 2007.

32. Haryanto, A., S. Fernando, S. Adhikari, "Ultrahigh Temperature Water Gas Shift Catalysts to Increase Hydrogen Yield from Biomass Gasification", *Catalysis Today*, Vol. 129, pp. 269-274, 2007.

33. Tabakova, T., F. Boccuzzi, M. Manzoli, D. Andreeva, "FTIR Study of Low-Temperature Water-Gas Shift Reaction on Gold/Ceria Catalyst", *Applied Catalysis A: General*, Vol. 252, pp. 385-397, 2003.

34. Fu, Q., A. Weber, M. Flytzani-Stephanopoulos, "Nanostructured Au-CeO_2 Catalysts for Low-Temperautre Water-Gas Shift", *Catalysis Letters*, Vol. 77, No. 1-3, pp. 87-95, 2001.

35. Kim, C. H., L. T. Thompson, "On the Importance of Nanocrystalline Gold for Au/CeO_2 Water-Gas Shift Catalysts", *Journal of Catalysis*, Vol. 244, pp. 248-250, 2006.

36. Andreeva, D., V. Idakiev, T. Tabakova, L. Ilieva, P. Falaras, A. Bourlinos, A. Travlos, "Low-Temperature Water-Gas Shift Reaction over Au/CeO_2 Catalysts" *Catalysis Today*, Vol. 72, pp. 51-57, 2002.

37. Idakiev, V., T. Tabakova, K., Tenchev, Z. Y. Yuan, T. Z. Ren, B. L. Su, "Gold Nanoparticles Supported on Ceria-Modified Mesoporous Titania as Highly Active Catalysts for Low-Temperature Water-Gas Shift Reaction", *Catalysis Today,* Vol. 128, pp. 223-229, 2007.

38. Sakurai, H., T. Akita, S. Tsubota, M. Kiuchi, M. Haruta, "Low-Temperature Activity of Au/CeO_2 for Water Gas Shift Reaction, and Characterization by ADF-STEM, Temperature-Programmed Reaction, and Pulse Reaction", *Applied Catalysis A: General*, Vol. 291, pp. 179-187, 2005.

39. Sandoval, A., A. Gomez-Cortes, R. Zanella, G. Diaz, J. M. Saniger, "Gold Nanoparticles: Support Effects for the WGS Reaction", *Journal of Molecular Catalysis A: Chemical*, Vol. 278, No. 1-2, pp. 200-208, 2007.

40. Andreeva, D., I. Ivanov, L. Ilieva, J. W. Sobczak, G. Avdeev, T. Tabakova, "Nanosized Gold Catalysts Supported on Ceria and Ceria-Alumina for WGS Reaction: Influence of the Preparation Method", *Applied Catalysis A: General*, Vol. 333, pp. 153-160, 2007.

41. Si, R., M. Flytzani-Stephanopoulos, "Shape and Crystal-Plane Effects of Nanoscale Ceria on the Activity of Au-CeO_2 Catalysts for the Water-Gas Shift Reaction", *Angewandte Chemie International Edition*, Vol. 47, pp. 2884-2887, 2008.

42. Tabakova, T., F. Bocuzzi, M. Manzoli, J. W. Sobczak, V. Idakiev, D. Andreeva, "Effect of Synthesis Procedure on the Low-Temperature WGS Activity of Au/Ceria Catalysts", *Applied Catalysis B: Environmental*, Vol. 49, pp. 73-81, 2004.

43. Luengnaruemitchai, A., S. Osuwan, E. Gulari, "Comparitive Studies of Low-Temperature Water-Gas Shift Reaction over Pt/CeO_2, Au/CeO_2, and Au/Fe_2O_3 Catalysts", *Catalysis Communications*, Vol. 4, pp. 215-221, 2003.

44. Denkwitz, Y., A. Karpenko, V. Plzak, R. Leppelt, B. Schumacher, R. J. Behm, "Influence of CO_2 and H_2 on the Low-Temperature Water-Gas Shift Reaction on Au/CeO_2 Catalysts in Idealized and Realistic Reformate", *Journal of Catalysis*, Vol. 246, pp. 74-90, 2007.

45. Schubert, M. M., S. Hackenberg, A. C. Veen, M. Muhler, V. Plzak, R. J. Behm, "CO Oxidation over Gold Catalysts – "Inert" and "Active" Support Materials and Their Role for the Oxygen Supply during Reaction", *Journal of Catalysis*, Vol. 197, No. 1, pp. 113-122, 2001.

46. Tabakova, T., V. Idakiev, D. Andreeva, I. Mitov, "Influence of the Microscopic Properties of the Support on the Catalytic Activity of Au/ZnO, Au/ZrO_2, Au/Fe_2O_3, Au/Fe_2O_3-ZnO, Au/Fe_2O_3-ZnO_2 Catalysts for the WGS Reaction", *Applied. Catalysis A: General*, Vol. 202, No. 1, pp. 91-97, 2000.

47. Li, Y., Q. Fu, M. Flytzani-Stephanopoulos, "Low-Temperature Water-Gas Shift Reaction over Cu- and Ni-Loaded Cerium Oxide Catalysts", *Applied Catalysis B: General*, Vol. 27, No. 3, pp. 179-191, 2000.

48. Haruta, M., "Size- and Support-Dependency in the Catalysis of Gold", *Catalysis Today*, Vol. 36, No.1, pp. 153-157, 1997.

49. Panagiotopoulou, P., J. Papavasiliou, G. Avgouropoulos, T. Ioannides, D. I. Kondarides, "Water-Gas Shift Activity of Doped Pt/CeO_2 Catalysts", *Chemical Engineering Journal*, Vol. 134, No. 1-3, pp. 16-22, 2007.

50. Andreeva, D., I. Ivanov, L. Ilieva, M. V. Abrashev, R. Zanella, J. W. Sobczak, W. Lisowski, M. Kantcheva, G. Avdeev, K. Petrov, "Gold Catalysts Supported on Ceria Doped by Rare Earth Metals for Water Gas Shift Reaction: Influence of the Preparation Method", *Applied Catalysis A: General*, Vol. 357, pp. 159-169, 2009.

51. Andreeva, D., M. Kantcheva, I. Ivanov, L. Ilieva, J. W. Sobczak, W. Lisowski, "Gold Supported on Ceria Doped by Me^{3+} (Me = Al and Sm) for Water Gas Shift Reaction: Influence of Dopant and Preparation Method", *Catalysis Today*, Vol. 158, pp. 69-77, 2010.

52. Yu, Q., W. Chen, Y. Li, M. Jin, Z. Suo, "The Action of Pt in Bimetallic Au-Pt/CeO_2 Catalyst for Water-Gas Shift Reaction", *Catalysis Today*, Vol. 158, pp. 324-328, 2010.

53. Leppelt, R., B. Schumacher, V. Plzak, M. Kinne, R. J. Behm, "Kinetics and Mechanism of the Low-Temperature Water-Gas Shift Reaction on Au/CeO_2 Catalysts in an Idealized Reaction Atmosphere", *Journal of Catalysis*, Vol. 244, pp. 137-152, 2006.

54. Jacobs, G., P. M. Patterson, L. Williams, E. Chenu, D. Sparks, G. Thomas, B. H. Davis, "Water-Gas shift: in situ Spectroscopic Studies of Noble Metal Promoted Ceria Catalysts for CO Removal in Fuel Cell Reformers and Mechanistic Implications", *Applied Catalysis A: General*, Vol. 262, pp. 177-187, 2004.

55. Rodriguez, J. A., "Gold-Based Catalysts for the Water-Gas Shift Reaction: Active Sites and Reaction Mechanism", *Catalysis Today*, Vol. 160, pp. 3-10, 2011.

56. Chen, Y., J. Cheng, P. Hu, H. Wang, "Examining the Redox and Formate Mechanisms for Water-Gas Shift Reaction on Au/CeO_2 Using Density Functional Theory", Surface Science, Vol. 602, pp. 2828-2834, 2008.

57. Meunier, F. C., C. Reid, A. Goguet, S. Shektman, C. Hardacre, R. Burch, W. Deng, M. Flytzani-Stephanoulos, "Quantitative Analysis of the Reactivity of Formate Species Seen by DRIFTS over a $Au/Ce(La)O_2$ Water-Gas Shift Catalyst: First Unambiguous Evidence of the Minority Role of Formates as Reaction Intermediates", *Journal of Catalysis*, Vol. 247, pp. 277-287, 2007.

58. Jacobs, G., E. Chenu, P. M. Patterson, L. Williams, D. Sparks, G. Thomas, B. H. Davis, "Water-Gas Shift: Comparative Screening of Metal Promoters for Metal/Ceria Systems and Role of the Metal", *Applied Catalysis A: General*, Vol. 258, pp. 203-214, 2004.

59. Kim, C. H., L. T. Thompson, "Deactivation of Au/CeO_x Water Gas Shift Catalysts", *Journal of Catalysis*, Vol. 230, pp. 66-74, 2005.

60. Tibiletti, D., A. Goguet, D. Reid, F. C. Meunier, R. Burch, "On the Need to use Steady-State or Operand Techniques to Investigate Reaction Mechanisms: As in situ DRIFTS and SSITKA-Based Study Example", *Catalysis Today*, Vol. 113, pp. 94-101, 2006.

61. Pozdnyakova, O., D. Teschner, A. Wootsch, J. Kröhnert, B. Steinhauer, H. Sauer, L. Toth, F.C. Jentoft, A. Knop-Gericke, Z. Paal, R. Schlögl, "Preferential CO Oxidation in Hydrogen (PROX) on Ceria-Supported Catalysts, Part I: Oxidation State and Surface Species on Pt/CeO_2 under Reaction Conditions", *Journal of Catalysis*, Vol 237, pp. 1-16, 2006.

62. Manasilp, A., E. Gulari, "Selective CO Oxidation over Pt/Alumina Catalysts for Fuel Cell Applications", *Applied Catalysis B: Environmental*, Vol. 37, pp. 17-25, 2002.

63. Laguna, O. H., M. A. Centeno, G. Arzamendi, L. M. Gandia, F. Romero-Sarria, J. A. Odriozola, "Iron-Modified Ceria and Au/Ceria Catalysts for Total and Preferential Oxidation of CO (TOX and PROX)", *Catalysis Today*, Vol. 157, No. 1-4, pp. 155-159, 2010.

64. Laguna, O. H., F. Romero-Sarria, M. A. Centeno, J. A. Odriozola, "Gold Supported on Metal-Doped Ceria Catalysts (M = Zr, Zn and Fe) for the Preferential Oxidation of CO (PROX)", *Journal of Catalysis*, Vol. 276, No. 2, pp. 360-370, 2010.

65. Schubert, M. M., A. Venugopal, M. J. Kahlich, V. Plzak, R. J. Behm, "Influence of H_2O and CO_2 on the Selective CO Oxidation in H_2-Rich Gases over Au/α-Fe_2O_3", *Journal of Catalysis*, Vol. 222, No. 1, pp. 32-40, 2004.

66. Tabakova, T., G. Avgouropoulos, J. Papavasiliou, M. Manzoli, F. Boccuzzi, K. Tenchev, F. Vindigni, T. Ioannides, "CO-Free Hydrogen Production over Au/CeO_2-Fe_2O_3 Catalysts: Part 1. Impact of the Support Composition on the Performance for the Preferential CO Oxidation Reaction", *Applied Catalysis B: Environmental*, Vol. 101, No. 3-4, pp. 256-265, 2011.

67. Schubert, M. M., M. J. Kahlich, H. A. Gasteiger, R. J. Behm, "Correlation Between CO Surface Coverage and Selectivity/Kinetics for the Preferential CO Oxidation over Pt/γ-Al_2O_3/α-Fe_2O_3: An in-situ DRIFTS Study", *Journal of Power Sources*, Vol. 84, No. 2, pp. 175-182, 1999.

68. Liotta, L. F., G. Di Caro, G. Pantaleo, A. M. Venezia, "Supported Gold Catalysts for CO Oxidation and Preferential Oxidation of CO in H_2 Stream: Support Effect", *Catalysis Today*, Vol. 158, No. 1-2, pp. 56-62, 2010

69. Piccolo, L., H. Daly, A. Valcarcel, F. C. Meunier, "Promotional Effect of H_2 on CO Oxidation over Au/TiO_2 Studied by Operand Infrared Spectroscopy", *Applied Catalysis B: Environmental*, Vol. 86, No. 3-4, pp. 190-195, 2009.

70. Quinet, E., L. Piccolo, F. Morfin, P. Avenier, F. Diehl, V. Caps, J. L. Rousset, "On the Mechanism of Hydrogen-Promoted Gold-Catalyzed CO Oxidation", *Journal of Catalysis*, Vol. 268, No. 2, pp. 384-389, 2009.

71. Schumacher, B., Y. Denkwitz, V. Plzak, M. Kinne, R. J. Behm, "Kinetics, Mechanism, and the Influence of H_2 on the CO Oxidation Reaction on a Au/TiO_2 Catalyst", *Journal of Catalysis*, Vol. 224, No. 2, pp. 449-462, 2004.

72. Ayastuy, J. L., M. P. Gonzalez-Marcos, M. A. Gutierrez-Ortiz, "Promotion Effect of Sn in Alumina-Supported Pt Catalysts for CO-PROX", *Catalysis Communications,* Vol. 12, No. 10, pp. 895-900, 2011.

73. Kahlich, M. J., H. A. Gasteiger, R. J. Behm, "Kinetics of the Selective CO Oxidation in H_2-Rich Gas on Pt/Al_2O_3", *Journal of Catalysis*, Vol. 171, pp. 93-105, 1997.

74. Bissett, E. J., S. H. Oh, R. M. Sinkevitch, "Pt Surface Kinetics for a PrOx Reactor for Fuel Cell Feedstream Processing", *Chemical Engineering Science*, Vol. 60, pp. 4709-4721, 2005.

75. Ayastuy, J. L., M. P. Gonzalez-Marcos, M. A. Gutierrez-Ortiz, "Effect of Process Variables on Pt/CeO_2 Catalyst Behavior for the PROX Reaction", *International Journal of Hydrogen Energy*, Vol. 31, pp. 2231-2242, 2006

76. Ayastuy, J. L., M. P. Gonzalez-Marcos, A. Gil-Rodriguez, J. R. Gonzalez-Velasco, M. A. Gutierrez-Ortiz, "Selective CO Oxidation over $Ce_xZr_{1-x}O_2$-Supported Pt Catalysts", *Catalysis Today*, Vol. 116, pp. 391-399, 2006.

77. Wootsch, A., C. Descorme, D Duprez, "Preferential Oxidation of Carbon Monoxide in the Presence of Hydrogen (PROX) over Ceria-Zirconia and Alumina-Supported Pt Catalysts", *Journal of Catalysis*, Vol. 225, pp. 259-266, 2004.

78. Korotkikh, O., R. Farrauto, "Selective Catalytic Oxidation of CO in H_2: Fuel Cell applications", *Catalysis Today*, Vol. 62, pp. 249-254, 2000.

79. Liu, X., O. Korotkikh, R. Farrauto, "Selective Catalytic Oxidation of CO in H_2: Structural Study of Fe Oxide-Promoted Pt/Alumina Catalyst", *Applied Catalysis A: General*, Vol. 226, pp. 293-303, 2002.

80. Igarashi, H., H. Uchida, M. Suzuki, Y. Sasaki, M. Watanabe, "Removal of Carbon Monoxide from Hydrogen-Rich Fuels by Selective Oxidation over Platinum Catalyst Supported on Zeolite", *Applied Catalysis A: General*, Vol. 159, pp. 159-169, 1997.

81. Igarashi, H., H. Uchida, M. Watanabe, "Mordenite-Supported Noble Metal Catalysts for Selective Oxidation of Carbon Monoxide in a Reformed Gas", *Chemistry Letters*, Vol. 329, No. 11, pp. 1262-1263, 2000.

82. Watanabe, M., H. Uchida, K. Ohkubo, H. Igarashi, "Hydrogen Purification for Fuel Cells: Selective Oxidation of Carbon Monoxide on Pt-Fe/Zeolite Catalysts", *Applied Catalysis B: Environmental*, Vol. 46, pp. 595-600, 2003.

83. Echigo, M., N. Shinke, S. Takami, S. Higashiguchi, K. Hirai, T. Tabata, "Development of Residual PEFC Cogeneration Systems: Ru Catalyst for CO Preferential Oxidation in Reformed Gas", *Catalysis Today*, Vol. 84, No. 3-4, pp. 209-215, 2003.

84. Han, Y. F., M. J. Hahlich, M. Kinne, R. J. Behm, "Kinetic Study of Selective CO Oxidation in H_2-Rich Gas on a Ru/γ-Al_2O_3 Catalyst", *Physical Chemistry Chemical Physics*, Vol. 4, No. 2, pp. 389-397, 2002.

85. Worner, A., C. Friedrich, R. Tamme, "Development of a Novel Ru-Based Catalyst System for the Selective Oxidation of CO Mixtures", *Applied Catalysis A: General*, Vol. 245, No. 1, pp. 1-14, 2003.

86. Han, Y. F., M. J. Hahlich, M. Kinne, R. J. Behm, "CO Removal from Realistic Methanol Reformate via Preferential Oxidation – Performance of a Rh/MgO Catalyst and Comparison to Ru/γ-Al_2O_3, and Pt/γ-Al_2O_3", *Applied Catalysis B: Environmental*, Vol. 50, pp. 209-218, 2004.

87. Jain, S. K., E. M. Crabb, L. E. Smart, D. Thompsett, A. M. Steele, "Controlled Modification of Pt/Al_2O_3 for the Preferential Oxidation of CO in Hydrogen: A Comparative Study of Modifying Element", *Applied Catalysis B: Environmental*, Vol. 89, pp. 349-355, 2009.

88. Schubert, M. M., M. J. Kahlich, G. Feldmeyer, M. Hüttner, S. Hackenberg, H. A. Gasteiger, R. J. Behm, "Bimetallic PtSn Catalyst for Selective CO Oxidation in H_2-Rich Gases at Low Temperatures", *Physical Chemistry Chemical Physics*, Vol. 3, pp. 1123-1131, 2001.

89. Garrido, G. I., F. C. Patcas, G. Upper, M. Turk, S. Yilmaz, B. Kaushaar-Czarnetzki, "Supercritical Deposition of Pt on SnO_2-Coated Al_2O_3 Foams: Phase Behavior and Catalytic Performance", *Applied Catalysis A: General*, ,Vol. 338, No. 1-2, pp. 58-65, 2008.

90. Grass, K., H. G. Lintz, "The Kinetics of Carbon Monoxide Oxidation on Tin (IV) Oxide Supported Platinum Catalysts", *Journal of Catalysis*, Vol. 172, No. 2, pp. 446-452, 1997.

91. Tillmann, S., G. Samjeske, K. A. Friedrich, H. Baltruschat, "The Adsorption of Sn on Pt (111) and its Influence on CO Adsorption as studied by XPS and FTIR", *Electrochimica Acta*, Vol. 49, No. 1, pp. 73-83, 2003.

92. Liu, H., L. Ma, S. Shao, Z. Li, A. Wang, Y. Huang, T. Zhang, "Preferential CO Oxidation on Ce-Promoted Pt/γ-Al_2O_3 Catalysts under H_2-Rich Atmosphere", *Chinese Journal of Catalysis*, Vol. 28, No. 12, pp. 1077-1082, 2007

93. Arteaga, G. J., J. A. Anderson, C. H. Rochester, "FTIR Study of CO Adsorption on Coked $Pt\text{-}Sn/Al_2O_3$ Catalysts", *Catalysis Letters*, Vol. 58, pp. 189-194, 1999.

94. Schubert, M. M., H. A. Gasteiger, R. J. Behm, "Surface Formates as Side Products in the Selective CO Oxidation on Pt/γ-Al_2O_3", *Journal of Catalysis*, Vol. 172, pp. 256-258, 1997.

95. Guerrero, S. J. T. Miller, E. E. Wolf, "Activity and Selectivity Control by Niobium for the Preferential Oxidation of CO on Pt Supported Catalysts", *Applied Catalysis A: General*, Vol. 328, No. 1, pp. 27-34, 2007

96. deMonerval, L. C., A. Chaqroune, B. Coq, F. Figueras, "Characterization of Mono- and Bi-Metallic Platinum Catalysts Using CO FTIR Spectroscopy – Size Effects and Topological Segregation", *Journal of the Chemical Society – Faraday Transactions*, Vol. 93, No. 20, pp. 3715-3720, 1997.

97. Balakrishnan, K., J. Schwank, "FTIR Study of Bimetallic Pt-Sn/Al_2O_3 Catalysts", *Journal of Catalysis*, Vol. 138, No. 2, pp. 491-499, 1992.

98. Llorca, J., N. Homs, J. Arana, J. Sales, P. R. de la Piscina, "FTIR Study of the Interaction of CO and CO_2 with Silica-Supprted Pt-Sn Alloy", *Applied Surface Science*, Vol. 134, No. 1-4, pp. 217-224, 1998.

99. Bulushev, D. A., I. Yuranov, E. I. Suvurova, P. A. Buffat, L. Kiwi-Minsker, "Highly Dispersed Gold on Activated Carbon Fibers for Low-Temperature CO Oxidation", *Journal of Catalysis*, Vol. 224, pp. 8-17, 2004.

100. Aksoylu, A. E., M. Freitas, M. F. R. Pereira, J. L. Figueiredo, "The Effects of Different Activated Carbon Supports and Support Modifications on the Properties of Pt/AC Catalysts", *Carbon*, Vol. 39, pp. 175-185, 2001.

101. Aksoylu, A. E., M. Freitas, J. L. Figueiredo, "Bimetallic Pt-Sn Catalysts Supported on Activated Carbon. I. The Effects of Support Modification and Impregnation Strategy", *Applied Catalysis A: General*, Vol. 192, pp. 29-42, 2000.

102. Aksoylu, A. E., M. Freitas, J. L. Figueiredo, "Bimetallic Pt-Sn Catalysts Supported on Activated Carbon. II. CO Oxidation", *Catalysis Today*, Vol. 62, pp.337-346, 2000.

103. Ozkara, S., A. E. Aksoylu, "Selective Low Temperature Carbon Monoxide Oxidation in H_2-Rich Gas Streams over Activated Carbon Supported Catalysts", *Applied Catalysis A: General*, Vol. 251, pp. 75-83, 2003.

104. Baltacioglu, F. S., B. Gulyuz, A. E. Aksoylu, Z. I. Onsan, "Low Temperature CO Oxidation Kinetics over Activated Carbon Supported Pt-SnO_x Catalysts", *Turkish Journal of Chemistry*, Vol. 31, pp. 455-464, 2007

105. Simsek, E., S. Ozkara, A. E. Aksoylu, Z. I. Onsan, "Preferential CO Oxidation over Activated Carbon Supported Catalysts in H_2-Rich Gas Streams Containing CO_2 and H_2O", *Applied Catalysis A: General*, Vol. 316, pp. 169-174, 2007.

106. Soykal, I., *Preferential Oxidation Performance of Pt-Sn/AC Catalysts*, MS Thesis, Bogazici University, 2006.

107. Gulmen, M. A., A. Sumer, A. E. Aksoylu, "Adsorption Properties of CO in Low-Index Pt_3Sn Surfaces", *Surface Science*, Vol. 600, pp. 4909-4921, 2006.

108. Sumer, A., M. A. Gulmen, A. E. Aksoylu, "CO and O Coadsorption on Pt_3Sn Studied by DFT: Changes in the Adsorptive Properties of the Surface with Alloying and Coverage", *Surface Science*, Vol. 602, No. 9, pp. 1636-1642, 2008.

109. Sumer, A., A. E. Aksoylu, "A Theoretical Investigation of Pt_3Sn (102) Surface Alloy and CO-Pt_3Sn (102) Cystem", *Surface Science*, Vol. 600, No. 10, pp. 2026-2039, 2006.

110. Biniak, S., G. Szymanski, J. Siedlewski, A. Swiatkowski, "The Characterization of Activated Carbons with Oxygen and Nitrogen Surface Groups", *Carbon*, Vol. 35, No. 12, pp. 1799-1810, 1997.

111. Rodriguez-Reinoso, F., M. Molina-Sabio, "Textural and Chemical Characterization of Microporous Carbons", *Advances in Colloid and Interface Science*, Vol. 76-77, pp. 271-294, 1998.

112. Nakagawa, K., S. R. Mukai, T. Suzuki, H. Tamon, "Gas Adsorption on Activated Carbons from PET Mixtures with a Metal Salt", *Carbon*, Vol. 41, pp. 823-831, 2003.

113. Auer, E., A. Freund, J. Pietsch, T. Tacke, "Carbons as Supports for Industrial Precious Metal Catalysts", *Applied Catalysis A: General*, Vol. 173, pp. 259-271, 1998.

114. Roman-Martinez, M. C., D. Cazorla-Amoros, A. Linares-Solano, C. Salinas-Martinez de Lecea, H. Yamashita, M. Anpo, "Metal-Support Interaction in Pt/C Catalysts. Influence of the Support Surface Chemistry and the Metal Precursor", *Carbon*, Vol. 33, No. 1, pp. 3-13, 1995.

115. Li, L., P. A. Quinlivan, D. R. U. Knappe, "Effects of Activated Carbon Surface Chemistry and Pore Structure on the Adsorption of Organic Contaminants from Aqueous Solution", *Carbon*, Vol. 40, pp. 2085-2100, 2002.

116. Pradhan, B. K., N. K. Sandle, "Effect of Different Oxidizing Agent Treatments on the Surface Properties of Activated Carbons", *Carbon*, Vol. 37, pp. 1323-1332, 1999.

117. Strelko Jr., V., D. J. Malik, M. Streat, "Characterization of the Surface of Oxidized Carbon Adsorbents", *Carbon*, Vol. 40, pp. 95-104, 2002.

118. Montoya, A., F. Mondragon, T. N. Truong, "CO_2 Adsorption on Carbonaceous Surfaces: A Combined Experimental and Theoretical Study", *Carbon*, Vol. 41, pp. 29-39, 2003.

119. Severini, F., L. Formaro, M. Pegoraro, L. Posca, "Chemical Modification of Carbon Fiber surfaces", *Carbon*, Vol. 40, pp. 735-741, 2002.

120. Figueiredo, J. L., M. F. R. Pereira, M. M. A. Freitas, J. J. M. Orfao, "Modification of the Surface Chemistry of Activated Carbons", *Carbon*, Vol. 37, pp. 1379-1389, 1999.

121. Shim, J. W., S. J. Park, S. K. Ryu, "Effect of Modification with HNO_3 and NaOH on Metal Adsorption by Pitch-Based Activated Carbon Fibers", *Carbon*, Vol. 39, pp. 1635-1642, 2001.

122. Boonamnuayvitaya, V., S. Sae-ung, W. Tanthapanichakoon, "Preparation of Activated Carbons from Coffee Residue for the Adsorption of Formaldehyde", *Separation Purification Technology,* Vol. 42, pp. 159-168, 2005.

123. Puziy, A.M., O. I. Poddubnaya, A. Martinez-Alonso, F. Suarez-Garcia, J. M. D. Tascon, "Surface Chemistry of Phosphorus-Containing Carbons of Lignocellulosic Origin", *Carbon*, Vol. 43, pp. 2857-2868, 2005.

124. Dandekar, A., R. T. K. Baker, M. A. Vannice, "Characterization of Activated Carbon, Graphitized Carbon Fibers and Synthetic Diamond Powder Using TPD and DRIFTS", *Carbon,* Vol. 36, No. 12, pp. 1821-1831, 1998.

125. El-Hendawy, A. A., A. J. Alexander, R. J. Andrews, Forrest G, "Effects of Activation Schemes on Porous, Surface and Thermal Properties of Activated Carbons Prepared from Cotton Stalks", *Journal of Analytical and Applied Pyrolysis*, Vol. 82, pp. 272-278, 2008.

126. ShamsiJazeyi, H., T. Kaghazchi, "Investigation of Nitric Acid Treatment of Activated Carbon for Enhanced Aqeous Mercury Removal", *Journal of Industrial and Engineering Chemistry*, Vol. 16, No. 5, pp. 852-858, 2010.

127. Zhang, Z., M. Xu, H. Wang, Z. Li, "Enhancement of CO_2 Adsorption on High Surface Area Activated Carbon Modified by N_2, H_2 and Ammonia", *Chemical Engineering Journal*, Vol. 160, pp. 571-577, 2010.

128. Prahas, D., Y. Kartika, N. Indraswati, S. Ismadji, "Activated Carbon from Jackfruit Peel Waste by H_3PO_4 Chemical Activation: Pore Structure and Surface Chemistry Characterization", *Chemical Engineering Journal,* Vol. 140, pp. 32-42, 2008.

129. Kohl, S., A. Drochner, H. Vogel, "Quantification of Oxygen Surface Groups on Carbon Materials via Diffuse Reflectance FT-IR Spectroscopy and Temperature Programmed Desorption", *Catalysis Today*, Vol. 150, pp. 67-70, 2010.

130. Macias-Garcia, A., M. A. Diaz-Diez, E. M. Cuerda-Correa, M. Olivares-Marin, J. Gañan-Gomez, "Study of the Pore Size Distribution and Fractal Dimension of HNO_3-Treated Activated Carbons", *Applied Surface Science,* Vol. 252, No. 17, pp. 5972-5975, 2006.

131. Shin, S., J. Jang, S. H. Yoon, I. Mochida, "A Study on the Effect of Heat Treatment on Functional Groups of Pitch Based Activated Carbon Fiber Using FTIR", *Carbon*, Vol. 35, No. 12, pp. 1739-1743, 1997.

132. Przepiorski, J., M. Skrodzewicz, A. W. Morawski, "High Temperature Ammonia Treatment of Activated Carbon for Enhancement of CO_2 Adsorption", *Applied Surface Science*, Vol. 225, pp. 235-242, 2004.

133. Silva, A. M. T., B. F. Machado, J. L. Figueiredo, J. L. Faria JL, "Controlling the Surface Chemistry of Carbon Xerogels Using HNO_3-Hydrothermal Oxidation", *Carbon*, Vol. 47, pp. 1670-1679, 2009.

134. Girgis, B.S., E. Smith, M. M. Louis, A. A. El-Hendawy, "Pilot Production of Activated Carbon from Cotton Stalks Using H_3PO_4", *Journal of Analytical and Applied Pyrolysis*, Vol. 86, pp. 180-184, 2009.

135. Yong, Z., V. G. Mata, A. Rodrigues, "Adsorption of Carbon Dioxide on Chemically Modified High Surface Area Carbon-Based Adsorbents at High Temperatures", *Adsorption*, Vol. 7, pp. 41-50, 2001.

136. Groszek, A. J., "Heats of Adsorption and Desorption of CO_2, CH_4, SO_2, O_2 and N_2 on Microporous Carbons", *Carbon*, Vol. 35, No. 9, pp. 1399-1405, 1999.

137. Plaza, M.G., C. Pevida, A. Arenillas, F. Rrubiera, J. J. Pis, "CO_2 Capture by Adsorption with Nitrogen Enriched Carbons", *Fuel*, Vol. 86, No. 14, pp. 2204-2212, 2007.

138. Lozano-Castello, D., D. Cazorla-Amoros, A. Linares-Solano, "Usefullness of CO_2 Adsorption at 273 K for the Characterization of Porous Carbons", *Carbon*, Vol. 42, No. 7, pp. 1233-1242, 2004.

139. Yong, Z., V. Mata, A. E. Rodrigues, "Adsorption of Carbon Dioxide at High Temperature – a Review", *Separation and Purification Technologies*, Vol. 26, pp. 195-205, 2002.

140. Son, W., J. Choi, W. Ahn, "Adsorptive Removal of Carbon Dioxide Using Polyethyleneimine-Loaded Mesoporous Silica Materials", *Microporous and Mesoporous Materials*, Vol. 113, pp. 31-40, 2008.

141. Sircar, S., T. C. Gulden, M. B. Rao, "Activated Carbon for Gas Separation and Storage", *Carbon*, Vol. 34, No. 1, pp. 1-12, 1996.

142. Shafeeyan, M. S., W. M. A. W. Daud, A. Houshmand, A. Shamari, "A Review on Surface Modification of Activated Carbon for Carbon Dioxide Adsorption", *Journal of Analytical and Applied Pyrolysis*, Vol. 89, pp. 143-151, 2010.

143. Zhou, H., D. Li, G. Gong, Y. Tian, Y. Chen, "Adsorption of Soluble Metal Ions from Red Mud by Modified Activated Carbon", *Key Engineering Materials*, Vol. 368-372, pp. 1541-1544, 2008.

144. Frere, M., G. de Weireld, R. Jadot, "Characterization of Porous Carbonaceous Sorbents Using High Pressure CO_2 Adsorption Data", *Journal of Porous Materials*, Vol. 5, pp. 275-287, 1998.

145. Rodriguez-Reinoso, F., "The Role of Carbon Materials in Heterogeneous Catalysis", *Carbon*, Vol. 36, No. 3, pp. 159-175, 1998.

146. Pevida, C., M. G. Plaza, B. Arias, J. Fermoso, F. Rrubiera, J. J. Pis, "Surface Modification of Activated Carbons for CO_2 Capture", *Applied Surface Science*, Vol. 254, pp. 7165-7172, 2008.

147. Pellerano, M., P. Pre, M. Kacem, A. Delebarre, "CO_2 Capture by Adsorption on Activated Carbons Using Pressure Modulation", *Energy Procedia*, Vol. 1, pp. 647-653, 2009.

148. Himeno, S., T. Komatsu, S. Fujita, "High-Pressure Adsorption Equilibra of Methane and Carbon Dioxide on Several Activated Carbons", *Journal of Chemical and Engineering Data*, Vol. 50, No. 2, pp. 369-376, 2005.

149. Martin, C. F., M. G. Plaza, J. J. Pis, F. Rubiera, C. Pevida, T. A. Centeno, "On the Limits of CO_2 Capture Capacity of Carbons", *Separation Purification Technologies*, Vol. 74, pp. 225-229, 2010.

150. An, H., B. Feng, S. Su, "CO_2 Capture Capacities of Activated Carbon Fibre-Phenolic Resin Composites", *Carbon*, Vol. 47, pp. 2396-2405, 2009.

151. Dastgheib, S. A., T. Karanfil, W. Cheng, "Tailoring Activated Carbons for Enhanced Removal of Natural Organic Matter from Natural Waters", *Carbon*, Vol 42, pp. 547-557, 2004.

152. Chen, W., F. S. Cannon, J. R. Rangel-Mendez, "Ammonia-Tailoring of GAC to Enhance Perchlorate Removal. I: Characterization of NH_3 Thermally Tailored GACs", *Carbon*, Vol. 43, No. 3, pp. 573-580, 2005.

153. Somy, A., M. R. Mehrnia, H. D. Amrei, A. Ghanizadeh, M. Safari, "Adsorption of Carbon Dioxide Using Impregnated Activated Carbon Promoted by Zinc*", International Journal of Greenhouse Gas Control*, Vol. 3, pp. 249-54, 2009.

154. Lillo-Rodenas, M. A., D. Cazorla-Amoros, A. Linares-Solano, "Understanding Chemical Reactions between Carbons and NaOH and KOH: An Insight into the Chemical Activation Mechanism", *Carbon*, Vol. 41, No. 2, pp. 267-275, 2003.

155. Diaz, E., E. Munoz, A. Vega, S. Ordonez, "Enhancement of the CO_2 Retention Capacity of X Zeolites by Na- and Cs-Treatments", *Chemosphere*, Vol. 70, No. 8, pp. 1375-1382, 2008.

156. Guo, B., L. Chang, K. Xie, "Adsorption of Carbon Dioxide on Activated Carbon", *Journal of Natural Gas Chemistry*, Vol. 15, pp. 223-229, 2006.

157. Song, H. K., K. H. Lee, "Adsorption of Carbon Dioxide on Chemically Modified Carbon Adsorbents", *Separation Science and Technology*, Vol. 33, No. 13, pp. 2039-2057, 1998.

158. Akın, A. N., *Development of Coprecipitated Cobalt-Alumina Catalysts for the Production of C_1-C_4 Hydrocarbons by Carbon Monoxide Hydrogenation*, Ph. D. Dissertation, Boğaziçi University, 1996.

159. Ma, L., *Hydrogen Production from Steam Reforming of Light Hydrocarbons in an Autothermic System*, Ph. D. Dissertation, University of South Wales, 1995.

160. Selen, B., *Production of Hydrogen from Light Hydrocarbons via Indirect Partial Oxidation on Bimetallic Catalysts*, MS. Thesis, Boğaziçi University, 2003.

161. Avci, A. K., *Computational and Experimental Investigation of Catalytic Hydrocarbon Fuel Processing for Autothermal Hydrogen Production*, Ph. D. Dissertation, Boğaziçi University, 2003.

162. Caglayan, B. S., A. K. Avci, Z. I. Onsan, A. E. Aksoylu, "Production of hydrogen over bimetallic Pt-Ni/δ-Al_2O_3: I. Indirect Partial Oxidation of Propane", *Applied Catalysis A: General*, Vol. 280, pp. 181-188, 2005.

163. Caglayan, B. S., Z. I. Onsan, A. E. Aksoylu, "Production of hydrogen over bimetallic Pt-Ni/δ-Al_2O_3: II. Indirect Partial Oxidation of LPG", *Catalysis Letters*, Vol. 102, No. 1-2, pp. 63-67, 2005.

164. Gökaliler, F.; B. S. Caglayan, Z. I. Önsan, A. E. Aksoylu, "Hydrogen Production by Autothermal Reforming of LPG for PEM Fuel Cell Applications", *International Journal of Hydrogen Energy,* Vol. 33, pp. 1383-1391, 2008.

165. Damyanova, S., J. M. C. Bueno, "Effect of CeO_2 loading on the Surface and Catalytic Behaviors of CeO_2-Al_2O_3-Supported Pt Catalysts", *Applied Catalysis A: General,* Vol. 253, No. 1, pp. 135-150, 2003.

166. Grisel, R. J. H., B. E. Nieuwenhuys, "A Comparative Study of the Oxidation of CO and CH_4 over Au/MOx/Al_2O_3 Catalysts", *Catalysis Today,* Vol. 64, No. 1-2, pp. 69-81, 2001.

167. Kimura, M., T. Miyao, S. Komori, A. Chen, K. Higashiyama, H. Yamashita, M. Watanabe, "Selective Methanation of CO in Hydrogen-Rich Gases Involving Large Amounts of CO_2 over Ru-Modified Ni-Al Mixed Oxide Catalysts", *Applied Catalysis A: General*, Vol. 379, pp. 182-187, 2010.

168. Liu, Q., Z. Liu, L. W. Liao, X. Dong, "Selective CO Methanation over Amorphous Ni-Ru-B/ZrO_2 Catalyst for Hydrogen-Rich Gas Purification", *Journal of Natural Gas Chemistry*, Vol. 19, pp. 497-502, 2010.

169. Xavier, K. O., R. Sreekala, K. K. A. Rashid, K. K. M. Yusuff, B. Sen, "Doping Effects of Cerium Oxide on Ni/Al_2O_3 Catalysts for Methanation", *Catalysis Today*, Vol. 49, pp. 17-21, 1999.

170. Kim, S. H., S. W. Nam, T. H. Lim, H. I. Lee, "Effect of Pretreatment on the Activity of Ni Catalyst for CO Removal Reaction by Water-Gas Shift and Methanation", *Applied Catalysis B: Environmental,* Vol. 81, pp. 97-104, 2008.

171. Zhang, F., P. Wang, J. Koberstein, S. Khalid, S. Chan, "Cerium Oxidation State in Ceria Nanoparticles Studied with X-Ray Photoelecton Spectroscopy and Absorption Near Edge Spectroscopy", *Surface Science*, Vol. 563, pp. 74-82, 2004.

172. Hwang, K., S. Ihm, J. Park, "Enhanced CeO_2-Supported Pt Catalysts for Water-Gas Shift Reaction", *Fuel Processing Technology*, Vol. 91, No. 7, 2010.

173. Tabakova, T., F. Bocuzzi, M. Manzoli, J. W. Sobczak, V. Idakiev, D. Andreeva, "A Comparative Study of Nanosized IB/Ceria Catalysts for Low-Temperature Water-Gas Shift Reaction", *Applied Catalysis A: General*, Vol. 298, pp. 127-143, 2006.

174. Kundakovic, L., D. R. Mullins, S. H. Overbury, "Adsorption and Reaction of H_2O and CO on Oxidized and Reduced Rh/CeO_x (111) Surfaces", Surface Science, Vol. 457, No. 1-2, pp. 51-62, 2000.

175. Okamoto, H., T. B. Massalski, "The Au-Fe (Gold-Iron) System", *Bulletin of Alloy Phase Diagrams*, Vol. 5, p. 383, 1984.

176. Binet, C., M. Daturi, J. C. Lavalley, "IR Study of Polycrystalline Ceria Properties in Oxidized and Reduced States", *Catalysis Today*, Vol. 50, No. 2, pp. 207-225, 1999.

177. Daniell, W., T. Weingand, H. Knözinger, "Redox Properties of Re_2O_7/Al_2O_3 as Investigated by FTIR spectroscopy of Adsorbed CO", *Journal of Molecular Catalysis A: Chemical*, Vol. 204-205, pp. 519-526, 2003.

178. Cheung, K. C., P. Guo, M. H. So, L. Y. S. Lee, K. P. Ho, W. L. Wong, K. H. Lee, W. T. Wong, Z. Y. Zhou, K. Y. Wong, "Electrocatalytic Reduction of Carbon dioxide by a Polymeric Film of Rhenium Tricarbonyl", *Journal of Organometallic Chemistry*, Vol. 694, No. 17, pp. 2842-2845, 2009.

179. Beamson, G. A. J. Papworth, C. Phillipps, A. M. Smith, R. Whyman, "Selective Hydrogenation of Amides Using Bimetallic Ru/Re and Rh/Re Catalysts", *Journal of Catalysis*, Vol. 278, pp. 228-238, 2011.

180. Azzam, K. G., I. V. Babich, K. Seshan, L. Lefferts, "Role of Re in Pt-Re/TiO_2 Catalyst for Water Gas Shift Reaction: A Mechanistic and Kinetic Study", *Applied Catalysis B: Environmental*, Vol. 80, pp. 129-140, 2008.

181. Daly, H. J. Ni, D. Thompsett, F. C. Meunier, "On the Usefulness of Carbon Isotopic Exchange for the Operando Analysis of Metal-Carbonyl Bands by IR over Ceria-Containing Catalysts", *Journal of Catalysis*, Vol. 254, pp. 238-243, 2008.

182. Mohamed, M. M., K. S. Khairou, "Fabrication and Characterization of Bimetallic Pt-Au Nanowires Supported on FSM-16 and Their Catalytic Activities Toward Water-Gas Shift Reaction", *Journal of Colloid and Interface Science*, Vol. 354, pp. 100-108, 2011.

183. Arunajatesan, V. , B. Subramaniam, K. W. Hutchenson, F. E. Herkes, "In Situ FTIR Investigations of Reverse Water Gas Shift Reaction Activity at Supercritical Conditions", *Chemical Engineering Science*, Vol. 62, pp. 5062-5069, 2007.

184. Teschner, D., A. Wootsch, O. Pozdnyakova-Tellinger, J. Kröhnert, E. M. Vass, M. Havecker, S. Zafeiratos, P. Schnörch, P. C. Jentoft, A. Knop-Gericke, R. Schlögl, "Partial Pressure Dependent in situ Spectroscopic Study on the Preferential CO Oxidation in Hydrogen (PROX) over Pt/Ceria Catalysts", *Journal of Catalysis*, Vol. 249, No. 2, pp. 318-327, 2007.

185. Schweicher, J., A. Bundhoo, A. Frennet, N. Kruse, H. Daly, F. Meunier, "DRIFTS/MS Studies During Chemical Transients and SSITKA of the CO/H_2 Reaction over Co-MgO Catalysts", *Journal of Physical Chemistry C*, Vol. 114, No. 5, pp. 2248-2255, 2010.

186. Sumer, A., A. E. Aksoylu, "Adsorption-Induced Surface Electronic Reconstruction of Pt and Pt-Sn Alloys during CO Adsorption", *Journal of Physical Chemistry C*, Vol. 113, pp. 14329-14334, 2009.

187. Paffett, M. T., S. C. Gebhard, R. G. Windham, B. E. Koel, "Chemisorption of CO, H_2 and O_2 on Ordered Sn/Pt (111) Surface Alloys", *Journal of Physical Chemistry*, Vol. 94, No. 17, pp. 6831-6839, 1990.

188. Mawhinney, D.B., J. T. Yates Jr, "FTIR Study of the Oxidation of Amorphous Carbon by Ozone at 300 K — Direct COOH Formation", *Carbon*, Vol. 39, No. 8, pp. 1167-1173, 2001.

189. Sircar, S., D. V. Cao, "Heat of Adsorption", *Chemical Engineering Technology*, Vol. 25, pp. 945-948, 2002.